STABILITY OF AMPHIBOLE AND CARBONATE IN AN OXIDIZED UPPER MANTLE AND THE GENESIS OF CARBONATITES

by

Margaret E. Wallace (BSc. Hon.)

Submitted in partial fulfilment of the requirements
for the degree of
Doctor of Philosophy (Geology)
University of Tasmania
(March, 1989)

This thesis contains no material which has been accepted for the award of any other higher degree or graduate diploma in any tertiary institution and to the best of the author's knowledge and belief, the thesis contains no material previously published or written by another person, except when due reference is made in the text of the thesis.

Margaret E. Wallace

Margaret E. Wallace

Abstract

Amphibole, phlogopite, dolomite and magnesite are the volatile-bearing mineral phases in the upper mantle. As such, their stability effects the H_2O and CO_2 content of the mantle and therefore solidus positions and phase relationships.

The stability of pargasitic amphibole in the upper mantle is a function of water content and bulk rock composition. Under water-undersaturated conditions, the stability of amphibole controls the solidus position. Under these conditions, amphibole is stable to the highest pressures and temperatures in fertile peridotites and its pressure and temperature stability limits are decreased as bulk rock composition becomes more refractory.

At high pressures (>21 kb), the temperature stability limit of dolomite and magnesite are controlled by the reaction carbonate + Cpx -> sodic, dolomitic carbonatite melt + Al phase (Gt/Sp). In the system (dolomite (5%)-bearing Pyrolite + 0.2% H_2O) this reaction, and therefore the high pressure solidus, occurs at 930°C. It is the lowest temperature peridotite solidus found to date.

At low pressures (<21 kb), the stability limit of dolomite is controlled by the reaction Dol + Opx -> Cpx + Ol + CO_2. This produces an S-shaped solidus in Pyrolite (H_2O, CO_2 undersaturated) similar to that found in the CMAS system. The sodic, dolomitic carbonatite melt field is bounded by the solidus and amphibole-out boundary. The melt becomes melilititic at temperatures above the stability limit of amphibole. The pressure and temperature stability limits of the carbonatite depend on the stability field of amphibole which is a function of water content and bulk rock composition.

The carbonatite melt field is limited to between 21-31 kb and 930-1075°C suggesting that carbonatite melts are only formed in areas which are oxidized and have oceanic (or rift valley) type geotherms. Carbonatite melts may migrate rapidly to the surface; however during upward melt migration the melt would cross the reaction boundary carbonatitic melt + Opx -> Cpx + Ol + CO_2 causing metasomatism of spinel lherzolite to olivine wehrlite. This process also causes Na, K, P, and LREE metasomatism of the lithosphere at ≤ 60 kms depth. This is additional to and differs mineralogically and chemically from Ti, Fe, Al metasomatism by crystallization of hydrous basaltic melts as they migrate across the amphibole-out boundary, i.e. metasomatism at up to 80-90 kms depth.

These processes are illustrated in peridotite nodules from the Tumut-Eucumbene Tunnel, N.S.W. This suite is distinctive as it contains amphibole, dolomite and magnesite. Mineral textures suggest that this suite records amphibole related Fe-Ti-Al metasomatism and the trapping of a carbonate-rich melt.

Acknowledgements

Prof. D.H. Green is thanked for suggesting the project, for his help and close supervision through-out the experimental studies, and for providing the xenolith samples from the Tumut-Eucumbene tunnel.

Keith Harris provided valuble assistance in the high pressure lab, both with teaching the experimental techniques and with running the experiments.

Wieslaw Jablonski helped with the use of the microprobe and took the S.E.M. pictures forming Figures 11 and 21.

Simon Stephens prepared the probe mounts and is thanked for developing techniques enabling the Na-carbonatite melt (which was very soft and water-soluble) to be polished.

Wayne Taylor and Malcolm Wallace helped with the use of computers. Wayne Taylor is particularly acnowledged for suggesting the magnesite buffer used in the experimental studies.

John Adam and Phil Robinson ran the X.R.F. analyses of the Eucumbene Tunnel xenoliths.

John Adam and Wayne Taylor are thanked for their discussions on the project along with other members of the Tasmanian petrology group, Trevor Falloon, Nick Odling, Tony Crawford, Rick Varne, Kurt Mengel, Steve Eggins and Joe Stoltz.

This project was undertaken while the author was recipient of a Commonwealth Post-Graduate scholarship.

Contents

INTRODUCTION 1

CHAPTER

1. THE EFFECT OF BULK ROCK COMPOSITION ON THE STABILITY OF AMPHIBOLE IN THE UPPER MANTLE

Introduction 3
Starting Material 4
Experimental Techniques 7
Experimental Results 7
Comparison with other work 10
Discussion 12
Mineral Chemistry 14
Conclusions 23

2. PHASE RELATIONS IN THE SYSTEM "CARBONATE-BEARING PYROLITE + 0.2% H_2O" AND THEIR EFFECT ON UPPER MANTLE PROCESSES

Introduction 25
Previous work in the Peridotite + H_2O + CO_2 system 26
Experimental Techniques 29
Experimental Results 31
Mineral Chemistry 43
Discussion 47
Conclusions 55

3. COMPOSITION OF A PRIMARY CARBONATITE MELT

Introduction 57
The Nature of 'Primary' Carbonatite 58
Experimental Techniques 60
Experimental Results 62
Discussion 68
Conclusions 73

CHAPTER

4. CARBONATE-RICH ULTRAMAFIC XENOLITHS FROM TUMUT-EUCUMBENE TUNNEL, N.S.W.

Introduction 74
Locality 75
Petrology 76
Mineral Chemistry 81
Whole Rock Chemistry 90
Conditions of Crystallization 94
Discussion 96
Conclusions 102

REFERENCES 103

APPEDICES

A. Natural Peridotitic Amphibole Database 119
B. Mineral Chemistry of (Tinaquillo + 0.2%H_2O) Experiments 149
C. Mineral Chemistry of (Carbonate-bearing Pyrolite + 0.2%H_2O) Experiments 157
D. List of Probe Mounts and Eucumbene Sample Numbers 168

List of Figures

1. Plot of SiO_2, Al_2O_3, TiO_2, FeO, CaO and Na_2O vs MgO for natural amphibole-bearing peridotites 5
2. Phase relationships of Tinaquillo peridotite under water-saturated and water under-saturated conditions 9
3. Comparison of amphibole stability in experimental peridotites 10
4. Comparison between natural and experimental amphibole compositions 17
5. Na vs K cation abundance of experimental and natural lherzolitic amphiboles 19
6. Ti vs Na cation abundance of experimental and natural lherzolitic amphiboles 22
7. Previous work in the peridotite + H_2O + CO_2 system 27
8. fO_2 range of magnesite-periclase-graphite buffer 31
9. Phase relationships in pyrolite + 0.2% H_2O + 1.4% $MgCO_3$ 32
10. Modal proportion of phases in carbonate-bearing pyrolite + 0.2% H_2O experiments 36
11. Scanning electron micrographs of carbonate-bearing H_2O undersaturated pyrolite experimental probe mounts 40
12. Mg# vs temperature of formation of silicate minerals in carbonate-bearing H_2O undersaturated pyrolite experiments 43
13. Al^6 vs Na cation abundance of experimental clinopyroxenes 44
14. Cross-section of large clinopyroxene crystal 45
15. Amphibole compositions from carbonate-bearing H_2O undersaturated pyrolite experiments 46
16. Carbonate compositions from carbonate-bearing H_2O undersaturated pyrolite experiments 46
17. Peridotite and dolomite-bearing peridotite solidi under a variety of water saturation conditions 48
18. Melt crystalization paths in an oxidized H_2O and CO_2-bearing mantle 50
19. Cross-section of an idealized continent of pyrolite composition 52
20. Experimental capsule and buffer assembly design 62
21. Scanning electron micrographs of sandwich experiments 64
22. Mineral compositions of silicate phases from sandwich experiments 66
23. Locality diagram for Tumut-Eucumbene 75

24. Thinsection microphotographs of carbonate in Tumut-Eucumbene xenoliths 80
25. Composition of silicate phases in Tumut-Eucumbene xenoliths 85
26. Clinopyroxene composition of xenoliths 86
27. Amphibole composition of xenoliths 87
28. Ti vs Mg# of amphibole in xenoliths 87
29. Spinel composition of xenoliths 88
30. Composition of carbonate phases in xenoliths 89
31. Major element abundance vs MgO of xenoliths 92
32. Rare earth element concentration of xenoliths 93
33. Trace element content of xenoliths 94
34. Relationship between Cr-diopside series xenoliths, Fe-rich xenoliths and banded xenolith samples 98
35. Pressure and temperature path of xenolith crystallization 99

List of Tables

1. Chemical compositions of experimentally studied peridotites 6
2. Experimental run conditions for Tinaquillo peridotite + H_2O 8
3. Chemical compositions of pyrolite starting mixes 30
4. Carbonate-bearing pyrolite + 0.2% H_2O run conditions 33
5. Starting compositions used in sandwich experiments 61
6. Run conditions of sandwich and reversal experiments 63
7. Analyses of mineral phases from sandwich experiments 65
8. Representative mineral compositions from reversal experiments 67
9. Comparison between selected natural and experimental carbonatites 69
10. Summary of texture and mineral phases present in Tumut-Eucumbene xenoliths 77
11. Representative mineral analyses of xenolith phases 82
12. Bulk rock compositions for Tumut-Eucumbene xenoliths and host rock 91
13. Xenolith conditions of crystallization 95

INTRODUCTION

The aim of this thesis was to determine the effect of H_2O and CO_2, therefore the minerals amphibole, dolomite and magnesite, upon mantle processes. The thesis work has been presented in four chapters. The first chapter describes experimental work in the Tinaquillo peridotite + H_2O system. The stability of amphibole and its effect on solidus positions is discussed.

Chapter 2 presents an experimental study in pyrolite + H_2O + CO_2 (undersaturated). In this study a carbonatite melt was discovered co-existing with amphibole lherzolite under oxidizing conditions. A general melting model for an oxidized H_2O and CO_2 bearing mantle is presented.

Chapter 3 describes the nature of the carbonatite melt. A Na-rich dolomitic melt was produced in equilibrium with an amphibole-bearing lherzolite by a series of sandwich experiments. Implications of a primary Na-rich dolomitic magma to the problems of carbonatite genesis are discussed.

Chapter 4 presents descriptions of natural carbonate-bearing lherzolite nodules from Tumut-Eucumbene, N.S.W. Mineralogy, petrology and whole rock chemistry of the xenoliths are provided. Interpretation of xenolith genesis is based on the experimental phase relationships determined in Chapters 1 and 2.

Partial results of this work have been published in;

Wallace, M.E. and Green, D.H. (1988). An experimental determination of primary carbonatite magma composition. *Nature*, 335, 343-346.

Green, D.H. and Wallace M.E. (1988). Mantle metasomatism by ephemeral carbonatite melts. *Nature*, 336, 459-462.

Green, D.H., Barsdell M., Crawford A.J., Eggins S.M., Falloon T.J., and Wallace M.E. (1987). Petrology of upper mantle processes in the S.W. Pacific. *Proc. Pacif. Rim Congr. A.I.M.M. Victoria* . 621-632

Methods

The high pressure experimental techniques used are described in each chapter. Probe analyses were performed on a JEOL JXA-50A electron microprobe with an EDAX attachment and calibrated on pure Cu (operating conditions = 15 kv, $7*10^{-10}$A). This has an analytical precision of 0.2 wt%. Electron micrographs (Figures 11 and 21) were taken on a Philips 505 S.E.M. Bulk rock X.R.F. analyses (Chapter 4) were performed on an automated Phillips PW1410 spectrometer.

1. THE EFFECT OF BULK ROCK COMPOSITION ON THE STABILITY OF AMPHIBOLE IN THE UPPER MANTLE

Introduction

Pargasitic amphibole has been widely recognised in mantle lherzolites and has attracted attention of petrologists since Oxburgh (1964) suggested that its presence as a phase in the upper mantle would explain the high K content of mantle derived basalts. The crystal chemistry of primary or equilibrated amphiboles in spinel and garnet lherzolites has been extensively studied (Dawson and Smith, 1982; Wilkinson and LeMaitre, 1987). These amphiboles occur predominantly in lherzolitic nodules hosted by basanitic to alkali basaltic lavas (Francis, 1976; Nickel and Green, 1984; Takahashi; 1980) or as an equilibrium phase in Alpine peridotites (Green, 1964; Bonatti *et al.*, 1986; Roden *et al.*, 1984; Henry and Medaris, 1980). In most samples, amphibole occurs as small interstitial grains, but it is occasionally found as grains rimming spinel or as thin lamellae replacing clinopyroxene. It is often associated with Ti-bearing phlogopite.

There have been several experimental investigations of the stability of amphibole at high pressure and temperature. The maximum pressure and temperature stability of amphibole under water-saturated conditions has been determined for pyrolite (Green, 1973), Salt Lake Crater spinel lherzolite (Kushiro, 1970) and St. Paul's peridotite (Millhollen *et al.*, 1974). In these compositions, amphibole was found to break down at temperatures between 980 and 1050°C at pressures between 25 and 28 kb.

Hill and Boettcher (1970) demonstrated that amphibole was stable to higher temperatures when the activity of water is less than 1.0 . Holloway's (1973) experiments showed that at 8 kb, pargasitic amphibole is stable to the highest temperatures when X_{H2O} = 0.4 . The maximum in temperature stability of amphibole at lower water activity has been confirmed in ultramafic rocks by Green (1973) using pyrolite, Millhollen and Wyllie (1974) using hornblendite, and Merrill and Wyllie (1975) using hornblende eclogite.

Closed system experiments with pyrolite (Green, 1973) have demonstrated that under water-undersaturated conditions (aprox. 0.2 wt% H_2O) the shape and position of the solidus is controlled by the stability of amphibole. Amphibole is stable up to 1150°C and

28 kb in pyrolite. Above 28 kb the solidus 'backbends' from 1150°C to 1000°C as a result of the interaction of the solidus with the amphibole breakdown reaction (amphibole -> garnet + pyroxene + olivine ± ilmenite ± phlogopite). At pressures greater than 28 kb, where amphibole is not stable and the amount of water is greater than can be accommodated by phlogopite, the peridotite + 0.2% H_2O solidus will be similar to the water-saturated solidus. This relationship can not be extrapolated to open systems with C-O-H fluid since Taylor and Green, (1988) have recently demonstrated that the peridotite solidus in open system experiments at low oxygen fugacities ($H_2O + CH_4 > CO_2$ fluid) is not controlled by the breakdown of amphibole. At higher oxygen fugacities, in open systems, the solidus is determined by melting involving carbonatite liquids. This will be discussed in Chapter 2.

The purpose of this study is to investigate the effect that bulk rock composition has on amphibole stability and therefore the position of the solidus in ultramafic rocks in a closed system, under water-undersaturated, high temperature and high pressure conditions. The phase relations for the depleted Tinaquillo peridotite composition over a range of temperatures and pressures were determined. This enabled mapping of the solidus position and the stability limits of amphibole in a refractory bulk rock composition.

Starting Material

Amphibole-bearing peridotites span a wide range of chemical compositions and the occurrance of amphibole does not appear to be restricted to any particular bulk rock composition. Figure 1, presents a plot of MgO vs SiO_2, FeO, NaO_2, CaO, Al_2O_3, and TiO_2 content of amphibole-bearing peridotites from Hoggar, Ataq, Tariat, Lake Bullenmerri, Finero, Fen, Alpe Arami, Balmuccia, Zabargad, Timor, Tinaquillo and the Austridic complex. (Chemical analyses and sample descriptions are provided in Appendix A). Compositions of the experimentally studied peridotites; Pyrolite, Tinaquillo peridotite, and North Hessian Depression spinel lherzolite are also shown for comparison.

This diagram demonstrates that amphiboles can occur in extremely refractory as well as fertile lherzolites. The samples fall along the mantle array (Palme and Nickel, 1985) and although a fair amount of chemical scatter is evident, they are neither significantly nor uniformly enriched in Na, Fe, or Ti. Most of the chemical scatter is provided by samples

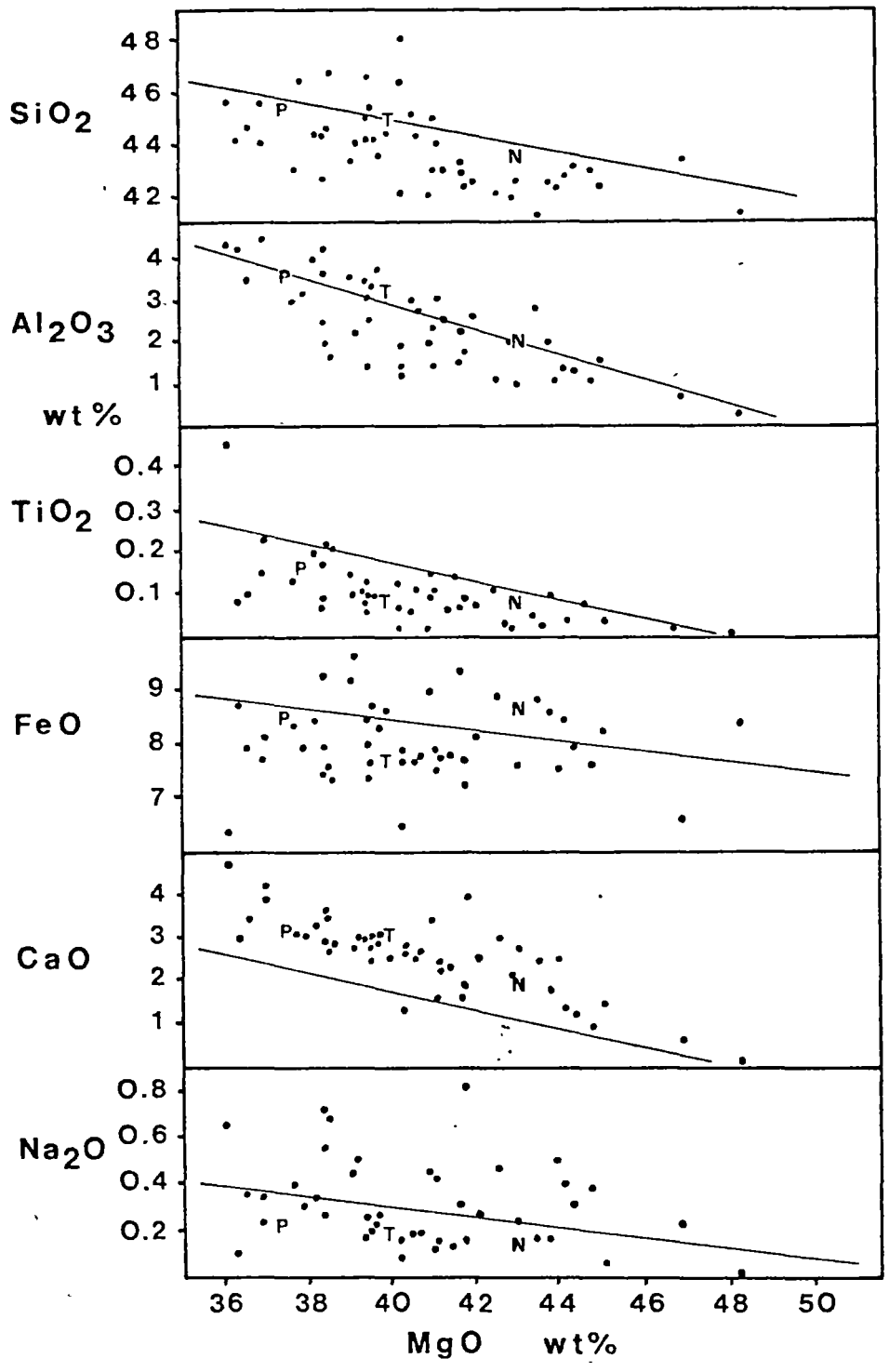

Figure 1. Plot of SiO_2, Al_2O_3, TiO_2, FeO, CaO and Na_2O vs MgO for natural amphibole bearing peridotites. P = pyrolite, T = Tinaquillo peridotite, N = North Hessian Depression composition. —— regression line for oceanic spinel lherzolite xenoliths (Maaloe and Aoki, 1977). Natural lherzolite data from Varne, 1970; Griffin, 1973; Frey and Green, 1974; Frey and Prinz, 1978; Ernst, 1978; Leavy and Hermes, 1979; Girod *et al.*, 1981; Berry, 1981; Obata and Morten, 1982; Nickel and Green, 1984; Griffin *et al.*, 1984; Bonatti *et al.*, 1986; Press *et al.*, 1986; Nixon, 1987; Dautria *et al.*, 1987; O'Reilly and Griffin, 1988; and Seyler and Mattson, 1989.

from Lake Bullenmerri, Victoria and generally, samples with high Na-contents tend to have large modal proportions of amphibole.

The Tinaquillo peridotite, a natural spinel lherzolite composition from Green, (1963), was selected for this project in order to study amphibole stability in a rock composition representative of depleted mantle peridotite. Results from experiments on the Tinaquillo composition can be directly compared with those from a previous study (Green, 1973) which documented the stability of amphibole in Hawaiian pyrolite, an enriched peridotite composition. Experimental methods used in this study are similar to those of Green (1973) thus enabling direct comparisons to be made. Compared to pyrolite, the Tinaquillo peridotite is depleted in TiO_2, K_2O, Na_2O, has slightly lower CaO and Al_2O_3, and contains more MgO (Table 1). It is similar to estimates of upper mantle compositions based on averages of spinel lherzolite compositions (Maaloe and Aoki, 1977).

To diminish the dominance of olivine in the crystallized mineral assemblage, a composition equivalent to Tinaquillo minus 40% olivine of $Fo_{91.1}$ composition has been used in the experimental runs. This starting mix was prepared from analytical reagent grade chemicals which were ground under acetone and sintered at 1000°C. Olivine was present in all runs, confirming that all mineral assemblages are olivine dominated and therefore peridotitic.

Table 1. Chemical Compositions of Experimentally Studied peridotites

	Pyrolite	Pyrolite -40% Ol	Tinaquillo	Tinaquillo -40% Ol	N.H.D	N.H.D.+1.5% mica-60% Ol	Salt Lake Crater	St.Paul's Peridotite
SiO2	45.20	47.90	44.95	47.50	43.40	47.20	48.02	42.22
TiO2	0.71	1.18	0.08	0.13	0.08	0.25	0.22	0.30
Al2O3	3.54	5.91	3.22	5.35	2.00	5.60	4.88	4.42
Fe2O3	0.48	0.20	0.09	0.15	-	-	1.94	2.86
FeO	8.04	8.63	7.58	7.38	8.60	6.69	8.15	4.45
MnO	0.14	0.13	0.14	0.18	0.13	0.07	0.14	0.13
MgO	37.50	28.80	40.03	32.80	43.10	33.59	32.35	34.61
CaO	3.08	5.14	2.99	4.97	1.80	4.43	2.97	3.92
Na2O	0.57	0.95	0.18	0.30	0.13	0.35	0.66	0.43
K2O	0.13	0.22	0.02	0.03	0.03	0.42	0.07	0.11
NiO	0.20	0.13	0.26	0.43	0.42	0.30		0.27
Cr2O3	0.43	0.72	0.45	0.75	0.30	1.08	0.25	0.50
Mg/Mg+Fe2+	0.893	0.856	0.904	0.888	0.899	0.899	0.876	0.933
Mg/Mg+Fe	0.890	0.855	0.903	0.887	0.899	0.899	0.865	0.915

N.H.D. = North Hessian Depression Analyses are from Green, (1973), Jaques and Green, (1980), Mengel and Green, (1988), Kushiro, (1970), and Millhollen et al., (1974)

Experimental Techniques

All experiments were carried out in piston - cylinder apparatus at the University of Tasmania. Samples were sealed in small capacity (2.2 mm O.D) Ag_{75} Pd_{25} and large capacity (3.5 mm O.D) $Ag_{50}Pd_{50}$ capsules and placed in NaCl or NaCl-pyrex sleeves. The desired water content was added to the capsule by microsyringe and checked by weighing the capsule before and after welding. Where very small quantities of water were needed in the water - undersaturated ($P_{H2O}<P_{Total}$) runs, a starting mix containing amphibole was synthesized. This was achieved by mixing 80 mg of peridotite with 1.8 to 2.0 wt% water and crystallizing the sample at 15 kb and 925 to 950°C for 72 hours, producing a subsolidus mineral assemblage of olivine, pyroxenes, spinel and amphibole. The sample was then ground under acetone and dried overnight at 250°C. Smaller (12 mg) portions were then run under various pressure and temperature conditions. No fO_2 buffer was used, but phase compositions suggest that fO_2 was in the MW-buffer range.

Experimental runs were performed using the "piston-in" technique with no friction correction applied. The stated pressures are accurate to within 1 kb. Temperatures were measured using a $Pt/Pt_{90}Rh_{10}$ thermocouple automatically controlled to within $\pm$ 5°C of the set point. No correction was applied for the effect of pressure on emf. Temperatures are accurate to $\pm$ 10°C.

Experimental charges were examined under the optical microscope. Solid phases were analyzed using a JEOL JX-50A electron microprobe.

Experimental Results

Water-saturated conditions , The phase relations for Tinaquillo under water-saturated conditions are presented as a function of temperature and pressure in Figure 2a and are listed in Table 2. Many of the experiments were run by K. Mengel in 1985 as part of a project on the North Hessian Depression, W. Germany (Mengel and Green, 1989). Analytical data were obtained as part of the present study. Olivine, orthopyroxene and clinopyroxene are present in all water-saturated runs. The spinel to garnet phase transition occurs at approximately 20 kb between 1000 and 1100°C. The assemblage present at 950°C and 20 kb contained garnet only while both phases occured at 20 kb and 980°C.

Table 2. Experimental run conditions for Tinaquillo peridotite under water saturated and water undersaturated conditions

Run#	P (kb)	T (°C)	%H2O	Run Time (hrs)	Starting Mix	Phases
Water-saturated runs						
1979	10	1000	1.0	120.0		Ol,opx,cpx,sp,gl
1570*	15	900	1.0	64.5		Ol,opx,cpx,sp,amph
1565*	15	950	10.0	45.0		Ol,opx,cpx,sp,amph
1571*	15	1000	1.0	27.0		Ol,opx,cpx,sp,gl
1583*	20	950	1.0	72.0		Ol,opx,cpx,gt,amph
2055	20	980	0.6	71.5		Ol,opx,cpx,sp,gt,gl
1582*	25	950	1.0	73.5		Ol,opx,cpx,gt,amph
1585*	25	1000	1.0	47.5		Ol,opx,cpx,gt,gl
2024	27	950	0.6	72.0		Ol,opx,cpx,gt
1578*	28	1000	1.0	72.0		Ol,opx,cpx,gt
1572*	30	950	1.0	48.0		Ol,opx,cpx,gt
1574*	30	1000	1.0	76.0		Ol,opx,cpx,gt
1586*	30	1050	1.0	43.0		Ol,opx,cpx,gt,gl
Starting Mixes						
1833	15	950	1.8	48.0		Ol,opx,cpx,sp,amph
1872	15	925	2.0	72.0		Ol,opx,cpx,sp,amph
1912	15	925	2.0	72.0		Ol,opx,cpx,sp,amph
1960	15	925	2.0	72.0		Ol,opx,cpx,sp,amph
Water-undersaturated runs						
1998	10	970		120.3	1912	Ol,opx,cpx,sp,amph
2007	10	1000		~140	1912	Ol,opx,cpx,sp
1920	15	1000		96.0	1912	Ol,opx,cpx,sp,amph
1952	15	1025		96.0	1912	Ol,opx,cpx,sp,gl
1944	20	1000		96.0	1912	Ol,opx,cpx,gt,amph
1902	20	1025		94.4	1872	Ol,opx,cpx,sp,gt,amph
1848	20	1100		48.0	1833	Ol,opx,cpx,sp,gt
1859	25	1000		72.0	1833	Ol,opx,cpx,gt,amph
1895	25	1025		72.0	1872	Ol,opx,cpx,gt,amph
1890	25	1050		72.0	1872	Ol,opx,cpx,gt
1840	25	1100		23.0	1833	Ol,opx,cpx,gt
1842	28	1050		42.0	1833	Ol,opx,cpx,gt
1838	28	1100		22.0	1833	Ol,opx,cpx,gt,gl

* Runs by K. Mengel, 1985
Phases = Olivine (Ol), orthopyroxene (opx), clinopyroxene (cpx), spinel (sp), garnet (gt), amphibole (amph), glass (gl)

The solidus was determined by optical examination of crushed samples. Above solidus mineral assemblages contain visible melt phases and have larger crystals than those in the subsolidus runs. The amphibole breakdown curve coincides with the solidus (within 25°C) from 5 to 26 kb. The amphibole dehydration reaction has been bracketed to between 25 and 27 kb at 950°C. Amphibole is present in all subsolidus runs below 27 kb (confirmed by microprobe).

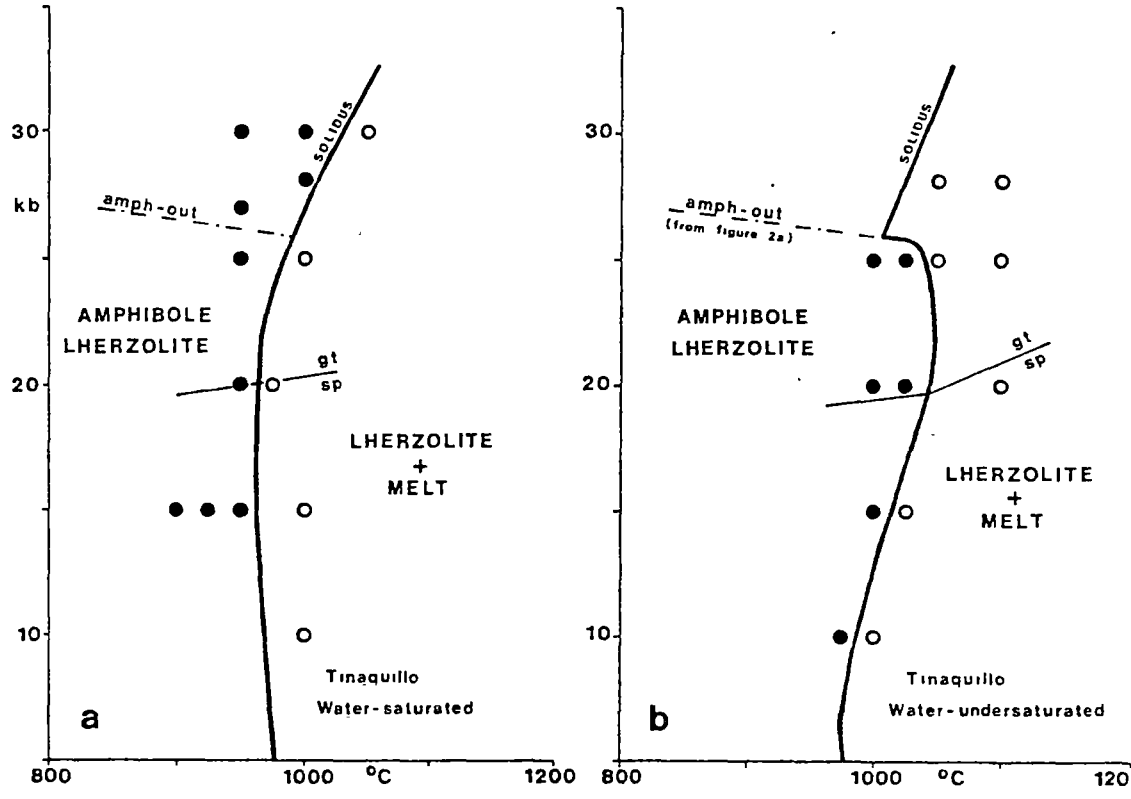

Figure 2. Phase relationships of Tinaquillo peridotite under (a) water-saturated and (b) water under-saturated conditions.

Water -undersaturated conditions , Experimental phase relationships for the Tinaquillo water-undersaturated system are presented in Figure 2b. The water undersaturated ($P_{H2O} < P_{Total}$) solidus has a curved, convex upward shape similar to that found in pyrolite + 0.2% H_2O (Green, 1973). The solidus appears to be controlled by the stability of pargasitic hornblende. In this bulk rock composition, amphibole is stable only up to 1025°C at pressures of 20 and 25 kbs, and to 1000°C at 15 kb. It is present in all of the sub-solidus samples. Probe analyses show that the amphibole is Cr-rich pargasite. It was not possible to optically confirm the presence of melt in the 1050°C runs, however Mg# values (Mg/Mg+Fe) of olivine crystals increase sharply when the solidus is crossed,

indicating that a melt phase is present. At 1100°C, small pools of melt and quench outgrowths on primary crystal phases were observed in crushed samples. The spinel lherzolite to garnet lherzolite transition occurs at 20 kb. At high pressures (>26 kb) where amphibole is not stable, the peridotite water undersaturated solidus is similiar to the water saturated solidus (Green 1973).

Comparison with other work

Water - saturated conditions, The water-saturated solidus and amphibole-out curve has been determined for Hawaiian Pyrolite (Green, 1973), Salt Lake Crater spinel lherzolite (Kushiro, 1970) and St. Paul's peridotite (Millhollen *et al.*, 1974). Under water-saturated conditions the Tinaquillo amphibole-out curve appears to coincide with the solidus, while amphibole is stable above the solidus for the other compositions (Figure 3). Pyrolite has the most accurately determined solidus curve constrained between 950°C and 980°C at 20 kb and 1000°C to 1020°C at 10 kb. The St. Paul's peridotite amphibole melting curve is constrained between 1000°C and 1050°C at 10 kb and 20 kb (Millhollen *et al.*, 1974). Kushiro (1970) has bracketed the Salt Lake Crater lherzolite between 1000°C and 1030°C at 15 kb, 17 kb to 20 kb at 1000°C, and 900°C to 950°C at 23 kb.

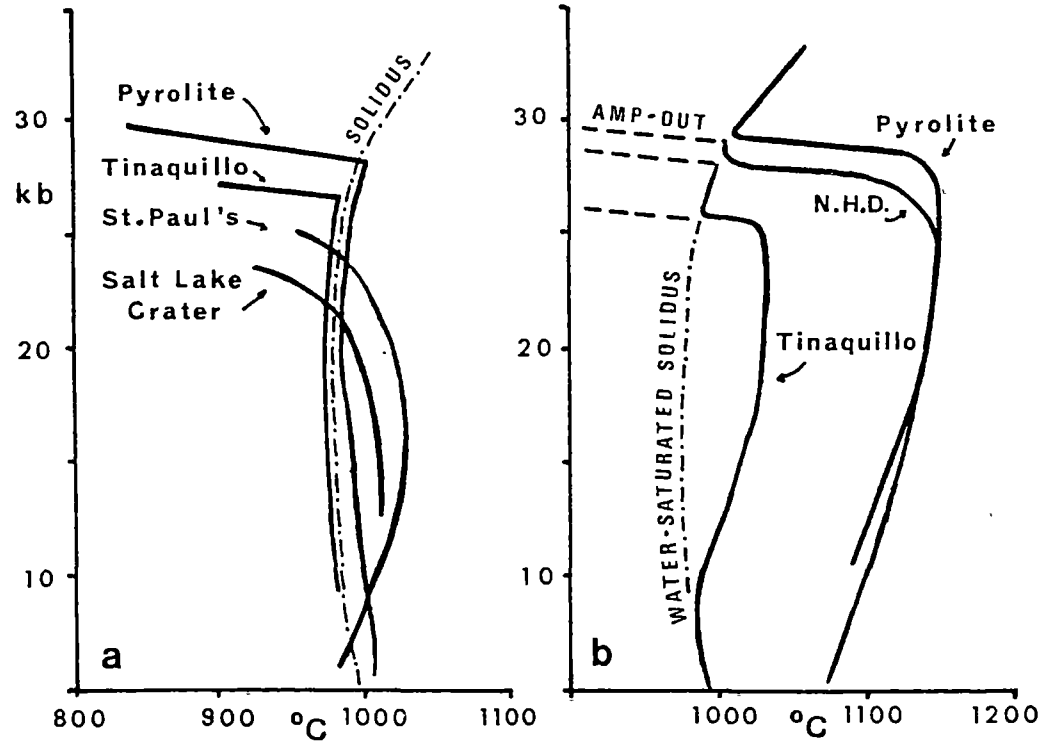

Figure 3. Comparison of amphibole stability in Tinaquillo peridotite, pyrolite, North Hessian Depression spinel lherzolite, St. Paul's peridotite and Salt Lake Crater spinel lherzolite under (a) water-saturated and (b) water under-saturated conditions. Data are derived from Green, (1973), Kushiro (1970), Millhollen et al., (1974), and Mengel and Green, (1988).

The solidus-amphibole out relationships have also been determined for Peridotites A, B, C and D of Mysen and Boettcher (1975). However, their results are not consistent with those of other researchers, possibly due to misinterpretation of the vapor phase, difficulty in optically determinating amphibole from pyroxenes and their use of CO_2 as a dilutant to control the activity of water.

The position of the water-saturated solidus does not appear to change significantly with bulk rock composition (within the experimental limits), however, amphibole is stable to higher temperatures above the solidus in the more alkali enriched compositions.

Water-undersaturated solidus , Figure 3b compares the Tinaquillo water-undersaturated solidus with that of pyrolite (Green, 1973) and the North Hessian Depression (N.H.D.) composition (Mengel and Green, 1989). Under water-undersaturated conditions, in a closed system, the solidus is controlled by the upper stability limit of amphibole. Amphibole is stable up to 1025°C and 26 kb in Tinaquillo composition and 1150°C and 28 to 29 kb in Pyrolite and N.H.D. compositions. The high temperature and pressure stability limits of pargasitic amphibole appear to be controlled by the availability of H_2O and bulk rock composition, particularly bulk rock alkali content as demonstrated by the high temperature (~1150°C) stability of amphibole in the refractory N.H.D. composition which was modified by the addition of 1.5% mica.

The modal proportion of pargasitic amphibole in a water-saturated lherzolite appears to depend upon bulk rock alkali content. A fertile composition such as pyrolite contains approximately 30% amphibole while a more refractory composition such as the Tinaquillo peridotite contains 10 to 15% amphibole. Excess H_2O forms a vapor phase. Under water-undersaturated conditions, however, the modal proportion of amphibole is dependent on H_2O content. Bulk rock alkali content will control amphibole stability rather than the modal proportion of amphibole in the assemblage. Excess alkalis, those not needed to stabilize amphibole, will reside in clinopyroxene and phlogopite.

Under increasing temperature and pressure conditions, pargasitic amphibole requires a larger proportion of alkalis (or increasing crystallographic A-site occupancy) to remain stable. This is reflected in the amphibole crystal chemistry from the pyrolite and Tinaquillo experiments. Assuming complete H_2O-site occupancy, Na + K / H_2O cation ratios of pargasitic amphibole equal 0.35 to 0.40 at 950°C, and 0.4 to 0.45 at 1100°C. Amphibole will only be stable if bulk rock composition can support the appropriate high

Na + K / H_2O cation ratio for any particular pressure and temperature condition. If there are not enough alkalis in the composition (or excess H_2O is added) the amphibole will breakdown to form olivine, pyroxenes, garnet and melt. Due to the lower concentration of alkalis in the Tinaquillo composition, amphibole breakdown occurs at lower temperatures and pressures, when Na + K / H_2O = 0.45, compared to pyrolite where amphibole breaks down when Na + K / H_2O = 0.6.

Discussion

Results of the experiments on Tinaquillo - 40% ol + 0.2% H_2O indicate first, that bulk rock composition and water content are the major factors controlling the stability of pargasitic amphibole. Second, that under water-undersaturated conditions, the position of the peridotite solidus is controlled by the stability of amphibole and third, that under conditions in which a range of bulk rock compositions have been hydrated at some lower temperature and are reheated, or adiabatically move to lower temperature, then the bulk rock composition with the least amount of alkalis (generally the most refractory composition) will begin to melt at the lowest temperatures. This is contrary to the melting relationships intuitatively expected since under most mantle conditions fertile lherzolite compositions will melt at lower temperatures than will more refractory ones.

Comparison of the solidus positions for pyrolite and Tinaquillo peridotite can form the basis for discussion of the melting behavior of a chemically inhomogeneous mantle. If the mantle is anhydrous, then the geotherm does not intersect the solidus. If however, there is a small amount of water in the upper mantle, then a diapir travelling upwards along an oceanic-type geotherm will cross the solidus and freeze by the formation of amphibole. A fertile peridotite assemblage will solidify at higher temperatures and therefore deeper in the mantle, than will a more refractory one.

Green, (1973) suggested that the low velocity zone, particularly in oceanic-crustal regions, is a direct result of the intersection of the geotherm with the peridotite solidus for $P_{H2O}<P_{Total}$. Also, that the depth or 'roof' of the low velocity zone is insensitive to changes in temperature, between 1000 and 1150°C, or water content (from H_2O=0 to 0.4%). Results of this study show that the high temperature, high pressure limit of amphibole lherzolite stability (the 'ledge' or 'step' on the dehydration solidus) is dependant upon amphibole composition and therefore water content and bulk rock

composition. The 'ledge' or 'step' will occur at 1150°C, 28 to 30 kb for a peridotite of fertile Hawaiian pyrolite composition and 1040°C, 24 to 25 kb for a more refractory peridotite of Tinaquillo composition.

At mantle temperatures and pressures between the two amphibole-out boundaries (for example 26 kb, 1080°C), a fertile peridotite will consist of olivine, pyroxenes, garnet and amphibole, while a more refractory composition will still contain melt. This melt fraction will be very small (<2%) and Fe, Ti, Al, Na and K rich, probably within the olivine basanite to nephelinite range suggested by Green (1970). It will also concentrate H_2O, Cl, and LREE, the most incompatible elements in a solidifying magma. The smaller the amount of melt, (controlled by the refractory nature of the assemblage) the higher would be the concentration of incompatible elements in the melt.

The melt fraction can behave in a variety of ways. It may migrate upwards along lithospheric fractures and if uncontaminated erupt as a volatile-rich nephelinitic magma. McKenzie (1984) has argued in favour of the ability of very small percentages of melt to segregate efficiently from their residual mantle material. It is more likely, however, due to the small proportion of melt present that it will be cooled against or react with the country rock and solidify at depth forming small amphibole-rich veins or segregations. In addition, this alkali-rich melt will react with and enrich (metasomatize) ajoining fertile peridotites which because of their alkali-rich composition have already solidified.

Features of this type (amphibole veins and selvages and metasomatism of adjoining peridotite) have been described from many localities, in particular the Geronimo Volcanic Field, Arizona (Kempton *et al.*, 1984; 1987) and Dish Hill, California (Wilshire and Trask, 1971; Wilshire *et al.*, 1980).

The best described example of H_2O-undersaturated chemically inhomogeneous mantle material is provided from studies of the St. Paul's peridotite (Frey, 1970; Melson *et al.*, 1972; Roden *et al.*, 1984). This locality contains three types of material, low K spinel peridotites containing minor pargasitic amphibole, fertile peridotites containing mainly kaersutitic amphibole and hornblende mylonites. Samples from this locality are LREE enriched and isotopically related. Roden *et al.*. (1984) have suggested that the samples record an 155 m.y.o. episode of LREE enrichment and that this enriching component was derived from the same mantle which was being enriched (auto-metasomatism). In addition, they suggested, (based on isotopic evidence), that the hornblende mylonite samples represent a crystallized metasomatic component which

due to its small size has re-equilibrated with the host lherzolite assemblage during a later metamorphic event.

Descriptions of the St. Paul's peridotite are consistent with the interpretation that it represents crystallization of inhomogeneous mantle material in the lithosphere. With diapiric uprise, a fertile peridotite will solidify into a pargasitic amphibole-rich peridotite, while more refractory areas will consist of K-poor peridotite plus an alkali and LREE enriched melt. In the St. Pauls peridotite, this melt has pooled and crystallized as amphibole segregations, later metamorphosed to hornblende mylonite schlieren. In addition the melt has enriched (metasomatized) the ajoining fertile peridotite by reaction with clinopyroxene and pargasite to form kearsutitic (high Ti) amphibole. This process is insitu and therefore auto-metasomatic.

The St. Pauls peridotite provides an instructive example of the upper mantle, in particular the lower part of the lithosphere, within the spinel lherzolite stability field. When the water content of this type of assemblage exceeds 0.4% by continued melt migration, the assemblage will become watersaturated and melting will occur. Due to the high concentration of amphibole in such an enriched and metasomatized lherzolite, it may be suitable as a source rock for producing alkali-basalts, as demonstrated by Roden *et al.*'s (1984) study of the St. Pauls peridotite.

Mineral Chemistry

The aim of this section is to compare the mineral chemistry of samples from this experimental study with samples of natural amphibole-bearing peridotites. In addition to the Tinaquillo analyses, experimental amphiboles are provided from studies of pyrolite (Green, 1973, many charges were analysed as part of this study) and the N.H.D. peridotite plus 1.5% mica (Mengel and Green, 1989). These additional analyses are provided in Appendix B.

A database of natural samples is presented in Appendix A. This contains published analyses of pargasitic amphiboles from peridotites. Analyses of co-existing phases (ol, opx, cpx, sp, gt and mica) where published are also included. Sample numbers, locations, and references are listed at the beginning of Appendix A.

This data set contains only pargasitic amphiboles which are in equilibrium with a Cr-rich diopside series assemblage. These amphiboles are generally Cr-rich and Ti-poor. Care was taken to exclude Ti-rich kaersutites which are megacrysts, which occur in Al-augite series samples, or which form by reaction with basaltic magmas. K-richterites were also excluded as they form only in Al-poor xenoliths associated with kimberlites. Amphiboles formed within eclogite nodules or MARID sequence rocks were omitted as they are chemically distinct from peridotitic amphiboles (They have low Mg#s and a much higher Fe, Ti and K content). The data set provides analyses of amphiboles from over 40 localities. Samples range from xenoliths in alkali basalts and kimberlites to alpine peridotites and peridotite lenses in gneiss, and are considered to provide a representative collection of amphibole bearing lherzolites.

Olivine,

Olivines occur in the Tinaquillo peridotite experiments as small (5 to 10 um) tabular grains. They show a limited compositional range with Mg# varying from 88.9 to 89.8 in subsolidus assemblages and from 89.5 to 89.7 in above solidus runs. (Mg#s of olivine in pyrolite samples range from 86 to 89). These high Mg#s reflect the residual nature of the Tinaquillo composition and indicate that only a small degree of melting has occurred with the breakdown of amphibole.

Orthopyroxenes

Orthopyroxene was the most abundant phase found in the Tinaquillo experiments. It occurs as large prismatic grains which are generally inclusion free. All of the orthopyroxenes were enstatites which range in Mg# from 88.0 to 91.0 (pyrolite opx Mg# = 85 to 88). Tinaquillo orthopyroxenes contain higher Mg contents and lower Fe and Ca than pyrolite samples. No Ti was detected. The experimental orthopyroxenes fall well within the chemical range of orthopyroxenes in natural peridotite samples (Mg# 86.3 to 92.6).

Clinopyroxenes

Clinopyroxenes did not occur in great abundance in the Tinaquillo experiments. They are present as small elongate grains and due to their small grainsize were quite difficult to analyse by electron microprobe. They are Cr-diopsides with Mg#s ranging between 89.5 and 91.5. Na contents range between 0.0 and 1.0 wt.% and increase with pressure. Compared to the pyrolite samples, Tinaquillo clinopyroxenes contain less Ti, Fe and Na, thus reflecting bulk rock composition.

No chemical zoning was detected in subsolidus runs, however, above solidus clinopyroxenes have Fe-rich quench rims. Calculation of temperature by the two pyroxene geothermometer (Wells, 1977) based on the diopside - enstatite miscibility gap generally yielded temperatures within 60°C of the experimentally set value. (Temperature calculations were not accurate for 950°C runs because the crystals were too small to provide good chemical analyses). Experimental samples are very similar in composition to natural clinopyroxenes which range in Mg#s from 84.4 to 95.5.

In general, natural clinopyroxene samples contain less Ti, Al and Fe as bulk rock composition becomes more refractory. This corresponds to an increase in Ca. Na values in natural samples tend to be erratic. There is a good correlation of Na increasing with Cr content. This appears to reflect the modal proportion of clinopyroxene within samples. Both Cr and Na contents increase with decreasing modal amounts of clinopyroxene. The same relationship is visible in the amphibole crystal chemistry.

Garnets

No spinels were analysed from the Tinaquillo runs due to their small grain size. Garnet analyses, however, were obtained from the 20 to 30 kb samples. These were from large, very poikilitic grains containing abundant inclusions of orthopyroxene. Tinaquillo garnets range from Mg# 79 to 82 and like the pyroxenes have lower Ti and Fe and higher Mg contents than those in pyrolite. Garnet Cr content increases with pressure. Experimental garnets have compositions similar to natural samples except that they have unusually high concentrations of Cr and Ti. This may be due to small inclusions of pyroxene and possibly of ilmenite.

Amphiboles

All experimental and natural lherzolitic amphiboles are pargasites with high Cr and low Ti contents (Figure 4). Amphibole compositions generally reflect bulk rock composition especially with respect to Fe and Cr contents and Mg#s. As a result, the Tinaquillo amphiboles contain low contents of Ti, Fe, Na, K and high concentrations of Mg and Cr when compared with pyrolite samples. Mg#, Cr and Ti contents of amphiboles are low in runs near the dehydration solidus. Amphiboles in these runs are present as small elongate crystals and analyses were difficult to obtain. The lower Mg# and Cr contents in some near-solidus amphiboles suggest that there may be some quench outgrowth indicating the presence of a very small amount of melt.

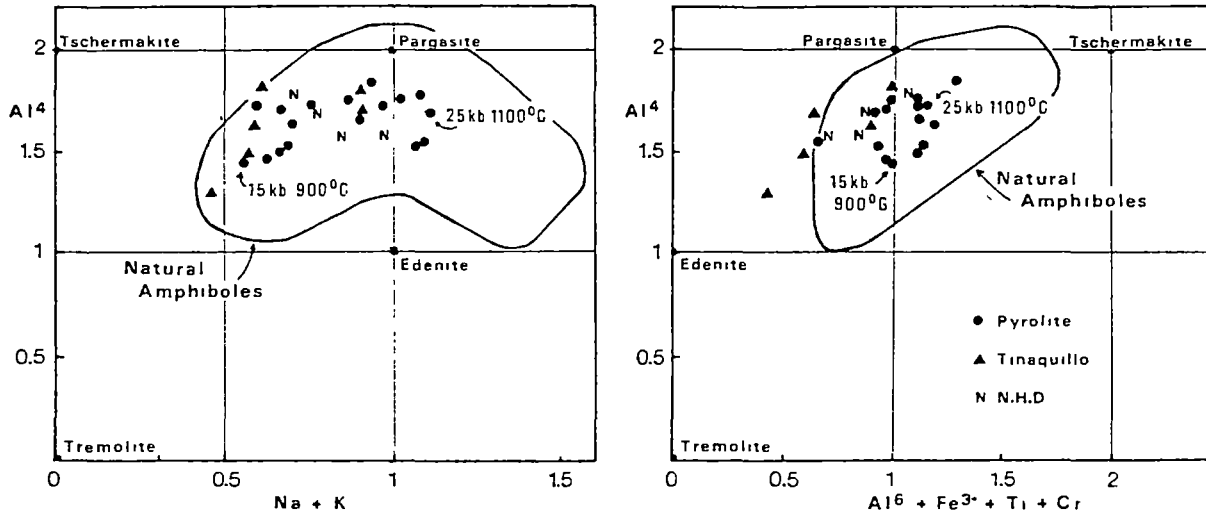

Figure 4. Comparison between (a) natural and (b) experimental amphibole compositions. Data are presented in Appendix A and Appendix B.

The Cr content in both natural and experimental amphibole samples is quite variable. In natural samples, this may be related to the affinity of amphibole with spinel. In many localities, amphiboles which appear to be in chemical equilibrium with a Cr-diopside series assemblage are found rimming spinel. The Al and Cr content of amphibole has been shown to decrease with proximity to spinel grains (Best, 1974; Francis, 1976). At many localities amphibole is most abundant in samples with little or no spinel.

The Cr content of amphiboles from experimental samples is also variable, both within samples and between them. Cr content does not reflect the presence of garnet or spinel, nor the modal abundance of amphibole. It is possible that many analyses of experimental amphiboles are contaminated by tiny spinel inclusions.

The concentration of Ti, Al and Na in experimental amphiboles, although generally bulk rock composition dependent, increases with temperature and pressure. This is due to increasing edenitic substitution and the dominance of the Ti over Fe tschermakite component with increasing pressure. The relationship is similar to that found in Jenkin's (1983) experimental studies.

The Al^4 concentration of amphibole, often investigated as a geothermometer (Robinson *et al.*, 1982), increases with metamorphic grade. This results in a change of

amphibole composition from tremolite to hornblende then pargasite which is accompanied by a change in crystal habit from thin elongate prisms to short stout equidimentional grains. Na content is controlled by increasing richterite or glaucophane component. Richterite, though only stable in Al-deficient rocks, is the highest pressure amphibole found in mantle environments (Veblen and Ribbe, 1982).

These amphibole Ti, Al, and Na temperature and pressure relationships, however, are not apparent in natural lherzolite samples. Ti, Al, or Na contents in natural pargasitic amphiboles do not correlate with temperature, calculated using Well's thermometer on co-existing pyroxenes, nor pressure as indicated by the presence or absence of garnet. The Ti, Na, and K concentrations differ greatly between localities and are often much higher in natural samples than in the experimental ones.

Figure 5, presents a plot of Na vs. K cation abundance for both experimental and natural samples. The natural samples fall into three groups.

1) Low K samples, These amphiboles contain < 0.04 cations of K (based on 23 oxygens) and can be found in samples from Ichinomegata, Tinaquillo, Timor, Miyamori, the Norwegian Western Gneiss (Lein), Mt.Leura, Fen, Oregon and the Ronda peridotite. (Samples from P'Aspet and the Lizard peridotite also contain low K abundances, however, only one published analysis was obtained from each of these localities.)

2) High K low Na samples, These amphibole samples have K concentrations > 0.5 cations and Na concentrations < 0.8 cations. Sample localities include Finero, Zabargad, Alpe Arami,and Austridic complex (=Nonsberg peridotite).

3) High Na and K samples, These samples contain Na cation abundances > 0.8 and variable K abundances which range from 0 to 0.35 cations. They are characterized by containing > 1.0 cations of combined Na plus K. High Na and K samples occur at Lake Bullenmerri, Lake Gnotuk, W. Eifel, Nunivak, Jagersfontein, Massif Central, and Malaita. Samples from Tariat, N.H.D. Deudesfeld, San Carlos, Grand Canyon, Hawaii, and Ataq also fall within this category, as do the kimberlite pargasitic amphiboles from Monestry, Bultfontein, Belsbank and Lesotho.

Only samples in group 1 fall within the compositional range expected for hydrated peridotites and compare well with the experimental samples. It is suggested that the amphiboles from these localities form by simple hydration of a peridotite assemblage, most likely by hydration of clinopyroxene to form pargasitic amphibole, or by crystallization of an H_2O-bearing melt during normal diapiric uprise of a lherzolitic assemblage.

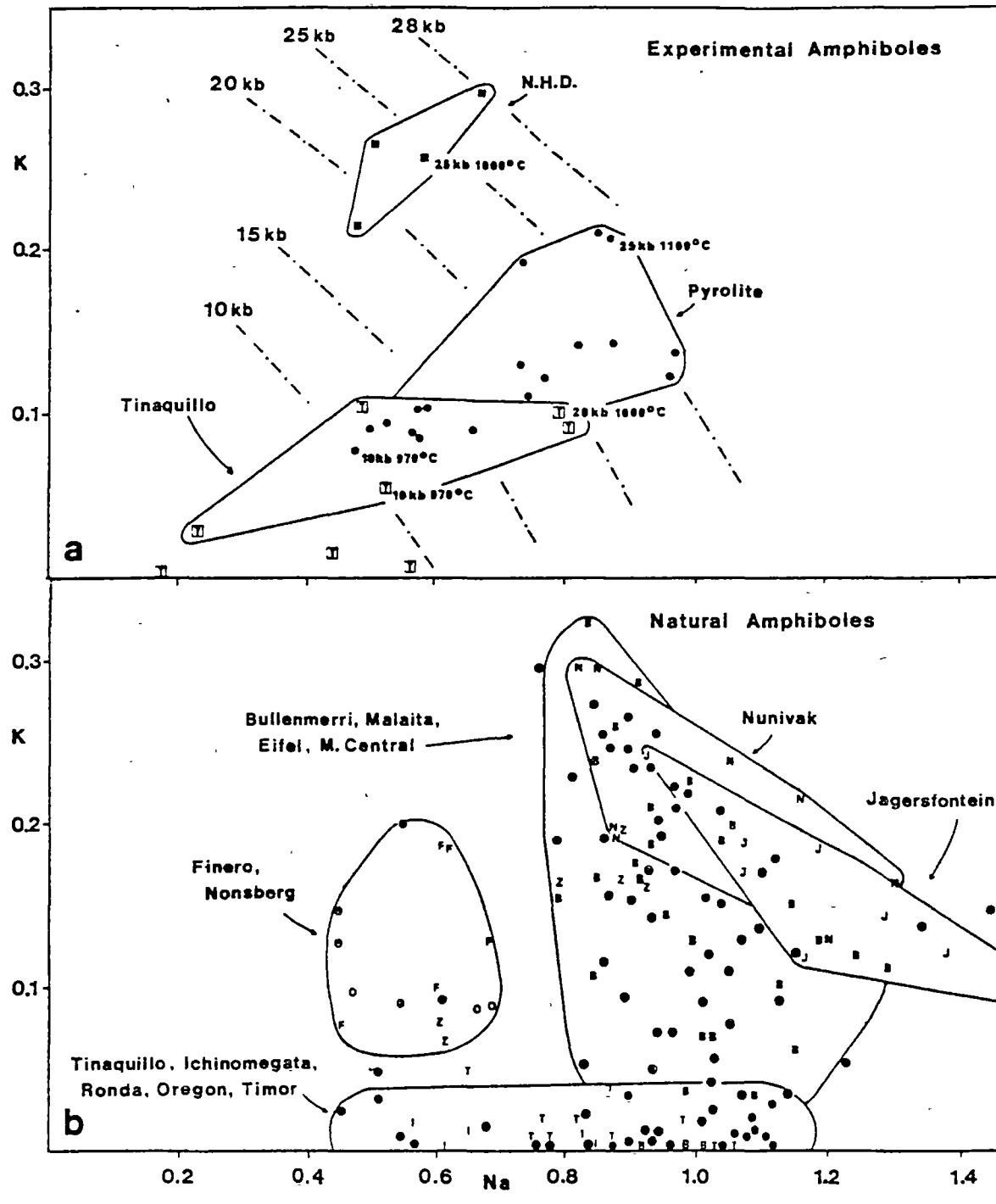

Figure 5. Na vs K cation abundances of (a) experimental and (b) natural lherzolitic amphiboles. Data from Appendix A and B. B = samples from Lake Bullenmerri, F = Finero, I = Ichinomegata, J = Jagersfontein, N = Nunivak Island, O = Nonsberg peridotite, T = Tinaquillo, Z = Zabargad.

Amphiboles in group 2 are K enriched and in this respect similar to experiments on the N.H.D. composition plus 1.5% mica (Mengel and Green, 1989). Many of these localities contain mica. The high K-content of amphiboles may reflect alkali element partitioning between amphibole and mica, however, the possibility that these samples have formed or been modified by reaction with a K-rich fluid or melt can not be ruled out.

Amphiboles in group 3 contain very high K plus Na contents, much higher than would normally be expected by simply hydrating peridotite. These amphiboles have near complete crystallographic A-site occupancy, a feature which suggests that they could be stable up to 30 kb, 1150-1200°C. They are, however, generally in equilibrium with spinel, not garnet, and co-existing pyroxene temperatures, calculated using the Well's (1977) geothermometer, do not exceed 1025°C. Bulk rock compositions from group 3 localities are not particularly fertile, nor are source regions characterized by any generally recognised peculiarities.

Amphiboles with high Na + K / H_2O ratios could form by a variety of processes. They may crystallize as an equilibrium phase in lherzolite under very high temperature and pressure conditions, form in peridotites which are extremely fertile or have very low water contents, or alternatively they may crystallize under normal mantle conditions (15-25 kb) but undergo additional alkali enrichment by reaction with Na-rich, H_2O poor melts or fluids.

It is unlikely that these alkali-rich amphiboles have formed under extremely high temperatures and pressures as they are not in equilibrium with garnet and co-existing pyroxene temperatures range from only 870 to 1025°C. Some amphiboles may have high alkali contents due to fertile bulk rock compositions or low H_2O concentrations, however, bulk rock compositions, where published, are rarely more fertile than pyrolite (Figure 1), nor are the modal proportions of amphibole generally low, as would be expected if amphibole formation was controlled by low water content. The most likely cause of high Na + K amphiboles, therefore, appears to be alkali enrichment (metasomatism) either during or after amphibole formation. This enrichment may be due to reaction with basaltic melts, carbonatitic melts (as described in Chapters 2 and 3), alkali-rich fluids, or a combination of both melts and fluids.

Lherzolite enrichment by reaction with basaltic melt has been well documented. It is usually described as modal metasomatism (Harte, 1983) and involves the precipitation

of amphibole and mica (Wilshire *et al.*, 1980; O'Reilly, 1987; Kempton *et al.*, 1987). Basalt related metasomatism is often characterized by veins rich in kaersutitic (high Ti) amphibole and Al-augite series clinopyroxene. Samples commonly show a compositional zoning between vein and host lherzolite assemblage.

The concentration of Na and K in both experimental and natural amphibole samples is independent of the concentration of Ti (Figure 6). This feature suggests that alkali enrichment of amphiboles may be, but is usually not, related to basaltic melt induced metasomatism. It suggests, in fact, that amphibole mineral chemistry records two types of melt or fluid interaction and that these types of reaction interact differently at different localities.

Figure 6 shows that Ti concentration in experimental amphiboles is bulk rock composition dependant. The Ti-tschermakite component in pargasitic amphiboles increases with increasing temperature and with decreasing pressure. Bulk rock composition, however, appears to be the dominant factor in controlling amphibole crystal chemistry.

The plot of Ti vs Na cation content of natural amphiboles displays two trends. Increasing Ti is correlated with increasing Na in samples from Finero, Nonsberg, Tinaquillo, Ronda, Ichinomegata and Timor (group 1 and 2 localities). Samples from these localities have similar chemistry to experimental amphiboles and are interpreted to have formed by simple hydration. Metasomatism, if present, does not involve the addition of elements, but is restricted to auto-metasomatism related to normal peridotite crystallization.

Amphibole samples from Lake Bullenmerri, Nunivak Island, Eifel, Malaita, Massif Central, S.W. Oregon and Jagersfontein (group 3 localities), show a different trend, one in which Ti content is independant of Na content. Ti, Na and K contents of these samples indicate that enrichment processes are important at these localities, and that amphibole chemistry records both Na and K metasomatism and basaltic-related Ti, Al and Fe metasomatism.

The occurrance of two distinct types of peridotite metasomatism, Ti-Al-Fe and K-LREE, has been increasingly recognised in the past few years (Hawkesworth *et al.*, 1984; Menzies *et al.*, 1987). It is suggested by a dichotamy in the behavior of K and Ti from xenolith bulk rock analyses (eg, Massif Central, Downes, 1987) and by an enrichment in K and LREE in some samples whilst others contain modal enrichments of Na, K, P, Fe, Si, and LREE (eg, Hoggar, Dautria *et al.*, 1987).

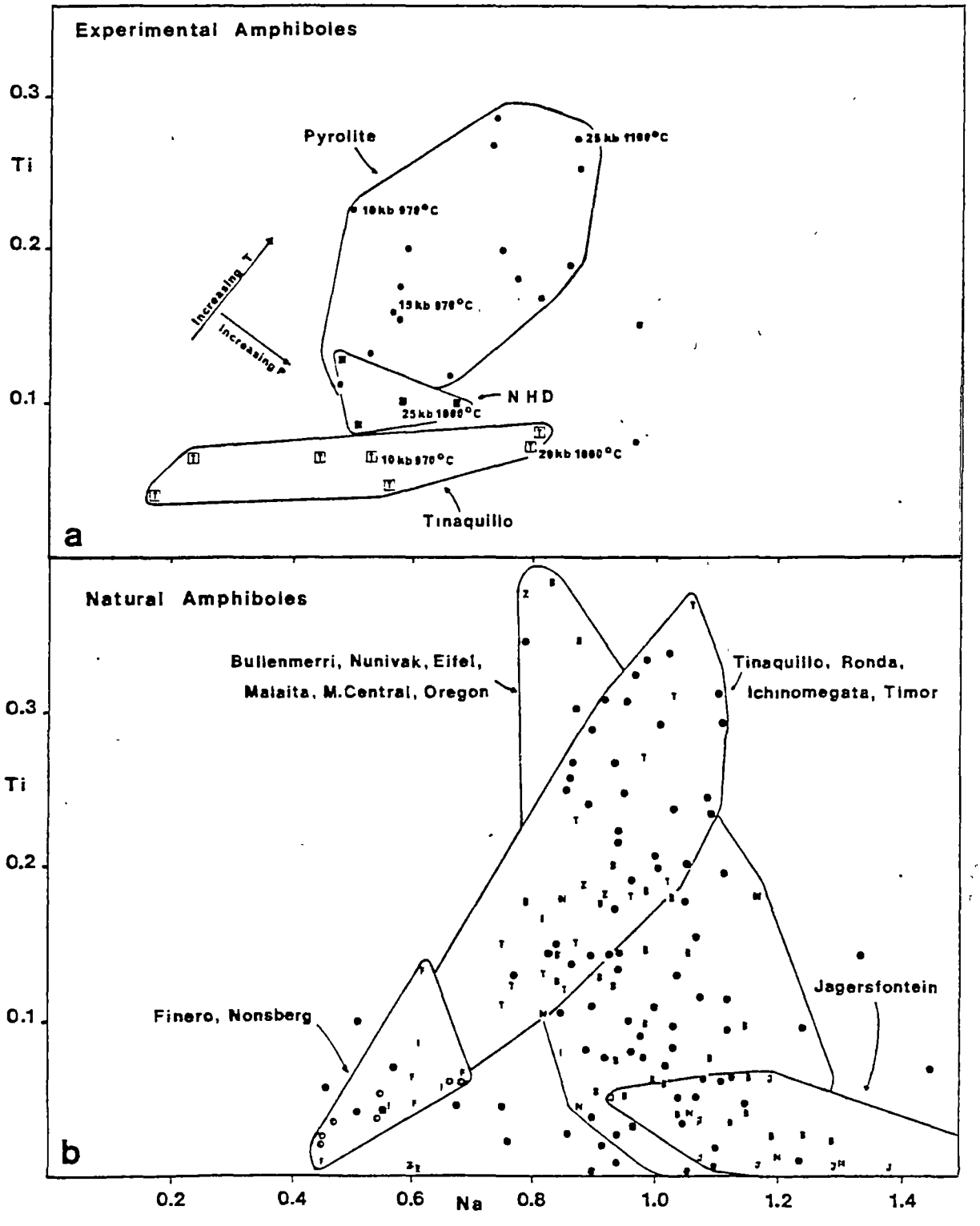

Figure 6. Ti vs Na cation abundances of (a) experimental and (b) natural lherzolitic amphiboles. Data from Appendix A and B. B = samples from Lake Bullenmerri, F = Finero, I = Ichinomegata, J = Jagersfontein, N = Nunivak Island, O = Nonsberg peridotite, T = Tinaquillo, Z = Zabargad.

K-LREE enrichment, usually described as cryptic metasomatism (Dawson 1984), is not as well understood as basaltic-melt related Ti-Al-Fe metasomatism. It has usually been interpreted as involving reaction with a hydrous alkali-rich fluid (Menzies and Wass, 1983; Hawkesworth *et al.*, 1984). It is possible, however, that Na and K enrichment involves reaction with a carbonatite melt, particularly because mantle derived carbonatite is alkali-rich and H_2O poor, therefore, ideal for enriching existing amphiboles while not creating new crystals. Carbonatite related metasomatism will be further discussed in Chapter 2. The Na, K and Ti compositions of natural amphiboles from group 3 localities appear to reflect reaction with migrating melts or fluids rather than bulk rock composition, temperature, or pressure.

Summary

The mineral chemistry of amphibole-bearing peridotites is dependent on a variety of factors, the most important being bulk rock composition, temperature, pressure and water content. In general, olivine and pyroxene compositions reflect bulk rock composition. Amphibole Mg#s and Cr contents are also bulk rock composition dependent. The abundance of Na, K, Ti, and Al in experimental samples is partially controlled by pressure and temperature. In natural amphibole samples, however, these elemental abundances have been modified, probably by reaction with volatile rich melts or fluids. The crystal chemistry of pargasitic amphiboles is complex. This study has indicated that additional work is necessary in order to understand the compositions of natural mantle amphiboles. It also suggests that amphibole compositions may become increasingly important in unraveling peridotite-melt relationships under mantle conditions.

Conclusions

1) Under water-saturated conditions, the position of the peridotite solidus is not affected by bulk rock composition (within experimental limits). Amphibole is stable for ~20°C above the solidus in fertile peridotite compositions. Its temperature stability decreases as bulk rock composition becomes more refractory.

2) Under water under-saturated conditions, the peridotite solidus is controlled by the stability of amphibole, which is a function of bulk rock composition and H_2O content.

Amphibole is stable above the water saturated solidus for ~160°C in fertile compositions such as pyrolite. Its stability is decreased to ~ 60°C above the water-saturated solidus for a more refractory composition such as theTinaquillo peridotite. The water-undersaturated solidus is deflected accordingly.

3) The stability of amphibole under water-undersaturated conditions is controlled by the avaliability of Na and K and possibly Ti. Increasing glaucophane, richterite, edenite and Ti-tschermakite substitutions stabilize amphiboles to higher temperatures and pressures. This is demonstrated by the high temperature of amphibole stability in Mengel and Green's (1989) experiments on N.H.D. composition which is refractory in nature but spiked with phlogopite giving it a high alkali content.

4) Under water-undersaturated conditions, the most fertile fraction of a crystallizing mantle diapir with an inhomogeneous composition will solidify first while a more refractory component will still contain melt. This melt is alkali-rich with the ability to metasomatise adjacent regions. This feature indicates that Ti, Fe, Al and Na metasomatism is a normal occurance that should be associated with upward migration and solidification of an H_2O bearing mantle diapir.

5) The mineral chemistry of olivine and pyroxenes in both natural and experimental compositions reflects bulk rock composition, temperature and pressure.

6) The Na, Al and Ti contents of experimental amphiboles increase with temperature and pressure. This relationship is not obviously present in natural samples. In natural amphibole samples Na, Al and Ti abundances appear to record reaction (metasomatic) with migrating fluids or melts.

2. PHASE RELATIONS IN THE SYSTEM "CARBONATE - BEARING PYROLITE + 0.2% H_2O" AND THEIR EFFECT ON UPPER MANTLE PROCESSES

Introduction

It is well established that the mantle is composed of solids (crystals), liquids (melts) and gases (vapor phases). The solid components as deduced from xenoliths in undersaturated mafic magmas and kimberlites consist predominantly of olivine, orthopyroxene, clinopyroxene, garnet and spinel with minor amounts of amphibole, phlogopite, apatite, ilmenite and rutile. Sulphides and carbonates are also present, but are very rare. Magmas derived from the upper mantle vary greatly, ranging from olivine tholeiites to olivine melilitites, nepheline-rich phonolites, kimberlites and carbonatites. Primary magma composition depends on the melting relations among the stable crystalline phases combined with the effect of volatiles, and melting relations, with or without volatiles, vary greatly with pressure and temperature.

H-O-C species are the most abundant volatile components in mantle fluids. S-F-Cl-K species are also present but in minor quantities. The form of the volatiles H-O-C is a function of the redox state and therefore of depth within the mantle. The redox state in the lower mantle is currently in debate with some authors estimating that it is relatively reduced, falling within the MW - IW buffer range (Deines, 1980; Ryabckikov *et al.*, 1981). In this range, the components C-O-H exist as carbon, CH_4, and H_2O. The upper mantle, on the other hand, is believed by many authors to be fairly oxidized in the MW - QFM range (Pasteris, 1987; Eggler, 1983). Under these conditions CO_2 and carbonates are stable. For this reason, the phase relationships in the Peridotite-H_2O-CO_2 system involving the minerals amphibole, phlogopite, dolomite and magnesite can provide a major framework for understanding upper mantle petrology.

This study presents the phase relationships for the system Peridotite (Pyrolite) + 0.5-2.5% CO_2 + 0.2% H_2O. This represents an enriched mantle composition under both H_2O and CO_2 vapor-undersaturated conditions and as such is believed to resemble significant regions of the upper mantle.

Previous work in the Peridotite + H_2O + CO_2 system

Simple system studies , Eggler (1974; 1976; 1978) conducted the first experimental studies in the Peridotite + H_2O + CO_2 system with simple system experiments in CMS-CO_2 (CaO-MgO-SiO_2-CO_2). These experiments produced a characteristic bent solidus (Figure 7a) which is concave towards high temperatures at high pressures and concave towards low temperatures in the low pressure region. The high and low pressure solidi are divided by a 'solidus ledge' at 28 kb. These experiments demonstrated the importance of the decarbonation reaction " Opx + Dolomite -> Cpx + Ol + Vapor ". This reaction boundary intersects the solidus at an invariant point E76 (Point I6 in Wyllie, (1978)). Eggler (1978) later extrapolated data from these experiments to include H_2O and concluded that the low pressure solidus should coincide with the break-down of amphibole.

Wyllie and Huang (1975; 1976) produced a theoretical Peridotite + H_2O + CO_2 solidus by extrapolating decarbonation reactions to high temperatures and pressures. Their results showed the solidus at 26 kb and 1200°C with a large inversion in the solidus such that two melting intervals separated by a solid and vapor field were encountered with increasing temperature from 26 to 32 kb. At higher pressure the carbonate peridotite solidus was at 1200°C whereas below 22 kb the peridotite + CO_2 solidus was at 1460°C (15 kb). Wyllie (1978) excluded this feature from subsequent papers.

The nature of the melt on the high pressure solidus has been described by both authors as "Haplocarbonatitic" (Eggler, 1976; Wyllie and Huang, 1975). The composition of the melt in CMS-CO_2 was investigated by Wendlandt and Mysen (1980). They found a carbonatitic liquid above the high pressure solidus at 30 kb and a silicate liquid above the low pressure solidus at 15 kb (Figure 7a).

Complex system studies To date, only two experimental studies in the Peridotite + H_2O + CO_2 system have been published. Results of these studies are presented in Figures 7b and 7c.

Figure 7b is derived from Brey and Green (unpublished data, partially reported in Brey *et al.*, 1983). An Hawaiian pyrolite - 40% Ol + 0.3% H_2O + 5% CO_2 composition was used and experiments were run at 25 kb, 1100°C; 27 kb, 1050°C, 1100°C, 1140°C; and 29 kb, 1100°C for between 4 and 6.5 hours. No buffer was used. These runs were

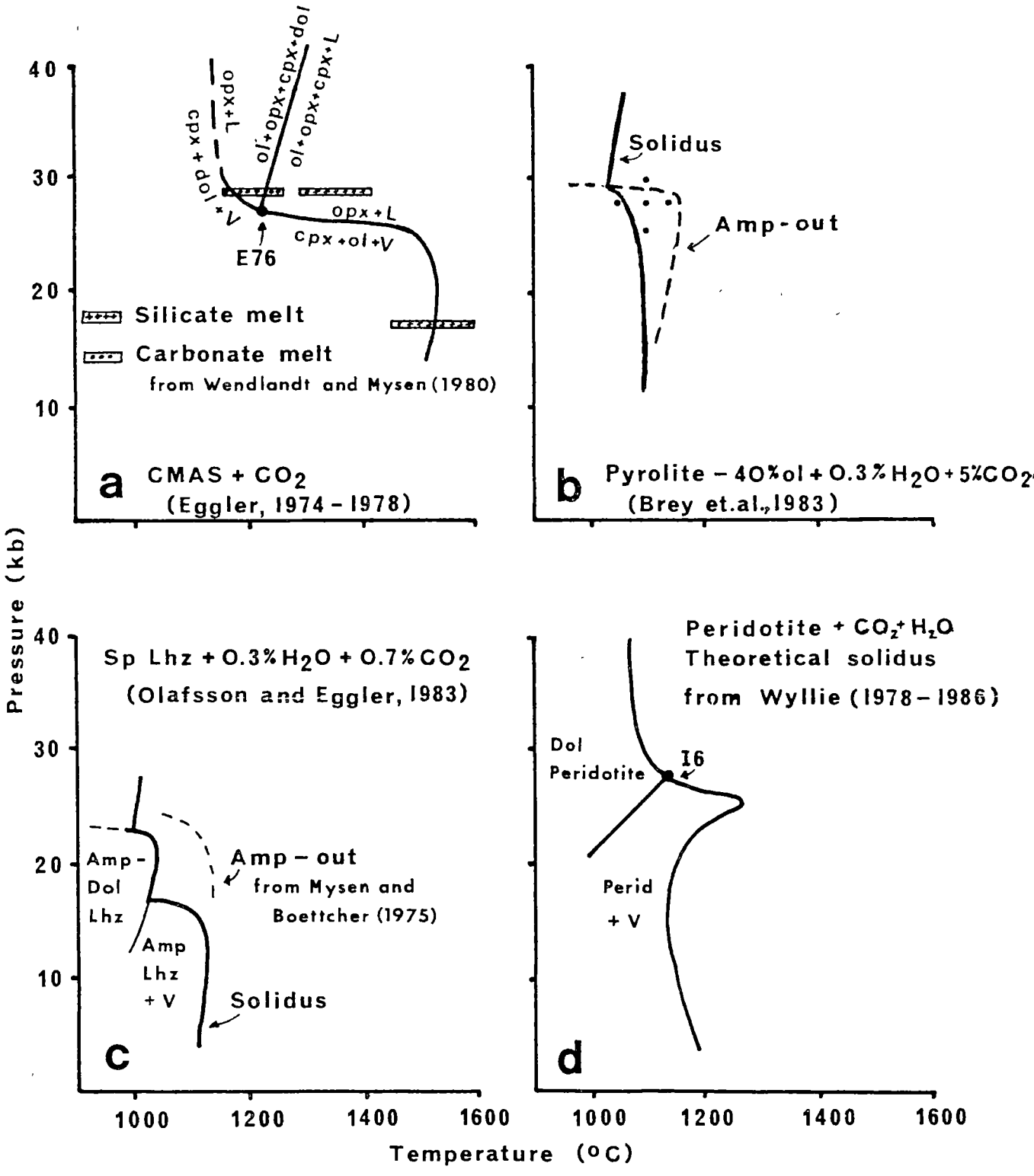

Figure 7. Previous work in the peridotite + H_2O + CO_2 system; a) CMAS + CO_2 experiments of Eggler, (1974-1978) and Wendlandt and Mysen, (1980), b) Pyrolite + H_2O + CO_2 experiments from Brey et al., (1983), c) Spinel lherzolite + H_2O + CO_2 from Olafsson and Eggler, (1983) and d) Theoretically constructed peridotite + H_2O + CO_2 solidus from Wyllie (1978-1986).

re-examined as part of the present study. Probe analyses of the mineral phases are presented in Appendix B. All runs contained ol, opx, cpx, and gt. Primary amphibole was present only in the run at 27 kb, 1050°C. The remaining runs contained quench amphibole which is compositionally distinct containing high Ti and very low Cr concentrations. All of the amphiboles were pargasitic in nature.

Phlogopite was present in the 29 kb, 1100°C run. A carbonate mineral was identified optically in the 27 kb, 1050°C run but was not found by microprobe. The texture of polished probe mounts (when compared with later experiments) suggested that a melt phase was present throughout the entire temperature and pressure range studied. The composition of the melt was not determined.

The above observations significantly alter the phase relationships from the version of the solidus diagram published by Wyllie (1987), particularly with respect to the CO_2-carbonate transition and therefore Wyllie's point I6. There were insufficient P-T points in this series of experiments to determine the correct position of the solidus or decarbonation reaction. The amphibole dehydration reaction was restricted to between 1050 and 1100°C at 27 kb. These results suggested that amphibole temperature stability was lower (~60-80°C) in the H_2O - CO_2 system than in Green's, (1973) water-undersaturated pyrolite system (i.e. the same amphibole peridotite composition but without carbonate).

Results of Olafsson and Eggler's (1983) experiments are presented in Figure 7c. Their research was conducted on a Hawaiian spinel lherzolite (Peridotite B of Mysen and Boettcher, 1975) with 0.3 wt% H_2O and 0.7 wt% CO_2. Experiments were run for between 3 and 15 hours and produced a double humped solidus convex to higher temperatures. The low pressure solidus was produced by the breakdown of amphibole while the high pressure solidus was controlled by both the stability of dolomite and of amphibole. Amphibole was not detected in any of their above-solidus experiments.

Wyllie (1978 - 1986) has produced a theoretical solidus for the peridotite + H_2O + CO_2 system (Figure 7d). This solidus position was based on an assumption that amphibole breaks down at low temperatures and does not intersect the solidus. The distinctive solidus ledge (Figure 7d) was produced by combining the peridotite + CO_2 solidus based on CMS +CO_2 experiments of Eggler (1978) with Green's (1973)

pyrolite + H_2O saturated solidus. This particular phase topology has not been confirmed by experimental studies.

Recent papers by Eggler (1987; 1988) and Wyllie (1987; 1988) have reviewed the phase relationships presented in the above diagrams and have attempted to explain the discrepancies in experimental results. Wyllie (1987) suggested that Brey *et al.*'s, (1983) experiments produced a CO_2 vapor-present solidus while the Olafsson and Eggler (1983) experiments resulted in a vapor-absent solidus. Consideration of the experimental methods used and the results described, however, does not support this interpretation. Wyllie (1987) concluded that the differences between phase diagrams are caused by the intersection relationships between the solidus and the limits of amphibole stability. Discussion of mantle processes, however, is still hampered by the limited constraints on solidus positions, fluid-melt volatile partitioning and near solidus melt compositions (Eggler, 1987).

Experimental Techniques

The present study was based on the composition; Hawaiian Pyrolite (mg# 87) - 40% Ol + 0.2% H_2O + 1.4% $MgCO_3$ or 5% $CaMg(CO_3)_2$. Chemical analysis of Hawaiian pyrolite (87) and the starting mixes are presented in Table 3. The pyrolite mix was prepared from analytical reagent grade chemicals, ground under acetone and sintered at 1000°C. This was the same mix used by Taylor and Green, (1988) and Odling (PhD thesis in prep.).

To diminish the dominance of olivine in the run products, 40% olivine ($Mg_{91.6}Fe_{8.1}Mn_{0.1}Ni_{0.2}$) was removed from the composition. All the experimental runs remained saturated in olivine. Water (0.2% H_2O) was added to the composition by preparing a starting mix as in the Tinaquillo experiments (Chapter 1). This starting mix contained 80 mg of sample plus 2.0 wt% H_2O added by microsyringe. This mix was run at 15 kb and 925°C for 48 hours and produced a sub-solidus mineral assemblage of olivine, pyroxenes, spinel and amphibole (~30%). The assemblage was ground under acetone and dried overnight at 250°C, leaving about 0.3% H_2O in the bulk composition bound in the amphibole crystal structure. The mix was then diluted by adding 20% dry

Table 3. Chemical compositions of pyrolite starting mixes

	Pyrolite (87) - 40%Ol	Pyrolite (87) - 40%Ol + 1.4% Magnesite	Pyrolite (87) - 40%Ol + 5% Dolomite
SiO2	47.64	46.98	45.39
TiO2	1.20	1.18	1.14
Al2O3	6.29	6.21	5.99
Cr2O3	0.65	0.64	0.62
FeO	7.79	7.68	7.42
MgO	29.76	30.01	29.38
CaO	5.19	5.12	6.38
Na2O	0.86	0.85	0.82
K2O	0.16	0.16	0.15
P2O5	0.25	0.25	0.24
CO2	—	0.72	2.28
H2O	0.20	0.20	0.19
Total	100.00	100.00	100.00

pyrolite and 1.4 wt% $MgCO_3$ or 5.0 wt% $CaMg(CO_3)_2$. The magnesite contained 0.02% Fe and 0.3% Ca. The dolomite contained 21.79% MgO, 30.08% CaO, 0.2% SiO_2, 0.035% Fe_2O_3, and 0.03% P_2O_5. Small 10 to 12 mg portions of the final mixed assemblage were used in each experiment.

Experimental runs were buffered using the reaction $MgCO_3 \rightarrow C + MgO + O_2$, (Magnesite -> Carbon + Periclase + O_2). The fO_2 range of this buffer, (MPG), calculated for 20 kb, is presented in Figure 8. Also shown are fO_2 calculations based on the O'Neill and Wall, (1987), oxygen geobarometer, using coexisting ol, opx and spinel mineral analyses from this experimental project. The MPG buffer provides fO_2 conditions near MW between 10 and 40 kb and is similar in range to the EMOG buffer (Eggler and Baker, 1982).

The buffer assembly consisted of 10 to12 mg of starting mix sealed inside a $Ag_{75}Pd_{25}$ capsule. (Iron loss is minimal when using $Ag_{75}Pd_{25}$ capsules and was not detected in subsequent probe analyses). This assemblage was placed within a large sealed $Ag_{50}Pd_{50}$ capsule and surrounded by magnesite. A small amount of water was added to the buffer to promote hydrogen diffusion.

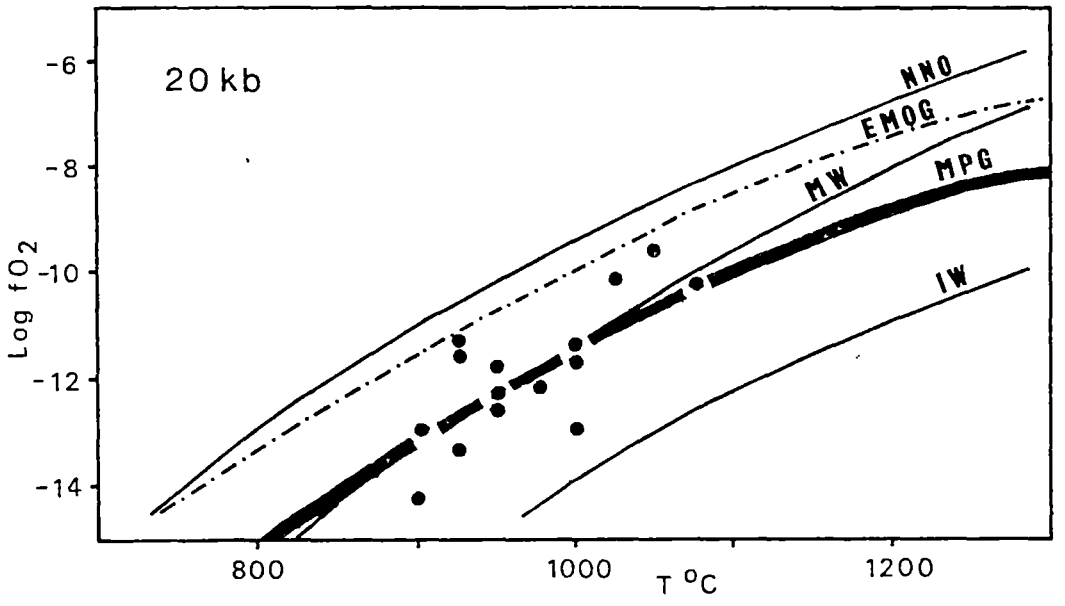

Figure 8. Calculated fO_2 range of magnesite-periclase-graphite (MPG) buffer used in experimental project (W.R. Taylor, pers. com., calculated using thermodynamic data from Robie et al., 1979). Calculations are approximate because no thermodynamic data ~~was~~ were available for magnesite at high pressure. NNO = nickel nickel oxide, EMOG = enstatite magnesite olivine graphite, MW = magnetite wustite, IW = iron wustite, • = calculated fO_2 from carbonate and amphibole-bearing pyrolite experimental runs using olivine, orthopyroxene and spinel oxygen geobarometer of O'Neill and Wall, (1987).

Experimental runs were performed using the 'piston-in' technique. NaCl sleeves were used and no pressure correction was applied. The stated experimental pressures were considered accurate to within 1 kb. Temperatures were measured using a $Pt/Pt_{90}Rh_{10}$ thermocouple and were accurate to within $10^{o}C$.

Experimental Results

The temperature and pressure phase relationships in the Pyrolite + 0.2% H_2O + 1.4% $MgCO_3$ system between 15 and 32 kb are presented in Figure 9. Individual run results are listed in Table 4. Olivine, opx, cpx and gt or sp were present in all the run products. Additional phases include amphibole, dolomite, magnesite, ilmenite, apatite and rutile. No phlogopite was present.

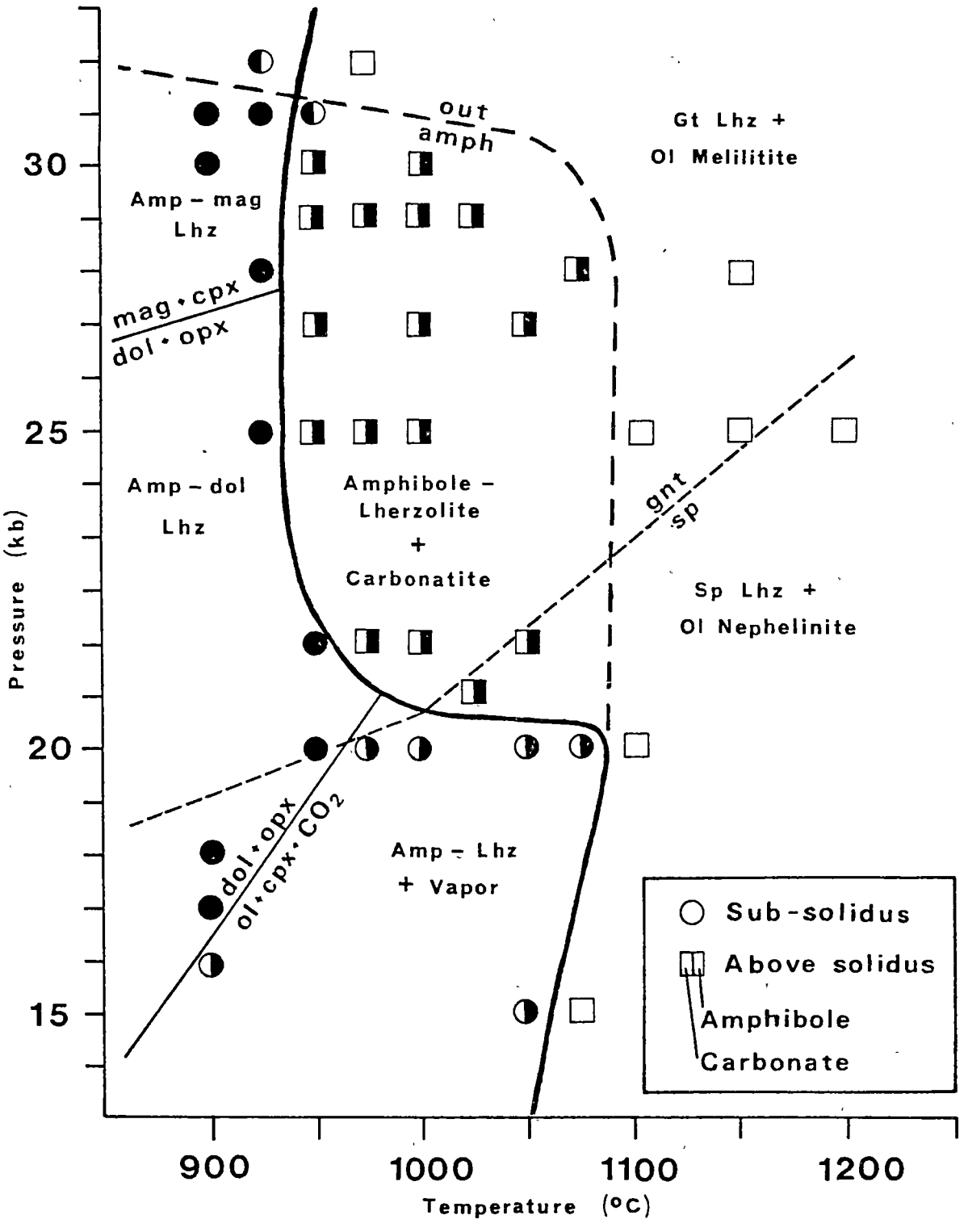

Figure 9. Phase relationships in Pyrolite + 0.2% H_2O + 1.4% $MgCO_3$

Table 4. Carbonate-bearing pyrolite + 0.2% H2O run conditions

Run#	P,Kb	T, C	Time, Hrs	H2O added to charge	Phases
Starting Mixes					
2167	15	925	48	1.9	Ol,Opx,Cpx,Amp,Sp
2257	15	925	48	2	Ol,Opx,Cpx,Amp,Sp
2282	15	925	48	2.4	Ol,Opx,Cpx,Amp,Sp
2326	15	925	48	2	Ol,Opx,Cpx,Amp,Sp
2386	15	925	48	2.6	Ol,Opx,Cpx,Amp,Sp
2408	15	925	48	2.1	Ol,Opx,Cpx,Amp,Sp
2447	15	925	48	2.4	Ol,Opx,Cpx,Amp,Sp
2460	15	925	58	2.5	Ol,Opx,Cpx,Amp,Sp

Run#	P,Kb	T, C	Time, Hrs	Starting Mix	Phases
Pyrolite + 0.2%H2O + 1.4%MgCO3 (Magnesite Buffer)					
2414	15	1050	23	2408	Ol,Opx,Cpx,Amp,Sp
2379	15	1075	26.5	2326	Ol,Opx,Cpx,Sp,S-melt
2406	16	900	24	2386	Ol,Opx,Cpx,Amp,Sp,Il,Rutile
2403	17	900	22	2386	Ol,Opx,Cpx,Amp,Sp,Il,Dolomite
2400	18	900	22	2386	Ol,Opx,Cpx,Amp,Sp,Il,Dolomite,Apatite
2367	20	950	24	2326	Ol,Opx,Cpx,Amp,Gt,Sp,Dolomite
2407	20	975	22	2386	Ol,Opx,Cpx,Amp,Gt,Il
2278	20	1000	24	2257	Ol,Opx,Cpx,Amp,Sp,Il
2321	20	1050	24	2282	Ol,Opx,Cpx,Amp,Sp,Il
2354	20	1075	6	2326	Ol,Opx,Cpx,Amp,Sp
2314	20	1100	24	2282	Ol,Opx,Cpx,Sp,S-melt
2344	21	1025	26	2326	Ol,Opx,Cpx,Amp,Sp,Il,C-melt
2296	22	950	24	2282	Ol,Opx,Cpx,Amp,Gt,Il,C-melt,dolomite
2388	22	975	24	2326	Ol,Opx,Cpx,Amp,Gt,Il,C-melt
2279	22	1000	24	2257	Ol,Opx,Cpx,Amp,Gt,Il,C-melt
2290	22	1050	25	2282	Ol,Opx,Cpx,Amp,Sp,Il,C-melt
2440	25	975	24.5	2408	Ol,Opx,Cpx,Amp,Gt,Il
2235	25	1000	8	2167	Ol,Opx,Cpx,Amp,Gt,Il,C-melt
2246	25	1100	8	2167	Ol,Opx,Cpx,Gt,S-melt
2262	25	1150	8	2257	Ol,Opx,Cpx,Gt,S-melt
2267	25	1200	5	2257	Ol,Opx,Cpx,Sp,S-melt
2319	27	1000	24	2282	Ol,Opx,Cpx,Amp,Gt,Il,C-melt
2300	27	1050	24	2282	Ol,Opx,Cpx,Amp,Gt,Il,C-melt
2410	28	1075	24	2386	Ol,Opx,Cpx,Amp,Gt,Il,C-melt
2272	28	1150	6	2257	Ol,Opx,Cpx,Gt,S-melt
2392	29	950	26	2386	Ol,Opx,Cpx,Amp,Gt,Il
2390	29	975	24	2326	Ol,Opx,Cpx,Amp,Gt,Il,C-melt
2384	29	1000	27	2326	Ol,Opx,Cpx,Amp,Gt,Il,Mag,C-melt
2405	29	1025	24	2386	Ol,Opx,Cpx,Amp,Gt,Il,C-melt

Table 4. cont.

Run#	P,Kb	T, C	Time, Hrs	Starting Mix	Phases
Pyrolite + 0.2%H2O + 1.4%MgCO3 (Magnesite Buffer)					
2428	30	900	46	2408	Ol,Opx,Cpx,Amp,Gt,Il,Mag,Apatite
2399	30	950	24	2386	Ol,Opx,Cpx,Amp,Gt,Il,C-melt
2419	30	1000	24	2408	Ol,Opx,Cpx,Gt,Il,S-melt
2444	31	925	2	2408	Ol,Opx,Cpx,Gt,Il
Pyrolite + 0.2%H2O + 1.4%MgCO3 (Hematite Buffer)					
2429	30	900	24	2408	Ol,Opx,Cpx,Amp,Sp,Il,Magnesite
2434	31	925	26	2408	Ol,Opx,Cpx,Gt,Il,Magnesite
2441	31	950	8	2408	Ol,Opx,Cpx,Il,Magnesite
Pyrolite + 0.2%H2O + 5%CaMg(CO3)2					
2450	25	925	24	2447	Ol,Opx,Cpx,Amp,Gt,Il,Dolomite
2454	25	950	24	2447	Ol,Opx,Cpx,Amp,Gt,Il,C-melt
2457	27	950	25	2447	Ol,Opx,Cpx,Amp,Gt,Il,C-melt
2464	28	925	24	2447	Ol,Opx,Cpx,Amp,Gt,Il,Magnesite
2479	31	900	24	2447	Ol,Opx,Cpx,Amp,Gt,Il,Magnesite
2483	32	925	24	2447	Ol,Opx,Cpx,Gt,Il,Magnesite
2488	32	975	26.25	2447	Ol,Opx,Cpx,Gt,Il,S-melt

The solidus occurs between 925 and 950°C above 20 kb, between 1075 and 1100°C at 20 kb, and at 1050°C at 15 kb. It has the characteristic S - shape described in simple system experiments by Eggler (1974). Above 20 kb, the solidus position coincides with the disappearance of dolomite, while below 20 kb, the solidus coincides with disappearance of amphibole. The inflection point between the high and low pressure solidi (I6) is controlled by the intersection of the solidus and the decarbonation reaction at approximately 21 kb and 975°C. The P - T field between the high pressure solidus and amphibole-out boundary contains an Na-rich dolomitic carbonatite melt. This melt becomes melilititic at temperatures above the stability field of pargasitic amphibole.

The high temperature and pressure reaction boundaries (29-32 kb, 925-950°C) were difficult to determine. Carbonate phases were not stable in the high pressure runs due to exhaustion of the magnesite buffer used. Several additional experimental runs were carried out using a hematite buffer. Carbonate phases were stable in these latter runs, however, increased oxygen fugacity promoted the formation of spinel rather than garnet. The solidus of the magnesite-bearing spinel lherzolite assemblage occurs above 950°C.

Phase relations in the system pyrolite + H_2O + CO_2 are dominated by the intersection of the following reaction boundaries; the carbonate-bearing peridotite solidus which is controlled by melting reactions including the minerals dolomite and magnesite; the dehydration melting of amphibole-bearing peridotite assemblages; the decarbonation reaction, dolomite to CO_2; and the dolomite peridotite to magnesite peridotite transition.

Figure 10 summarizes the calculated modal abundances of olivine, orthopyroxene, clinopyroxene and amphibole found within experimental charges. Modal proportions were calculated using the Pet-Mix program of Le Maitre, (1981) which is based on the compositions of co-existing mineral phases. All phases (ol, opx, cpx, amph, gt, sp, mag, dol, ilm, apatite and rutile) where present were used (data are provided in Appendix C). The carbonatite melt composition used was determined from sandwich experiments (Chapter 3) and the silicate melt composition was taken from run # T-2246 (25 kb, 1100°C). This diagram indicates that substantial changes in mineral modal proportions occur as reaction boundaries are crossed. Nine reactions (excluding the garnet to spinel transition) are present. These are summarized in Figure 10 and described below.

<u>Sub-solidus reactions</u>

Decarbonation reaction

(a) $CaMg(CO_3)_2 + 4MgSiO_3 \rightarrow 2Mg_2SiO_4 + CaMgSi_2O_6 + 2CO_2$

Dolomite Opx Ol Cpx Vapor

This reaction has been well documented (Eggler ,1976; 1978; Brey *et al.*, 1983; Newton and Sharp, 1975) since its intersection with the solidus at point I6 results in the distinctive solidus ledge found in peridotite + H_2O + CO_2 system experiments. The position of this reaction boundary is approximately 2 kb higher in this study than was determined in previous experimental studies. This is a direct consequence of the role of water in these experiments. At pressures below the decarbonation reaction, water must partition between the fluid phase and amphibole. The decarbonation boundary increases in pressure as the activity of CO_2 in the fluid becomes less than one.

Dolomite to magnesite transition

(b) $CaMg(CO_3)_2 + 2MgSiO_3 \rightarrow 2MgCO_3 + CaMgSi_2O_6$

Dolomite Opx Magnesite Cpx

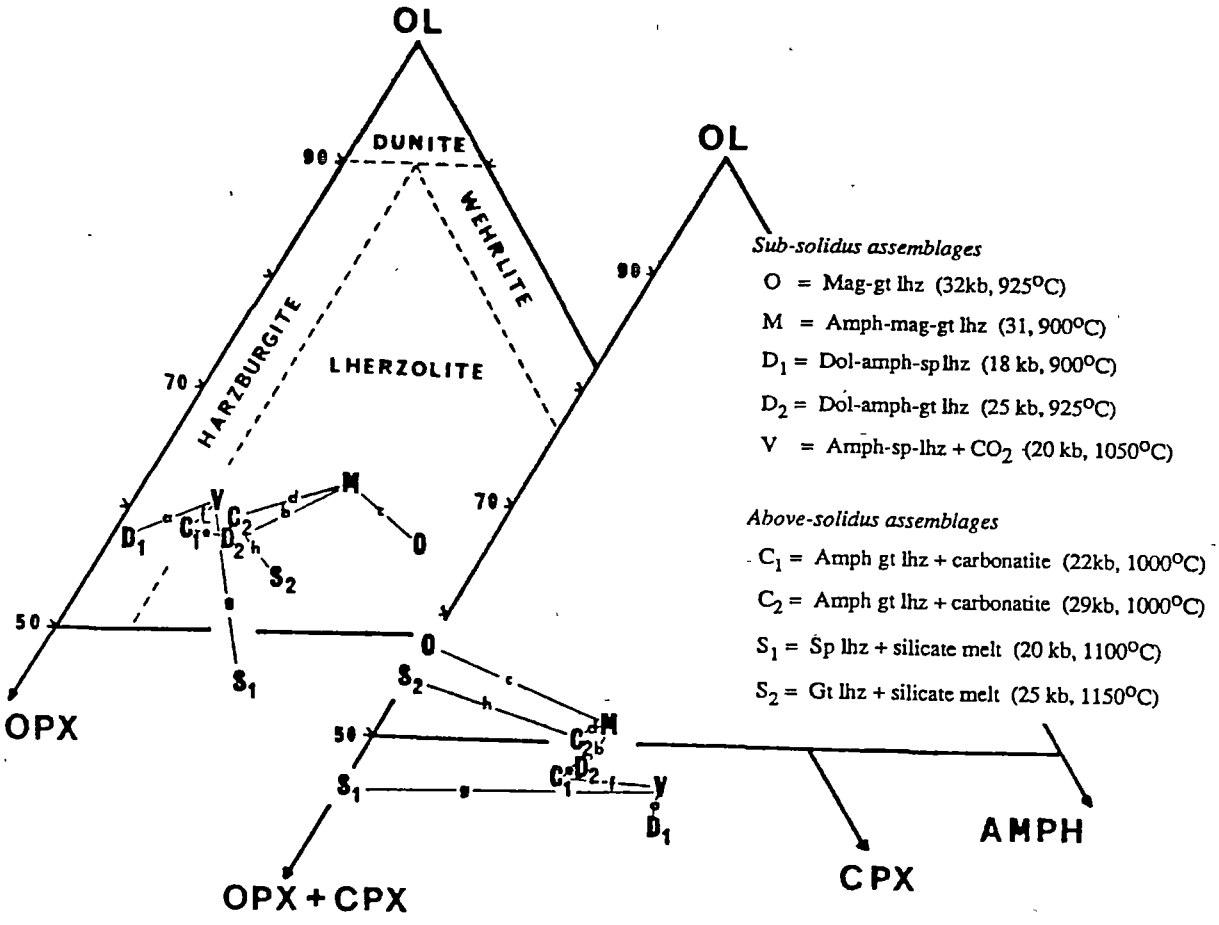

Sub-solidus reactions

(a) dolomite + opx -> ol + cpx + CO_2 (D_1 -> V)

(b) dolomite + opx -> magnesite + cpx (D_2 -> M)

(c) amph + opx -> Jadeitic cpx + gt + ol + H_2O (M -> O)

Solidus reactions

(d) magnesite + cpx + ol + amph -> carbonatite + opx + gt (M -> C_2)

(e) dolomite + cpx + ol + amph -> carbonatite + opx + gt (D_2 -> C_1)

(f) ol + amph + CO_2 -> carbonatite + opx + gt (V -> C_1)

(g) amph + opx -> silicate melt + cpx (V -> S_1)

Above solidus reactions

(h) carbonatite + amph + opx -> silicate melt + cpx +ol (C_2 -> S_2)

Figure 10. Modal proportion of phases in carbonate-bearing H_2O-undersaturated pyrolite experiments. Modal proportions were calculated using the Petmix program (Le Maitre, 1981)

This reaction has been constrained to lie between 25 and 28 kb at 925°C. The P - T position and slope of the reaction ~~is~~ has been presented as similar to that determined by Brey *et al.*, (1983) (26 kb at 925°C) and within 2 kb of the determination of Olafsson and Eggler (1983).

Sub-solidus amphibole-out reaction

(c) $NaCa_2Mg_4Al_3Si_6O_{22}(OH)_2 + 5MgSiO_3 \rightarrow$

Amphibole Opx

$NaAlSi_2O_6 + 2CaMgSi_2O_6 + Mg_3Al_2Si_3O_{12} + 2Mg_2SiO_4 + H_2O$

Jadeite Diopside Gt Ol Vapor

The breakdown of amphibole occurs at 31 kb (900°C) and produces an H_2O rich vapor plus a peridotite assemblage containing abundant jadeite-rich clinopyroxene.

Solidus reactions

High Pressure solidus

(d) $10MgCO_3 + 2NaAlSi_2O_6 + 4CaMgSi_2O_6 + 3Mg_2SiO_4 \rightarrow$

Magnesite Jadeite Diopside Ol

$2Mg_{2.5}Ca_2Na(CO_3)_5 + 12MgSiO_3 + Mg_3Al_2Si_3O_{12}$

Carbonatite Opx Gt

(e) $2NaAlSi_2O_6 + 5CaMg(CO_3)_2 + 3Mg_2SiO_4 \rightarrow$

Jadeite Dolomite Ol

$2MgSiO_3 + CaMgSi_2O_6 + 2Mg_{2.5}Ca_2Na(CO_3)_5 + Mg_3Al_2Si_3O_{12}$

Opx Diopside Carbonatite Gt

Reactions (d) and (e) are produced by the breakdown of carbonate plus cpx to produce an Na-rich dolomitic carbonatite melt (composition determined in Chapter 3), plus an aluminous phase (gt or sp). This corresponds with an increase in orthopyroxene and decrease in olivine abundance (i.e. a harzburgitic rather than dunitic residue is expected). These reaction boundaries occur between 925 and 950°C and are approximately 50°C lower than the water-saturated silicate solidus. These solidus reactions also occur at lower temperatures than Eggler's predicted solidus reaction 'cpx + dolomite + vapor -> opx + CO_2 rich melt' (Eggler, 1976; 1978). The effect of amphibole on lowering the solidus position has not yet been determined. Its effectiveness as a water-bearing phase, in addition to being an additional mineral component may have resulted in the very low solidus temperature determined in this study.

Solidus 'Ledge' Reactions

(f) $2NaCa_2Mg_4Al_3Si_6O_{22}(OH)_2 + 9Mg_2SiO_4 + 10CO_2 \rightarrow$

Pargasite Ol Vapor

$2Mg_{2.5}Ca_2Na(CO_3)_5 + 3Mg_3Al_2Si_3O_{12} + 12MgSiO_3 + 2H_2O$

Carbonatite Garnet Opx Vapor

(f_2) $2NaAlSi_2O_6 + 4CaMgSi_2O_6 + 13Mg_2SiO_4 + 10CO_2 \rightarrow$

Jadeite Diopside Ol Vapor

$2Mg_{2.5}Ca_2Na(CO_3)_5 + Mg_3Al_2Si_3O_{12} + 22MgSiO_3$

Carbonatite Garnet Opx

Calculation of modal proportions indicates that the solidus-ledge reaction in this set of experiments is produced by carbonatite crystallizing into amphibole plus CO_2 vapor (reaction f). This reaction indicates that the carbonatite melt contains a small amount of dissolved H_2O. The peridotite + CO_2 system is predicted to contain a similar shaped solidus. In this system the solidus ledge would be produced by carbonatite crystallizing into Na-rich jadeitic clinopyroxene plus CO_2 (reaction f_2). The P-T position of this ledge has since been determined (Falloon and Green, 1989, submitted for publication).

Amphibole breakdown reaction

(g) $NaCa_2Mg_4Al_3Si_6O_{22}(OH)_2 + 7MgSiO_3 \rightarrow$

Pargasite Opx

$NaCaMg_3AlSi_6O_{18} + CaMgSi_2O_6 + 2Mg_2SiO_4 + Mg_3Al_2Si_3O_{12} + H_2O$

Silicate melt Cpx Ol Gt Vapor

* silicate melt composition has been simplified from run #2246, 25 kb, 1100°C.

The shape of the amphibole stability curve in this system is similar to that in pyrolite + 0.2% H_2O as determined by Green (1973). The upper temperature stability limit of amphibole (1080°C), however, is 50 to 100°C lower than in the water-undersaturated system. This is due to the addition of CO_2 and the consequent appearance of a vapor phase. The observed effect of a vapor phase is to lower the solidus. The activity of water in the pyrolite + CO_2 + H_2O experiments at 15 kb, 1080°C was higher than the activity of water in the amphibole pyrolite composition synthesized in Green's (1973)

experiments, at the same pressure and temperature conditions (i.e. a fluid absent amphibole spinel lherzolite assemblage). The amphibole breakdown reaction is similar to 'opx + amph + sp -> ol + cpx + melt' as determined by Holloway (1973) and produces an alkali basaltic melt.

Above solidus reaction

(h) $2Mg_{2.5}Ca_2Na(CO_3)_5 + NaCa_2Mg_4Al_3Si_6O_{22}(OH)_2 + 33MgSiO_3 \rightarrow$

Carbonatite Pargasite Opx

$3NaCaMg_3AlSi_6O_{18} + 3CaMgSi_2O_6 + 15Mg_2SiO_4 + 10CO_2 + H_2O$

Silicate melt Cpx Ol Vapor

Silicate melt is produced by the breakdown of amphibole in the presence of the carbonatite melt. The silicate melt contains substantial amounts of dissolved H_2O and CO_2. Silicate and carbonate melt immiscibility was not investigated, however, experimental melt textures suggest that silicate and carbonate melts may be immiscible at high pressures (28 to 32 kb) particularly at temperatures less than 1050°C. Brey and Green's (1975-1977) experiments indicate that a melilitite melt would be stable in the intermediate pressure (20 to 28 kb) region. At low pressure (10 kb), CO_2 is much less soluble in the silicate melt and melting is similar to that for pyrolite + H_2O (Green, 1973). From 10 to 20 kb a transitional region of increasing CO_2 solubility in silicate melt is inferred.

Phase fields

The reactions presented above divide the phase relation diagram (Figure 9) into five fields due to the release of H_2O by the breakdown of amphibole and CO_2 from dolomite. These fields are; 1) amphibole-dolomite peridotite, 2) amphibole peridotite + CO_2-rich vapor, 3) magnesite peridotite + H_2O-rich vapor, 4) amphibole peridotite + carbonatite melt, and 5) gt/sp peridotite + carbonate rich siliceous melt. The fields are illustrated in Figure 11 and described below.

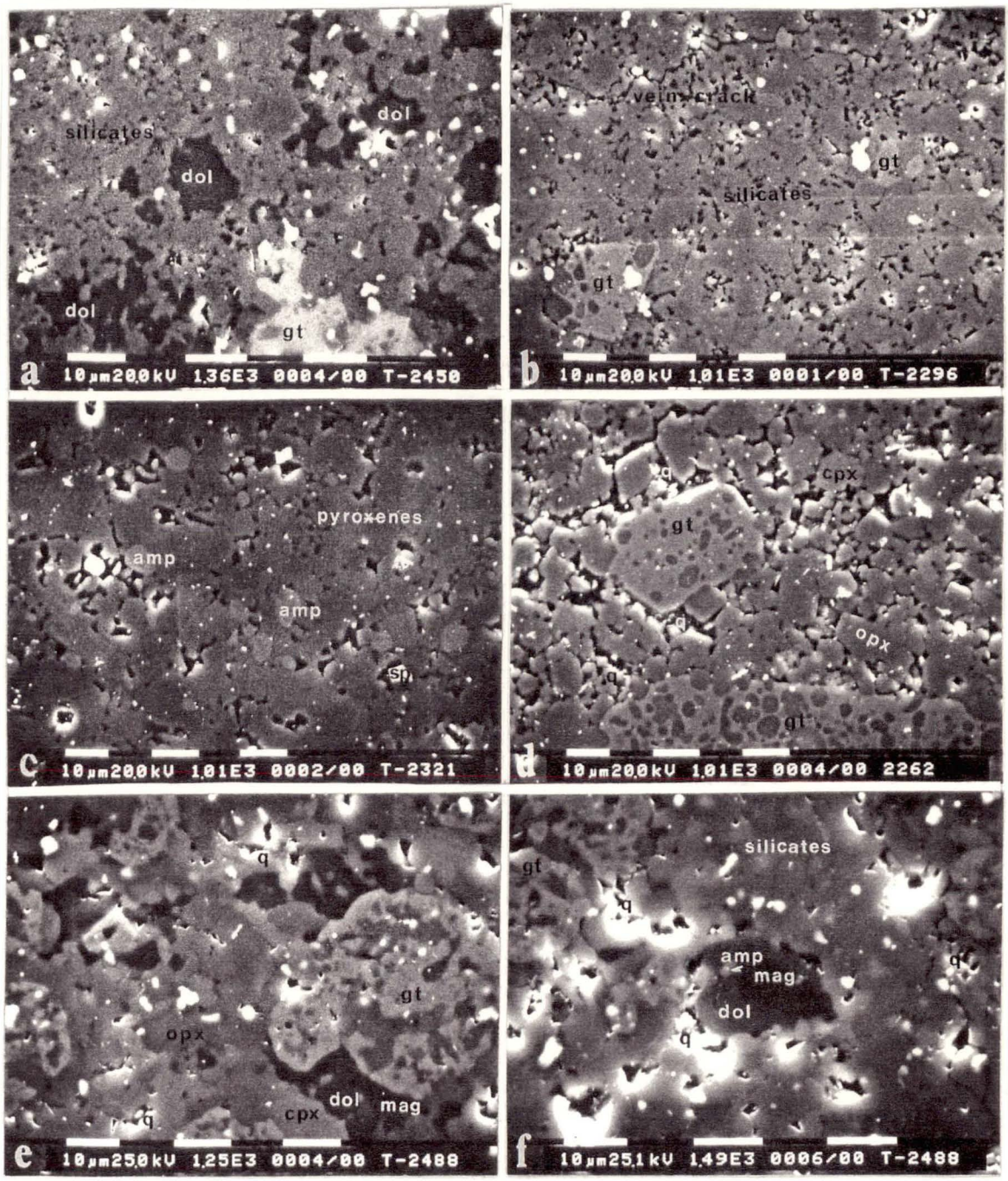

Figure 11. Scanning electron micrographs of carbonate-bearing H_2O-undersaturated Pyrolite experimental probe mounts. Order of increasing brightness of mineral phases = (magnesite, dolomite, olivine, orthopyroxene, clinopyroxene, amphibole, garnet, spinel). a) Sample T-2450, 25 kb, 925°C, 24 hrs. Subsolidus field, dolomite-amphibole-garnet lherzolite assemblage, sample contains very little intergranular void space. b) Sample T-2296, 22 kb, 950°C, 24 hrs. Carbonatite melt field, amphibole-garnet-lherzolite assemblage, silicate grains are larger than those in the subsolidus region. Intergranular void spaces (missing melt?), veins and decompression cracks are common. Garnets are generally large and euhedral. c) Sample T-2321, 20 kb, 1050°C, 24 hrs. CO_2 vapor field, spinel-amphibole-lherzolite assemblage. Samples characteristically have large grains and non-interconnected void space. d) Sample T-2262, 25 kb, 1150°C, 8 hrs. Silicate-melt field, garnet lherzolite assemblage. Samples have very large crystal grains and a net-work of interconnecting intergranular space. Melt is missing but small patches of quench crystals (Ti-rich amphibole and mica) are present. e,f) Sample T-2488, 32 kb, 975°C, 26.25 hrs. High pressure silicate-melt field, garnet lherzolite plus melt assemblage. Silicate-melt has quenched into amphibole and pyroxenes. Carbonate-rich melt forms pools of dolomite and magnesite and characteristically contains a small crystal of amphibole.

Amphibole and Dolomite (magnesite) -bearing Peridotite , Runs in this field are generally fine grained and devoid of pore space (Figure 11a). This suggests that all the H_2O is contained in amphibole and the CO_2 is locked up in carbonate. If a fluid phase is present, it must be very small. The carbonate is dolomite in runs below 27 kb, and magnesite in runs above 27 kb. Dolomite and magnesite do not coexist. Ilmenite is the characteristic Ti phase. Rutile is common as large angular grains.

Experimental charges in this field often contain apatite, a phase not found in above-solidus runs. This suggests that apatite may partition into a carbonate melt more readily than into a silicate melt and is supported by its occurrence in natural samples as discrete euhedra in melt pods (Griffin *et al.*, 1984; O'Reilly, 1987) and its abundance as a phenocryst phase in carbonatite magmas (LeBas, 1977; Heinrich, 1966).

Amphibole peridotite + CO_2 Samples in this field contain ol, opx, cpx, amphibole and spinel (Figure 11c). Ilmenite occurs in runs with temperatures less than 1050°C. No other phases have been observed. Samples have fairly large crystal grains (~10-20um for 24 hour runs, spinel grains are much smaller). Abundant bubbles and fluid inclusions have been observed in crushed samples. These are too small for infra-red analysis and are believed to be predominantly CO_2. Probe mounts contain abundant intergranular void space. These spaces appear to be discrete voids with no interconnecting fabric such as are present in samples from above-solidus runs.

Magnesite peridotite + H_2O Only one sample was obtained from this high pressure field since the amphibole-out boundary is near the limits of the experimental apparatus. This sample was a medium grained ol, opx, cpx, gt assemblage with abundant small patches of magnesite. It had a very compact texture, although intergranular void space was present. These voids did not appear to be interconnected. Abundant fluid inclusions could be observed in the crushed sample. These are assumed to be predominantly H_2O.

The most distinctive feature of the sample was its high proportion of clinopyroxene and the absence of K-bearing phases. Phlogopite, an easily identifiable phase in experimental mounts was not present. (In this project, phlogopite was only found as a quench phase in above-solidus silicate melt rich runs). It is possible that K is soluble in H_2O rich fluid at high pressures as suggested by Ryabchikov and Boettcher (1980). This is compatible with its high abundance with H_2O and CO_3^{2-} in diamond micro-inclusions (Navon *et al.*, 1988).

Amphibole + carbonatite melt field Samples from this field were medium grained and characterised by very large poikilitic garnets (Figure 11b). Grains tended to have good crystal shapes and regular outlines. Textures were typical of above-solidus runs. Grains were separated by interconnected void space and veins or cracks were common (possibly a feature of decompression). Ilmenite and amphibole were present in all runs.

Carbonatite melt (between 2-5% of the charge) was easily observed in crushed samples due to its high birefringence. It was, however, difficult to find in probe mounts. The melt appeared to quench to a very fine grained assemblage of dolomite, magnesite and Na carbonate. This material polished out of samples easily and the Na carbonate phases were water soluble. Carbonate material was occasionally concentrated as small pools or as veins. Na and Ca-rich quench rims were common on cpx and amphibole grains. The composition of the carbonate melt was obtained using a series of sandwich experiments. This technique and the experimental results are discussed in Chapter 3.

Carbonated silicate melt field Samples from this field were coarse grained and contained a high proportion of visible melt (Figure 11d). Melt in the high temperature, low pressure samples had quenched into a fine grained carbonate (dolomite and magnesite) and silicate (amphibole, pyroxenes and phlogopite) assemblage. The melt appears to be melilititic in nature and melt patches were strongly birefringent when observed in crushed samples. It was not possible to determine whether the melt contained immiscible silicate and carbonate segregations. It is chemically inhomogeneous but this may be due to quench modification.

The high pressure melt area (32 kb, 950°C) differed from the low pressure high temperature area. Samples were rather coarse grained with large patches of carbonate melt and smaller interconnecting patches of quench silicates (Figure 11e and 11f). The carbonate melt areas contained cores of magnesite rimmed by dolomite, neither of which had good euhedral shapes. The carbonate patches often contained one or two small crystals of amphibole (Mg#87). Amphibole is not considered to be stable at 32 kb, so that the grains probably resulted from quenching. The charge had a compact texture, with interstitial voids concentrated into areas of silicate quench crystals. These grains were predominantly pyroxenes, although some amphiboles were present. No quench phlogopite was observed. The distribution of quench silicates and carbonate melt pods suggested that liquid immiscibility may be important at these high pressures and at near-solidus conditions. Similar results were obtained in Brey and Green's (1976) high pressure (30-40 kb) experiments on the solubility of CO_2 in olivine melilitite melts.

Mineral Chemistry

Silicates, Representative mineral analyses from this series of experiments are presented in Appendix C. Mg# vs temperature of formation of the silicate minerals, ol, opx, cpx and amph, have been plotted in Figure 12. Olivine and orthopyroxene Mg#s range between 86.2 and 91.0 and are not significantly different from those found in the pyrolite + H_2O (CO_2 absent) experiments of Green (1973) (analyses in Appendix B). The Mg# ratios of the silicate phases have not been altered by the presence of carbonatite melt, but Mg# is higher in minerals formed above the stability of amphibole, where a silicate melt is present.

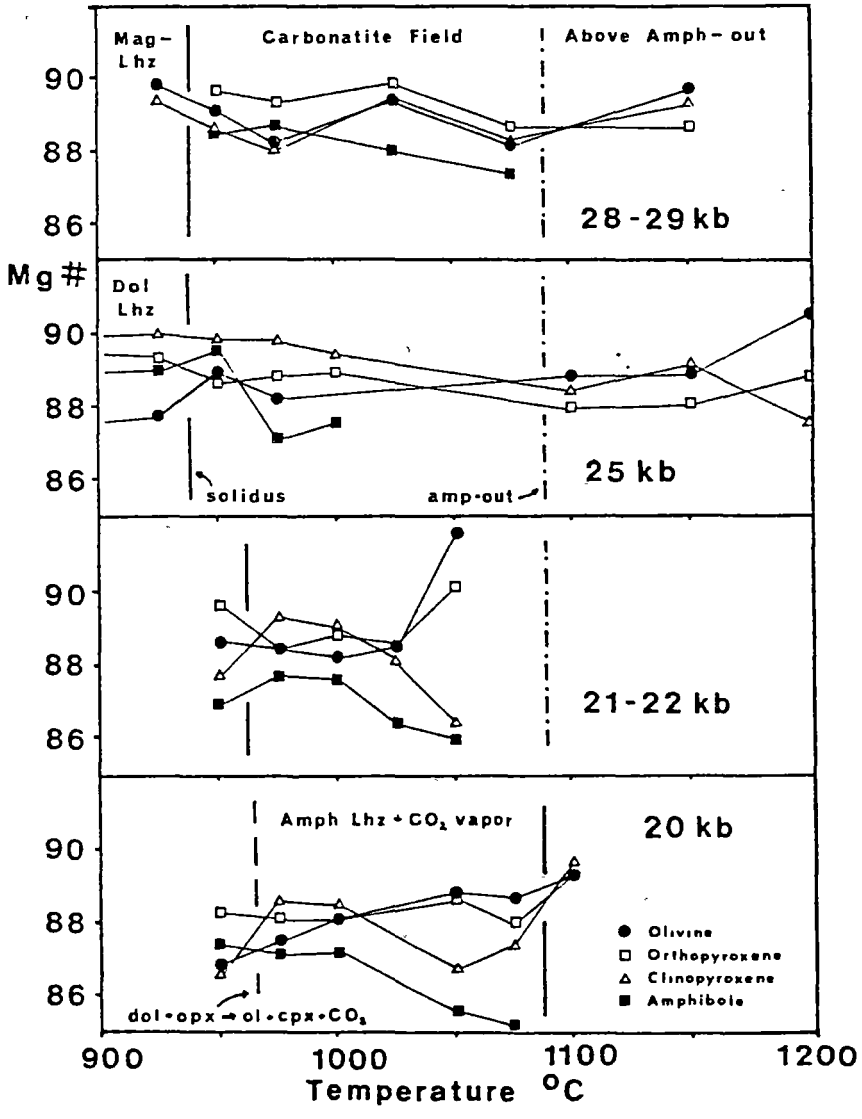

Figure 12. Mg# vs temperature of formation of silicate minerals from carbonate-bearing pyrolite + 0.2 H_2O experiments.

Preferential partioning of Fe over Mg into melt appears to be characteristic of silicate melts, but not of carbonate melts. Primary carbonatites, therefore, will have much higher Mg#s than primary silicate melts.

Amphibole and clinopyroxene mineral chemistry was expected to reflect the presence of carbonatite melt due to the solidus reaction which produces carbonatite melt plus CaMg-rich diopsidic silicates at the expence of AlNa-rich jadeitic or pargasitic ones. This chemical modification is not present in the amphiboles and clinopyroxenes analysed, but probably, due to the small size of the crystal grains, has been obscured by Na-carbonate rich melt rims. The relationship is further complicated by the need for amphiboles and clinopyroxenes to contain an increasingly high jadeitic or pargasitic component in order to remain stable at higher pressures and temperatures.

Figure 13 presents a plot of Al^6 vs Na cation abundance of sub-solidus and above solidus clinopyroxenes. Clinopyroxene analyses from pyrolite + H_2O (CO_2 absent) are included for comparison. This diagram shows that clinopyroxenes which coexist with carbonate melt are substantially enriched in Na, but that Na enrichment is not correlated with the enrichments in Al^6 needed to fulfil charge balance requirements. In addition, these clinopyroxenes have lower Mg abundances and lower, but scattered Ca values.

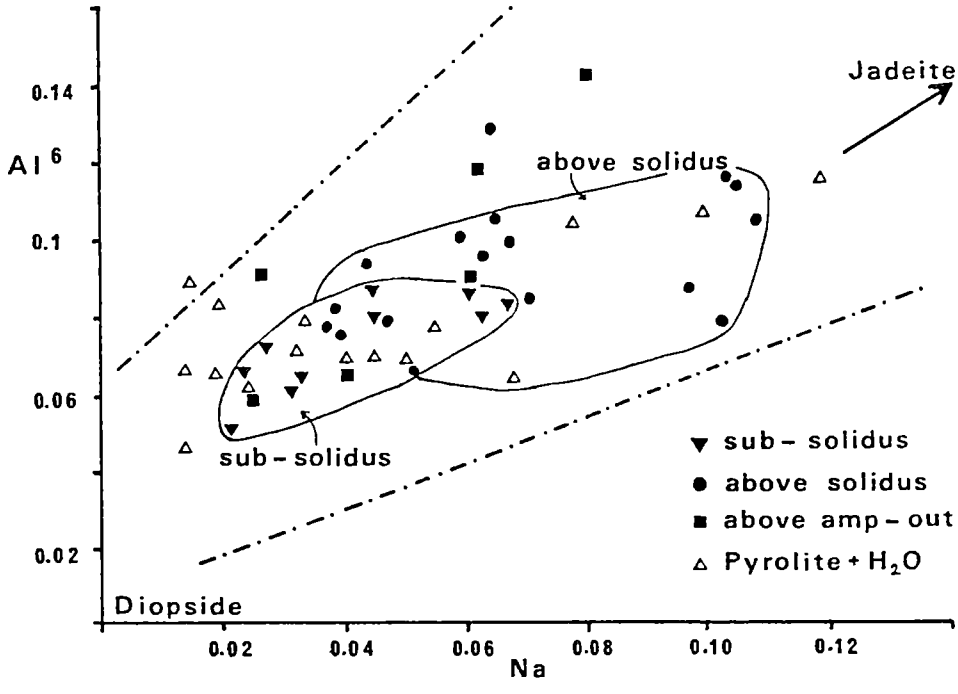

Figure 13. Al^6 vs Na cation abundance of experimental clinopyroxenes - - - - - limits of natural lherzolitic clinopyroxene composition

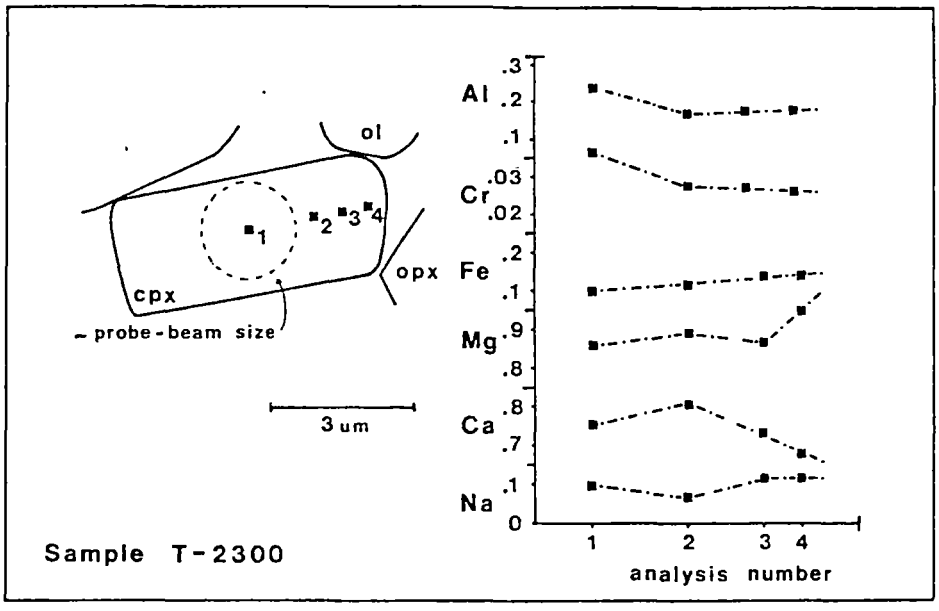

Figure 14. Cross-section of a large clinopyroxene crystal, Sample T-2300

Detailed cross-sections of large clinopyroxene grains (Figure 14) have demonstrated that this relationship is caused by rims of Na, Ca, Mg - rich carbonate melt on many, if not all, of the clinopyroxenes analysed. The melt-rims are not visible optically or by scanning electron microscope, but are present on all the silicate phases. They are particularly hard to detect on amphiboles and clinopyroxenes where the presence of Na does not indicate a bad or contaminated analysis.

Amphibole compositions from the carbonate-bearing pyrolite + 0.2% H_2O experiments are presented in Figure 15. Amphiboles in above-solidus runs are very Na-rich and, like the clinopyroxenes, Na is not correlated with Al^6 suggesting that Na enrichment is an artifact of small Na-rich quench rims of carbonatite melt. With the exception of Na content, the amphiboles are not significantly different from the Pyrolite + H_2O experimental analyses. Amphiboles quenched from silicate melt are kaersutitic with distinctively low Mg#s (Mg# = 73-78).

Carbonates, Both dolomite and magnesite were present in the experimental charges. Their mineral chemistry is shown in Figure 16. They are Mg-rich phases and trend towards end member compositions with pressure. Mg#s of carbonate minerals are

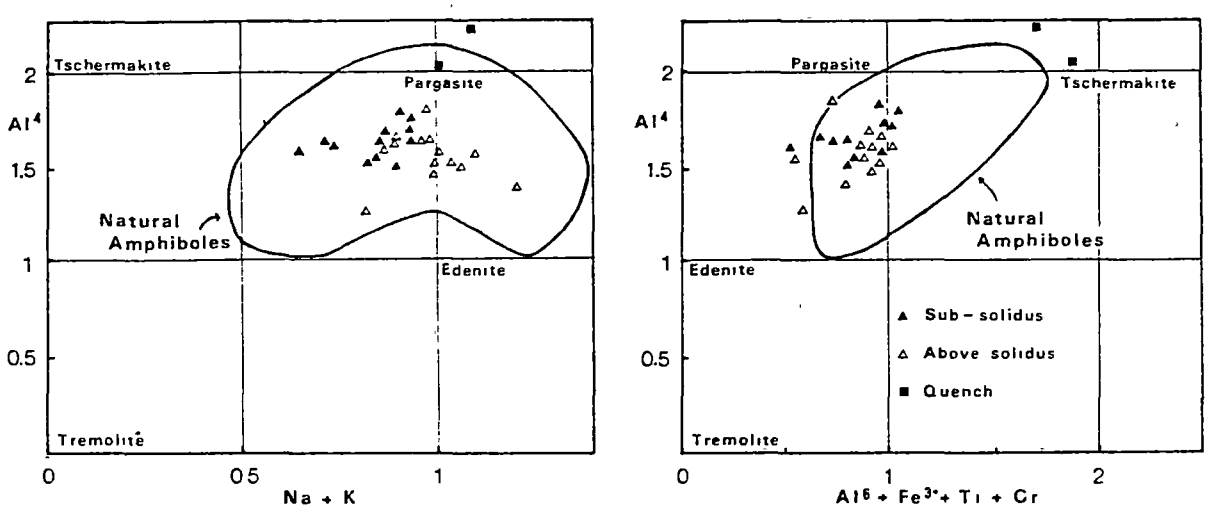

Figure 15. Amphibole compositions from carbonate-bearing pyrolite + 0.2% H_2O experiments

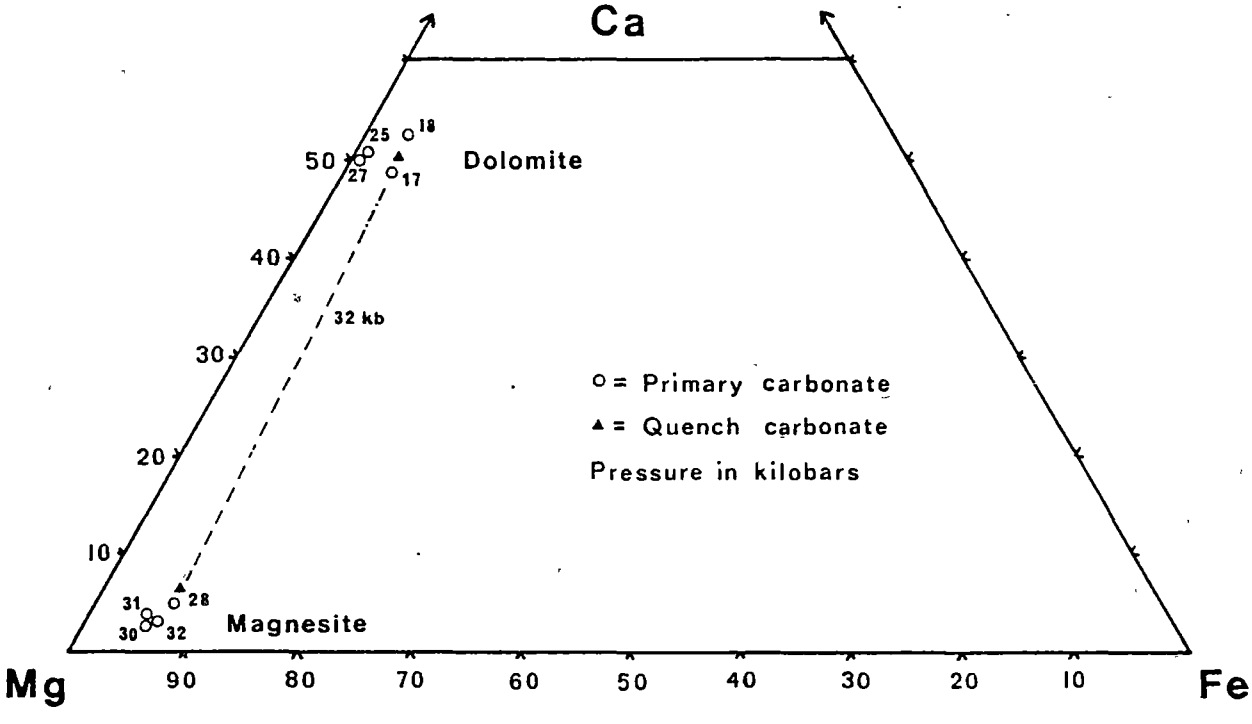

Figure 16. Carbonate compositions from carbonate-bearing pyrolite + 0.2% H_2O experiments

substantually higher than those in coexisting silicates. The quench carbonates from the high pressure (32 kb) experiment are also shown.

Summary

Mineral chemistry from the dolomite-bearing pyrolite + 0.2% H_2O experiments is not significantly different from experiments on Pyrolite + 0.2% H_2O (CO_2 absent) (Green 1973). Mg# of mineral phases has not been effected by the coexistance of a carbonatite melt. Na, Al and Ca cation ratios of clinopyroxenes and amphiboles are probably modified by silicate-melt partitioning. This relationship, however has been obscured by melt-rich rims found coating the silicate phases. Carbonate phases have higher Mg# than coexisting silicates, and their compositions become more Mg-rich with pressure.

Discussion

The results of this study enable solidus positions to be predicted for carbonate-bearing pyrolite under a variety of H_2O and CO_2 saturation conditions. Figure 17 compares the solidi curves for H_2O bearing pyrolite with that of carbonated pyrolite in a closed system under oxidizing conditions. Figure 17a indicates the solidus position for dry-pyrolite from Green and Ringwood (1970). The pyrolite H_2O undersaturated and H_2O saturated solidi, figures 17b and 17c, are from Green (1973).

The carbonate-bearing water-absent pyrolite solidus, presented in Figure 17d, has not yet been determined experimently. The high pressure solidus for carbonate-bearing pyrolite is predicted to be based on the reaction 'ol + cpx + dolomite -> opx + Al-phase + melt', and is therefore similar in shape to the H_2O undersaturated carbonate-bearing solidus. It has not been established whether H_2O is an important component in the above reaction. This reaction is expected to occur at higher temperatures in the water-absent system than in water-undersaturated carbonate-bearing pyrolite since the presence of amphibole as an additional phase will lower the solidus temperature. The low pressure solidus would be similar to the dry-pyrolite solidus, as predicted from Eggler's (1974,1976) simple system experiments.

Figure 17e presents the water undersaturated carbonate-bearing pyrolite solidus which was experimentally determined in the present study. The main features displayed in this

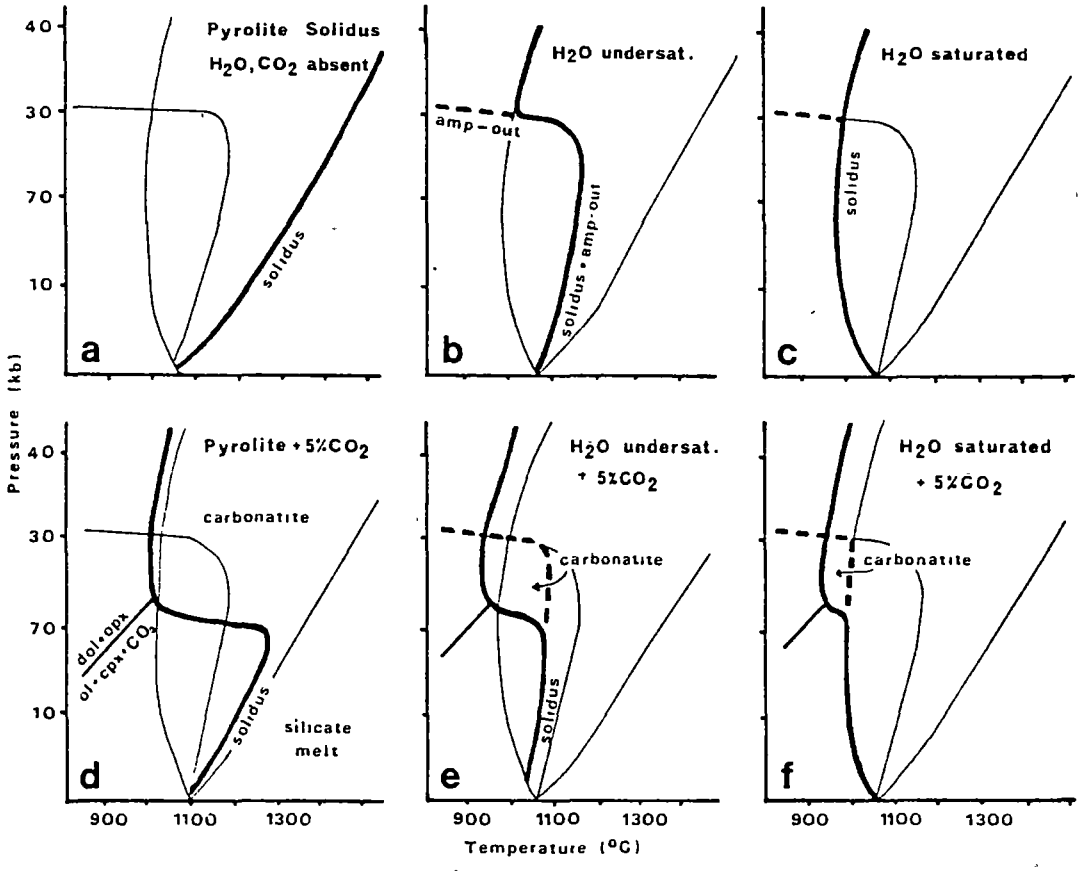

Figure 17. Peridotite and dolomite-bearing peridotite solidi under a variety of water saturation conditions. (a) pyrolite solidus (Green and Ringwood, 1970), (b) water undersaturated pyrolite solidus (Green, 1973), (c) water-saturated pyrolite solidus (Green, 1973), (d) predicted carbonate-bearing pyrolite solidus, (e) carbonate-bearing water undersaturated solidus (this study), (f) predicted carbonate-bearing, water-saturated pyrolite solidus.

diagram are first, that the high pressure solidus is 50°C lower in temperature than the H_2O saturated solidus and is, therefore, the lowest temperature solidus determined to date. Second, that the addition of CO_2 lowers the amphibole melting temperature. These features are significant since they restrict the temperature range over which a carbonatite melt will be stable. This carbonatite field, dependent on the stability of amphibole, will also contract as the bulk rock composition becomes more refractory (Chapter 1).

The presence of a high pressure (>30 kb) carbonatite field is still a matter of speculation. Carbonate and silicate melt immiscibility will be an important process at high

pressures. The presence of a high pressure carbonate melt, however, may help explain the origin of the K-richterite and phlogopite often found in deep-seated nodules. Oxygen fugacity will also have a significant effect on the stability of a carbonate-rich melt, particularly in the region between 30 and 60 kb, if this is a transition zone between oxidized upper mantle and one which becomes more reduced with depth or if the mantle is inhomogeneus and composed of both oxidized and reduced areas.

Figure 17f shows the solidus position expected in a carbonate-bearing peridotite under water-saturated conditions. In this example, the low pressure solidus is predicted to be similar to the H_2O saturated solidus, while the high pressure solidus is expected to be the same as the water undersaturated carbonate-bearing peridotite solidus. The restricted temperature stability of amphibole under watersaturated conditions, as compared to water undersaturated conditions, will contract the temperature interval over which a carbonatite melt is stable.

The phase relationships present within the mantle depend on bulk rock composition, oxygen fugacity, pressure, temperature and the volatile species present. The sequence of petrological and therefore physical properties expected in any part of the mantle can be represented by tracing along a geotherm through the appropriate phase fields and in particular establishing the pressure and temperature conditions under which a melt may be present. In mantle regions composed of a fertile carbonate-bearing H_2O undersaturated peridotite, four scenerios of melt generation and migration are possible. These are presented in Figure 18 which shows the solidus boundaries for 'dolomite bearing pyrolite +0.2% H_2O' intersected by four theoretical geotherms.

Geotherm C, (Figure 18), represents a high pressure continental geotherm similar to the geotherm calculated for the Kaapvaal craton by Finnerty and Boyd (1987). This geotherm crosses the solidus at approximately 67 kb, liberating a kimberlite-type melt by the dissolution of magnesite and possibly phlogopite (Wyllie, 1980). This melt may reach the surface by crack propagation or may promote diapiric uprise of the magmatic assemblage to progressively lower pressure regions. The diapir will contain ol, opx, cpx and gt as crystal phases and H_2O and CO_2 dissolved in the kimberlite melt. If the interstitial melt component migrates upwards along this geotherm it will cross the solidus at 40 kb as the carbonate component reacts with opx to form a cpx-rich magnesite-gt-peridotite assemblage.

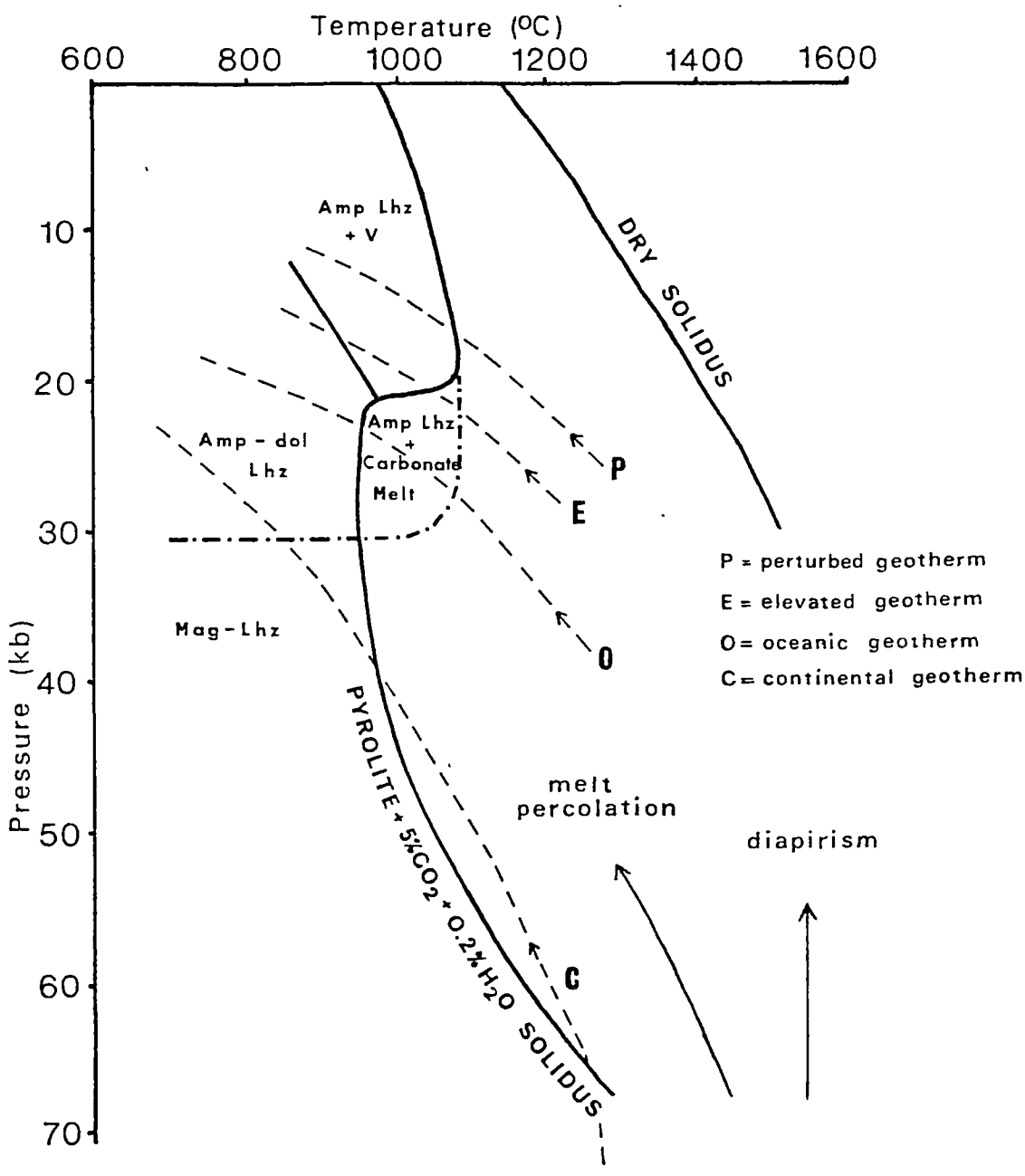

Figure 18. Melt crystallization paths in an oxidized H_2O and CO_2 bearing upper mantle

Geotherm O, displays the sequence of events along an oceanic geotherm, for example the Malaita geotherm calculated by Nixon and Boyd (1979). This is similar to the geothermal gradient predicted for rift valleys such as the St. Laurence Valley and the Fen complex (Mitchel *et al.*, 1982; Sachteleben and Seck, 1981). A partially molten assemblage of garnet peridotite plus H_2O, CO_2 bearing melilitite melt would migrate

upwards until it crossed the amphibole dehydration boundary. Amphibole would crystallize out of the melt and in regions with a normal mantle composition, leave an Na-rich dolomitic carbonatite. This carbonatite melt-rich assemblage will then migrate crossing the carbonatite solidus, enabling the melt to react with its host lherzolite and freeze forming a dolomite-bearing peridotite. Unless the carbonate melt was released and rose to the surface quickly, (e.g. along cracks where it is unable to react to form cpx + CO_2) its presence in the mantle environment would not be detected.

Geotherm E represents a slightly hotter path for melt migration. Melts travelling upwards along this geotherm will behave similarly to those found along the oceanic geotherm described above, by first crystallizing amphibole and therefore the silicate component, out of the migrating melt. With further cooling, the carbonatite melt component would cross the solidus ledge. This would be visible through the metasomatizing reaction Melt + opx + sp -> jadeitic cpx + CO_2. The melt component would react-out leaving an assemblage of cpx-rich peridotite (wehrlite) plus abundant CO_2-rich fluid inclusions.

This reaction also helps explain the occurance of massive gas exsolution at depths of approximately 80 km, close to the spinel stability field, which Bailey (1987) has suggested may provide the trigger for high velocity volcanic erruptions. If the CO_2-rich fluid does not escape and regional cooling occurs, the wehrlite assemblage may react again in the subsolidus region and on crossing the carbonation reaction (Cpx + Ol + CO_2 -> Dol + Opx), produce a dolomite, amphibole-rich peridotite.

Geotherm P, represents a perturbed or elevated geotherm, similar to that constructed for S.E. Australia by O'Reilly and Griffin (1985). This geotherm is too hot to intersect the carbonatite field. As a spinel lherzolite assemblage plus ol-melilitite melt crosses the solidus under these conditions, the silicate components will crystalize into amphibole and opx while CO_2 will become trapped as inclusions.

An idealized cross-section of a continental land mass can be drawn by assuming that the geothermal gradient becomes progressively hotter from the centre to the edge of continents. Figure 19 presents cross-sections of an idealized continent overlying lithosphere of pyrolite composition under conditions with CO_2 only, H_2O saturated and H_2O undersaturated, and with both CO_2 and H_2O as the volatile species. The X-axes

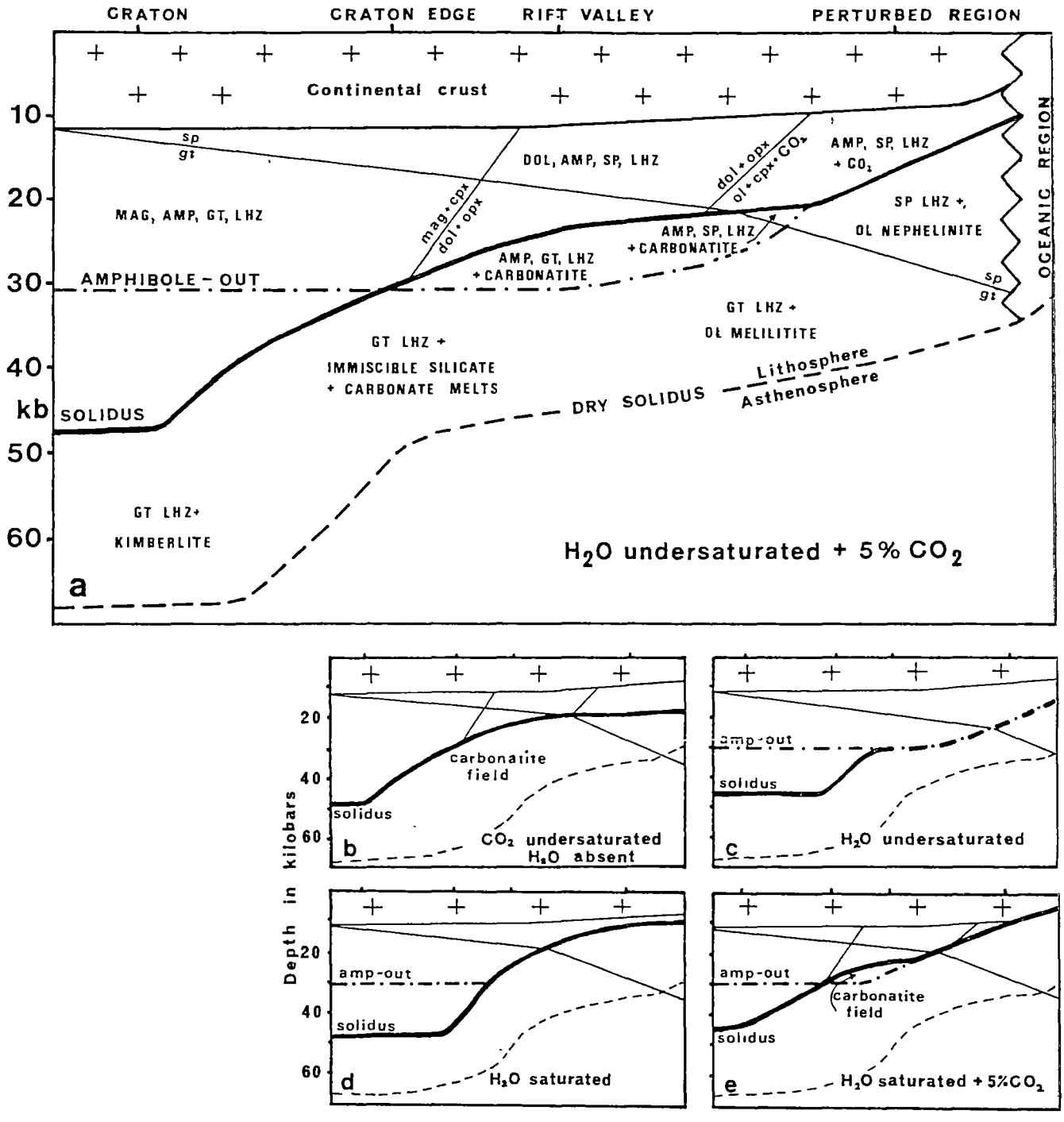

Figure 19. Cross-section of an idealized continent of pyrolite composition

display progressively hotter geotherms while the Y-axes show depth in kb. Four geotherms have been indicated; the continental geotherm from the Kaapvaal craton (Finnerty and Boyd 1987) , the geotherm calculated for the Kaapvaal periphery (Finnerty and Boyd 1987), the geotherm calculated from Malaita (Nixon and Boyd 1979) and the perturbed geotherm from S.E. Australia (O'Reilly and Griffin 1985).

These cross-sections demonstrate the change in mineral phase relationships and solidus positions caused by the addition of H_2O and CO_2 to a mantle peridotite assemblage. They do not take into account inhomogeneities in the mantle caused by such factors as fO_2, bulk rock composition, presence of the volatiles F, Cl, S, or trace elements. The presence of F and Cl is believed to stabilize amphibole to higher temperatures (Holloway and Ford, 1975), while the availability of sulphur may lower solidus temperatures and pressures by stabilizing sulphides as an additional phase. Lower fO_2 (<EMOG) will cause reducing conditions and destabilise the carbonate minerals. This will result in completely different peridotite phase relationships as demonstrated by Taylor and Green's (1988) experiments with pyrolite + H_2O + CH_4.

Since the solidus positions are at differing pressures and temperatures for different H_2O-CO_2 conditions, melts formed in a mantle region with a particular volatile content may migrate and enrich adjoining regions which contain different volatile contents or chemical compositions.

The phase boundaries presented in Figure 19 demonstrate many features found in natural lherzolite samples. The slope of the garnet to spinel boundary demonstrates why most lherzolites from cratonic environments contain garnet while those from cratonic edges contain spinel. Carbonatitic magmas are restricted to rift valley or ocean island environments. This is confirmed in natural samples by the presence of carbonatites in rift valleys (east Africa, Fen and Alno) or oceanic environments (Malaita and the Cape Verde Islands). Carbonatites would not be expected in continental areas with a high geothermal gradient such as S. E. Australia, or the Red Sea or in intra-plate oceanic islands with high geotherms and high degrees of melt such as Hawaii (O'Reilly, 1987; McGuire, 1988; Sen, 1987).

Dolomite bearing peridotites also have a very restricted range and should be found near craton edges. It is peculiar that few natural samples are seen. Many authors, for example, Eggler (1974),and Boyd and Gurney (1982), suggest that dolomite would not survive the ascent in erupting magmas, but would decompose into CO_2 and pyroxenes. (Magmatic ascent involves adiabatic pressure decrease not movement along a geotherm).

Perhaps the most interesting feature presented in Figure 19, however, is the occurrence of two solidus ledges, one based on the occurrence of amphibole, the classic low velocity

zone (Green 1973), and the other formed by the freezing of carbonatite melt. Each can be viewed as a region of metasomatism. In some instances the two ledges are geographically distinct, allowing two distinct metasomatic episodes to be detected, while in other places the two ledges are close together and would result in multiple metasomatic episodes which would be indistinguishable. The relationship between the carbonate-bearing peridotite solidus (zone of carbonate related K and LREE metasomatism) and the amphibole dehydration boundary (zone of basaltic melt generated Fe, Al, and Ti metasomatism) is dependant on both the regional pressure and temperature conditions and host-rock volatile contents.

The occurance of two types of metasomatism has been increasingly recognised in the past few years (Hawkesworth *et al.*, 1984; Menzies *et al.*, 1987; Nixon, 1987). It is suggested by a dichotomy in the behavior of K and Ti from xenolith bulk rock analysis eg, Massif Central (Downes, 1987) or by an enrichment in K and LREE in some samples whilst others contain modal enrichments of Na, K, P, Fe, Si, LREE eg, Hoggar (Dautria *et al.*, 1987). It was strongly suggested by comparison of mineral chemistry between natural and experimental amphibole samples in this study (Chapter 1).

Ti, Al, Fe enrichment is the dominant type of metasomatism, and perhaps the best understood. It has often been described as modal metasomatism (Harte, 1983) because of the common occurance of amphibole and phlogopite. Isotope and trace element characteristics of localities with Fe, Al and Ti metasomatism are consistent with an interpretation that they form by basaltic-melt migration (Irving and Frey 1984; Roden *et al.*, 1984). In extreme cases this results in Fe-rich lherzolites such as those from Kiama, N.S.W. (O'Reilly, 1987) and southwestern Japan (Goto and Arai, 1987).

K-LREE metasomatism has been observed in samples from many localities, and is generally described as cryptic metasomatism (Dawson, 1984). It is believed to involve a hydrous alkali-rich fluid rich in Rb, Ba, Na, Ca, and Sr (Menzies and Hawkesworth, 1987; Meen, 1987). At many localities, this type of metasomatism may be caused by a carbonatitic melt rather than fluid, particularly since a melt can transport much greater quantities of Na, K, Rb, Sr, Ba, and LREE. In addition, a carbonatite melt has a low viscosity so that it may readily migrate and metasomatise adjoining mantle regions. Phase relationships at high temperatures and pressures suggest that metasomatism may result from lherzolite reaction with either silicate melts, carbonatite melts or volatile (H_2O, CO_2) rich fluids.

The presence of an amphibole crystallization ledge at higher temperatures and pressures than the carbonatite ledge is significant, since it provides amphibole as a crystal phase which may absorb Na, K and the LREEs deposited as the carbonatite melt crystallizes. In areas which do not contain amphibole (its formation controlled by the availability of H_2O), the clinopyroxenes will become very enriched in LREEs. This has been documented by Kempton, (1987) who concluded that Na and LREE enrichment is most extreme in high Cr# clinopyroxenes from samples without amphibole (high Cr#s reflect low modal proportions).

Metasomatism by fluids may be important at high pressures (>30 kb), as the presence of a carbonate rich melt above the stability of amphibole has not yet been established. The high pressure MARID nodules found as kimberlite inclusions are believed to be conduit linings resulting from the passage of hydrous fluids (Kramers *et al,*. 1983; Smith, 1983; Menzies, 1987) as are the low pressure glimerites and micaceous pyroxenites (Menzies *et al.,* 1987). Oxygen fugacities also will play an important role at these pressures as the mantle is believed to contain less O_2 with depth.

It has long been recognised that metasomatised mantle material would provide an ideal fertile source rock for intraplate basaltic liquids which characteristically have high incompatible element contents. The occurrence of metasomatized xenoliths worldwide, with similar geochemistry, mineralogical characteristics and many which formed over a restricted temperature range, indicate that there is a petrogenetic relationship linking metasomatism and intra-plate volcanism. The stability relationships of dolomite and amphibole provide this relationship. Phase relations in the system dolomite-bearing peridotite + 0.2 % H_2O provide a fairly simple model by which to further explore the types and timing of metasomatic enrichment, both as a process to form mantle inhomogeneities and as one to explain their occurrence.

Conclusions

1) Experiments in carbonate-bearing pyrolite + 0.2% H_2O produced an S-shaped solidus similar to that found in CMAS. The high pressure solidus limb is controlled by the stability of carbonate and results from the reaction 'magnesite + cpx + ol -> carbonatite melt + opx + gt. It occurs at 920°C and is the lowest temperature solidus found to date. The low pressure solidus is controlled by the stability of amphibole. The amphibole

breakdown reaction consumes pargasite plus orthopyroxene to produce a silicate melt plus olivine, clinopyroxene and H_2O vapor.

2) Carbonatite melt is stable in the temperature and pressure region between the solidus and amphibole breakdown reaction (930-1070°C, 21-31 kb). The melt is a Na-rich dolomitic carbonatite which quenches to dolomite, magnesite, and Na carbonate minerals.

3) The melt becomes melilititic above the stability of amphibole. It appears to segregate into immiscible silicate and carbonate components at high pressure (P > 30 kb).

4) Phase relationships in carbonate-bearing pyrolite + 0.2% H_2O indicate that mantle regions containing CO_2 and H_2O contain two major crystallization ledges. At 30 kb a barrior is created by the formation of amphibole, the classic low velocity zone, while at 22 kb a ledge is formed by the crystallization of carbonatite by the reaction carbonatite + gt + opx -> jadeitic cpx + ol + CO_2. This corresponds to the zone of Fe, Al, Ti metasomatism and K, LREE metasomatism respectively.

3. COMPOSITION OF A PRIMARY CARBONATITE MELT

Introduction

Carbonatites have been defined by Streckeisen (1980), as igneous rocks containing greater than 50% carbonate minerals. The majority of carbonatites are Ca rich and are composed of calcite (sovites and alvikites) and dolomite (beforsites) with minor amounts of ferroan carbonate. Apatite, phlogopite, magnetite, aegirine, aegirine-augite and pyrochlore are common mineral phases. Cation abundance is in the order Ca > Mg > Fe > (Na + K) (LeBas, 1981). These carbonatites characteristically contain high contents of Sr, Ba, Nb and rare earth elements, are associated with ijolites and other alkali-rich igneous rocks and are often surrounded by large sodic or potassic fenitization halos.

Na-carbonatites, (natro-carbonatites), form another group of carbonatitic magmas. The only naturally occuring example is from Oldoinyo Lengai, an active volcano in the Gregory Rift Valley, Northern Tanzania (Dawson, 1962). This lava consists predominantly of Na_2O, K_2O, CaO, and CO_2 with traces of SiO_2 and Al_2O_3 (Dawson *et al.*, 1987). The crystallized lava contains acicular to prismatic crystals of the alkali carbonate mineral nyerereite $(Na_{0.82}K_{0.18})_2Ca(CO_3)_2$ with minor amounts of gregoryite $(Na_{0.78}K_{0.05})_2Ca_{0.17}CO_3$ (McKie and Frankis, 1977).

Kimberlite associated carbonatite material has been reported (Dawson and Hawthorne, 1973; Mitchell and Clarke, 1976; Emeleus and Andrews, 1975; Clement, 1975). This carbonate material, however, does not contain the characteristic chemical or mineralogic characteristics mentioned above and may therefore be regarded as petrogenetically distinct (Mitchell, 1979; LeBas, 1977).

Isotopic studies (C, O, Sr, Nd and Pb) have established that most carbonatites are derived from mantle source regions (Deines and Gold, 1973; Sheppard and Dawson, 1975; Nelson *et al.*, 1988). It is still undetermined, however, whether they are derived by partial melting of the mantle (Lancelot and Allegre, 1974; Koster Van Groos, 1975; Dawson, 1962) or by exsolution from a CO_2 rich phonolitic or nephelinitic magma (Donaldson and Dawson, 1978; Freestone and Hamilton, 1980; Rankin and LeBas, 1974; and LeBas, 1977; 1987).

The experimental work described in Chapter 2 determined the pressure and temperature stability field of carbonatite magma in fertile peridotite under oxidizing (MPG) conditions. It did not however, distinguish whether natural carbonatites are formed by the melting of peridotite as the carbonate-bearing peridotite solidus is crossed, or if they formed as a segregation from a CO_2 rich basaltic melt as it migrates to lower pressures and temperatures along an oceanic-type geotherm crystallizing clinopyroxene and amphibole.

The experimental study in Chapter 2 documented the existence of primary carbonatite melt. The aim of this chapter is first, to determine the chemical composition and nature of the melt and second, to examine whether the experimental melt is suitable as a parental melt for deriving naturally occurring carbonatites. The experimental 'primary' carbonatite composition was determined by conducting a series of layered or sandwich experiments with sequentially changing melt compositions in order to produce a carbonatite melt which is in chemical equilibrium with a spinel or garnet lherzolite assemblage.

The nature of 'primary' carbonatite

Early research (pre-1960), determined that carbonatites were magmatic rocks. These studies focused mainly on the source region for carbonatites, whether they are mantle derived (Eckermann, 1948; Holmes, 1950; Koster van Groos, 1975) or formed by the melting of sedimentary limestone or trona (Milton 1968). Isotope studies (Powell, 1966; Bell *et al.*, 1973; Deines and Gold, 1973) eventually concluded that most carbonatites are derived from mantle source regions. Primary carbonatite magmas were believed to be Ca-rich (Heinrich, 1966) as demonstrated by experiments, (Wyllie, 1965; 1966; 1978) on the genesis of kimberlites. These experiments produced calcitic and dolomitic melts from CO_2 and H_2O rich peridotite sources. These experiments are now interpreted by some authors as relating to kimberlite-type carbonate segregations or ocellii, not to carbonatitic magmas (Le Bas, 1987; Twyman and Gittins, 1987).

In 1962, J.B. Dawson reported the occurrence of natro-carbonatite lavas from Oldoinyo Lengai and suggested that many Ca-carbonatites were not primary, but were originally Na and K rich carbonatites which had lost their alkalis to aqueous solutions involved in fenetization. This hypothesis was supported by Deans and Roberts, (1984) and Clarke and Roberts, (1986) who described large lath-shaped crystals, texturally similar to nyerereite but now replaced by calcite, from Tinderet and Homa Mountains, Kenya.

Similar mineral textures have also been described in samples from Kaiserstuhl and Fort Portal (Keller, 1981; Nixon and Hornung, 1973).

Fluid inclusions in apatites from Ca-carbonatites have been shown to trap fluids rich in Ca, Na, K, sulphide and halide molecules, thus supporting an origin from an alkaline rich magma not dissimilar to a natro-carbonatite (Rankin and LeBas, 1974; Rankin, 1977; Aspden, 1980).

An origin for Ca-carbonatite by replacement of original natro-carbonatite is further supported by comparison between the two magma types. Both lava types are associated with alkali ignoeus rocks, for example, nephelinite, phonolite, pyroxenite, ijolite, and fenite. Isotope values are in the same range for Oldoinyo Lengai as for older Ca-carbonatites (O'Neil and Hay, 1973; Deines and Gold, 1973; Sheppard and Dawson, 1975).

Recent research by Dawson *et al.*, (1987), has documented a change over time in the chemical composition of the Oldoinyo Lengai carbonatite due to reaction with Ca-rich surficial waters. This study indicated that the lava had become Ca-rich at the expense of Na and K, over a 20 year period, due to the alteration of nyerereite to form the mineral pirsonite ($Na_2Ca_2(CO_3)_2 \cdot 2H_2O$). This mineral is believed to provide the missing link between young Na-carbonatites and the older Ca-carbonatites.

Current general opinion is that many carbonatites may be derived from Na-rich carbonatite magmas which have lost their alkalis due to fenitization processes. These Na-rich melts, however, are generally considered to be evolved and evolving melts rather than primary melts and debate continues over the constituents of a 'primary' carbonatite. This problem has frustrated petrologists, since some carbonatites and their related magmas have undergone intense crystal fractionation and host rock assimilation (Donaldson *et al.*, 1987).

Most researchers are of the opinion that Na-carbonatites are derived as an immiscible segregation from a carbonated nephelinite magma (LeBas, 1987). This interpretation is based on experimental liquid immiscibility studies, particularly that of Koster van Groos and Wyllie, (1966; 1968; 1973) who demonstrated liquid immiscibility between Na-rich silicate and carbonate components along the join $NaAlSi_3O_8$-Na_2CO_3 (at 1 kb and above 870°C), and the studies of Freestone and Hamilton, (1980) which demonstrate that Na-rich carbonatite magmas are immiscible at high pressures (7.6 kb) with nephelinite and

phonolite magmas. Liquid immiscibility is enhanced by the addition of K, P and Ti while the addition of water causes the immiscibility field to shrink (Wendlandt and Harrison, 1979; Freestone, 1978; Mysen *et al.*, 1981). Kjarsgaard and Hamilton (1988) have recently reported immiscibility in Na-poor compositions at 5 kb using the join albite-calcite and anorthite-calcite.

Twyman and Gittins, (1985; 1987) are amongst the few researchers currently supporting a primary origin for carbonatites. They have suggested that if a primary carbonatite magma exists, it would be an alkalic olivine sovite with approximately 8% $Na_2O + K_2O$.

The debate is ongoing with several researchers reverting to pre-1960 hypotheses which suggest that Na-carbonatite magmas are a partial melt of fenetised lower crust (Morogan and Martin, 1985) or assimilated trona deposits (Peterson and Marsh, 1986).

Experimental Techniques

A first approximation of the primary carbonatite melt composition appeared in the dolomite-bearing pyrolite + H_2O experiments (Chapter 2). Probe mounts of the initial experiments contained intergranular void spaces where melt was expected. This feature suggested that the melt was either very soft or was water soluble. The remaining probe mounts were prepared using oil and care was taken not to permit samples to come into contact with water or acetone.

Intergranular void spaces in the oil-polished probe mounts contained small broken crystals of material which appeared to be an assemblage of dolomite plus magnesite. This material was too fine grained to provide single crystal analyses. Analysis showed it to be Mg and Ca rich with minor Na and P and to be generally silica free. A further indication of the melt composition was provided by a small vein of pure Na_2CO_3 which was present in sample T-2388 (22 kb, 975°C). It was interpreted that the melt quenched to an assemblage of dolomite, magnesite and Na-carbonate.

A series of sandwich experiments was then conducted in order to determine the primary carbonatite melt composition. Experimental capsules were constructed to contain a basal layer of carbonate (10%) plus an upper layer of amphibole pyrolite plus 5% dolomite

Table 5. Starting compositions used in sandwich experiments

	Pyrolite+0.2%H2O + 5% dolomite	Na2CO3	Carbonatite #1	Carbonatite #2	Carbonatite #3
SiO2	45.39	-	-	-	-
TiO2	1.14	-	-	-	-
Al2O3	5.99	-	-	1.96	-
Cr2O3	0.62	-	-	-	-
FeO	7.42	-	5.20	5.12	5.20
MgO	29.38	-	15.70	15.32	16.70
CaO	6.38	-	10.50	22.53	19.80
Na2O	0.82	58.48	21.00	10.24	12.50
K2O	0.15	-	-	-	-
P2O5	0.24	-	-	-	-
CO2	2.28	41.52	47.60	44.83	45.80
H2O	0.19	-	-	-	-
Total	100.00	100.00	100.00	100.00	100.00

(90%). The amphibole pyrolite composition was similar to that used in previous experiments (Chapter 2). It was made by precrystallizing pyrolite - 40% olivine + 2% H_2O at 15 kb, 925°C for 48 hours into an amphibole-rich assemblage (approx. 0.4% H_2O) and then mixing in 5% dolomite. Model carbonatite compositions were prepared using Na_2CO_3, dolomite, magnesite and siderite minerals ground together without the use of water or acetone. The initial sandwich experiment used pure Na_2CO_3 as the carbonate melt layer. The resulting melt formed the basis for the melt composition in the second experiment. Five such experiments were carried out in this iterative manner. Compositions of the carbonatite starting mixes are presented in Table 5.

The starting assemblage was placed in small diameter $Ag_{75}Pd_{25}$ inner capsules, surrounded by a magnesite buffer and enclosed in large diameter $Ag_{50}Pd_{50}$ capsules (Figure 20). NaCl sleeved assemblies were used. Samples were run for 3 hours. Experiments were performed using the piston-in technique with no friction correction applied. Pressures are accurate to within 1 kb and temperatures were automatically controlled and are considered accurate to $\pm 10^{o}C$. Experimental run conditions are provided in Table 6.

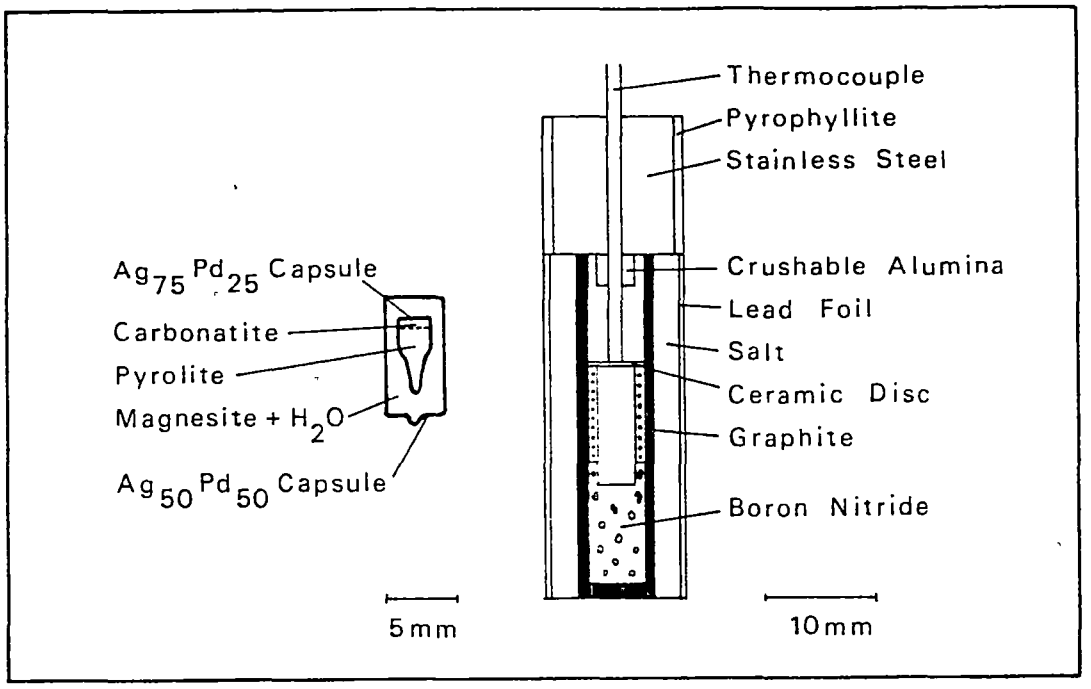

Figure 20. Experimental capsule and buffer assembly design

Experimental Results

These were as follows:

T-2467, This experiment contained pure Na_2CO_3 as the carbonatite layer and was run at 22 kb, 975°C for 3 hours. The resultant assemblage contained an NaMgCa-rich carbonatite melt (analysis presented in Table 7) which quenched to large tabular crystals with NaMg-rich carbonate cores and CaMgNa-rich carbonate rims. Large hexagonal-shaped crystals of eckermanite, an Na-amphibole were also present in the melt layer (Figure 21). The peridotite assemblage contained ol, opx, pargasitic amphibole, and an ekermanitic amphibole. The assemblage closely resembled results of experiments by McNeil and Edgar, (1987) on a Na-metasomatised upper mantle (pyrolite) composition. It is concluded that the starting melt layer contained far too much Na to be in equilibrium with a peridotite assemblage. A large area scan of the melt layer provided the composition for Carbonatite mix #1.

T-2508, Carbonatite mix #1 was used as the basal layer in this run. The run temperature was increased from 975 to 1000°C to hold the experiment well within the carbonatite stability field. This run resulted in a melt layer composed of dolomite, Na-Mg carbonate and Na-Ca carbonate (Figure 21). The Na-carbonate grains were lath-shaped while the dolomite formed large blocky crystals. The dolomite crystals are interpreted as quench, rather than primary, because of their radiating habit and low Mg# (88.8). The pyrolite layer contained ol, opx, amph, il and primary dolomite (Mg# 99.3). It contained neither clinopyroxene nor an aluminous phase (gt or sp). Mineral compositions were not

Table 6. Run conditions of sandwich and reversal experiments

Run#	Composition	P (kb)	T (°C)	Time (hrs)	Phases
Starting Mix					
T-2526	Pyrolite+2%H2O	15	925	48	ol,opx,cpx,amp,sp
T-2516	Pyrolite+2%H2O	15	925	48	ol,opx,cpx,amp,sp
Sandwich Runs					
T-2467	90%(Py+5%dol)+10%(Na2CO3)	22	975	3	ol,opx,amp,Na-amp melt = NaMg-carb, CaMgNa-ca
T-2508	90%(Py+5%dol)+10%(Carbonatite1)	22	1000	3	ol,opx,amp,ilm,dol melt = dol, NaMg-carb, NaCa-c
T-2517	90%(Py+5%dol)+10%(Carbonatite2)	22	1000	3	ol,opx,cpx,amph,Na-amph melt = dol, mag
T-2518	90%(Py+5%dol)+10%(Carbonatite3)	22	1000	3	ol,opx,cpx,amp,ilm,sp melt = dol, NaMgCa-carb
T-2534	90%(Py+5%dol)+10%(Carbonatite3)	25	1000	3	ol,opx,cpx,amp,gt melt = dol, NaMgCa-carb
Reversals					
T-2476	95%(Py)+5%(Na2CO3)	25	920	24	ol,amp,Na-amp,mag
T-2490	98%(Py)+2%(Carbonatite1)	25	900	24	ol,opx,cpx,amp,ilm,ap,mag
T-2493	98%(Py)+2%(Carbonatite1)	19	1000	24	ol,opx,cpx,amp,ilm,
T-2535	98%(Py)+2%(Carbonatite3)	22	900	26	ol,opx,cpx,amp,ilm,sp,dol
T-2539	98%(Py)+2%(Carbonatite3)	18	1000	4	ol,opx,cpx,amph,ilm,sp

similar to those found in pyrolite formed under the same temperature and pressure conditions as reported in Chapter 2 (Figure 22).

T-2517, Carbonatite composition #2 was used as the basal layer in this experiment. In this composition, Al was added to the carbonatite layer in an attempt to stabilize an Al-phase in the pyrolite. This experiment resulted in a pyrolite assemblage of ol, opx, cpx, amphibole and Na-rich amphibole. Modal proportions of amphibole were extremely high (> 60%). The melt consisted of dolomite, magnesite and unreacted corundum (Al_2O_3) crystals. It was concluded that there was too much water in the assemblage and that this had promoted the growth of amphibole. This result seemed to be caused by either the sample absorbing H_2O during preparation or by hydrogen diffusion during the experiment.

T-2518, Carbonatite #3 composition was used in this experiment (similar to carbonatite mix #2 but without Al). The experiment resulted in a carbonatite melt composed of Na-Mg-Ca carbonate plus dolomite quench crystals and a pyrolite assemblage of

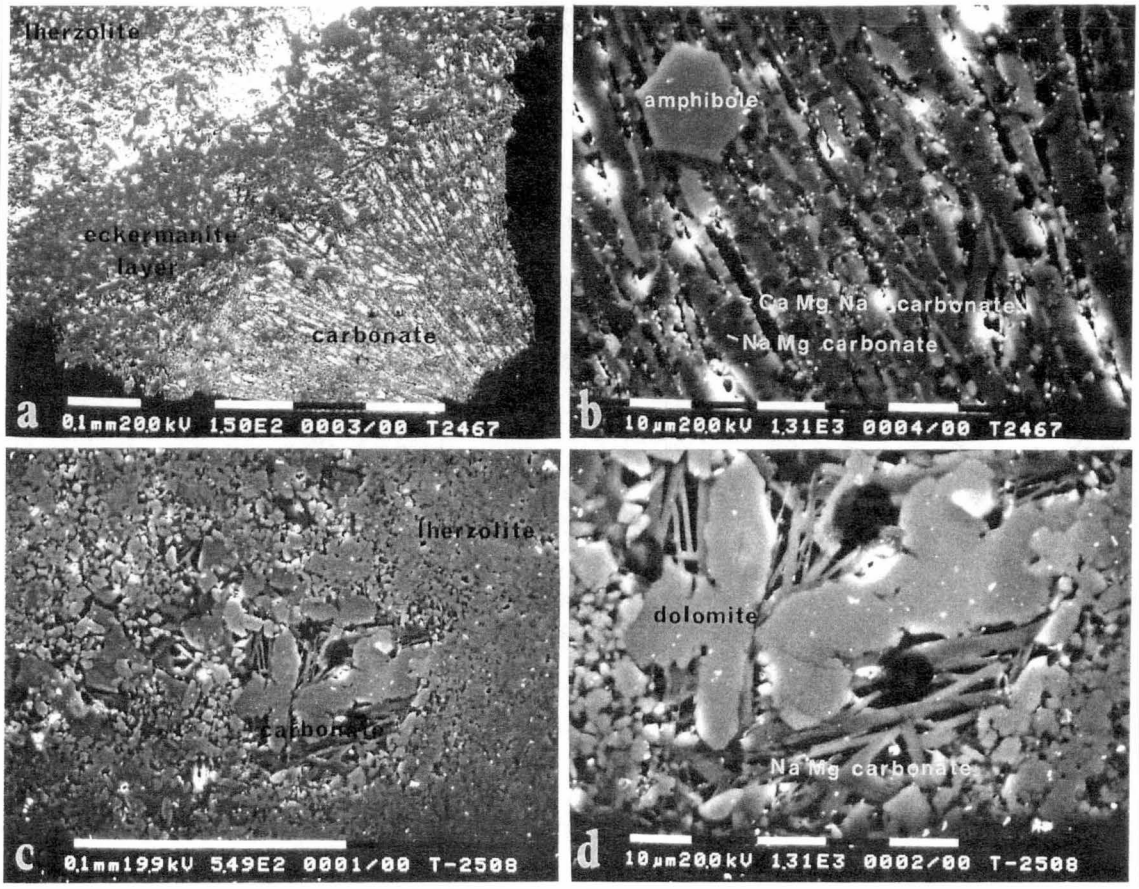

Figure 21. Scanning electron micrographs of sandwich experiments a,b) Sample T-2467 90%(amphibole pyrolite + 5% dolomite) + 10% Na_2CO_3 run at 22 kb, 975°C for 3 hours. Lherzolite is composed of olivine, orthopyroxene and amphibole, reaction corona between lherzolite layer and carbonatite is composed of echermanite (Na-amphibole). Carbonatite layer is composed of NaMg-caerbonate crystals with CaMgNa-rich carbonate rims. c,d) Sample T-2508, 90%(amphibole pyrolite + 5% dolomite) + 10% carbonatite #1 composition run at 22kb, 1000°C for 3 hours. Pyrolite assemblage consists of olivine, orthopyroxene and amphibole. Carbonatite pools are composed of dolomite and NaMg carbonate minerals (analyses presented in Table 7).

ol, opx, cpx, amph, il, and sp (Table 7). The pyrolite assemblage contained minerals with a similar chemistry to those in the (pyrolite + 5% dolomite + 0.2% H_2O) experiments reported in Chapter 2. It was noteworthy that K_2O and P_2O_5, not present in the carbonatite layer but minor constituents of the pyrolite layer, were now strongly concentrated in the quenched carbonate - rich pools. The mobility of the elements K_2O and

Table 7 Representative mineral compositions from sandwich experiments

	T-2467				Phases in melt			T-2508						Phases in melt		
	Melt	Ol	Opx	Amp	Amp	Na Carb	Quench	Melt	Ol	Opx	Amp	Ilm	Dol	Dol	Quench	Quench
P2O5	0 38	-	-	-	-	0.27	0 25	0 43	-	-	-	-	0 18	-	0.65	0 73
SiO2	1.99	40.67	56 00	46 48	53.46	0.32	1.85	1 32	40 39	55 14	45.70	6.79	-	-	-	0.39
TiO2	0 16	-	0 27	1.59	1.24	-	0.25	-	-	0.37	1.56	43 48	-	-	-	-
Al2O3	1 17	-	2 88	11 99	5 80	0.31	1.54	0 38	0 25	3 38	11.83	0 67	0 16	-	-	0 37
Cr2O3	-	-	0 45	1 00	0.60	-	-	-	-	0.62	1.62	1 29	-	-	-	-
FeO	4.83	11.67	6 47	3 81	3.58	3 51	7.62	5 01	12 21	7 96	4.96	25 48	0.25	4 87	4 34	4 83
NiO	-	0.31	-	-	-	-	-	-	0 39	-	-	-	-	-	-	-
MnO	-	-	-	-	-	-	0 39	-	-	-	-	-	-	0 26	-	-
MgO	14 67	47.36	33.25	19 35	19 93	25 33	6 41	16 00	46 76	31.52	18.53	19 20	19 86	21.72	3.82	18.22
CaO	6 98	-	0.67	10.20	2 53	1 98	32.68	19 19		1.01	10.26	2 82	29 33	36 22	25 18	5 84
K2O	0 19	-	-	0.51	0 09	-	0 24	0.18	-	-	0.29	-	-	-	0 95	0 27
Na2O	22 96	-	-	4 66	9.66	24.76	2 84	11.90	-	-	3 26	-	-	-	14.74	18 54
Cl	0.07	-	-	-	-	-	-	0 07	-	-	-	-	-	-	0 12	0 09
Total	53.40	100 00	100.00	99 60	96.87	56 47	54.07	54.48	100.00	100.00	98.00	100 00	49.78	63 06	49 81	49 28
P	0 0308	-	-	-	-	0 0199	0.0206	0 0338	-	-	-	-	0.0145	-	0 0631	0 0633
Si	0 1895	1.0046	1.9340	6 4579	7 4715	0 0282	0.1809	0.1229	1.0008	1.9205	6 4611	0.3019	-	-	-	0 0395
Ti	0 0118	-	0.0069	0 1664	0 1304	-	0.0182	-	-	0 0098	0 1659	1 4548	-		-	-
Al	0.1312	-	0 1173	1.9630	0.9549	0.0315	0 1773	0 0417	0.0073	0 1386	1.9705	0 0349	0.0177	-	-	0 0446
Cr	-	-	0 0124	0.1097	0.0658	-	-	-	-	0.0171	0 1811	0 0455	-	-	-	-
Fe	0.3859	0.2410	0 1869	0 4430	0 4184	0.2567	0 6216	0 3900	0.2531	0 2318	0.5869	0 9482	0 0203	0 3235	0 4144	0 4138
Ni	-	0.0061	-	-	-	-	-	-	0.0078	-	-	-	-	-	-	-
Mn	-	-	-	-	-	-	0 0321	-	-	-	-	-	-	0 0176	-	-
Mg	2 0869	1.7437	1.7116	4 0078	4.1515	3.3033	0 9315	2.2195	1 7267	1.6363	3.9054	1.2731	2 8699	2 5737	0 6503	2 7822
Ca	0.7144	-	0 0250	1.5178	0 3781	0 1856	3 4153	1.9136		0 0378	1.5533	0 1345	3 0467	3 0850	3 0775	0 6406
K	0.0230	-	-	0 0912	0 0165	-	0 0294	0 0211	-	-	0 0530	-	-	-	0 1386	0.0358
Na	4 2493	-	-	1.2561	2 6175	4 2013	0.5378	2 1463	-	-	0.8932	-	-	-	3 2610	3 6822
Cl	0 0109	-	-	-	-	-	-	0 0105	-	-	-	-	-	-	0.0228	0.0154
Total	7 8337	2.9954	3.9942	16 0129	16.2046	8 0265	5 9647	6 8995	2 9956	3 9919	15 7703	4 2031	5 9692	5.9998	7.6277	7.7174
Mg#	84.4	87 9	90 2	90 0	90 8	92 8	60 0	85.1	87 2	87 6	86.9	57.3	99 3	88 8	61.1	87 1
Ca	22.4	0 0	1 3	25 4	7.6	5.0	68 7	42 3	0 0	2.0	25 7	5 7	51.3	51.6	74 3	16 7
Mg	65.5	87 9	89 0	67 1	83 9	88 2	18.7	49.1	87.2	85 9	64 6	54 0	48 3	43 0	15 7	72.5
Fe	12.1	12 1	9 7	7 4	8.5	6 9	12 5	8 6	12.8	12 2	9 7	40 2	0 3	5 4	10 0	10 8

	T-2518									T-2534					
	Melt	Ol	Opx	Cpx	Amp	Ilm	Sp	Quench Dol	Quench Na mn	Ol	Opx	Cpx	Amp	Gt	Dol
P2O5	0 48	-	-	-	-	-	-	-	4 22	-	-	-	-	-	-
SiO2	2 94	40 91	55 43	51.25	45.67	-	-	0 37	0 19	40.87	54 95	52.79	45 91	41 54	-
TiO2	0.45	-	0.26	1.10	1.57	55 17	0.61	-	0 23	-	0 27	0 83	2.16	1 54	-
Al2O3	1 95	-	2.71	5.18	11 69	0 32	58.53	0.28	-	-	2 87	5 4	13.2	19	-
Cr2O3	0.22	-	0.50	0 95	1 40	0.87	8 02	-	-	-	0.5	0 86	1.03	1.07	-
FeO	4.61	12 32	7 90	4.04	4 86	29.75	12 27	4 35	9 78	12 94	7.7	4 07	4 66	10 1	3 21
NiO	-	0 45	-	-	-	-	0 35	-	-	-	-	-	-	0 29	-
MnO	-	-	-	-	-	-	-	-	-	46.07	32.17	17 45	19 48	20 64	17 58
MgO	14.19	46 03	32 25	17.50	18 74	13.89	20 04	16 70	8 88	0.12	1 46	17 58	10 23	5 8	26 96
CaO	21.29	0 30	0.94	19.24	11.00	-	0.18	30 50	8.75	-	-	-	0 45	-	-
K2O	0 35	-	-	-	0.60	-	-	-	1.34	-	-	1.01	2 88	-	-
Na2O	4 99	-	-	0.74	2 48	-	-	-	22 84	-	-	-	-	-	-
Cl	-	-	-	-	-	-	-	-	0.19	-	-	-	-	-	-
Sum	51 49	100.00	100 00	100.00	98.00	100 00	100 00	52.71	56.43	100	100	100	100	100	47.75
P	0 0383	-	-	-	-	-	-	-	0.3300	-	-	-	-	-	-
Si	0 2752	1.0138	1 9300	1.8609	6 4607	-	-	0 0357	0.0177	1.0132	1 917	1 9008	6 3384	3.0037	-
Ti	0 032	-	0 0068	0 0301	0 1666	1 9126	0.0118	-	0.0166	-	0 0071	0 0225	0 2239	0 084	-
Al	0.2144	-	0 1114	0 2218	1 9494	0.0172	1.7859	0.0317	-	-	0.1179	0.2293	2.1474	1.6196	-
Cr	0.0161	-	0.0138	0 0274	0 1571	0.0318	0 1642	-	-	-	0 0138	0.0245	0 112	0.0612	-
Fe	0 3604	0.2553	0.2299	0.1226	0.5747	1 1470	0 2656	0 3471	0.7736	0 2683	0 2268	0 1226	0 5379	0 611	0 2785
Ni	-	0.0090	-	-	-	-	0.0074	-	-	-	-	-	-	0.0179	-
Mn	-	-	-	-	-	-	-	-	-	1 7021	1.6727	0 9365	4.0094	2.2248	2 7217
Mg	1 9776	1.7002	1.6738	0 9473	3 9512	0 9542	0.7732	2 3723	1 2511	0 0032	0 0547	0.6782	1.5137	0 4497	2 9996
Ca	2.1326	0.0080	0.0350	0 7483	1 6658	-	0 0049	3 1153	0 8868	-	-	-	0 0798	-	-
K	0 0418	-	-	-	0 1076	-	-	-	0 1621	-	-	0 0708	0 7705	-	-
Na	0.905	-	-	0.0518	0 6798	-	-	0 0925	4.1872	-	-	-	-	-	-
Cl	-	-	-	-	-	-	-	-	0 0312	-	-	-	-	-	-
Sum	5.9934	2.9862	4.0006	4.0103	15.7129	4 0630	3.0130	3 9946	7.6643	2.9868	4 01	3 9851	15.733	8.0718	5 9998
Mg#	84.6	86 9	87 9	88 5	87.3	45.4	74 4	87 2	61 8	86 4	88.1	88 4	88.2	78 5	90.7
Ca	47.7	0 4	1.8	41.2	26 9		0 5	53 4	30 5	0.2	2.8	39	25	13 7	50
Mg	44 2	86.6	86 3	52.1	63.8	45 4	74 1	40.7	43 0	86 2	85 6	53 9	66.2	67 7	45.4
Fe	8.1	13 0	11 9	6.7	9.3	54.6	25.4	5.9	26 6	13 6	11 6	7.1	8.9	18 6	4 6

P_2O_5 suggest that chemical equilibrium had taken place. The melt composition is considered to be a good approximation of a primary carbonatite. Note that the concentrations of K_2O and P_2O_5 in the melt reflect the strong partitioning of these components into the melt and are determined by the relative proportion of carbonatite and peridotite layers. There are no criteria in these experiments which constrain the K_2O and P_2O_5 contents of primary carbonatite. The Na_2O concentration reported (4.99 wt%) may be low due to volatilization of Na during electron microprobe analysis.

T-2534, This experiment was similar to T-2518 but run at 25 kb, rather than 22 kb, in order to be in the garnet stabilty field. The peridotite assemblage contained similar ol, opx, cpx, amph and garnet mineral chemistry to the (pyrolite + 5% dolomite + 0.2% H_2O) experiments. The melt was not analysed because a suitably large homogeneous melt pool was not intersected during preparation of the probe mount.

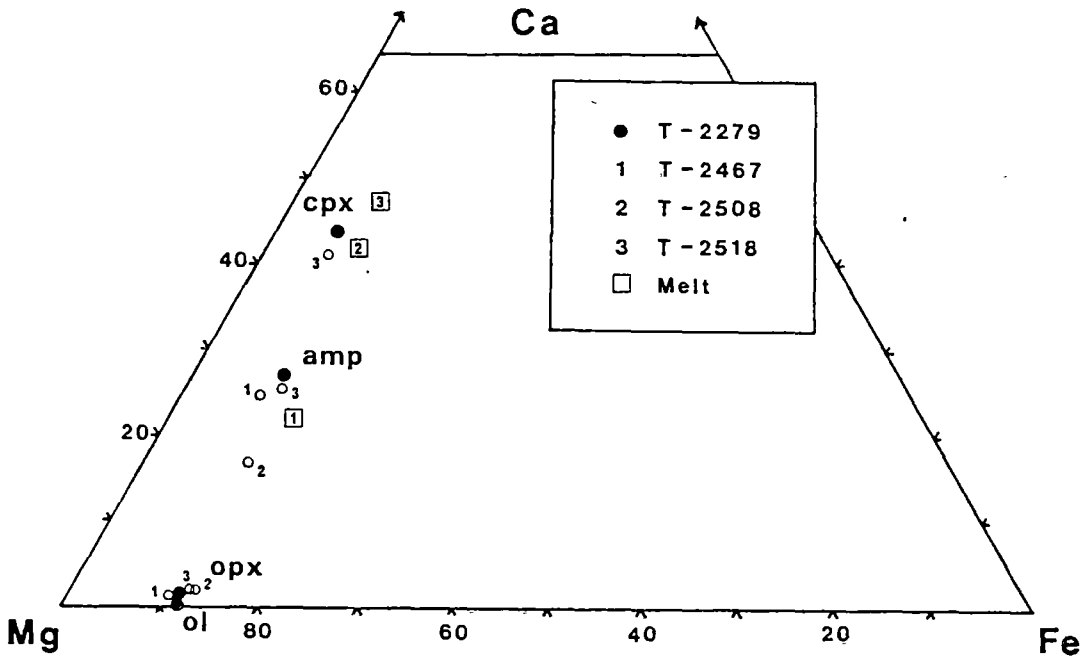

Figure 22. Mineral compositions of silicate phases in sandwich experiments and comparison with (pyrolite - 40% olivine + 1.4% magnesite) phases at 22 kb, 1000°C (Sample T-2279)

Reversal experiments

Reversal experiments were run as a check on first, the solidus position and second, the composition of the melt. Experiments T-2535 and T-2539 confirmed the solidus relationships found. In these experiments 2 to 5 wt% of the carbonatite melt was added and mixed into the amphibolitized pyrolite. Sample T-2535 was run in the dolomite stability field at 22 kb, 900°C for 22 hrs. This resulted in an amphibole-bearing spinel lherzolite assemblage with approximately 2% dolomite. Sample T-2539 was run in the sub-solidus CO_2 field at 18 kb, 1000°C for 4 hours. The resultant assemblage contained ol, opx, cpx, amph, ilm, and spinel. No carbonate phases were present and the sample contained abundant fluid inclusions. These were assumed to be CO_2. The mineral chemistry of both runs (Table 8) confirmed the solidus position and suggested that the experimental 'primary' carbonatite composition is similar to the carbonatite melt in equilibrium with a mantle peridotite assemblage.

Table 8. Representative mineral compositions from reversal experiments

	T-2439, 98% Amph-pyrolite + 2% Carbonatite#3, 18kb,1000C,4hrs					T-2535, 98%Pyrolite + 2%Carbonatite#3, 22kb, 900C,26hrs					
	Ol	Opx	Cpx	Amp	Ilm	Ol	Opx	Cpx	Amph	Ilm	Dol
SiO2	40.62	55.75	52.50	45.91	-	40.25	55.19	53.22	44.98	0.72	0.37
TiO2	-	0.30	0.73	2.12	54.18	-	0.20	0.27	1.64	48.65	-
Al2O3	-	2.87	3.31	12.49	0.25	-	2.17	2.80	14.93	0.77	0 22
Cr2O3	-	0.39	0.62	0.96	1.67	0.28	0.29	-	0.56	1.47	-
FeO	11.51	7.55	3.94	5.35	30.53	11.92	7.77	5.78	5.24	35.78	2.93
NiO	0.43	-	-	-	-	0.35	-	-	-	-	-
MgO	47.45	32.20	17.17	18.76	13.37	47.20	33.62	16.42	18.88	12.23	17.89
CaO	-	0.94	21.48	11.11	-	-	0.76	20.85	10.29	0.37	30.19
K2O	-	-	-	0.46	-	-	-	-	0.28	-	-
Na2O	-	-	0.25	2.83	-	-	-	0.65	3.20	-	-
Total	100.00	100.00	100.00	100.00	100.00	100.00	100.00	100.00	100.00	100.00	51.60
Si	1.0034	1.9356	1.9109	6.3762	-	0.9973	1.9221	1.9460	6.2207	0.0344	0.0355
Ti	-	0.0079	0.0199	0.2218	1.8896	-	0.0052	0.0075	0.1705	1.7384	-
Al	-	0.1174	0.1422	2.0435	0.0137	-	0.0889	0.1209	2 4339	0.0433	0.0247
Cr	-	0.0107	0.0180	0.1060	0.0611	0.0054	0.0080	-	0 0612	0.0553	-
Fe	0.2377	0.2192	0.1199	0 6213	1.1842	0.2471	0.2263	0.1769	0.6057	1.4216	0.2351
Ni	0.0085	-	-	-	-	0.0071	-	-	-	-	-
Mg	1.7470	1.6665	0.9316	3.8831	0.9246	1.7432	1.7451	0.8949	3.8909	0.8662	2.5559
Ca	-	0.0351	0.8377	1.6531	-	-	0.0285	0.8170	1.5242	0.0188	3.1006
K	-	-	-	0.0815	-	-	-	-	0.0501	-	-
Na	-	-	0.0178	0.7627	-	-	-	0.0462	0.8578	-	-
Total	2.9966	3.9924	3.9980	15.7492	4.0731	3.0000	4.0242	4.0092	15.8150	4.1780	5.9519
Mg#	88.0	88.4	88.6	86.2	43.8	87.6	88.5	83.5	86.5	37.9	91.6
Ca	0.0	1.8	44.3	26.8	0.0	0.0	1.4	43.3	25.3	0.8	52.6
Mg	88.0	86.8	49.3	63.1	43.8	87.6	87.3	47.4	64.6	37.6	43.4
Fe	12.0	11 4	6.3	10.1	56.2	12.4	11.3	9.4	10.1	61.6	4.0

Discussion

Results of this experimental study have shown that primary carbonatite melt, co-existing with amphibole-bearing peridotite at 22 kb, 1000°C, is an Na-rich dolomitic carbonatite with a high Mg# (84.5) and low silica content (2.94 wt% SiO_2). The experimental primary carbonatite melt is enriched in K_2O and P_2O_5 (exact concentrations were not determined) and is significantly Al_2O_3 and TiO_2 poor. Sodium concentration of the melt may be higher than shown due to volatilization of Na by the probe.

Due to the complexities of the sandwich experiments, the melt composition was only determined at 22kb, 1000°C. Additional experiments would be required to document the change in melt composition with pressure, temperature and different source composition (ie, eclogite as suggested by Nelson *et al.*, 1988).

The melt quenches into a series of water-soluble Na-Mg-Ca carbonate minerals plus dolomite. This is similar to natural carbonatite samples which tend to quench into microcrystalline aggregates rather than glass (Cooper *et al.*, 1975), however, the presence of NaMg carbonate minerals is distinctive. Previously only the Na, Ca and Fe-rich carbonate minerals Nyereriete, Fairchildite, Pirsonite and Gregorite, found at Oldoinyo Lengai, have been associated with carbonatites (Cooper *et al.*, 1975; McKie and Frankis, 1977; Dawson *et al.*, 1987).

There has been little previous effort to identify the composition of a primary carbonatite mainly for lack of a suitable natural candidate. Natural carbonatites are rarely erruptive rocks, nor do they have a suitably high Mg#. They commonly display abundant evidence of crystal fractionation and are often obscured by low pressure fenitization processes. In, addition, it has been commonly accepted that carbonatites have formed by silicate-carbonate liquid immiscibility and crystal fractionation (LeBas, 1977) negating the need for identifying a primary carbonatite magma.

Recently, Eggler (1988), after an extensive review of the literature, selected what he believed to be two 'possible' primary carbonatites; the kimberlite-carbonatites of the Saguenay River Valley, Quebec (Mg#>64) from Gittins *et al.*, (1975), and the carbonatites from Fort Portal, Uganda (Mg#59 to 60) from von Knorring and DuBois (1961). Representative analyses are presented in Table 9. Eggler (1988), however, concluded that olivine melilitites or nephelinites are much more plausible as primary magmas.

Twyman and Gittins (1987) have presented a calculated primary carbonatite melt -a mildly alkalic olivine sovite with 8% combined Na_2O plus K_2O. Twyman and Gittins (1987) melt composition was based on adding 8.1% ($Na_2O + K_2O$) to an olivine sovite magma from the Argor intrusion, Ontario (Table 9). The experimental melt from this study differs from their calculated one by having lower Al_2O_3, TiO_2, FeO, and CaO concentrations and higher MgO. P_2O_5 and K_2O are enriched in both compositions.

The natro-carbonatite at Oldoinyo Lengai is commonly described as a parental rather than primary melt. It is however, the only naturally occurring Na-rich carbonatite and therefore a link between primary carbonatite compositions and many carbonatites formed by surficial replacement of Na-carbonate by the more stable Ca-carbonate minerals.

An attempt has been made to determine if there is a relationship between the selected naturally occurring carbonatites and the experimental melt determined in this project. The Ugandan carbonatite is an extrusive volcanic containing fine grains of pyroxene, olivine, biotite, magnetite, ilmentite, apatite and calcite. It is associated with a large fenitization halo (von Knorring and Dubois, 1961). It differs from the experimental primary carbonatite by having lower MgO, Na_2O, and higher CaO, FeO and SiO_2 contents. It is possible that a magma of this type may be near primary, having fractionated MgO in the

Table 9. Comparison between selected natural and experimental carbonatite compositions

	Experimental Carbonatite	Fort Portal Uganda	Saguenay Quebec	Oldoinyo Lengai	Gittins Primary composition	Experimental melt -61%dol,-7%ol -3%sp,-1%il	Experimental melt -20% magnesite +12% cpx
P2O5	0.48	3.32	4.80	1.13	5.92	3.04	0.71
SiO2	2.94	12.99	14.40	<.1	6.56	-	12.83
TiO2	0.45	1.74	2.50	0.01	1.09	-	0.66
Al2O3	1.95	3.03	2.30	0.03	10.66	0.13	2.88
Cr2O3	0.22	-	-	-	-	-	0.32
FeO	4.61	11.58	12.60	0.26	10.66	2.71	9.44
MnO	-	0.40	0.40	-	0.25	-	-
MgO	14.19	8.55	12.90	0.26	3.68	0.26	9.57
CaO	21.29	35.97	26.60	13.93	34.50	16.82	34 21
K2O	0.35	0.20	0.90	6.55	2.41	2.21	0.52
Na2O	4.99	0.73	0.10	30.30	5.74	31.57	7.36
CO2	-	14.79	17.20	33.90	28.17	-	-
Total	51.49	100.62	99.00	89.17	100.00	52.75	78.50

Fort Portal, Uganda, composition from Knorring and DuBois (1961), also includes 3.45% H2O+, 1.65% H2O-
Saguenay River, Quebec, composition from Gittins et al.,(1975), includes 2.9% H2O+, 0.55% BaO and 0.09% Sr
Natrocarbonatite BD118 from Oldoinyo Lengai (Dawson et al.,1987) includes 3.23% SO3, 1.2% F, 4.51% H2O+, 2.45% Cl.

form of olivine and assimilating SiO_2, CaO and FeO in the form of silicates. Loss of Na can be accounted for by low pressure fenitization processes. Calculation of the experimental melt - 20% magnesite + 12% cpx is presented in Table 9. It provides a reasonable approximation to the naturally occurring Ugandan magma if Na is excluded.

The kimberlite - carbonatite occurrence at Saguenay River, Quebec, consists of dykes composed of olivine, phlogopite, apatite, titaniferous magnetite, calcite Ti-salite and Ti-rich pargasite. They are not associated with a fenitization halo (Gittins *et al.*, 1975). This composition, similar to the Ugandan occurrence, may also be related to a primary carbonatite melt by the fractionation of dolomite and contamination by silicate phases. There is, however, no means of explaining the alkali loss, other than fractionation of a Na-Mg carbonate phase at depth. This is an extreme possibility and to date there is little supporting evidence for such a process. It is more likely that the Saguenay River carbonatites are formed by differentiation of a kimberlite, as suggested originally by Gittins *et al.*, (1975).

Due to the precipitation of olivine and dolomite, probable liquidus phases, Mg# does not appear to be a particularly good way of discriminating primary or near primary carbonatite magmas. Unfortunately alkali content is not very useful ether, since most natural carbonatites have lost Na and K during low pressure fenitization processes. Total alkali content rarely exceeds 2 wt% in carbonatites, and where alkalis are present they are bound in the silicate phases amphibole and phlogopite (Heinrich, 1966).

Calculations based on removal of phases from the experimental primary carbonatite melt in order to generate a Na-rich carbonatite such as found at Oldoinyo Lengai are presented in Table 9. Simple fractionation of dolomite (61%), olivine (7%), spinel (3%) and ilmenite (1%) are sufficient to produce an alkali-rich melt composition similar to the natural occurance at Oldoinyo Lengai. Under natural conditions fractionation of other minerals (eg, apatite, magnetite, phlogopite, nepheline or pyrochlore) would be expected. This would produce a wide variety of carbonatite compositions, of which Oldoinyo Lengai would be only one example.

These calculations suggest that Na-carbonatites may form as a result of differentiation of primary dolomitic magma by the fractional crystallization of Mg-rich phases (ol, pyroxenes and dolomite), and thus allowing the concentration of alkali elements. The origin of Ca-Mg rich carbonatites (sovites), on the other hand remains uncertain, they may be generated as deep seated accummulates, derived from a parental composition by loss of

alkalis to aqueous fluids, or form as Ca, Mg-rich immiscible magmas by low pressure kimberlite related processes.

High pressure and temperature crystallization paths of Na-rich dolomitic carbonatite have yet to be studied in order to identify the nature of deep seated cumulates, melt-host rock reaction, and possible eruptive carbonatite compositions. This is particularly important with respect to the variety of Na-Mg carbonate minerals found during this sequence of experiments. These have a similar shape to Nyerereite but different compositions. Their chemistry suggests that Mg-Na solid solutions may be important.

The experimental NaMg-carbonate crystals are the same shape as pseudomorphs described from Homa Montains, Kaiserstuhl, and Fort Portal (Clark and Roberts, 1986; Keller, 1981; Nixon and Hornung 1973), previously described as Nyerereite crystals. Little however is known about these calcite replaced minerals other than that they are tabular on {0001} and contain minor amounts of Na, K, Sr and P. It is likely that a wide range of water-soluble Na-Mg-Ca carbonate minerals are present in natural carbonatites. Phase relationships in the system Na-Mg-Ca in addition to those determined for Na-Ca-K carbonates by Cooper *et al.*, (1975) could provide insights into this problem.

The history from formation to eruption of any particular carbonatite magma is likely to be very complex. A carbonatite may be generated at 930 to 1070°C, 21 to 30 kb by melting of a dolomite-bearing peridotite or by crystallization of amphibole from an H_2O, CO_2-rich basaltic melt. The pressure and temperature range over which primary carbonatites are formed is controlled by bulk-rock compositon and water content. Carbonatite magmas appear to contain little dissolved H_2O, so the bulk of water, if present, must be incorporated in hydrous phases such as amphibole or mica. Na and K are partioned between the hydrous phases, clinopyroxene, and the melt.

Once formed. the melt would only survive if isolated from H_2O-rich fluids. At 22 to 30 kb water-saturation would result in lowering the stability of amphibole, thus incorporating the carbonatite into an ol-melilitite melt by the reaction 'carbonatite + pargasite + opx + gt -> silicate melt + cpx + ol + vapor (Chapter 2).

At pressures below 22 kb, the carbonatite melt would react with opx and olivine forming a clinopyroxene, amphibole and CO_2 rich assemblage (ie, metasomatising lherzolite to a wehrlite assemblage). The carbonatite may only survive this stage by quick upward

migration, possible by such a low viscosity melt, or by extensive country rock metasomatism and consumption of ol and opx, and thus creating a metasomatised envelope or channelway. This feature helps explain why carbonatites are last in the order placement and why they commonly contain apatite inclusions with low density CO_2 (Nesbitt and Kelly, 1977).

Upward melt migration would be a complex process involving crystal fractionation, host-rock alteration, decarbonation, and finally fenitization processes. Upward migration accompanied by fractionation of dolomite would lead to melts with increasing alkali composition. This process has been documented by Twyman and Gittins (1987) using amphibole compositions. They have found that amphiboles from the Argor and Goldray carbonatites, Ontario, are zoned with increasing Na and Fe and decreasing Ca and Mg from core to rim. This feature is compatible with fractionation of dolomite.

Once the magma becomes water-saturated either by crystallization of hydrous phases or reaction with the country rock, the melt will loss its alkali content to aqueous fluids. Low pressure fenetization processes are complex and generally result in the formation of amphibole, mica and feldspar halos surrounding carbonatite complexes and generally obscuring original melt - country rock relationships.

The relationship between alkali rich silicate magmas and carbonatites is related to T, P conditions, source rock compositions and volatile contents. Increasing temperature or water content will result in formation of melilitite magmas rather than carbonatites (Brey, 1975). Increasing pressure will enhance silicate-carbonate liquid immiscibility relationships. Source rock characteristics will play an important role in determining Na-K partitioning relationships. In addition, metasomatism of source rocks by carbonatite magmas may result in a large range of melt compositions.

The occurrence of Oldoinyo Lengai, a highly fractionated Na-rich magma is fortuitous. Its presence is due to the combination of many factors. It is anhydrous and U-Th isotope relationships suggest that it erupted less than 20 years after formation (Williams et al., 1986). The magma was preserved by travelling through a highly metasomatised stockwork system (Dawson, 1966) and finally, it was collected before reacting with the water-table. It is not surprising that examples such as this are extremely rare. The lavas at Oldoinyo Lengai have an evolved alkali-enriched composition that can be directly calculated back to the experimental composition. The Oldoino Lengai carbonatite is however, only one variant of a large range of possible eruptive carbonatite compositions.

This study has not ruled out the possibility that many carbonatites have formed by separation of an immiscible carbonate melt from a carbonated nephelinite magma. It has, however, demonstrated that primary carbonatites are formed under normal oxidized mantle conditions, and has provided another alternative to the currently proposed models on carbonatite genesis.

Conclusions

1) Primary carbonatite melt, coexisting with amphibole-bearing peridotite at 22 kb and 1000°C, is an Na-rich dolomitic carbonatite with a high Mg# (84.5) and low silica content. The melt is enriched in K_2O and P_2O_5, and is Al_2O_3 and TiO_2 poor.

2) The carbonatite melt quenches into an assemblage of dolomite plus water soluble Na, Mg carbonate minerals. The melt is texturally silmilar to naturally occuring carbonatites from Kaiserstuhl and Fort Portal particularly those normally described as containing calcite pseudomorphs of nyerereite crystals.

3) The Na-rich natrocarbonatite composition from Oldoinyo Lengai can be derived from the experimentally determined primary carbonatite compostion by crystal fractionation of dolomite and olivine. This suggests that the Oldoinyo Lengai composition is evolved rather than primary and that it may have fractionated from a mantle derived carbonatite melt rather than have formed as an immiscible segregation from a carbonated nephelinite magma.

4) The experimental confirmation that there are P, T, conditions for derivation of primary Na-rich dolomitic carbonatite from lherzolite does not rule out the possibility that many, naturally occurring carbonatites are derived by carbonate - silicate liquid immiscibility processes, however it poses a good alternative to these currently favoured models of carbonatite genesis.

4. CARBONATE-RICH ULTRAMAFIC XENOLITHS FROM TUMUT-EUCUMBENE TUNNEL, N.S.W.

Introduction

It is widely accepted by petrologists that H_2O and CO_2 are the major volatile species present in an oxidized upper mantle. Experimental studies in the system 'peridotite + H_2O + CO_2' have shown that H_2O is incorporated in the minerals amphibole and phlogopite, present as a fluid component, or dissolved in basaltic melts. This is consistent with observations of natural lherzolitic samples, many of which contain hydrous phases. Experiments have indicated that CO_2 where present, is incorporated in the carbonate minerals dolomite and magnesite, exists as free CO_2 vapor at low pressures, forms part of a carbonatite melt at high pressures and moderate temperatures, or occurs with H_2O as a dissolved species in basaltic melts at high temperatures. In natural samples CO_2 has been readily recognised as the dominant vapor component of fluid inclusions in peridotite xenoliths (Roedder, 1965; Anderson *et al.*, 1984) or as disolved CO_3 in basaltic to melilititic melts. Surprisingly however, very little carbonate material, other than late calcite veins, has been recognised or described from mantle xenoliths.

The few described occurrences of mantle carbonate include that in peridotites from the Colorado Plateau (Smith, 1979; 1987; McGetchin and Besancon, 1973), Spitzbergen (Amundsen, 1987; Amundsen *et al.*, 1987), and Kiama N.S.W. (Wass, 1979; Wass and Rogers, 1980). Carbonate occurances are also reported but not described from Shingu, Japan (Goto and Arai, 1987). Textural criteria suggest that the carbonate is a primary equilibrium phase at Colorado while at Spitzbergen and Kiama it appears to represent remnants of an immiscible carbonatite melt. Additional carbonate ocurrences include kimberlite-related carbonate-rich ocelli or segregations as described from Benfontein (Dawson and Hawthorne, 1973) and brucite-calcite occurrences interpreted to be a late replacement of dolomite (Berg, 1986). Many authors have suggested that the scarcity of carbonate in mantle xenoliths may be the result of an inability to survive ascent in erupting magmas (Eggler 1976; Boyd and Gurney, 1982; Smith, 1987).

The xenolith suite from Tumut-Eucumbene tunnel, N.S.W., is unusual in that the nodules contain abundant pods of carbonate material. The object of this study is to describe the petrology and mineralogy of this suite of xenoliths in order to interprete the origin of the carbonate. It is here suggested that the carbonate pods (composed of dolomite and magnesite) are remnants of an immiscible carbonatitic melt associated with the infiltration of a lherzolitic assemblage by a CO_2 and H_2O-rich basaltic magma.

Locality

The Tumut-Eucumbene locality (Figure 23) has been classified as part of the Snowy Mountains xenolith province in N.S.W. (O'Reilly, 1987). The xenoliths are from a nepheline basanite dyke, of probable Tertiary age, found cutting granite located at the Tumut-Eucumbene Tunnel Station 213, Snowy Mountains, N.S.W. This tunnel was built as part of the Snowy mountain hydro-developement project and is located between 36°05'S, 148°25'E and 36°05'S, 148°35'E. The nepheline basanite intrusion is approximately 8 feet across and composed of massive, fine grained alkali basalt with very abundant rounded inclusions of predominantly peridotite and minor amounts of eclogite and granulite (Lovering and White, 1964).

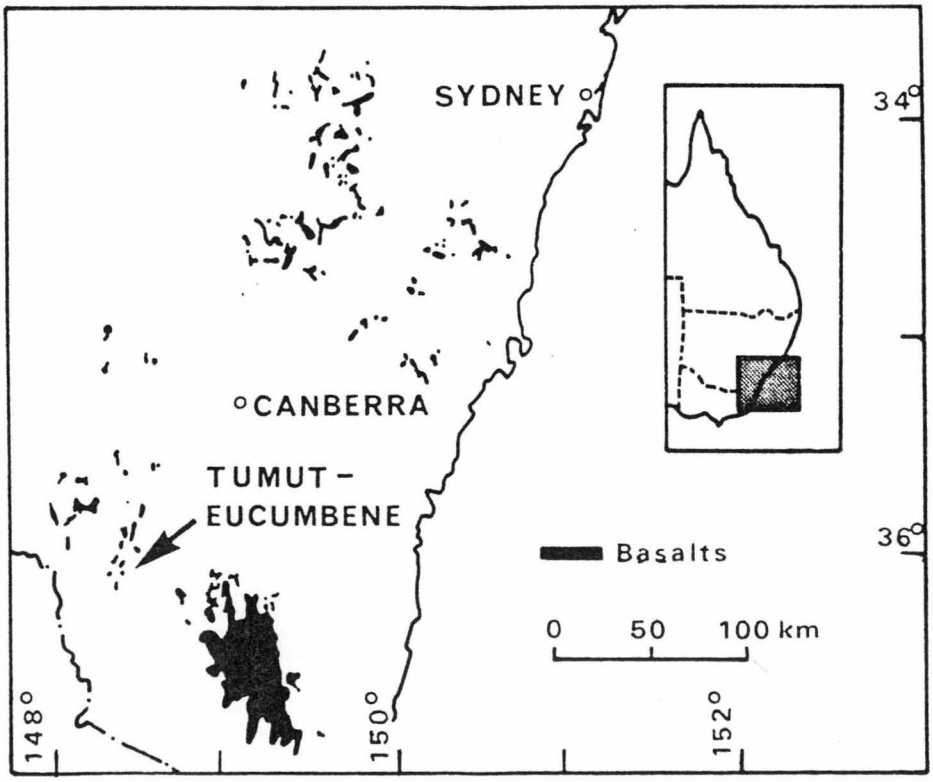

Figure 23. Locality diagram for Tumut-Eucumbene (adapted from Wass and Irving, 1976)

The samples in this study have been cut from 4 large handsamples (samples 46375 to 46378 in the University of Tasmania collection). Altogether 14 distinct nodules were obtained. These xenoliths vary in length from 3 to 12 cm. They are well rounded and the contact between the host lava and xenoliths is sharp. Some xenoliths have been invaded by the host lava but this is in the form of recognisable veins.

Little previous work has been undertaken on the inclusions. Irving (1974) noted that they contain amphibole and provided mineral analyses for a garnet-amphibole websterite (#2825C). Lovering and White (1964) reported that samples in their possession did not contain scapolite. Joplin (1963) listed three bulk rock analyses. The location has been recorded in the Xenmeg catalog (Wass and Irving, 1976).

Petrology

Samples have been classified into the Cr-diopside and Al-augite series suites using the terminology of Wilshire and Shervais (1975). This corresponds to Type I and Type II xenoliths of Frey and Prinz (1978). Textures, grainsize and mineral phases present in the xenoliths are summarized in Table 10.

Cr-diopside series

The sample suite contains four normal (Fe-poor) and six Fe-rich Cr-diopside series xenoliths. The 'normal' samples are spinel lherzolites with equigranular mosaic textures. Olivine mg# ranges from 90.7 to 88.2 (cpx = 93.0-90.8). All of the samples contain ol, opx, cpx, sp and minor amounts of Fe-Ni sulphides. In addition, samples N26B, N24 and N2 contain small mosaic-shaped pods of mixed carbonate material (dolomite and magnesite). Sample N2 is hydrous containing large discrete grains of pargasitic amphibole (mg# 87) and phlogopite (mg# 90). Amphibole and phlogopite do not occur in contact in the sample, suggesting a weak compositional layering.

Fe-rich Cr-diopside samples

The Fe-rich samples vary considerably in terms of texture, grainsize, and modal mineralogy. Olivine mg# ranges from 86.3 to 85.3. In thin section, olivine grains are clear where as orthopyroxene and clinopyroxene grains are cloudy white. It is difficult to optically distinguish orthopyroxene from clinopyroxene in these samples as the clinopyroxene does not display the distinctive light green colour commonly seen in Cr-rich

Table 10 Summary of textures and mineral phases present in xenoliths

Xenolith sample		Phases	Texture	Grain size	Comments
Cr Diopside series					
N26	Spinel lherzolite	Ol,opx,cpx,sp,sulphide	Equi. mosaic	Fine	
N26B	Spinel lherzolite	Ol,opx,cpx,sp,sulphide, carbonate	Equi. mosaic	Fine	-alot of serpentinization
N24	Spinel lherzolite	Ol,opx,cpx,sp,sulphide, carbonate	Equi. mosaic	Medium	-opx exsolving cpx
N2	Spinel lherzolite	Ol,opx,cpx,sp,amph,mica, sulphide,carbonate	Equi. mosaic - tabular	Medium	
Fe-rich samples					
N22	Spinel lherzolite	Ol,opx,cpx,sp,amph, sulphide,carbonate	Equi. mosaic	Medium	-alot of decompression melting, serpentinization
N10	Amph. peridotite	Ol,cpx,sp,amph, sulphide,carbonate	Equi. mosaic	Medium	-grades into amph +apatite vein
N21	Spinel lherzolite	Ol,opx,cpx,sp	Porphyroclastic	Coarse	
N3	Spinel lherzolite	Ol,opx,cpx,gt,sp,amph, sulphide,carbonate	Equi. mosaic - tabular	Medium	-banded
N18	Spinel lherzolite	Ol,opx,cpx,sp,sulphide	Protogranular	Coarse	-contains pyroxenite vein
N7	Spinel websterite	Opx,cpx,sp,amph sulphide,carbonate	Equi. mosaic	Medium	-banded, amph. rich layer
Al Augite series					
N4	Pyroxenite	Opx,cpx,il,amph sulphide,carbonate	Equi. mosaic	Medium	-decompression melting
N21A	Pyroxenite	Opx,cpx,il,amph carbonate	Equi. mosaic	Medium	-melt incursion and decompression melting
N15	Pyroxenite	Opx,cpx,il,amph sulphide,carbonate	Equi. mosaic	Medium	-banded and decompression melting
Granulites					
N26A	Garnet - Clinopyroxenite	Cpx,gt,feld	Equi. mosaic	Medium	

Samples have been listed in order of decreasing Cpx Mg#
Textures according to terminology of Mercier and Nicolas, (1975)
University of Tasmania sample numbers (46375-46378) of xenoliths are presented in Appendix D.

diopside. Spinels are brown and generally form small equigranular crystals. Samples are described below in order of decreasing cpx mg#. (Cpx has been used as a reference since it is the only phase common to all xenoliths.)

N22 (mg# cpx = 88.8), is a medium grained spinel lherzolite with an equigranular mosaic texture. The sample contains abundant amphibole as well as carbonate-rich pods. It is characterized by large amounts of brown coloured glass containing quench crystals of kaersutitic amphibole, spinel and carbonate. The glassy areas are interpreted as having been formed by decompression melting. Decompression melting plus approximately 20% serpentinization has obscured the original textural relationship between the carbonate-rich zones and the host silicate assemblage.

N10 (mg# cpx = 88.4), is an amphibole-rich peridotite which shows a gradual transition from an ol, sp, cpx assemblage (possibly once lherzolitic) to an amphibole, apatite-rich one. This change takes place over approximately 3 cm. Individual grains have an equigranular mosaic shape. Clinopyroxene grains are rare (only 2 small crystals were found over a large thin-section). Orthopyroxene crystals are not present. Amphibole in the olivine rich portion exists as discrete grains rimming spinel. Within the amphibole-rich zone, spinel decreases in abundance and amphibole becomes much larger in size, changing in composition from pargasite to Ti-rich pargasite. Cl-rich apatite grains also become abundant. These are dusty brown in colour and difficult to see in thin-section. They are easily recognisable using cathodoluminescence. The amphibole-rich area contains many carbonate pods and spherical shaped sulphide inclusions.

N21 (mg# cpx = 88.1), is an anhydrous spinel lherzolite with a coarse porphyroclastic texture. It has been classified as an Fe-rich sample because the clinopyroxenes are dusty white in thinsection, and the spinels have an anomalously low $Cr / Cr + Al + Fe^{3+}$ ratio. This sample does not contain carbonate nor any hydrous phases.

N18 (mg#cpx = 85.6), is a composite xenolith of protogranular spinel lherzolite cut by a 12mm wide pyroxenite vein. The contact between the vein and host lherzolite is sharp and apart from slight serpentinization there is no apparent modal change associated with the vein within the host lherzolite. The sample is cut by small late calcite veins. No primary carbonate was visible.

N7 (mg# cpx = 85.5), is an amphibole-bearing spinel websterite which is mineralogically layered. This layering represents varying concentrations of amphibole and clinopyroxene. The sample is medium-grained with an equigranular mosaic texture. No olivine was

present in the thin-section cut. The xenolith contains several small carbonate pods and sulphide spheres.

N3 (mg# cpx = 87.5), is a layered amphibole-rich spinel lherzolite with a medium-grained equigranular mosaic texture. Banding is due to clinopyroxene, amphibole and garnet rich layers. Sample N3 is the only xenolith of the Cr-diopside suite which contains garnet. No spinel was found. Minor sulphide and carbonate material are present.

The most unusual and distinctive feature of this nodule suite is the occurrence of carbonate veins and pods and their associated sulphide globules. Four types of carbonate material were found; 1) small dolomite - magnesite pods, 2) large magnesite - talc pods, 3) rare siderite and 4) late calcite viens. These are described below. Representitve samples are illustrated in Figure 24.

Small dolomite/magnesite pods occur in six of the samples (N26B, N24, N2, N3, N10, and N7). These carbonate pods are between 0.1 and 0.4 mm in size and consist of roughly equal proportions of dolomite and magnesite. They often, but not always, contain a small spherical shaped bleb of Fe-Ni-sulphide. The carbonate pods are sometimes surrounded by a small rim of talc. They do not appear to be related to the presence of amphibole nor any other phase. These pods are also unusual as they are anhedral with curvilinear margins and 120° triple point junctions with adjacent phases (Figure 24). This overall shape is usually indicative of textural equilibrium.

Large magnesite/talc pods are present in samples N22, N10, N2, and N7. They range in size from 0.2 mm to 2 mm and are quite irregular in shape. They consist predominantly of magnesite and talc. The magnesite is zoned becoming more Fe-rich towards the edge of the pods. The pods have a broad rim of fine grained silicates. These crystals are too small to provide single crystal analyses, but appear to be predominantly amphibole and clinopyroxene. Most pods contain Fe-Ni sulphide globules which have exsolved into pyrrhotite and pentlandite-rich phases. Sulphides are not found as interstitial phases or enclosed within the major silicate phases (except within the amphibole apatite vein of sample N10) as commonly seen in sulphide rich xenoliths (Frick, 1973; Dewaal and Calk, 1975; Dromgoole and Pasteris, 1987). They are only found within the carbonate-rich areas. Silicate grains adjacent to carbonate pods have disaggregated crystal rims and contain abundant fluid inclusions.

Rare siderite was found in sample N7. The siderite occurs in two small pods with dolomite and magnesite. It is not considered to be part of an equilibrium assemblage.

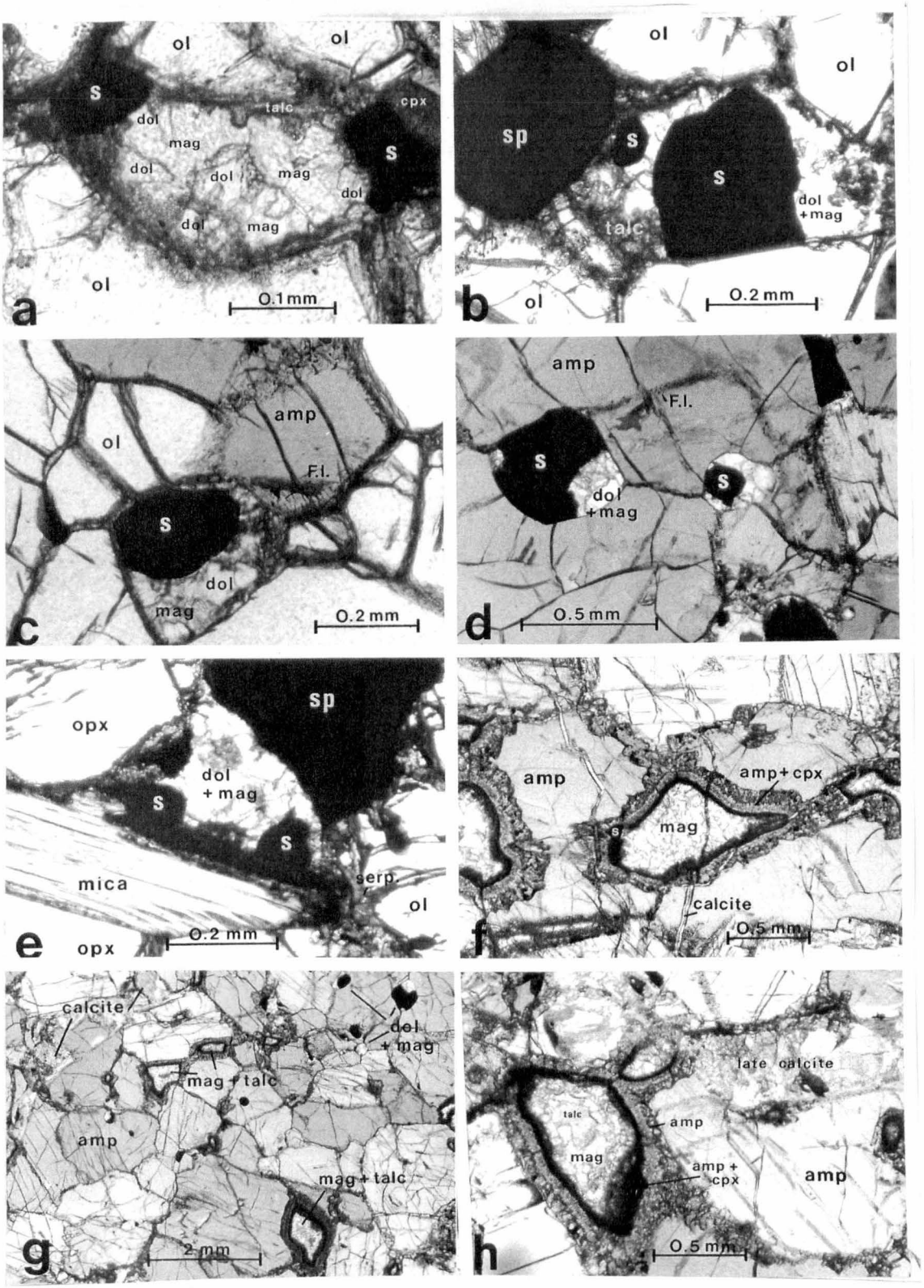

Figure 24. Thinsection photomicrographs of carbonate pods in Tumut - Eucumbene xenoliths. a, b) Small carbonate pods in sample N3. Note coexisting dolomite (dol) and magnesite (mag), and the characteristic sulphide spheres (s). Small carbonate pods are often surrounded by fine rim of talc. c, d) Small carbonate pods in sample N10. Note the abundant trains of fluid inclusions in amphibole crystals. e) Small carbonate pod in sample N2. f, g, h) Large magnesite - talc pods in sample N10. Carbonate pods are rimmed by fine crystals of amphibole and clinopyroxene. Surrounding amphibole grains contain abundant fluid inclusions. Magnesite pods are cut by late calcite veins.

Calcite veins are the youngest feature observed in the nodules. They crosscut both the large magnesite-talc pods and the nodule-basanite boundaries. These veins are very irregular in shape due to their tendency to migrate along grain boundaries. They appear to be associated with the transporting magma.

Al-augite series

Three pyroxenite xenoliths were present in the samples cut. These are websterites containing approximately equal amounts of ortho and clinopyroxene. They have medium-grained equigranular mosaic textures. There are no visible igneous microstructures. Ti-rich pargasitic amphiboles are present in all of the samples. The opaque phase is titaniferous magnetite and is green in color. All samples contain abundant brown glassy irregular shaped zones. These are interpreted as resulting from decompression melting of the amphibole and carbonate-rich areas. Amphiboles bordering the glass have red kaersutitic rims and the glass contains a quench assemblage of amphibole, clinopyroxene, carbonate and ilmenite.

Sample N15 is banded with an amphibole rich layer containing abundant sulphide grains. The sulphides are large, have euhedral shapes and appear to be in textural equilibrium with the silicate assemblage. All of the Al-augite series samples contain carbonate-rich areas. These have a very random shape due to decompression melting and reaction with the host assemblage.

Granulite

Sample N26A is an atypical sample consisting of cpx (mg# 92.3), gt, and sodic plagioclase. It has a medium grained equigranular mosaic texture and the garnets have kelyphite rims. There are no visible carbonate pods or sulphides in this sample, but it has been cut by late calcite veins. The presence of both Na-rich plagioclase and garnet indicates that the sample comes from a high temperature and pressure region, either the lower crust or upper mantle.

Mineral Chemistry

Mineral analyses of the silicate phases are presented in Table 11.

Olivines

Olivines display a wide range in chemical composition with Mg# ranging from $Fo_{85.4}$ to $Fo_{90.7}$ thus enabling two groups of samples, Fe-rich and Fe-poor, to be recognised

Table 11. Representative analyses of xenolith phases. 11a, Olivines, Eucumbene Tunnel

	N26	N26B	N21	N24	N2	N18	N10	N22	N3
SiO2	40.72	40.51	40.47	40.22	40.40	40.18	40.17	39.57	39.85
FeO	9.07	9.53	11.29	11.55	11.39	13.30	13.11	14.15	14.07
NiO	0.50	0.80	0.35	0.33	0.39	-	0.38	0.33	-
MgO	49.70	49 16	47.89	47.91	47.83	46.52	46.35	45.95	46.08
Total	100.00	100.00	100.00	100.00	100.00	100.00	100.00	100.00	100.00
Si	0.9962	0.9947	0.9990	0.9944	0.9980	0.9994	0.9999	0.9909	0.9954
Fe	0.1856	0.1958	0.2330	0.2388	0.2353	0.2767	0.2730	0.2964	0.2938
Ni	0.0099	0.0158	0.0070	0.0065	0.0077	-	0.0075	0.0066	-
Mg	1.8121	1.7991	1.7620	1.7658	1.7610	1.7245	1.7197	1.7152	1.7153
Total	3.0038	3.0053	3.0010	3.0055	3.0020	3.0006	3.0001	3.0091	3.0046
Mg#	90.7	90.2	88.3	88.1	88.2	86.2	86.3	85.3	85.4

Table 11b Orthopyroxenes, Eucumbene Tunnel

	Cr-diopside series									Al-augite series		
	N26	N26B	N2	N21	N24	N18	N3	N18 vein	N7	N4	N21A	N15
SiO2	56.53	56.03	55.95	55.16	56.09	55.09	55.60	54.86	54.39	54.03	53.88	53.89
TiO2	-	-	-	-	-	0.23	-	0.32	0.18	-	-	-
Al2O3	2.39	2.99	1.78	4.77	3.02	4.51	3.23	4.43	3.67	3.37	2.68	2.51
Cr2O3	0.42	0.25	0.31	0.20	0.25	-	-	-	0.25	-	-	-
FeO	5.76	6.21	7.19	7.09	7.52	8.74	9.65	9.03	11.23	13.50	13.68	14.52
MgO	34.62	34 20	33 47	32.82	33.63	31.90	31.20	31.33	30 48	29.44	28.57	28.05
CaO	0.28	0.32	0.34	0.60	0.35	0.87	0.32	1.04	0.38	0.40	0.46	0.37
Total	100.00	100.00	99.03	100.64	100.86	101.33	100.00	101.01	100.58	100.74	99.26	99.34
Si	1.9436	1.9304	1.9554	1.8970	1.9273	1.8966	1.9414	1.8984	1.9077	1.9113	1.9357	1.9413
Ti	-	-	-	-	-	0.0059	-	0.0083	0.0047	-	-	-
Al	0.0969	0.1214	0.0732	0.1932	0.1224	0.1830	0.1330	0.1807	0.1519	0.1404	0.1134	0.1065
Cr	0.0114	0.0069	0.0086	0.0055	0.0068	-	-	-	0.0069	-	-	-
Fe	0.1655	0.1788	0.2101	0.2038	0.2160	0.2516	0.2818	0.2613	0.3295	0.3993	0.4110	0.4374
Mg	1.7742	1.7560	1.7437	1.6822	1.7224	1.6370	1.6238	1.6159	1.5933	1.5523	1.5300	1.506
Ca	0.0105	0.0119	0.0127	0.0220	0.0130	0.0319	0.0121	0.0384	0.0143	0.0152	0.0176	0.0142
Total	4.0022	4.0054	4.0037	4.0037	4.0080	4.0060	3.9921	4.0029	4.0083	4.0185	4 0076	4.0054
Mg#	91.5	90.8	89.2	89.2	88.9	86.7	85.2	86.1	82.9	79.5	78.8	77.5
Ca	0.5	0.6	0.6	1.2	0.7	1.7	0.6	2.0	0.7	0.8	0.9	0.7
Mg	91.0	90.2	88.7	88.2	88.3	85.2	84.7	84.4	82.3	78.9	78.1	76.9
Fe	8.5	9.2	10.7	10.7	11.1	13.1	14.7	13.6	17.0	20.3	21.0	22.3

Table 11c. Clinopyroxenes, Eucumbene Tunnel

	Cr-diopside series											Al-augite series			Granulite
	N26	N26B	N24	N2	N22	N10	N21	N3	N7	N18	N18 vein	N4	N21A	N15	N26A
SiO2	53 91	54.25	53 21	53 96	51.77	53 95	51 65	51 80	50 88	51.73	51 51	50 89	51 33	51.52	51 00
TiO2	0 17	-	0 39	-	0 49	0.25	0 64	0.65	0 89	0.64	1 03	0 65	0 60	0 54	0 40
Al2O3	3 58	4.03	4 10	2 73	5 69	5 22	6 73	5 59	4 90	6 06	6 12	5 19	4 61	4 13	11 31
Cr2O3	1 13	0 87	0.52	0 95	1.27	0 92	0 75	0 40	0 53	0 64	0 42	0 24	0 34	0.24	0 44
FeO	2 17	2 57	2 88	2 92	3 56	3 45	3 86	3 79	4 45	4 82	5 26	5 92	6 34	6 39	1 95
MgO	16 10	16 25	16 30	16 24	15 74	14 73	16 03	14 86	14 78	16 05	16 37	14 21	14 52	14 27	13 08
CaO	21 87	21 93	23 00	22 31	20 33	20 14	18 97	21 66	22 10	19 27	18 49	21 60	20 78	21 34	22 26
Na2O	1 26	1 03	0 58	0 88	1 13	2 18	1.37	1 04	0 51	1.21	1 14	0 82	1 12	0 99	1 51
Total	100 18	100 94	100 96	100 00	100 00	100 84	100 00	99 80	99 05	100 42	100 34	99.52	99 64	99 42	101 96
Si	1 9461	1 9429	1 9144	1.9587	1 8806	1 9367	1 8690	1 8895	1 8807	1 8736	1 8662	1 8815	1 8965	1 9095	1 8048
Ti	0 0047	-	0.0105	-	0 0135	0 0068	0 0174	0 0179	0 0248	0 0176	0 0281	0 0182	0 0166	0 0152	0 0107
Al	0 1525	0 1702	0 1737	0 1169	0 2437	0 2208	0 2868	0 2403	0 2135	0.2585	0 2613	0 2261	0 2005	0 1805	0 4716
Cr	0 0321	0 0246	0 0147	0 0273	0 0366	0 0262	0 0213	0 0115	0 0156	0 0182	0.0120	0 0069	0 0100	0 0070	0 0123
Fe	0 0654	0 0771	0 0865	0 0886	0 1080	0 1037	0 1169	0 1157	0 1376	0 1461	0 1593	0 1830	0 1959	0 1981	0 0578
Mg	0 8661	0 8674	0 8741	0 8789	0 8524	0 7881	0 8644	0 8082	0 8144	0 8664	0 8841	0 7832	0 7994	0 7882	0 6896
Ca	0 8461	0 8416	0 8865	0 8677	0 7913	0 7747	0 7356	0 8467	0 8751	0 7476	0 7178	0.8555	0 8226	0 8476	0 8437
Na	0 0879	0 0717	0 0408	0 0621	0 0799	0 1517	0 0963	0 0734	0 0365	0 0851	0 0803	0 0586	0 0805	0 0711	0 1038
Total	4 0008	3 9955	4 0013	4 0002	4 0058	4 0088	4 0077	4 0033	3 9982	4 0130	4 0092	4 0131	4 0219	4.0171	3.9944
Mg#	93.0	91 8	91 0	90 8	88 8	88 4	88 1	87 5	85 5	85 6	84 7	81 1	80 3	79 9	92 3
Ca	47 6	47 1	48 0	47 3	45 2	46 5	42 8	47 8	47 9	42 5	40 8	47 0	45 3	46 2	53 0
Mg	48 7	48 6	47 3	47 9	48 7	47 3	50 3	45 6	44 6	49 2	50 2	43 0	44 0	43 0	43 3
Fe	3 7	4 3	4 7	4 8	6 2	6 2	6 8	6 5	7.5	8 3	9 0	10 0	10 8	10 8	3 6

Table 11d. Amphiboles, Eucumbene Tunnel

										Mica	Apatite	Gt	Feldspar	
	N2	N10	N10 vein	N22	N3	N7	N4	N21A	N15	N2	N10 vein	N3	N26A	N26A
P2O5	-	-	-	-	-	-	-	-	-	-	38 85	-	-	-
SiO2	42 12	43 37	42 96	44 22	41 76	41 08	42 19	42 16	42 07	37 99	2 06	41 78	42 05	56 01
TiO2	0 73	1 94	3 10	0 83	2 29	3 20	2 18	2 32	2 58	1 22	-	-	-	-
Al2O3	12 78	14 50	15 13	12 73	14 62	14 44	13 84	13 79	13 45	15 56	-	23 56	23 99	28 78
Cr2O3	1 54	1 27	-	2 01	0 42	0 42	0 28	0 49	0 42	0 93	-	0 22	0 27	-
FeO	4 59	5 06	5 35	5 90	5 94	6 92	8 87	9 27	9 81	4 36	0 35	12 91	7 50	-
MgO	17 21	17 00	16 45	17 49	16 81	14 93	15 89	15 63	14 48	21 99	1 22	17 29	18 91	-
CaO	10 82	10 39	10 37	10 33	11 23	11 62	10.92	10 72	11 06	-	49 60	5 41	7 56	10 49
K2O	1 32	0 66	0 66	0 78	0 31	1 85	0 18	0.25	0 90	8 96	-	-	-	0 24
Na2O	2 50	3.76	3 76	3 67	3 35	1 98	3 07	3 56	2 91	0 51	1 16	-	-	5 11
Cl	-	0 08	-	-	-	-	-	-	-	-	1 43	-	-	-
MnO	-	-	-	-	-	-	-	-	-	-	-	0 78	-	-
Total	93 62	98 05	97.78	97 95	96 72	96 45	97.42	98 18	97 68	91 51	94 68	101 95	100 27	100 64
P										-	1 3825	-	-	-
Si	6 2855	6 1728	6 1178	6 3291	6 0485	6 0340	6 1273	6 1019	6 1508	5 8624	0 0866	2 9754	2 9791	2 4997
Ti	0 0822	0 2079	0 3318	0 0889	0 2493	0 3530	0 2384	0 2522	0 2831	0 1415	-	-	-	-
Al	2 2585	2 4328	2 5403	2 1469	2 4955	2 4994	2 3688	2 3517	2 3171	2 8293	-	1 9777	2 0029	1 5139
Cr	0.1821	0 1434	-	0 2271	0 0477	0 0484	0 0320	0 0566	0 0488	0 1135	-	0 0123	0 0154	-
Fe	0 5733	0 6027	0 6372	0 7068	0 7198	0 8503	1 0778	1 1216	1 1996	0 5622	0 0124	0 7691	0 4442	-
Mg	3 8276	3 6072	3 4918	3 7309	3 6286	3 2687	3 4409	3 3716	3 1555	5 0571	0 0767	1 8356	1 9965	-
Ca	1 7302	1 5850	1 5819	1 5840	1 7420	1 8289	1 6998	1 6632	1.7316	-	2 2342	0 4126	0 5735	0 5017
K	0 2514	0 1199	0 1198	0 1428	0.0564	0 3471	0 0326	0 0468	0 1680	1 7647	-	-	-	0 0138
Na	0 7232	1 0387	1 0390	1 0190	0 9414	0 5648	0 8648	0 9986	0 8248	0 1523	0 0942	-	-	0 4419
Cl	-	0 0197	-	-	-	-	-	-	-	-	0 1022	-	-	-
Mn	-	-	-	-	-	-	-	-	-	-	-	0 0469	-	-
Total	15 9041	15 9300	15 8595	15 9756	15 9293	15 7948	15 8824	15 9643	15 8793	16 4830	3 9888	8 0295	8 0116	4 9711
Mg#	87 0	85 7	84 6	84 1	83 4	79 4	76 1	75 0	72 5	90 0	86 1	70 5	81 8	-
Ca	28 2	27 4	27 7	26 3	28 6	30 7	27 3	27 0	28 4	0 0	96 2	13 7	19 0	Ca = 62 4
Mg	62 4	62 2	61 1	62 0	59 6	55.0	55 3	54 8	51 8	90 0	3 3	60 8	66 2	Na = 46 2
Fe	9 4	10 4	11 2	11 7	11 8	14 3	17 3	18 2	19 7	10 0	0 5	25 5	14 7	K = 1 4

Table 11e, Spinels, Eucumbene Tunnel

	N26	N26B	N24	N2	N21	N3	N10	N7	N18	N10 vein	Titaniferous magnetites N4	N21A	N15
TiO2	-	-	0 24	0 35	0 47	-	-	0 55	0 80	-	42 64	46 05	43 79
Al2O3	39 62	48 15	51 12	27 95	56 57	59 15	47 13	46 47	50 42	65 74	1 31	1 06	0 99
Cr2O3	28 43	19 11	13 96	33 90	8 82	5 00	18 20	14 34	10 96	0.53	0 77	0 72	0 85
FeO	14 96	13 26	15.97	23 85	14 10	16 69	17.12	23 61	18 67	12 87	49 99	45 36	45 76
NiO	-	0 34	-	-	0 54	-	0 37	0.34	0 37	-	-	-	-
MgO	17 64	19 14	18 71	13 38	21 13	19 16	17.18	14 69	18 80	20 86	5 30	6 80	5 64
Total	100 65	100.00	100 00	99 43	101.64	100 00	100 00	100 00	100 01	100 00	100 00	100 00	97 03
Ti	-	-	0 0047	0 0079	0 0090	-	-	0.0115	0 0161	-	1 1463	1.2293	1 2132
Al	1 2973	1 5235	1 6038	0 9893	1 6990	1 8000	1 5127	1 5152	1 5829	1 9527	0 0551	0 0444	0 0428
Cr	0 6245	0 4056	0 2939	0 8049	0 1776	0 1020	0 3919	0 3136	0 2309	0 0107	0 0218	0 0202	0 0248
Fe2+	0 3399	0 2908	0 3463	0 5801	0 2901	0.3507	0 3803	0 5314	0 4005	0 2664	1 3222	1 1856	1 2467
Fe3+	0 0078	0 0071	0 0093	0 0190	0 0105	0 0098	0 0095	0 0148	0 0154	0 0049	0 1723	0 1608	0 1630
Ni	-	0 0074	-	-	0 0111	-	0 0084	0 0077	0 0078	-	-	-	-
Mg	0 7305	0 7657	0 7422	0 5989	0 8026	0 7375	0 6974	0 6059	0 7465	0 7836	0 2823	0 3597	0 3095
Total	3 0000	3 0000	3 0000	3 0000	3 0000	3 0000	3 0000	3 0000	3 0000	3 0182	3 0000	3 0000	3 0000
Mg#	67 8	72 0	67 6	50 0	72 8	67 2	64 1	52 6	64 2	74 3	15 9	21 1	18 0
Cr#	32 5	21 0	15 5	44 9	9 5	5 4	20 6	17 1	12.7	0 5	28 3	31 3	36 6

Table 11f, Carbonates

	N2 Dol	Mag	N3 Dol	Mag	N10 Mag	Mag	Mag(Mg)	Mag(Fe)	N7 Siderite	Dolomite	Magnesit	N18 Calcite	N7 Fe-calcit
SiO2	0 64	0 22	0 46	0 16	1 10	0 29	1 24	-	0 26	-	-	0 73	0 22
Al2O3	0 18	0 21	0 19	0 25	0 26	0 51	0 30	0 19	0 35	-	0 24	-	-
FeO	1 69	8 70	3 97	8 54	5 73	12 06	-	34 82	35 11	6 23	11 57	-	1 41
MnO	-	-	-	-	-	-	-	0 39	0 46	-	-	-	0 44
MgO	19 95	37 15	20 59	26 81	39 00	36 35	38 80	21 60	16 89	16 72	37 60	-	6 91
CaO	28 60	1 71	24 41	1 44	1 19	0 43	0 59	0 50	3 68	28 10	0 94	54 04	43 89
													SO3=0 19
Total	51 06	47 99	49 62	47 20	47 28	49 64	40 93	57 50	56 74	51 04	50 34	54 77	53 06
	Cations/6 oxygens												
Si	0 0600	0 0205	0 0452	0 0153	0 0987	0 0262	0 1209	-	0 0264	-	-	0 0736	0 0218
Al	0 0202	0 0228	0 0223	0 0271	0 0273	0 0547	0 0346	0 0219	0.0408	-	0 0250	-	-
Fe	0 1328	0 6686	0 3247	0 6660	0 4303	0 9143	-	2 7945	2 9360	0 5190	0 8646	-	0 1187
Mn	-	-	-	-	-	-	-	0 0313	0 0387	-	-	-	0 0377
Mg	2 7887	5 0882	2 9971	5 1184	5 2166	4 9098	5 6441	3 0899	2 5168	2 4820	5 0081	-	1 0338
Ca	2 8744	0 1679	2 5543	0 1441	0 1146	0 0413	0 0621	0 0512	0 3944	2 9988	0 0896	5 8526	4 7211
													SO3= 013
Total	5 8760	5 9680	5.9435	5 9710	5 8875	5 9463	5 8619	5 9889	5 9530	5 9998	5 9873	5 9262	5 9466
Mg#	95 5	88 4	90 2	88 5	92 4	84 3	100 0	52 5	46 2	82 7	85 3	-	89 7
Ca	49 6	2 8	43.5	2 4	2 0	0 7	1.1	0 9	6 7	50 0	1.5	100 0	80 4
Mg	48 1	85 9	51.0	86 3	90 5	83 7	98 9	52 1	43 0	41 4	84 0	0 0	17 6
Fe	2 3	11 3	55 5	11 2	7 5	15 6	0 0	47 1	50.2	8 6	14 5	0 0	2 0

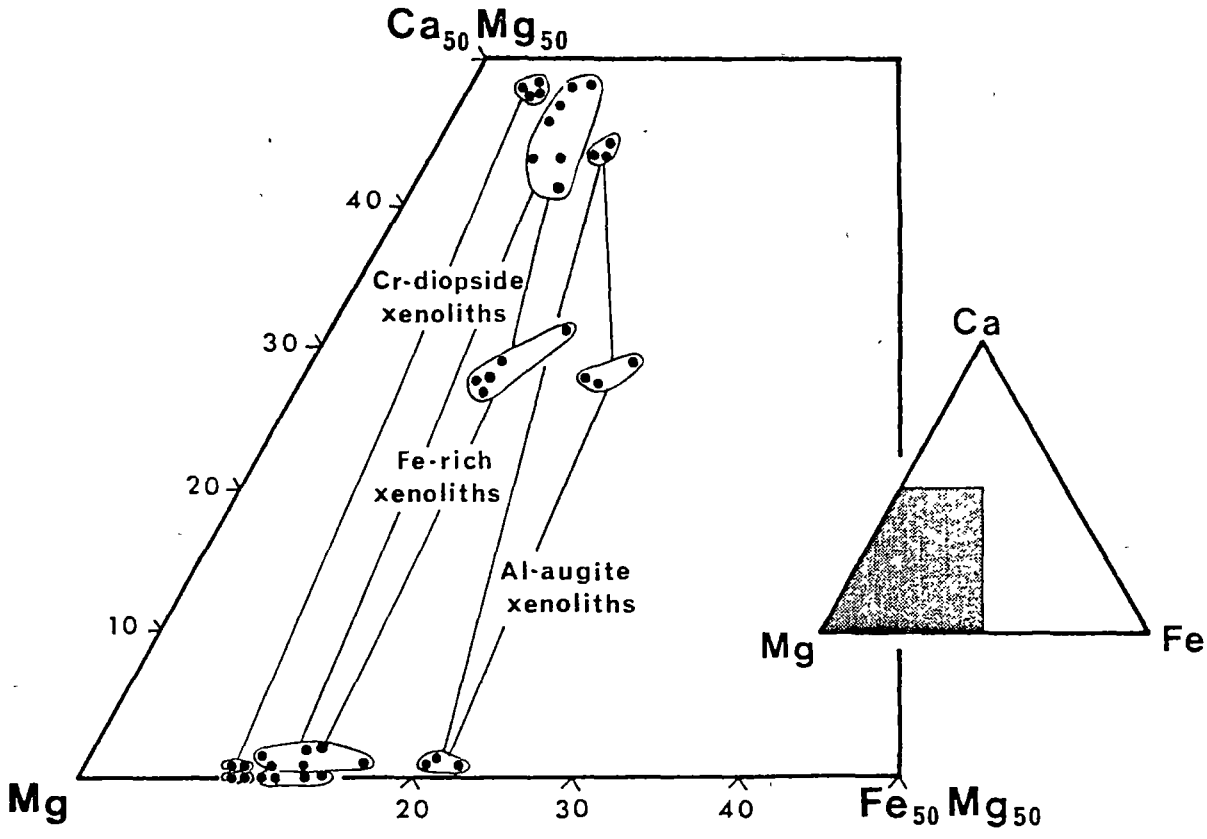

Figure 25. Composition of silicate phases in Tumut-Eucumbene xenoliths

within the Cr-diopside series xenoliths. Fe-poor samples have Mg# ranging from 88.2 to 90.7 and olivines in Fe-rich samples have Mg# between 85.4 and 88.2. These divisions appear to reflect an unusual enrichment in Fe rather than a depletion of Mg. Similar relationships are present in co-existing ortho and clinopyroxenes (Figure 25). NiO values range from 0 to 0.9wt% and increase with Mg#. Hydrous phases occur predominantly within the Fe-rich Cr-diopside series xenoliths.

Pyroxenes

Orthopyroxenes in the Cr-diopside suite xenoliths have Mg#'s ranging from 91.5 to 82.9 (enstatite to bronzite). These Mg#s are slighly higher than the olivine values (Figure 25). Orthopyroxenes in the pyroxenite samples range from Mg# 79.5 to 77.5 . Fe-series orthopyroxenes contain higher Al and lower Cr concentrations than those in the Fe-poor Cr-diopside series. Orthopyroxenes in sample N18 have high Ca and Ti cation abundances suggesting that the pyroxenite vein cutting the sample intruded at high temperatures, the high Ti reflecting an origin from a crystallising basaltic magma.

Clinopyroxenes have Mg# ranging from 90.8 to 93.0 in the Cr-diopside series, 85.5 to 88.8 in the Fe-rich Cr-diopside series and 79.9 to 81.1 in the Al-augite series. Figure 26 indicates that along with Fe, cpx's in the Fe-rich Cr-diopside suite have unusually high cation abundances of Al, Ti and are slightly higher in Na. This is accompanied by depletion in Cr, Mg, and Si. The banded samples N7 and N3 show the highest level of Fe and Ti enrichment and Cr depletion.

Amphiboles

Amphiboles range from pargasite to kaersutite (Figure 27) and have Mg#'s ranging from 70 to 88. All samples have a high Na content. Xenoliths N2 and N22 contain pargasites which have compositions similar to amphiboles in chemical equilibrium with a lherzolitic assemblage (high Cr, low Ti). Sample N2 has a particularly high K concentration, but not unexpected for an amphibole in equilibrium with phlogopite (Chapter 1). Amphiboles in samples N3, N7 and N10 contain a high tschermakite component, and as such do not resemble part of an equilibrium mantle assemblage. They are most likely part of an introduced secondary assemblage which has yet to arrive at complete chemical equilibrium with the host.

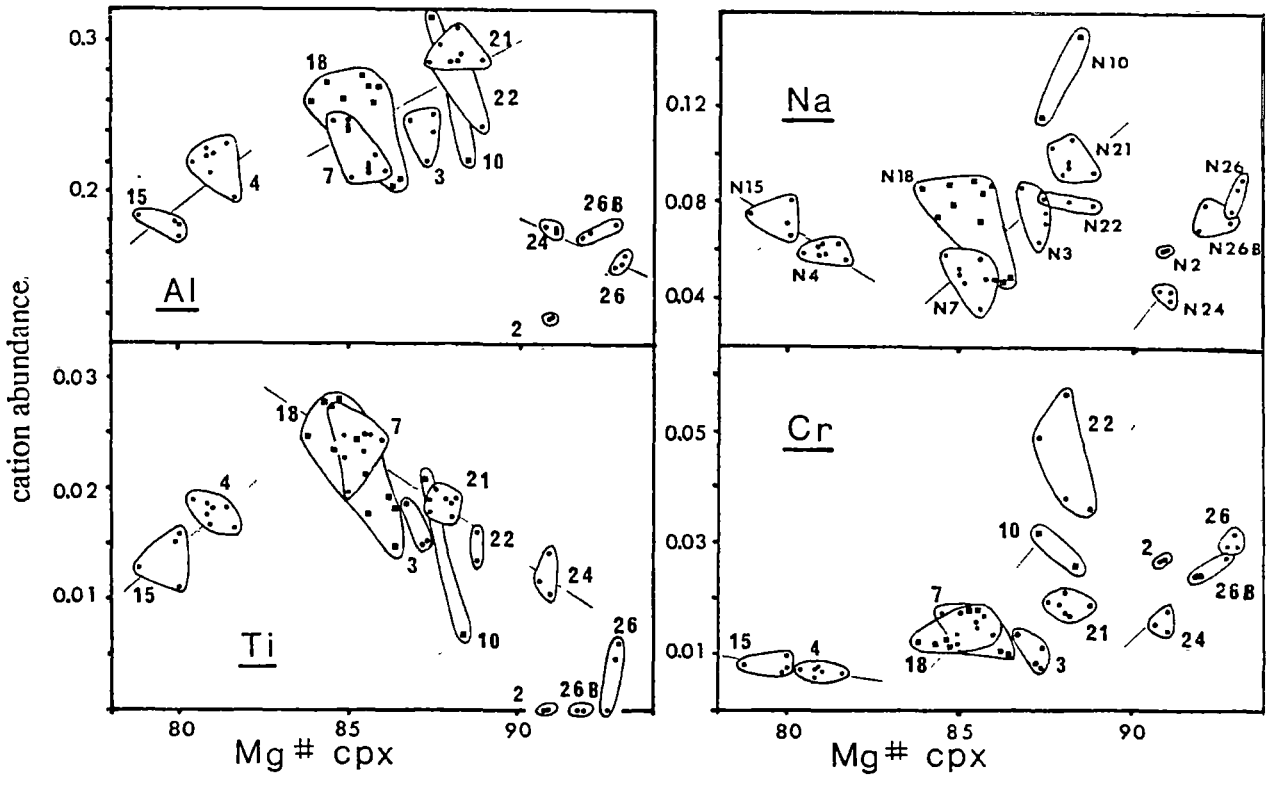

Figure 26. Clinopyroxene compositions of Tumut-Eucumbene xenoliths

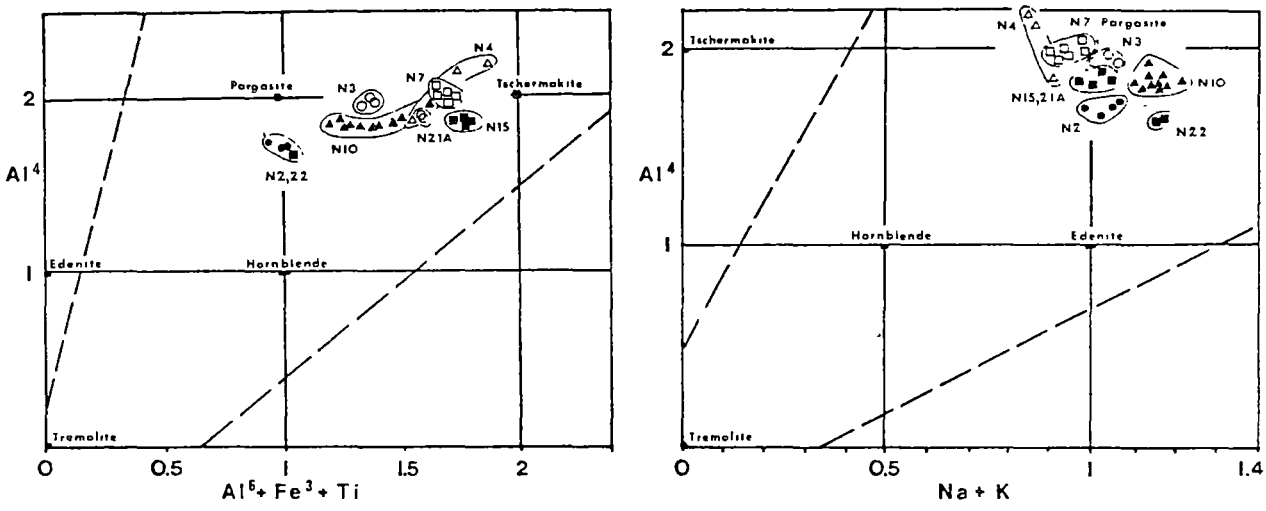

Figure 27. Amphibole composition of xenoliths

Sample N10 contains amphiboles which range from Ti-rich pargasite in the host peridotite assemblage to an almost kaersutitic composition in the amphibole-apatite rich area. This is a feature commonly associated with amphibole veined lherzolites (Wilshire *et al.*, 1980). Samples N15, N21A, N4 contain Ti-rich pargasitic amphiboles with compositions similar to those normally found in Al-augite series rocks. Sample N4

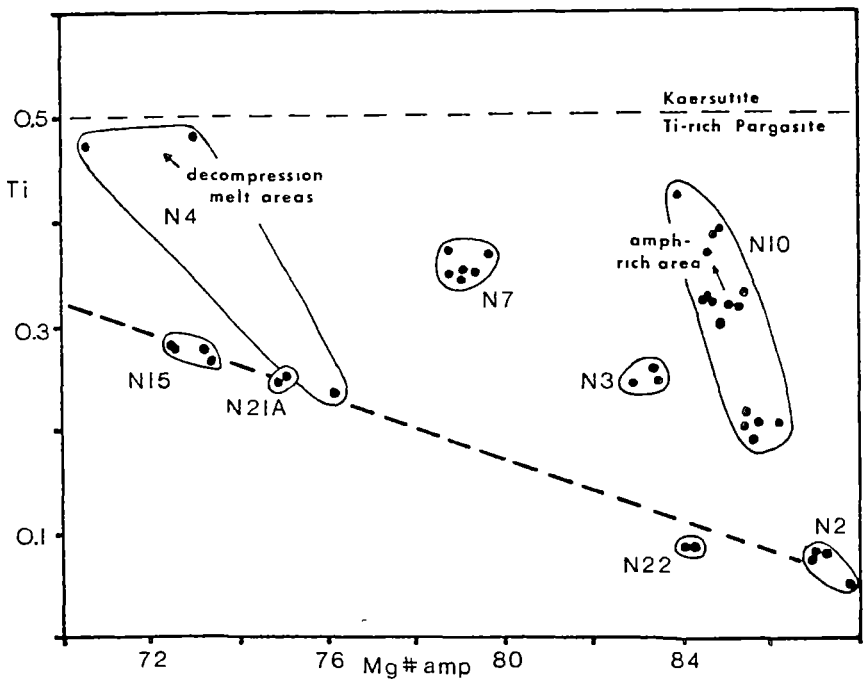

Figure 28. Ti cations vs Mg# of xenolith amphiboles

contains many amphiboles which have been altered by decompression melting. (Amphibole analyses from red colored amphibole rims have low Mg#s and are kaersutitic, Figure 28). Small amphibole phenocrysts precipitating out of the decompression melt areas have even more extreme compositions; they are true kaersutites with Mg#'s between 60 and 65.

Spinels,

Spinels are present in all the Cr-diopside series nodules. They are Mg-Cr rich spinels with Mg# ranging between 50 and 74 and Cr# between 0 and 45. All samples are slightly oxidized with a small Fe^{3+} component (Figure 29). The spinels show increasing Cr# with decreasing Mg#. The xenoliths can be divided into three groups; 1) Cr-diopside series

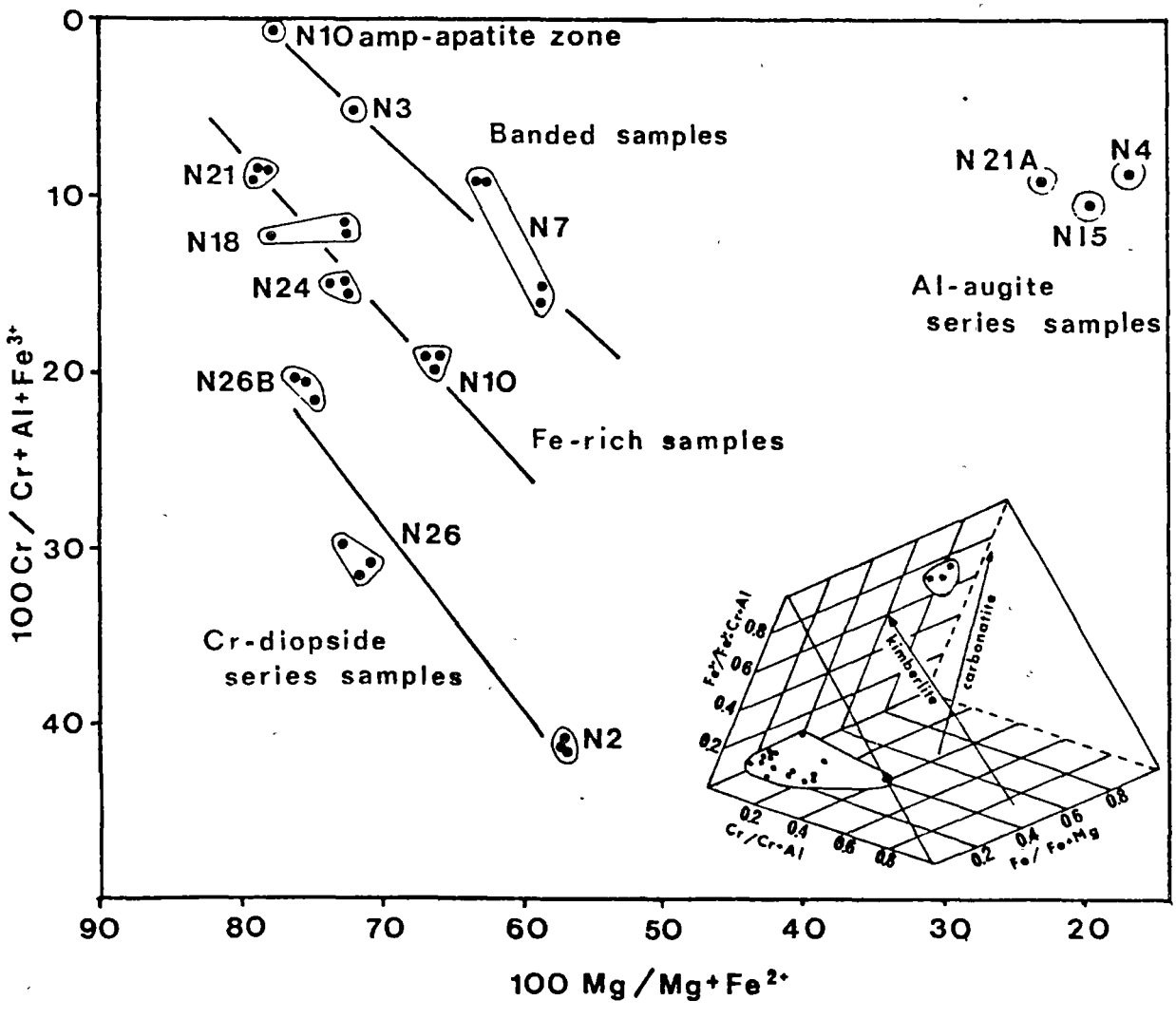

Figure 29. Spinel compositions of xenoliths

(N2, N26, N26B) which contain high Cr#/Fe# (=1.1 to 0.86) spinels, 2) Fe-rich Cr-diopside series which have intermediate Cr#/Fe# spinel ratios (0.4-0.6), and 3) banded samples N7, N3, and the N10 amphibole apatite-rich area which contain spinels with low Cr#/Fe# ratios (0.0-0.2). This division appears to reflect Al enrichment and Cr-depletion in the Fe-rich samples and extreme modification in the spinels from the banded samples. The relationship is contrary to that described from samples in which amphibole has formed at the expence of spinel. These spinels normally have high Cr and low Al abundances (Griffin *et al.*, 1984).

Carbonate,

Magnesite and dolomite compositions have been summarized in a $CaCO_3$-$MgCO_3$-$FeCO_3$ tertiary diagram (Figure 30). Four types of carbonate are present; small dolomite- magnesite pods, large magnesite-talc pods, rare siderite and late calcite. The small pods consist of magnesite (Mg# 82 to 98) and dolomite (Mg# 91 to 99) pairs. Mineral compositions are homogeneous within pods, but compositions of the pods vary

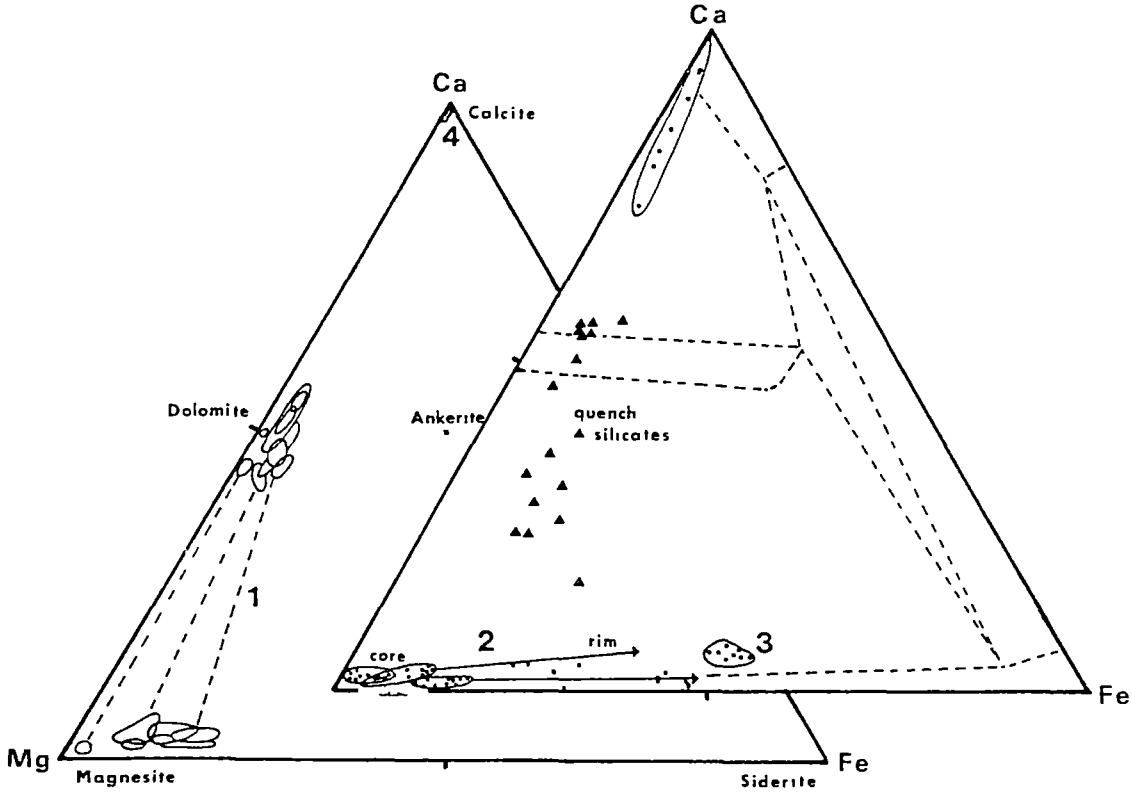

Figure 30. Composition of carbonate phases in xenoliths. 1 = small dolomite-magnesite pairs, 2 = large magnesite-talc pods, 3 = rare siderite, 4 = late calcite veins. - - - - phase relationships of carbonates at ~600°C and 15kb from Anovitz and Essene (1987).

within any thin-section. The high Mg# of the carbonate suggests that the pods are in approximate chemical equilibrium with the silicate assemblage. The presence of two carbonate minerals, however, suggests that the carbonate behaves as a discrete immiscible phase. Dolomite plus magnesite should not co-exist within a silicate assemblage unless on the reaction boundary 'dolomite + ol -> magnesite + cpx' (25kb, 900°C well within the garnet stability field). The presence of sulphide spheres rules out the possibility that they are exsolution features of one high pressure phase. Ca/Mg ratios of the co-existing dolomite and magnesite suggest that they crystallize from a carbonate melt at 800-900°C (12 kb) using the phase relationships determined by Irving and Wyllie (1975).

The large magnesite talc pods contain magnesite with Mg#s ranging from 98 to 50. The magnesite is zoned, becoming more Fe-rich towards the rims of the pods and towards sulphide grains. A reaction rim between the carbonate and silicate assemblage contains abundant small crystals of clinopyroxene and amphibole. Individual grain analyses have been plotted in Figure 30. The compositions of the silicates are only approximate due to the small (<probe beam) size of the crystals.

The siderite composition is $Mg_{43}Fe_{50.2}Ca_{6.7}(CO_3)_2$. Siderite was only found in two small pods where it appears to co-exist with dolomite and magnesite. It is not considered to be part of an equilibrium assemblage. Late calcite veins have the pure end-member calcite composition, suggesting that they formed under low temperature conditions. A vein of high Mg calcite was found in sample N7. The high Mg content of the calcite suggests formation at approxamately 900°C (Goldsmith and Newton, 1969). Accurate temperature estimation, however, requires co-existing calcite-dolomite pairs.

The mineral compositions of carbonates in the Fe-rich samples are similar to those in Fe-poor Cr-diopside series samples. The carbonate, mainly dolomite and magnesite with high Mg#, in the Al-augite series xenoliths has undergone decompression melting, obscuring its original composition. Decompression melting appears to have produced an assemblage of dolomite, magnesite, Ti-rich amphibole ± clinopyroxene, spinel and glass from an original carbonate, pargasite and clinopyroxene assemblage.

Whole Rock Chemistry

Major, trace and rare earth element analyses for samples N2 (Cr-diopside series), N22, N10, N18, N7 (Fe-rich Cr-diopside series), N10 vein (amphibole-apatite-carbonate vein), and N4 (Al-augite series) and the host basanite are presented in Table 12. Many of the

Table 12, Tumut-Eucumbene Tunnel, Bulk Rock Compositions

	N2	N4	N7	N10vein	N10	N18	N22	Host
SiO2	39.67	45.27	49.30	40.73	39.24	43.84	39.79	47.01
TiO2	0.08	1.60	0.70	2.77	0.65	0.27	0.22	2.16
Al2O3	1.50	9.16	6.18	10.29	5.01	3.13	3.13	12.70
Fe2O3	12.50	12.18	7.71	8.64	12.26	11.38	11.92	10.56
MnO	0.18	0.15	0.16	0.11	0.17	0.15	0.19	0.16
MgO	43.26	17.20	18.32	22.22	35.54	35.46	32.94	8.27
CaO	1.45	11.72	15.69	8.33	3.19	3.34	4.69	6.87
Na2O	<.20	0.85	0.62	2.59	0.93	0.24	0.90	3.89
K2O	0.01	0.06	0.03	0.47	0.16	0.05	0.14	2.69
P2O5	<.03	<.03	<.03	0.32	0.09	<.03	0.04	0.91
Loss	1.07	1.30	1.00	3.55	2.53	1.90	5.88	4.21
Total	99.72	99.49	99.71	100.02	99.77	99.76	99.84	99.43
Nb (ppm)	<1	2	2	19	8	1	21	116
Zr	3	27	26	27	8	15	52	488
Y	<2	20	16	21	9	4	6	32
Sr	12	147	108	713	220	37	146	1519
Rb	<2	<2	<2	3	<2	<2	2	54
Ni	1990	537	700	1290	1810	2000	1680	250
Cr	3870	173	5830	2990	5480	2510	4870	394
V	44	333	307	290	118	81	83	142
Ba	3	33	15	273	78	9	25	854
Sc	8	31	44	37	14	14	17	14
La (ppm)	<.35	1.38	2.00	13.70	4.65	1.74	4.50	86.90
Ce	0.93	5.03	5.37	46.40	16.40	4.06	11.50	175.00
Pr	<.31	1.29	0.82	7.66	2.62	0.59	1.64	18.70
Nd	0.36	8.46	4.68	37.30	12.10	2.72	8.55	74.70
Sm	<.23	2.76	1.71	8.66	2.63	0.69	2.19	13.20
Eu	<.22	0.97	0.62	2.90	0.91	<.22	0.85	3.99
Gd	<.2	3.46	2.53	7.47	2.31	0.68	2.05	10.00
Dy	<.19	3.55	2.81	5.04	1.78	0.58	1.54	6.87
Er	<.17	1.82	1.49	1.85	0.78	0.35	0.59	3.03
Yb	<.17	1.44	1.32	1.09	0.48	0.30	0.28	2.00

samples were too small for bulk rock analysis so that sample selection was generally based upon sample size, though an attempt was made to analyse representative samples from each group.

Major elements,

Abundances of the major elements SiO_2, TiO_2, Al_2O_3, Fe_2O_3, CaO, and Na_2O vs MgO have been plotted in Figure 31. In general, TiO_2, Al_2O_3, and CaO abundance decreases with increasing MgO where as SiO_2, Fe_2O_3, and Na_2O contents are erratic. With the exception of Fe_2O_3 and SiO_2, Cr-diopside series samples fall along the average oceanic spinel lherzolite array of Maaloe and Aoki (1977). In this suite, Cr# does not increase with Mg# as would be expected if the xenoliths were related by simple melt extraction (Frey and Green, 1974). Additional enrichment processes are required.

The samples are distinguished by a high but erratic concentration of Fe (analysed as Fe_2O_3). This may be related to the presence of Fe Ni sulphides, though the Ni content of the xenoliths is not particularly high. The presence of carbonate veins and pods may have a similar control over the irregularity of SiO_2 content. Sample N10 vein (or amphibole apatite-rich area) has extremely high concentrations of Na, Al, and Ti. This was expected due to a high proportion of amphibole in the sample and its 'metasomatised'

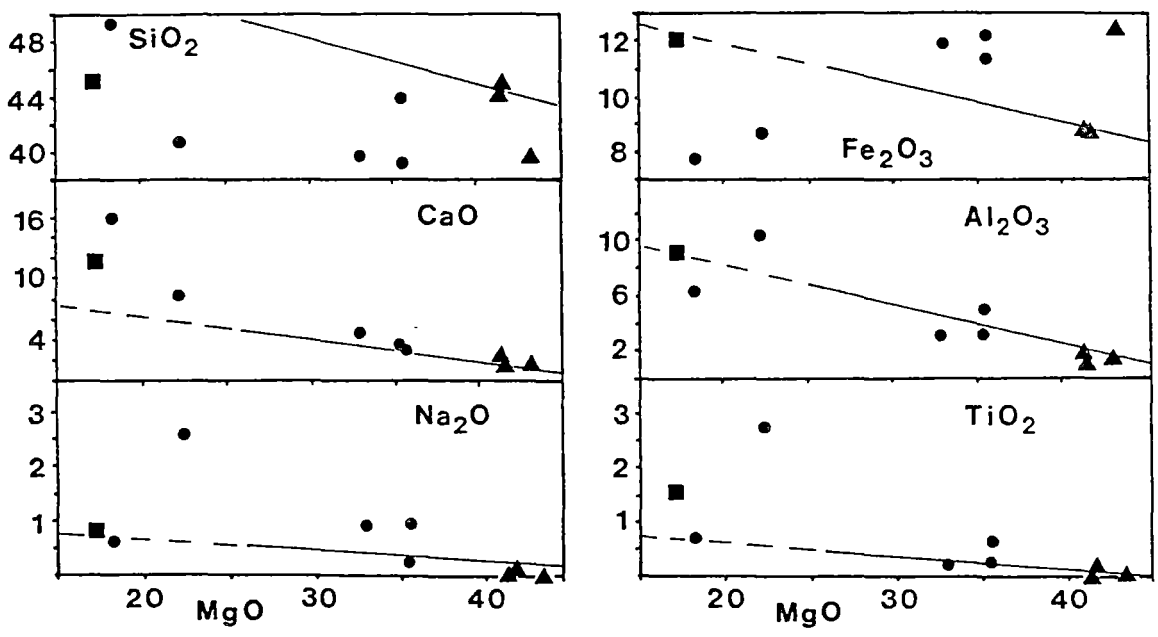

Figure 31. Major element abundance vs MgO of xenoliths. ▲ = Cr-diopside series samples, ● = Fe-rich Cr-diopside samples, ■ = Al augite series sample N4 ---- oceanic spinel lherzolite array from Maaloe and Aoki (1977)

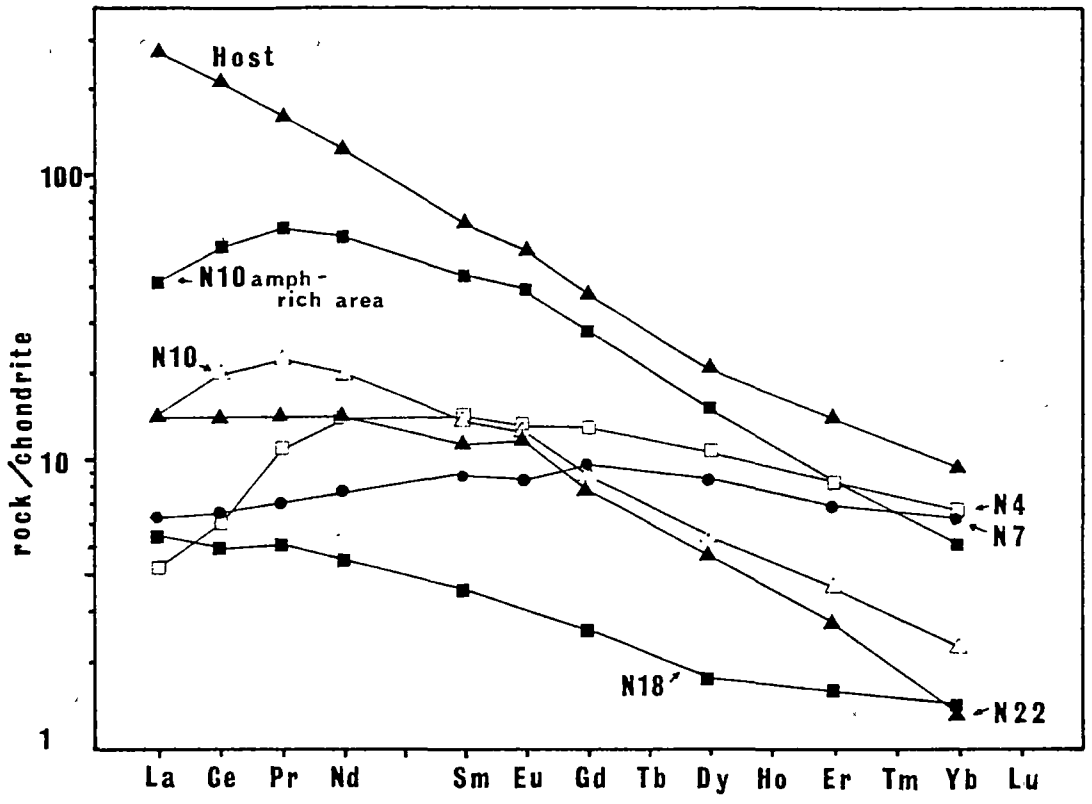

Figure 32. REE concentration of xenoliths. Samples have been normalized to chondrite values. Sample N2 has not been plotted as the concentration of many elements was below the detection limit.

appearance. Samples N10 and N22 also show enrichments of Na at the expense of Al. This is a common feature in samples where spinel has been consumed during the formation of amphibole. The low concentration of Fe in N10 vein and banded sample N7 is anomalous. In sample N10 this may be the result of unusually high enrichment of Al and Ti and the ability of these elements to substitute for Fe in clinopyroxene and amphibole. Sample N7, on the other hand, has an unusually high proportion of Ca, most of which resides in clinopyroxene and amphibole.

Trace elements,

All samples, with the exception of N4, N7 and refractory sample N2 are LREE enriched (Figure 32). Samples N10 and N10 vein have the most extreme amount of LREE enrichment. They show the classic pattern for S.E. Australian amphibole-rich lherzolites (O'Reilly and Griffin, 1988). This was not anticipated, however, because sample N10 has a high proportion of apatite, a feature usually resulting in La > Ce concentration. Samples N7 and N4 have similar REE patterns which are slightly and uniformly REE enriched in the middle and heavy REE. This suggests a possible relationship between the Al-augite series samples and banded Fe-rich xenoliths. Samples N22 and anhydrous sample N18 have low REE concentrations pointing out that the REE enrichment is highest in the Fe-'metasomatised' samples, especially those with a high modal proportion of amphibole.

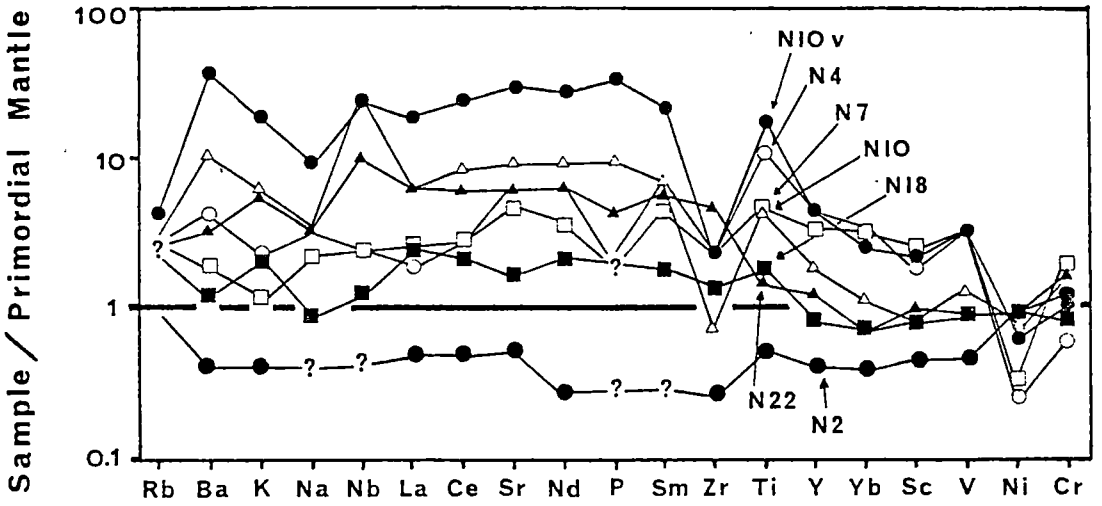

Figure 33. Trace element content of xenoliths normalized to primordial mantle. P.M. values from Wood, (1979) and Sun, (1982).

Trace elements normalized to primordial mantle have been plotted in Figure 33. With the exception of refractory sample N2, samples are enriched in incompatible elements Ba to Sm, close to PM in the moderately refractory elements Y to V, and depleted in the refractory elements Ni and Cr. Samples have a strong depletion in Zr and a moderate enrichment of Ti. Most extreme enrichment is seen in the amphibole-rich sample N10.

Much of this grouping is mineral dependent. Apatite, present in samples N10 and N22, concentrates P, Sr, and LREEs. P and Sr concentrations do not correlate suggesting that Sr is also found in the carbonate along with Nb. The Zr anomaly is peculiar especially since Zr is commonly associated with the presence of amphibole. These samples have an abundance of amphibole, yet a Zr depletion.

Conditions of Crystallization

Pressure, temperature and oxygen fugacity have been calculated based on the mineralogy of co-existing silicate phases. These are presented in Table 13.

Temperatures have been calculated using the Well's (1977) geothermometer for co-existing ortho and clinopyroxenes (estimated uncertainty of 70°C). The calculated temperatures range from 884°C to 1091°C. Most samples fall within the range of

Table 13. Xenolith conditions of crystallization

Xenolith #		Temperature (°C) Wells (1977)	O'Neill+Wall (1987)	Pressure (kb) Harley+Green (1982)	Nickel+Green (1985)	f(O2) O'Neill+Wall (1987)
Cr Diopside series						
N26	Spinel lherzolite	887	838	-	-	QFM -0.07
N26B	Spinel lherzolite	935	860	-	-	QFM -0.58
N24	Spinel wehrlite	902	827	-	-	QFM -0.21
N2	Spinel harzburgite	893	855	-	-	QFM -0.07
Fe-rich Cr Diopside series						
N22	Spinel lherzolite					
N21	Spinel lherzolite	1057	1006	-	-	QFM
N3	Spinel lherzolite	895	826	15.5	16.3	QFM -0.08
N18	Spinel lherzolite	1048	1001	-	-	QFM +.05
	vein	1091	-	-	-	-
N7	Spinel websterite	912	-	-	-	-
Al Augite series						
N4	Pyroxenite	884	-	-	-	-
N21A	Pyroxenite	905	-	-	-	-

890-940°C. These are relatively low temperatures for lherzolite nodules. Amphibole and carbonate do not occur in the high temperature samples N18 and N21. Amphibole-bearing samples have low temperatures (893-912°C).

The absence of plagioclase from the spinel lherzolite samples indicates that samples formed within a pressure range of 9 to 24 kb. Pressures of 15.5 kb and 16.3 kb were calculated from the garnet bearing sample N3 using respectively the Nickel and Green (1985) and Harley and Green (1982) geobarometers based on the Al content of orthopyroxene co-existing with garnet. This is a realistic pressure range for a sample containing both garnet and spinel. Oxygen Fugacity (fO_2) was determined using the calculations of O'Neill and Wall (1987) based on co-existing ol, opx, and spinel. Calculated fO_2's range from QFM(-0.6 to +0.05). This indicates that the assemblages formed under moderately oxidizing conditions and such a conclusion is consistant with the presence of carbonate minerals.

Discussion

Samples from the Tumut-Eucumbene tunnel can be divided into 4 groups based on their mineral chemistry:

1) Cr-diopside series, (normal mantle wall rock)
2) Fe-rich Cr-diopside series, (cryptically metasomatised samples)
3) Banded, Fe-rich samples including the amphibole peridotite, N10, (modally metasomatised samples)
4) Al-augite series samples, (deep seated melt).

These are discussed below.

Cr-diopside series samples are similar to those normally described as mantle wall rock. Silicates have high Mg#s and are Cr-rich (Frey and Green, 1974; Nickel and Green, 1984). The samples are predominantly dry except for N2 which contains Cr-rich pargasitic amphibole and phlogopite grains. All of the silicate phases in this suite appear to be in chemical equilibrium. There is no evidence to suggest that the hydrous phases are not primary. Sample N2, the only sample large enough for bulk rock analysis, has a depleted trace element pattern, consistent with the interpretation that the Cr-diopside series samples represent residual mantle material after melt extraction.

Fe-rich, Cr-diopside series nodules are characterized by samples with low Mg#s, colourless clinopyroxenes (in thinsection) and silicate phases rich in Ti, Al, and Fe. Samples analysed show a small but uniform enrichment in trace elements relative to primordial mantle. They show no textural or obvious modal evidence of enrichment. Chemical enrichment, therefore, is related to a process of cryptic metasomatism. Low temperature samples contain amphibole while high temperature samples do not. This is probably due to the stability limits of amphibole rather than to the degree of enrichment. Amphiboles are extremely rare in peridotite samples with calculated temperatures higher than 1000°C (Chapter 1). In experimental studies amphibole has been observed only up to 1150°C under optimum conditions (eg, a very fertile bulk rock composition and X_{H2O} = 0.6 (Holloway, 1973). Its stability is lowered by the addition of CO_2. In natural samples, amphibole is probably not stable over 1050°C.

In the Eucumbene tunnel Fe-rich samples, amphibole is present in sample N22. In this sample, the amphibole is considered to be in chemical equilibrium with the silicate assemblage. It is therefore not possible to determine whether it is an introduced phase, the result of modal metasomatism, or a residual silicate phase.

Sample enrichment of Fe, Al, and Ti coupled with depletions in Ni and Cr , apparent in the Eucumbene xenoliths, would be expected in lherzolites which have been infiltrated by a basaltic melt. This type of enrichment is often described as 'Fertilization' and related to hydrous and anhydrous mafic dykes. It is often seen in composite xenoliths (Harte, 1983). Fe, Al, and Ti enrichment has been described in samples from the western U.S. (Wilshire and Shervais, 1975; Wilshire *et al.*, 1980; Stewart and Boettcher, 1977; Kempton *et al.*, 1984) and eastern Australia (Irving, 1980; O'Reilly, 1987).

Banded Fe-rich samples contain silicate phases which are extremely enriched in Ti, Al, and Fe. They are characterized both by their banded or layered appearance and by silicate phases which are not in chemical equilibrium. Their layered appearance is probably the result of modal metasomatism, specifically, the addition of amphibole and clinopyroxene. The presence of non-equilibrated amphibole suggests that the fertilizing basaltic magma was H_2O rich and the extreme trace and LREE enrichment patterns of these samples indicate that the infiltrating magma provided a source of abundant incompatible elements.

Al-augite series samples have similar silicate compositions to samples that are inferred to have crystallized from basaltic melts at high pressures (Wilshire and Shervais, 1975; Frey and Prinz, 1978). They are unusual since they contain titaniferous magnetite as an opaque phase, abundant sulphide grains and carbonate minerals. Trace element patterns suggest that the Al-augite series xenoliths are manifestations of the metasomatizing magma. The samples may, on the other hand, be Al-augite series veins which have become metasomatized.

The relationship between these nodule types can be explained in terms of an infiltrating H_2O, CO_2-rich basaltic magma reacting with and metasomatising spinel lherzolite country-rock (Figure 34). Cr-diopside samples represent the host lherzolite assemblage. Fe-rich samples have been cryptically metasomatized and banded samples have undergone modal metasomatism by the infiltrating magma. Al-augite series samples represent either direct crystallization from the infiltrating magma, or veins which have been metasomatized. The presence of amphibole is temperature controlled.

Carbonate pods,

Carbonate pods are present only in low temperature (< 935°C) samples and have textures indicative of a quenched melt. The small dolomite -magnesite pods behave as an immiscible phase with respect to the silicate assemblage. The talc magnesite pods, on the other hand, show evidence of reaction with the host silicate assemblage as they contain

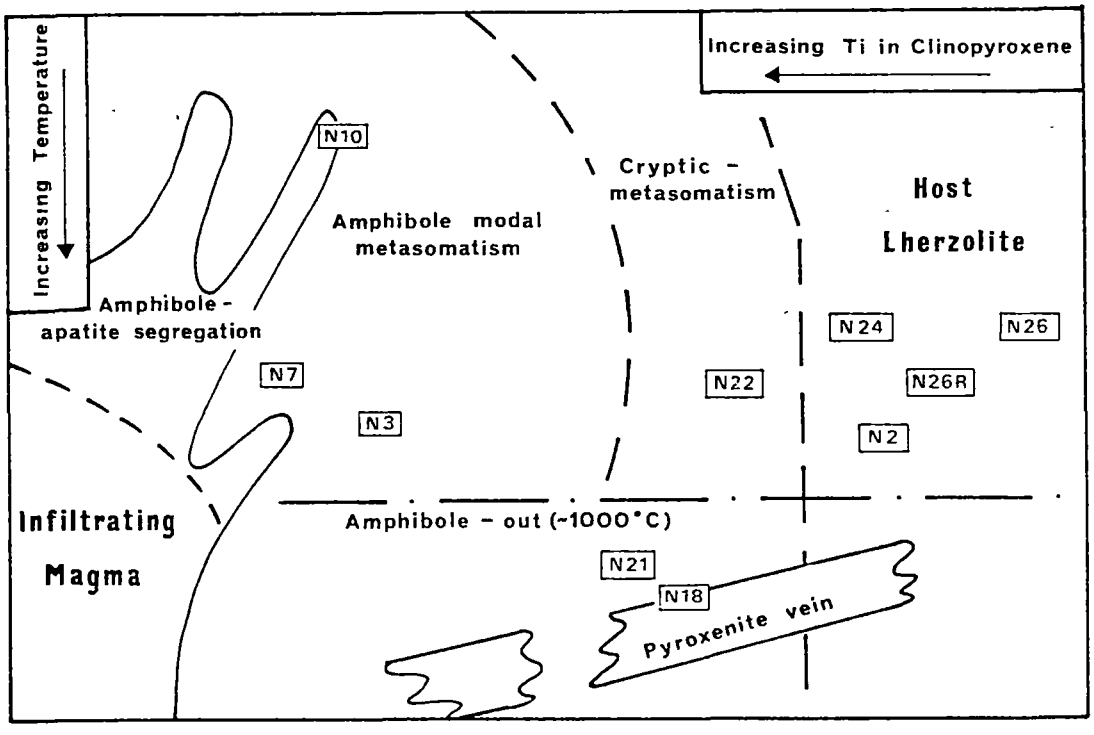

Figure 34. Relationship between Cr-diopside series xenoliths, Fe-rich xenoliths and banded xenolith samples

coronas of magnesite, silicates and abundant fluid inclusions. The presence of sulphide globules within the carbonate pods suggests that the magnesite-dolomite pairs are not formed as the result of decompression melting or exsolution from a single carbonate phase. It further demonstrates the ability of a carbonate-rich melt to scavenge and transport sulphide material. Since the carbonates are not a residual phase in the lherzolites, they were probably infiltrated into the lherzolite assemblage as part of the basaltic melt.

The features observed in the samples have been interpreted as an immiscible carbonate melt fraction associated with the metasomatizing basaltic melt under oxidizing conditions. This interpretation agrees with the phase relations seen in peridotite + H_2O + CO_2. Figure 35 presents an idealised geotherm for the Tumut-Eucumbene samples. It has been constructed on the basis of Well's calculated temperatures for co-existing pyroxenes. Pressure has been based on the orthopyroxene-garnet pair in sample N3. (This geotherm can only be very approximate since only one sample contains garnet). The geotherm is

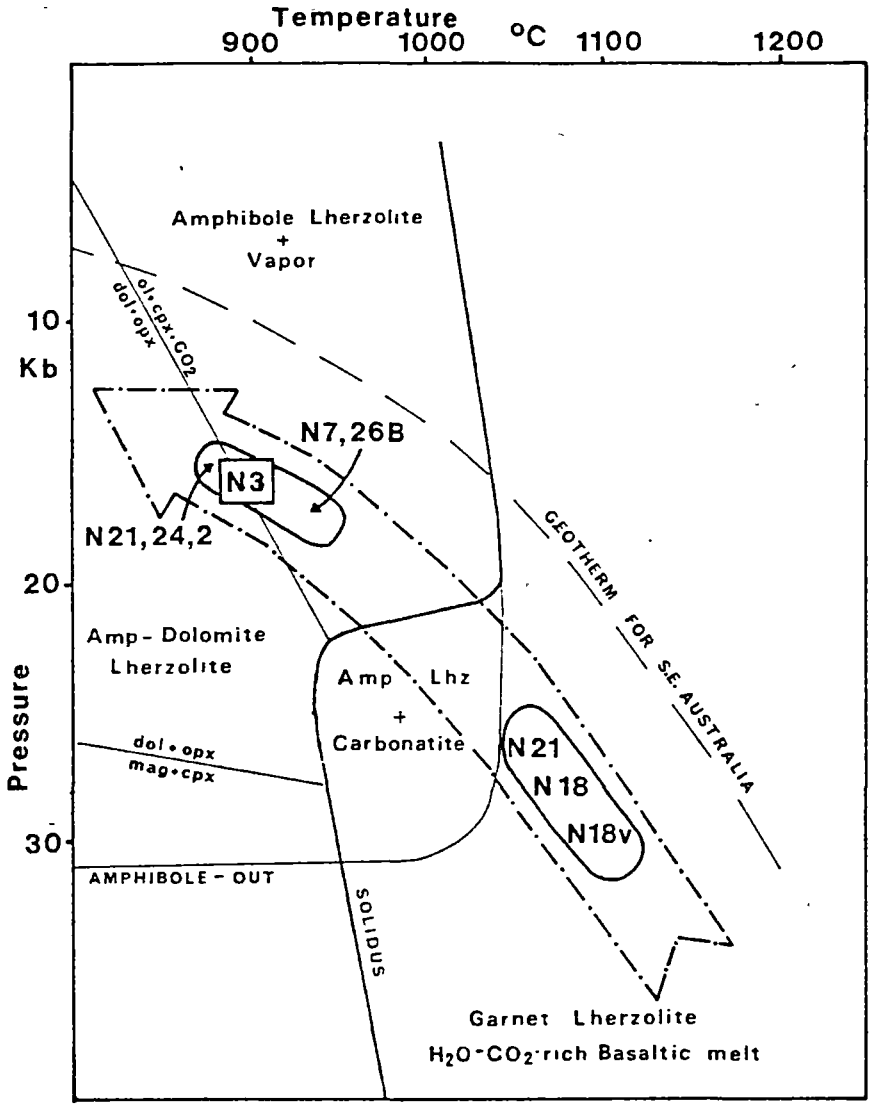

Figure 35. Pressure and temperature path of xenolith crystallization

constructed parallel to, but cooler, than the S.E. Australian geotherm of O'Reilly and Griffin (1985). Phase relationships for pyrolite + H_2O + CO_2 are also presented (Chapter 2). The amphibole-out boundary has been adjusted for a bulk rock composition less fertile than pyrolite.

Carbonate-silicate relationships are interpreted as representing the reaction between a diapiric H_2O, CO_2-rich basaltic melt and its lherzolitic host-rock as the diapir migrates upwards along an oceanic-type geotherm. At high temperatures and pressures (T > 1050°C) the assemblage would not be within the stability field of amphibole or carbonate.

H_2O and CO_2 would remain disolved in the basaltic melt and the lherzolite would consist of olivine, pyroxenes, spinel or garnet. Reaction between the basalt and lherzolite will be confined to Fe, Ti, and Al-enrichment of the lherzolite clinopyroxene, but result in little to no modal change.

As the amphibole stability boundary is crossed (T = 1050°C), the basaltic component will react with its host lherzolite resulting in the formation of Ti, Al-rich pargasitic amphibole. Water will be consumed by the developing amphibole and CO_2 will react with clinopyroxene to form a residual carbonatite melt. The composition of this melt is unknown, but will depend on Na, K and Ca partitioning between the carbonatite and amphibole. This melt has been preserved in the Tumut-Eucumbene xenoliths as small magnesite-dolomite pods. (Na-carbonate minerals would only be preserved if the sample remained completely dry after its formation and did not come into contact with water during eruption, weathering, sample collection or thin-section preparation.)

As the diapiric assemblage cooled further, it would cross into the amphibole lherzolite field (carbonatite + gt + opx -> cpx + ol +CO_2 vapor). The carbonatite melt would react with the silicate assemblage producing Na-rich clinopyroxene and amphibole with abundant CO_2-rich fluid inclusions. This event is preserved in the Tumut-Eucumbene xenoliths as large magnesite-talc pods and their associated silicate and CO_2-fluid inclusion-rich coronas. The lherzolites would become Na, K and LREE metasomatised at this stage.

If the assemblage cools further, it will cross the CO_2-dolomite boundary (ol + cpx + CO_2 -> dol + opx). It is expected that the assemblage would freeze at this stage, perhaps as in the Tumut-Eucumbene samples, preserving the original carbonate-silicate reactions.

The presence of sulphide as an additional component may lower the temperature and pressure of the solidus position from that established for pyrolite + CO_2 + H_2O.

Sulphides,

Although they are not a common feature, sulphides are increasingly being recognised in mantle samples (Dewaal and Calk, 1975; Lorand and Conquere, 1983; Irving, 1980). They are generally considered to have formed from an immiscible sulphide liquid, but the

origin of such a liquid remains under debate. Recent discussion has concentrated on whether the sulphides represent a co-genetic immiscible sulphide liquid or whether they were introduced by a late infiltrating magma or fluid. Their presence has been explained by the following processes:

1) Sulphides introduced by a contaminating magma (Dewaal and Calk, 1975; Irving, 1980)
2) Sulphides related to metasomatism and the introduction of amphibole (Lorand and Conquere, 1983; Clarke *et al.*, 1977)
3) Sulphides are residual from a partial melting event (Garuti *et al.*, 1984; Dromgoole and Pasteris, 1987; Tsai *et al.*, 1979).

The origin of the sulphides in the Tumut-Eucumbene tunnel samples can not be resolved conclusively. They are associated with an infiltrating Fe, Al, and Ti rich melt and are now concentrated in carbonate melt pools. It is not possible to determine whether they were part of the host lherzolite assembage which has been remobilized by the carbonate melt, or whether they were introduced by the infiltrating basaltic melt. The presence of large equigranular sulphide grains in the Al-augite suite sample N15 suggests that the latter explanation is most likely.

Summary

The textural and mineralogical features seen in samples from the Eucumbene Tunnel are consistant with an origin by infiltration of an H_2O, CO_2-rich, sulphide-bearing basaltic magma into a mantle lherzolite assemblage. The infiltrating magma has both cryptically and modally metasomatised the country rock. H_2O has reacted with the silicate assemblage producing amphibole. CO_2 and sulphur have segregated from the magma into immiscible carbonatitic and sulphide melts.

As the assemblage cooled, it travelled through the CO_2 field producing abundant fluid inclusions and the carbonate melt reacted with the silicate assemblage. The melt-peridotite reactions and carbonate melt were frozen once the P-T conditions were within the stability field of dolomite. From the basaltic melt, Fe, Al and Ti metasomatised the lherzolite, P, Na, K, Cl, F, Ca and H_2O formed amphibole and apatite and Mg, Ca and CO_2 formed carbonate melt. Fe,S, and Ni are precipitated as sulphides. In these samples, it was not possible to tell whether the carbonatite melt was alkali rich.

Conclusions

1) Xenoliths from the Tumut-Eucumbene tunnel can be divided into four groups based on their mineral chemistry;

1) Cr-diopside series, (normal mantle wall rock)
2) Fe-rich Cr-diopside series, (cryptically metasomatised samples)
3) Banded, Fe-rich samples, (modally metasomatised samples)
4) Al-augite series samples, (deep seated melt).

2) Xenoliths contain abundant carbonate pods and associated sulphide spheres. Four types of carbonate were recognised;

1) Small magnesite-dolomite pods, (trapped immiscible carbonatite melt)
2) Large magnesite-talc pods, (trapped carbonate melt which has reacted with the host silicate assemblage)
3) Rare siderite, magnesite. dolomite pods, (disequilibrium assemblage, possibly Fe-enriched)
4) Calcite veins, (late veins associated with transporting magma)

3) Whole rock analyses indicate that the samples are enriched in Fe, Al, Ti and LREE. Enrichment is greatest in banded, Fe-rich samples and samples with a high proportion of modal amphibole.

4) Temperature and pressure estimates indicate that samples were last equilibrated at 880 to 1100°C, most samples cluster within the range of 880 to 940°C.

5) Samples are related by reaction of an H_2O, CO_2-rich basaltic melt with a Cr-diopside series lherzolite assemblage.

6) Carbonate pods represent a trapped carbonatite melt, residual after the formation of pargasitic amphibole from a crystallizing basaltic magma under oxidizing conditions.

References

Amundsen H.E.F., 1987, Evidence for liquid immiscibility in the upper mantle: Nature, v. 327, p. 692-695

Amundsen H.E.F., Griffin W.L., and O'Reilly S.Y., 1987, The lower crust and upper mantle beneath northwestern Spitsbergen: Evidence from xenoliths and geophysics: Tectonophysics, v. 139, p. 169-185

Anderson T., O'Reilly S.Y., and Griffin W.L., 1984, The trapped fluid phase in upper mantle xenoliths from Victoria, Australia: implications for upper mantle metasomatism: Contrib. Mineral. Petrol., v. 88, p. 72-85

Anovitz L.M., and Essene E.J., 1987, Phase equilibria in the system $CaCO_3$-$MgCO_3$-$FeCO_3$: J. Petrol., v. 28, p. 389-414

Arai S., 1986, K/Na variation in phlogopite and amphibole of upper mantle peridotites due to fractionation of the metasomatizing fluids: J. Geol., v. 94, p. 436-444

Aspden J.A., 1980, The mineralogy of primary inclusions in apatite extracted from Alno ijolite: Lithos, v. 13, p. 263-268

Bailey D.K., 1987, Mantle metasomatism - perspective and prospect: Alkaline Igneous Rocks, in J.G. Fitton, and B.G.J. Upton, Eds, Oxford, Blackwell, p. 1-14

Bell K., Dawson J.B., and Farquhar R.M., 1973, Strontium isotope studies of alkalic rocks: The active carbonatite volcano Oldoinyo Lengai, Tanzania: Bull. Geol. Soc. Amer., v. 84, p. 1019-1030

Berg G.W., 1986, Evidence for carbonate in the mantle: Nature, v. 324, p. 50-51

Berry R.F., 1981, Petrology of the Hili Manu lherzolite, East Timor: J. Geol. Soc. Australia, v. 28, p. 453-469

Best M.G., 1974, Mantle-derived amphibole within inclusions in alkalic-basaltic lavas: J. Geophys. Res., v. 79, p. 2107-2113

Bonatti E., Ottonello G., and Hamlyn P.R., 1986, Peridotites from the island of Zabargad (St. John), Red Sea: Petrology and geochemistry: J. Geophys. Res., v. 91, p. 599-631

Boyd F.R., 1971, Pargasite - spinel peridotite xenolith from the Wesselton mine: Carnegie Inst. Wash. Yearb., v. 70, p. 138-142

Boyd F.R., and Gurney J.J., 1982, Low-calcium garnets: Keys to craton structure and diamond crystallization: Carnegie Inst. Wash. Yearbk., v. 81, p. 261-267

Brey G., 1978, Origin of olivine melilitites - chemical and experimental evidence: J. Volcanol. Geotherm. Res., v. 3, p. 61-88

Brey G., and Green D.H., 1975, The role of CO_2 in the genesis of olivine melilitite: Contrib. Mineral. Petrol., v. 49, p. 93-103

Brey G., and Green D.H., 1976, Solubility of CO_2 in olivine melilitite at high pressures and role of CO_2 in the Earth's upper mantle: Contrib. Mineral. Petrol., v. 55, p. 217-230

Brey G., and Green D.H., 1977, Systematic study of liquidus phase relations in olivine melilitite + H_2O + CO_2 at high pressures and petrogenesis of an olivine melilitite magma: Contrib. Mineral. Petrol., v. 61, p. 141-162

Brey G., Brice W.R., Ellis D.J., Green D.H., Harris K.L., and Ryabchikov I.D., 1983, Pyroxene-carbonate reactions in the upper mantle: Earth. Planet. Sci. Lett., v. 62, p. 63-74

Brown G.M., Pinsent R.H., and Coisy P., 1980, The petrology of spinel-peridotite xenoliths from the Massif Central, France: Amer. J. Sci., v. 280A, p. 471-496

Cawthorn R.G., 1975, The amphibole peridotite - metagabbro complex, Finero, Northern Italy: J. Geol., v. 83, p. 437-454

Clark M.G.C., and Roberts B., 1986, Carbonated melilitites and calcitized alkali carbonatites from Homa Mountain, western Kenya: A reinterpretation: Geol. Mag., v. 123, p. 683-692

Clarke D.B., Pe-Piper G.G., McKay R.M., Gill K.R., O'Hara M.J., and Gard J.A., 1977, A new potassium-iron-nickel sulphide from a nodule in kimberlite: Earth Planet. Sci. Lett., v. 35, p. 421-428

Clement C.R., 1975, The emplacement of some diatreme-facies kimberlites: Phys. Chem. Earth, v. 9, p. 51-59

Cooper A.F., Gittins J., and Tuttle O.F., 1975, The system Na_2CO_3-K_2CO_3-$CaCO_3$ at 1 kilobar and its significance in carbonatite petrogenesis: Amer. J. Sci., v. 275, p. 534-560

Dautria J.M., Liotard J.M., Cabanes N., Girod M., and Briqueu L., 1987, Amphibole-rich xenoliths and host alkali basalts: petrogenetic constraints and implications on the recent evolution of the upper mantle beneath Ahaggar (Central Sahara, Southern Algeria): Contrib. Mineral. Petrol., v. 95, p. 133-144

Dawson J.B., 1962, The geology of Oldoinyo Lengai: Bulletin Volcanologique, v. 24, p. 349-387

Dawson J.B., 1962, Sodium carbonate lavas from Oldoinyo Lengai, Tanganyika: Nature, v. 195, p. 1075-1076

Dawson J.B., 1966, Oldoinyo Lengai - an active volcano with sodium carbonatite flows: Carbonatites, in Tuttle O.F., and Gittins J., Eds, New York, Interscience, p. 155-168

Dawson J.B., 1984, Contrasting types of upper mantle metasomatism: in J. Kornprobst, Ed, Kimberlites 2: The mantle and crust-mantle relationships, Amsterdam, Elsevier, p. 289-294

Dawson J.B., and Hawthorne J.B., 1973, Magmatic sedimentation and carbonatitic differentiation in kimberlite sills at Benfontein, South Africa: J. Geol. Soc. London, v. 129, p. 61-85

Dawson J.B., and Smith J.V., 1982, Upper mantle amphiboles: a review: Mineral. Mag., v. 45, p. 35-46

Dawson J.B., Garson M.S., and Roberts B., 1987, Altered former alkalic carbonatite lava from Oldoinyo Lengai, Tanzania: Inferences for calcite carbonatite lavas: Geology, v. 15, p. 765-768

Dawson J.B., Gurney J.J., and Lawless P.J., 1975, Palaeogeothermal gradients derived from xenoliths in kimberlite: Nature, v. 257, p. 299-300

Dawson J.B., Hervig R.L., and Smith J.V., 1981, Fertile iron-rich dunite xenoliths from the Bultfontein kimberlite, South Africa: Fort. Min., v. 59, p. 303-324

Deans T., and Roberts B., 1984, Carbonatite tuffs and lava clasts of the Tinderet foothills, western Kenya: A study of calcified natrocarbonatites: J. Geol. Soc. London, v. 141, p. 563-580

Deer W.A., Howie R.A., and Zussman J., 1963, Rock forming minerals: London, Longmans,435p.

Deines P., 1980, The carbon isotopic composition of diamonds: relationship to diamond shape, color, occurrence and vapor composition: Geochim. Cosmochim. Acta, v. 44, p. 943-961

Deines P., and Gold D.P., 1973, The isotopic composition of carbonatite and kimberlite carbonates and their bearing on the isotopic composition of deep-seated carbon: Geochim. Cosmochim. Acta, v. 37, p. 1709-1733

Delaney J.S., Smith J.V., and Nixon P.H., 1979, Model for upper mantle below Malaita, Solomon Islands, deduced from chemistry of lherzolite and megacryst minerals: Contrib. Mineral. Petrol., v. 70, p. 209-218

DeWaal S.A., and Calk L.C., 1975, The sulfides in the garnet pyroxenite xenoliths from Salt Lake Crater, Oahu: J. Petrol, v. 16, p. 134-153

Donaldson C.H., and Dawson J.B., 1978, Skeletal crystalization and residual glass compositions in a cellular alkalic pyroxenite nodule from Oldointo Lengai: implications for evolution of the alkalic carbonatite lavas: Contrib. Mineral. Petrol., v. 67, p. 139-149

Donaldson C.H., Dawson J.B., Kanaris-Sutiriou R. Batchelor R.A., and Walsh J.N., 1987, The silicate lavas of Oldoinyo Lengai, Tanzania: N. Jb. Miner. Abh., v. 156, p. 247-279

Downes H., 1987, Tertiary and Quaternary volcanism in the Massif Central, France: The Alkaline Rocks, in Fitton J.G., and Upton B.G.J., Eds, Geol. Soc. London spec. pub. 30.

Dromgoole E.L., and Pasteris J.D., 1987, Interpretation of the sulphide assemblages in a suite of xenoliths from Kilbourne Hole, New Mexico: Mantle Metasomatism and Alkaline Volcanism, in E. Morris, and J.D. Pasteris, Eds, Geol. Soc. Am. Spec. Paper. 215, p. 25-46

Eckermann H. von., 1948, The alkaline district of Alno Island: Sver. Geol. Unders. Ser. C., p. 36

Eggler D.H., and Baker D.R., 1982, Reduced volatiles in the system C-O-H: Implications to mantle melting, fluid formation, and diamond genesis: High-pressure research in geophysics, in Akimoto S., and Manghnani M.H., Eds, Tokyo, Center for Academic Publications, p. 237-250

Eggler D.H., 1974, Effect of CO_2 on the melting of peridotite: Carnegie Inst. Wash. Yearbk., v. 73, p. 215-224

Eggler D.H., 1976, Does CO_2 cause partial melting in the low-velocity layer of the mantle?: Geology, v. 4, p. 69-72

Eggler D.H., 1978, The effect of CO_2 upon partial melting of peridotite in the system Na_2O-CaO-Al_2O_3-MgO-SiO_2-CO_2 to 35 kb, with an analysis of melting in a peridotite-H_2O-CO_2 system: Amer. J. Sci., v. 278, p. 305-343

Eggler D.H., 1983, Upper mantle oxidation state: evidence from olivine-orthopyroxene -ilmenite assemblages: Geophys. Res. Lett., v. 10, p. 365-368

Eggler D.H., 1987, Discussion of recent papers on carbonated peridotite, bearing on mantle metasomatism and magmatism: an alternative: Earth Planet. Sci. Lett., v. 82, p. 398-400

Eggler D.H., 1987, Solubility of major and trace elements in mantle metasomatic fluids: experimental constraints: Mantle metasomatism, in Menzies M.A., and Hawkesworth C.J., Eds, New York, Academic Press, p. 21-41

Emeleus C.H., and Andrews J.H., 1975, Mineralogy and petrology of kimberlite dyke and sheet intrusions and included peridotite xenoliths from South-West Greenland: Phys. Chem. Earth, v. 9, p. 179-197

Ernst W.G., 1978, Petrochemical study of lherzolitic rocks from the Western Alps: J. Petrol., v. 19, p. 341-392

Fabries J., Figueroa O., and Lorand J.P., 1987, Petrology and thermal history of highly deformed mantle xenoliths from the Montferrier basanites, Languedoc, southern France: A comparison with ultramafic complexes from the north Pyrenean zone: J. Petrol., v. 28, p. 887-919

Field S.W., Haggerty S.H., and Erlank A.J., 1986, Subcontinental lithospheric and asthenospheric metasomatism in the region of Jagersfontein, South Africa: Geol. Soc., v. 16, p. 235-237

Field S.W., Haggerty S.H., and Erlank A.J., 1989, Subcontinental metasomatism in the region of Jagersfontein, South Africa, Australian J. Earth Sci. Spec. Pub. 14, IV International Kimberlite Conference, in press

Finnerty A.A., and Boyd F.R., 1987, Thermobarometry for garnet peridotites: basis for the determination of thermal and compositional structure of the upper mantle: Mantle Xenoliths, in Nixon P.H., Ed, New York, John Wiley, p. 381-402

Francis D.M., 1976, The origin of amphibole in lherzolite xenoliths from Nunivak Island, Alaska: J. Petrol., v. 17, p. 357-378

Freestone I.C., and Hamilton D.L., 1980, The role of liquid immiscibility in the genesis of carbonatites: an experimental study: Contrib. Mineral. Petrol., v. 73, p. 105-117

Freestone I.C., 1978, Liquid immiscibility in alkali-rich magmas: Chem. Geol., v. 23, p. 115-123

Frey F.A., 1970, Rare earth abundances in a high temperature peridotite intrusion: Geochim. Cosmochim. Acta, v. 33, p. 1429-1447

Frey F.A., and Green D.H., 1974, The mineralogy, geochemistry and origin of lherzolite inclusions in Victorian basanites: Geochim. Cosmochim. Acta, v. 38, p. 1023-1059

Frey F.A., and Prinz M., 1978, Ultramafic inclusions from San Carlos, Arizona: Petrologic and geochemical data bearing on their petrogenesis: Earth Planet. Sci. Lett., v. 38, p. 129-176

Frick C., 1973, Ten kimberlites from Pofadder, Namaqualand, South Africa: Trans. Geol. Soc. S. Afr., v. 77, p. 31-36

Garuti G., Gorgoni C., and Sighinolfi G.P., 1984, Sulphide mineralogy and chalcophile and siderophile element abundances in the Ivrea-Verbano mantle peridotites (Western Italian Alps). Earth Planet. Sci. Lett., v.70, p.69-87

Girod M., Dautria J.M.,, and De Giovanni R., 1981, A first insight into the constitution of the upper mantle under the Hoggar area (Southern Algeria): the lherzolite xenoliths in the alkali basalts: Contrib. Mineral. Petrol., v. 77, p. 66-73

Gittins J., Hewins R.H., and Laurin A.F., 1975, Kimberlitic-carbonatitic dykes of the Saguenay River Valley, Quebec, Canada: Phys. Chem. Earth, v. 9, p. 137-148

Goto A., and Yokoyama K., 1988, Lherzolite inclusions in olivine nephelinite tuff from Salt Lake Crater, Hawaii: Lithos, v. 21, p. 67-80

Goto K., and Arai S., 1987, Petrology of peridotite xenoliths in Lamprophyre from Shingu, Southwestern Japan: Implications for origin of Fe-rich mantle peridotites: Contrib. Mineral. Petrol., v. 37, p. 137-155

Green D.H., 1963, Alumina content of enstatite in a Venezuelan high temperature peridotite: Geol. Soc. Amer. Bull., v. 74, p. 1397-1402

Green D.H., 1964, The petrogenesis of the high-temperature peridotite intrusion in the Lizard area, Cornwall: J. Petrol, v. 5, p. 134-188

Green D.H., 1970, Compositions of basaltic magmas as indicators of conditions of origin: application to oceanic volcanism: Royal Soc. Philos. Trans., v. 268, p. 707-721

Green D.H., 1973, Conditions of melting of basanite magma from garnet peridotite: Earth Planet. Sci. Lett., v. 17, p. 456-465

Green D.H., 1973, Contrasted melting relations in a pyrolite upper mantle under mid-oceanic ridge, stable crust and island arc environments: Tectonophysics, v. 17, p. 285-297

Green D.H., and Ringwood A.E., 1970, Mineralogy of peridotitic compositions under upper mantle conditions: Phys. Earth Planet. Interiors, v. 3, p. 359

Griffin W.L., 1973, Lherzolite nodules from the Fen alkaline complex, Norway: Contrib. Mineral. Petrol., v. 38, p. 135-146

Griffin W.L., Carswell D.A., and Nixon P.H., 1979, Lower-crustal granulites and eclogites from Lesotho, southern Africa: in Boyd F.R., and Meyer H.O.A., Eds, The mantle sample: inclusions in kimberlites and other volcanics. (Proc. Int. Kimberlite Conf., No. 2., Vol. 2), Washington D.C., American Geophysical Union, p. 59-86

Griffin W.L., Wass S.Y., and Hollis J.D., 1984, Ultramafic xenoliths from Bullenmerri and Gnotuk maars, Victoria: petrology of a subcontinental crust-mantle transition: J. Petrol., v. 25, p. 53-87

Harley S.L., and Green D.H., 1982, Garnet-orthopyroxene barometry for granulites and peridotites: Nature, v. 300, p. 697-701

Harte B., 1983, Mantle peridotites and processes - the kimberlite sample: in Hawkesworth C.J., and Norry M.J., Eds, Continental basalts and mantle xenoliths, Nantwich, Cheshire, Shiva Publishing Ltd., p. 46-91

Hawkesworth C.J., Rogers N.W., Van Calsteren P., and Menzies M.A., 1984, Mantle enrichment processes: Nature, v. 311, p. 331-335

Hay R.L., 1983, Natrocarbonatite tephra of Kerimasi volcano, Tanzania: Geology, v. 11, p. 599-602

Heinrich E.W., 1966, The Geology of Carbonatites: Chicago, Rand McNally.

Henry D.J., and Medaris L.G., 1980, Application of pyroxene and olivine-spinel geothermometers to spinel peridotites in Southwestern Oregon: Amer. J. Sci., v. 280A, p. 211-231

Hill R.E.T., and Boettcher A.L., 1970, Water in the earth's mantle: melting curves of basalt-water and basalt-water-carbon dioxide: Science, v. 167, p. 980-982

Holloway J.R., 1973, The system pargasite-H_2O-CO_2: a model for melting of a hydrous mineral with a mixed-volatile fluid - 1. Experimental results to 8 kbar: Geochim. Cosmochim. Acta, v. 37, p. 651-666

Holloway J.R., and Ford C.E., 1975, Fluid-absent melting of the fluoro-hydroxy amphibole pargasite to 35 kilobars: Earth. Planet. Sci. Lett., v. 25, p. 44-48

Holmes A., 1950, Petrogenesis of katungite and its associates: Am. Mineral., v. 35, p. 772-792

Irving A.J., and Frey F.A., 1984, Trace element abundances in megacrysts and their host basalts: Constraints on partition coefficients and megacryst genesis: Geochim. Cosmochim. Acta, v. 48, p. 1202-1221

Irving A.J., 1974, Geochemical and high pressure experimental studies of garnet pyroxenite and pyroxene granulite xenoliths from the Delegate basaltic pipes, Australia: J. Petrol., v. 15, p. 1-40

Irving A.J., 1980, Petrology and geochemistry of composite ultramafic xenoliths in alkalic basalts and implications for magmatic processes within the mantle: Amer. J. Sci., v. 280A, p. 389-426

Irving A.J., 1974, Pyroxene rich ultramafic xenoliths in the Newer Basalts of Victoria, Australia: Neues. Jb. Mineral. Abh., v. 120, p. 147-167

Jaques A.L., and Green D.H., 1980, Anhydrous melting of peridotite at 0-15 kb pressure and the genesis of tholeiitic basalts: Contrib. Mineral. Petrol., v. 73, p. 287-310

Jenkins D.M., 1983, Stability and composition relations of calcitic amphiboles in ultramafic rocks: Contrib. Mineral. Petrol., v. 83, p. 375-384

Joplin G.A., 1963, Chemical analysis of Australian rocks, Part 1: Igneous and metamorphic: Bull. Bur. Miner. Resour. Geol. Geophys. Aust., v. 65.

Keller J., 1981, Carbonatitic volcanism in the Kaiserstuhl alkaline complex: Evidence for highly fluid carbonatitic melts at the earth's surface: J. Volcanol. Geotherm. Res., v. 9, p. 423-431

Kempton P.D., 1987, Mineralogic and geochemical evidence for differing styles of metasomatism in spinel lherzolite xenoliths: enriched mantle source regions of basalts? In Menzies M.A., and Hawkesworth C.J., Eds, Mantle metasomatism, London, Academic Press, p. 45-89

Kempton P.D., Menzies M.A., and Dungan M.A., 1984, Petrography, petrology and geochemistry of xenoliths and megacrysts from the Geronimo volcanic field, southeastern Arizona: Kimberlites: 2, the mantle and crust-mantle relationships, in Kornprobst J., Ed, Devs. Petrology, vol 11B: Amsterdam, Elsevier, p. 71-74393p.

Kempton P.D., Dungan M.A., and Blanchard D.P., 1987, Petrology and geochemistry of xenolith-bearing alkalic basalts from the Geronimo Volcanic Field, south east Arizona, Evidence for polybaric fractionation and implications for mantle heterogeneity, in Morris E.M., and Pasteris J.D., Eds, Mantle metasomatism and alkali magmatism, Geol. Soc. Amer. Spec. Paper 215, p.347-370

Kjarsgaard B.A., and Hamilton D.L., 1988, Liquid immiscibility and the origin of alkali-poor carbonatites: Mineral. Mag., v. 52, p. 43-56

Knorring O. von., and DuBois C.G.B., 1961, Carbonatitic lava from Fort Portal area in western Uganda: Nature, v. 192, p. 1064-1065

Kornprobst J., Pineau F., Degiovanni R., and Dautria J.M., 1987, Primary igneous graphite in ultramafic xenoliths 1: Petrology of the cumulate suite in alkali basalt near Tisseiut (Eggere, Algerian Sahara): J. Petrol., v. 28, p. 293-311

Koster van Groos A.F., and Wyllie P.J., 1966, Liquid immiscibility in the system Na_2O-Al_2O_3-SiO_2-CO_2 at pressures to 1 kilobar: Amer. J. Sci., p. 234-255

Koster van Groos A.F., and Wyllie P.J., 1968, Liquid immiscibility in the join $NaAlSi_3O_8$-Na_2CO_3-H_2O and its bearing on the genesis of carbonatites: Amer. J. Sci., v. 266, p. 932-967

Koster van Groos A.F., and Wyllie P.J., 1973, Liquid immiscibility in the join $NaAlSi3O_8$-$CaAl_2Si_2O_8$-Na_2CO_3-H_2O: Amer. J. Sci., v. 273, p. 465-487

Koster van Groos A.F., 1975, The effect of high CO_2 pressures on alkali rocks and its bearing on the formation of alkalic ultrabasic rocks and the associated carbonatites: Amer. J. Sci., v. 275, p. 163-185

Kramers J., Roddick J., and Dawson J., 1983, Trace element and isotope studies on veined, metasomatic and 'MARID' xenoliths from Bultfontein, South Africa: Earth Planet. Sci. Lett., v. 65, p. 90-106

Kuno H., and Aoki K., 1970, Chemistry of ultramafic nodules and their bearing on the origin of basaltic magmas: Phys. Earth Planet. Interiors, v. 3, p. 273-301

Kushiro I., 1970, Stability of amphibole and phlogopite in the upper mantle: Carnegie Inst. Wash. Yearbk., v. 68, p. 245-247

Lambert I.B., and Wyllie P.J., 1968, Stability of hornblende and a model for the low velocity zone: Nature, v. 219, p. 1240-1241

Lancelot J.R., and Allegre C.J., 1974, Origin of carbonatitic magma in light of the Pb-U-Th isotope system : Earth Planet. Sci. Lett., v. 22, p. 233-238

Leavy B.D., and Hermes O.D., 1979, Mantle xenoliths from Southeastern New England: in Boyd F.R., and Meyer H.O.A., The Mantle Sample: Inclusions in Kimberlites and other Volcanics, Eds, Washington, p. 374-381

LeBas M.J., 1977, Carbonatite-nephelinite volcanism: an African case history: London, Wiley, Interscience.

LeBas M.J., 1977, Carbonatite-nephelinite volcanism: an African case history: London, Wiley, Interscience.

LeBas M.J., 1981, Carbonatite magmas: Mineral Mag., v. 44, p. 133-140

LeBas M.J., 1987, Nephelinites and carbonatites: in J.G. Fitton, and B.G.J. Upton, Eds, Alkaline Igneous Rocks, Oxford, Blackwell, p. 53-84

LeMaitre R.W., 1981, GENMIX - A generalised petrological mixing model program: Comput. Geosci., v.7, p.229-247

Lloyd F.E., and Bailey D.K., 1975, Light element metasomatism of the continental mantle: the evidence and the consequences: Phys. Chem. Earth , v. 9, p. 389-416

Lovering J.F., and White A.J.R., 1964, The significance of primary scapolite in granulitic inclusions from deep-seated pipes: J. Petrol., v. 5, p. 195-218

Maaloe S., and Aoki K., 1977, The major element composition of the upper mantle estimated from the composition of lherzolites: Contrib. Mineral. Petrol., v. 63, p. 161-173

McGetchin T.R., and Besancon J.R., 1973, Carbonate inclusions in mantle-derived pyropes: Earth. Planet. Sci. Lett., v. 18, p. 408-410

McGuire A.V., 1988, The mantle beneath the Red Sea margin: xenoliths from western Saudi Arabia: Tectonophysics, v. 150, p. 101-120

McGuire A.V., 1988, Petrology of mantle xenoliths from Harrat al Kishb: the mantle beneath Western Saudi Arabia: J. Petrol., v. 29, p. 73-92

McKenzie D., 1984, The generation and compaction of partially molten rock: J. Petrol., v. 25, p. 713-765

McKie D., and Frankis E.J., 1977, Nyerereite: A new volcanic carbonate mineral from Oldoinyo Lengai: Zeitschrift fur Krystallographie, v. 145, p. 73-95

McNeil A.M., and Edgar A.D., 1987, Sodium-rich metasomatism in the upper mantle: Implications of experiments on the pyrolite-Na_2O-rich fluid system at 950°C, 20 kbar: Geochim. Cosmochim. Acta, v. 51, p. 2285-2294

Medaris L.G., 1984, A geothermobarometric investigation of garnet peridotites in the western gneiss region of Norway: Contrib. Mineral. Petrol., v. 87, p. 72-86

Medaris L.G., 1980, Petrogenesis of the Lien Peridotite and associated eclogites, Almklovdalen, Western Norway: Lithos, v. 13, p. 339-353

Meen J.K., 1987, Mantle metasomatism and carbonatites; An experimental study of a complex relationship: Geol. Soc. Amer. Spec. Paper. 215, p. 91-99

Melson W.G., Hart S.R., and Thompson G., 1972, St. Paul's Rocks, equatorial Atlantic: petrogenesis, radiometric ages and implications on sea-floor spreading: Geol. Soc. Am. Mem. 132, p. 241-72

Mengel K., 1981, Petrographische und geochemische Untersuchungen an Tuffen des Habichtswaldes und seiner Umgebung und an deren Einschlussen aus der tieferen Kruste und dem oberen Mantel: PhD Diss. Universitst Gottingen (FRG).

Mengel K., and Green D.H., 1989, Stability of amphibole and phlogopite in metasomatized peridotite under water-saturated and water-undersaturated conditions: Australian J. Earth Sci. Spec. Pub. 14, IV International Kimberlite Conference, in press

Menzies M.A., 1987, Alkaline rocks and their inclusions: a window on the Earth's interior: The alkaline rocks, in Fitton J.G., and Upton B.G.J., Eds, Geol. Soc. London Spec. Pub. 30, p. 15-27

Menzies M.A., and Hawkesworth C.J., 1987, Mantle Metasomatism: London, Academic Press.

Menzies M., and Wass S.Y., 1983, CO_2 and LREE-rich mantle below eastern Australia; A REE and isotope study of alkaline magmas and apatite rich mantle xenoliths from the Southern Highlands Provence, Australia: Earth. Planet. Sci. Lett., v. 65, p. 287-302

Menzies M.A., Rogers N., Tindle A., and Hawkesworth C.J., 1987, Metasomatic and enrichment processes in lithospheric peridotites, an effect of asthenosphere-lithosphere interaction: Mantle Metasomatism, in Menzies M.A., and Hawkesworth C.J., Eds, London, Academic Press, p. 313-361

Mercier J.C.C., and Nicolas A., 1975, Textures and fabrics of upper mantle peridotites as illustrated by basalt xenoliths: J. Petrol., v. 16, p. 454-487

Merrill R.B., and Wyllie P.J., 1975, Kaersutite and kaersutite eclogite from Kakanui, New Zealand - Water-excess and water-deficient melting to 30 kilobars: Geol. Soc. Amer. Bull., v. 86, p. 555-570

Millhollen G.L.. and Wyllie P.J., 1974, Melting relations of brown-hornblende mylonite from St. Paul's rocks under water-saturated and water-undersaturated conditions to 30 kilobars: J. Geology, v. 82, p. 589-606

Millhollen G.L., Irving A.J., and Wyllie P.J., 1974, Melting interval of peridotite with 5.7 percent water to 30 kilobars: J. Geology, v. 82, p. 575-587

Milton C., 1968, The natro-carbonatite lava" of Oldoinyo Lengai, Tanzania: Geol. Soc. Amer. Spec. Paper 121, p. 202

Mitchell R.H., 1979, The alleged kimberlite-carbonatite relationship: Additional contrary mineralogical evidence: Amer. J. Sci., v. 279, p. 570-589

Mitchell R.H., and Clarke D.B., 1976, Oxide and sulphide mineralogy of the Peuyuk kimberlite, Somerset Island, N.W.T., Canada: Contrib. Mineral. Petrol., v. 56, p. 157-172

Mitchell R.H., and Janse A.J.A., 1982, A harzburgite-bearing monchiquite from Wawa, Ontario: Can. Mineral., v. 20, p. 211-216

Mori T., and Green D.H., 1978, Laboratory duplication of phase equilibria observed in natural garnet lherzolites: J. Geol., v. 86, p. 83-97

Morogan V., and Martin R.F., 1985, Mineralogy and partial melting of fenitized crustal xenoliths in the Oldoinyo Lengai carbonatitic volcano, Tanzania: Amer. Mineral., v. 70, p. 1114-1126

Mysen B.O., and Boettcher A.L., 1975, Melting of a hydrous mantle (parts 1 and 2): J. Petrol., v. 15, p. 520-548, 549-593

Mysen B., Ryerson F.J., and Virgo D., 1981, The structural role of phosphorus in silicate melts: Amer. Mineral., v. 66, p. 106-117

Nakamura N., 1974, Determination of REE, Ba, Fe, Mg, Na, and K in carbonaceous and ordinary chondrites: Geochim. Cosmochem. Acta, v. 38, p. 757-776

Navon O., Hutcheon I.D., Rossman G.R., and Wasserburg G.J., 1988, Mantle-derived fluids in diamond micro-inclusions: Nature, v. 355, p. 784-789

Neal C.R., 1988, The origin and composition of metasomatic fluids and amphiboles beneath Malaita, Solomon Islands: J. Petrol., v. 29, p. 149-180

Neal C.R., and Nixon P.H., 1986, Spinel-garnet relationships in mantle xenoliths from the Malaita alnoite, Solomon Islands, South-western Pacific: Trans. Geol. Soc. S. Africa, v. 88, p. 347-354

Nelson D.R., Chivas A.R., Chappell B.W., and McCulloch M.T., 1988, Geochemical and isotopic systematics in carbonatites and implications for the evolution of ocean-island sources: Geochim. Cosmochim. Acta, v. 52, p. 1-17

Nesbitt B.E., and Kelly W.C., 1977, Magmatic and hydrothermal inclusions in carbonatite of the Magnet Cove complex, Arkansas: Contrib. Mineral. Petrol., v. 63, p. 271-94

Newton R.C., and Sharp W.E., 1975, Stability of forsterite + CO_2 and its bearing on the role of CO_2 in the mantle: Earth Planet. Sci. Lett., v. 26, p. 239

Nickel K.G., and Green D.H., 1985, Empirical geothermobarometry for garnet peridotites and implications for the nature of the lithosphere, kimberlites and diamonds: Earth Planet. Sci. Lett., v. 73, p. 158-170

Nickel K.G., and Green D.H., 1984, The nature of the uppermost mantle beneath Victoria, Australia as deduced from ultramafic xenoliths: in Kornprobst J., Ed, Kimberlites: 2, The mantle and crust-mantle relationships, Devs Petrology, vol. 11A: Amsterdam, Elsevier, p. 161-178

Nixon P.H., 1987, Mantle Xenoliths: New York, Wiley.

Nixon P.H., and Boyd F.R., 1979, Garnet bearing lherzolites and discrete nodule suites from the Malaita alnoite, Solomon Islands, S.W. Pacific, and their bearing on oceanic composition and geotherm: in Boyd F.R., and Meyer H.O.A., Eds, The mantle sample: inclusions in kimberlites and other volcanics. (Proc. Int. Kimberlite Conf., No. 2., Vol. 2), x Washington D.C., American Geophysical Union, p. 400-423

Nixon P.H., and Hornung G., 1973, The carbonatite lavas and tuffs near Fort Portal, Western Uganda: Overseas Geol. Mineral Resources, v. 41, p. 168-179

Nixon P.H., Chapman N.A., and Gurney J.J., 1978, Pyrope-spinel (alkremite) xenoliths from kimberlite: Contrib. Mineral. Petrol., v. 65, p. 341-346

O'Neil J.R., and Hay R.L., 1973, $^{18}O/^{16}O$ ratios in cherts associated with the saline lake deposits of East Africa: Earth. Planet. Sci. Lett., v. 19, p. 257-266

O'Neill H.St.C., and Wall V.J., 1987, The olivine-orthopyroxene-spinel oxygen geobarometer, the nickel precipitation curve, and the oxygen fugacity of the Earth's upper mantle: J. Petrol., v. 28, p. 1169-1192

O'Reilly S.Y., 1987, Volatile-rich mantle beneath eastern Australia: Mantle Xenoliths, in P.H. Nixon, Ed, London, Wiley, p. 661-670

O'Reilly S.Y., and Griffin W.L., 1985, A xenolith-derived geotherm for southeastern Australia and its geophysical implications: Tectonophysics, v. 111, p. 41-64

O'Reilly S.Y., and Griffin W.L., 1988, Mantle metasomatism beneath western Victoria, Australia: 1. Metasomatic processes in Cr-diopside lherzolites: Geochim. Cosmochim. Acta, v. 53, p. 433-447

Obata M., 1980, The Ronda peridotite: garnet-spinel and plagioclase - lherzolite facies and the P-T trajectories of a high-temperature mantle intrusion: J. Petrol., v. 21, p. 533-572

Obata M., and Morten L., 1982, Remnants of some high-temperature peridotite and the transformation from spinel-lherzolite to garnet-peridotite observed in the ultramafic bodies in the Austridic metamorphic terraine, between Non and Ultimo Valleys, northern Italy: Terra Cognita, v. 2, p. 329

Olafsson M., and Eggler D.H., 1983, Phase relations of amphibole, amphibole-carbonate, and phlogopite-carbonate peridotite: petrologic constraints on the asthenosphere: Earth Planet. Sci. Lett., v. 64, p. 305-315

Oxburgh E.R., 1964, Petrological evidence for the presence of amphibole in the upper mantle and its petrogenetic and geophysical implications: Geol. Mag., v. 101, p. 1-19

Ozawa K, 1986, Partioning of elements between constituent minerals in peridotites from the Miyamori ultramafic complex, Kitakami mountains, northeast Japan: Estimation of P-T conditions and igneous composition of minerals: J. Fac. Sci. University of Tokyo, v. 21, p. 115-137

Ozawa K., 1988, Ultramafic tectonite of the Miyamori ophiolitic complex in the Kitakami Mountains, Northeast Japan: hydrous upper mantle in an island arc: Contrib. Mineral. Petrol., v. 99, p. 159-175

Palme H., and Nickel K.G., 1985, Ca/Al ratio and composition of the earth's upper mantle: Geochem. Cosmochem. Acta, v. 49, p. 2123-2132

Pasteris J.D., 1987, Fluid inclusions in mantle xenoliths: Mantle xenoliths, in Nixon P.H., Ed, New York, John Wiley, p. 691-707

Peterson T.D., and Marsh B.D., 1986, Sodium metasomatism and mineral stabilities in alkaline ultramafic rocks: implications for the origin of the sodic lavas of Oldoinyo Lengai: EOS, v. 67, p. 389-390

Powell J.L., 1966, Isotopic composition of strontium in carbonatites and kimberlites: Mineral Soc. India, p. 58-66

Press S., Witt G., and Seck H.A., 1986, Spinel peridotite xenoliths from the Tariat Depression, Mongolia. I: Major element chemistry and mineralogy of a primitive mantle xenolith suite: Geochem. Cosmochem. Acta, v. 50, p. 2587-2600

Rankin A.H., and Le Bas M.J., 1974, Nahcolite ($NaHCO_3$) in inclusions in apatites from some E. African ijolites and carbonatites: Mineral. Mag., v. 39, p. 564-570

Rankin A.H., 1977, Fluid-inclusion evidence for the formation conditions of apatite from the Tororo carbonatite complex of eastern Uganda: Mineral. Mag., v. 41, p. 155-164

Robie R.A., Hemingway B.S., and Fisher J.R., 1979, Thermodynamic properties of minerals and related substances at 298.15 K and 1 bar (10^5 pascals) pressure and at higher temperatures: Geol. Sur. Bull. 452, Washington, United States Government Printing Office

Robinson P., Spear F.S., Schumacher J.C., Laird J., Klein C., Evans B.W., and Doolan B.L., 1982, Phase relations of metamorphic amphiboles: natural occurrence and theory: Amphiboles: petrology and experimental phase relations, in Veblen D.R., and Ribbe P.H., Eds, Reviews in Mineralogy vol 9B Mineral. Soc. Amer., p. 3-42

Roden M.K., Hart S.R., Frey F.A., and Melson W.G., 1984, Sr, Nd, and Pb isotopic and REE geochemistry of St. Paul's Rocks: the metamorphic and metasomatic development of an alkali basalt mantle source: Contrib. Mineral. Petrol., v. 85, p. 379-400

Roedder E., 1965, Liquid CO_2 inclusions in olivine-bearing nodules and phenocrysts from basalts: Amer. Mineral., v. 50, p. 1746-1782

Ryabchikov I.D., and Boettcher A.L., 1980, Experimental evidence at high pressure for potassic metasomatism in the mantle of the earth: Amer. Mineral., v. 65, p. 915-919

Ryabchikov I.D., Green D.H., Wall W.J., and Brey G.P., 1981, The oxidation state of carbon in the reduced-velocity zone: Geochem. International, p. 148-158

Sachtleben T., and Seck H.A, 1981, Chemical control of Al-solubility in orthopyroxene and its implications for pyroxene geothermometry: Contrib. Mineral. Petrol., v. 78, p. 157-165

Schneider M.E., and Eggler D.H., 1984, Compositions of fluids in equilibrium with peridotite; Implications for alkaline magmatism-metasomatism: Kimberlites 1; Kimberlites and related rocks, in J. Kornprobst, Ed, Amsterdam, Elsevier, p. 383-394

Schneider M.E., and Eggler D.H., 1987, Fluids in equilibrium with peridotite minerals: complications for mantle metasomatism: Geochim. Cosmochim. Acta, v. 50, p. 7211-7242

Sen G., 1987, Xenoliths associated with the Hawaiian hot spot : in Nixon P.H., Ed, Mantle xenoliths, New York, John Wiley, p. 359-375

Seyler M., and Mattson P.H., 1989, Petrology and thermal evolution of the Tinaquillo peridotite, Venezuela: J. Geophys. Res., in press

Sheppard S.M.F., and Dawson J.B., 1975, Hydrogen, carbon and oxygen isotope studies of megacryst and matrix minerals from Lesothan, South African kimberlites: Phys. Chem. Earth., v. 9, p. 747-763

Smith C.B., 1983, Pb, Sr and Nd isotopic evidence for sources of southern African Cretaceous kimberlites: Nature, v. 304, p. 51-54

Smith D., 1979, Hydrous minerals and carbonates in peridotite inclusions from the Green Knobs and Buell Park kimberlitic diatremes on the Colorado Plateau: The Mantle Sample: Inclusions in Kimberlites and other Volcanics, in Boyd F.R., and Meyer H.O.A.,, Washington, p. 345-356

Smith D., 1987, Genesis of carbonate in pyrope from ultramafic diatremes on the Colorado Plateau, south western United States: Contrib. Mineral. Petrol., v. 97, p. 389-396

Stewart D.C., and Boettcher A.L., 1977, Chemical gradients in mantle xenoliths: Geol. Soc. Amer. Annual Mtg., v. 9, p. 1191-1192

Stolz A.J., and Davies G.R., 1988, Chemical and isotopic evidence from spinel lherzolite xenoliths for episodic metasomatism of the upper mantle beneath Southeast Australia: J. Petrol. Spec. Issue, p. 303-330

Stosch H.G., and Seck H.A., 1980, Geochemistry and mineralogy of two spinel peridotite suites from Dreiser Weiher, West Germany: Geochim. Cosmochim. Acta, v. 44, p. 457-470

Streckeisen A., 1980, Classification and nomenclature of volcanic rocks, lamprophyres, carbonatites and melilitic rocks.: Geol. Rundschau, v. 69, p. 194-207

Sun S.S., 1982, Chemical composition and origin of the Earth's primative mantle: Geochim. Cosmochim. Acta , v. 46, p. 179-192

Takahashi E., 1980, Thermal history of lherzolite xenoliths from the Ichinomegata Crater, Oga Peninsula, northeast Japan: Geochim. Cosmochim. Acta, v. 44, p. 1643-1658

Taylor W.R., and Green D.H., 1988, Measurement of reduced peridotite-C-O-H solidus and implications for redox melting of the mantle: Nature, v. 332, p. 349-352

Tsai H.M. Shieh T.N., and Meyer H.O.A., 1979, Mineralogy and S^{34}/S^{32} ratios of sulfides associated with kimberlite, xenoliths and diamonds: in Boyd F.R., and Meyer H.O.A., Eds, Kimberlites, diatremes and diamonds; their geology, petrology and chemistry. (Proc. Int. Kimberlite Conf., No. 2, Vol. 1),Washington D.C., American Geophysical Union, p. 87-103399p.

Twyman J.D., and Gittins J., 1985, Alkalic carbonatite magmas: parental or derivative: J. Geol., v. 142, p. 706-707

Twyman J.D., and Gittins J., 1987, Alkalic carbonatite magmas: parental or derivative: Alkaline Igneous Rocks, in Fitton J.G., and Upton B.G.J., Eds, Oxford, Blackwell, p. 85-94

Varne R., 1970, Hornblende lherzolite and the upper mantle: Contrib. Mineral. Petrol., v. 27, p. 45-51

Veblen D.R., and Ribbe P.H., 1982, Amphiboles: petrology and experimental phase relations; Mineral. Soc. Amer. Reviews in Mineralogy, v. 9B

Wass, S.Y., 1979, Fractional crytallization in the mantle of late-stage kimberlitic liquids-evidence in xenoliths from the Kiama area, NSW, Australia: in Nixon P.H., Ed, The Mantle Sample: Inclusions in Kimberlites and Other Volcanics: Washington, A.G.U., p. 266-373

Wass S.Y., and Irving A.J., 1976, XENMEG: a catalogue of occurrences of xenoliths and megacrysts in volcanic rocks of eastern Australia: Sydney, Australian Museum.

Wass S.Y., and Rogers N.W., 1980, Mantle metasomatism - precursor to continental alkaline volcanism: Geochim. Cosmochim. Acta, v. 44, p. 1811-1823

Wells P.R.A., 1977, Pyroxene thermometry in simple and complex systems: Contrib. Mineral. Petrol., v. 62, p. 129-139

Wendlandt R.F., and Harrison W.J., 1979, Rare earth partitioning between immiscible carbonate and silicate liquids and CO_2 vapor: results and implications for the formation of light rare earth-enriched rocks: Contrib. Mineral. Petrol., v. 69, p. 404-419

Wendlandt R.F., and Morgan P., 1982, Lithospheric thinning associated with rifting in East Africa: Nature, v. 298, p. 734-736

Wendlandt R.F., and Mysen B.O., 1980, Melting phase relations of natural peridotite + CO_2 as a function of degree of partial melting at 15 and 20 kbar: Amer. Mineral., v. 65, p. 37-44

Wilkinson J.F.G., and LeMaitre R.W., 1987, Upper mantle amphiboles and micas and TiO_2, K_2O and P_2O_5 abundances and (100Mg/Mg + Fe^{2+}) ratios of common basalts and andesites: implications for modal mantle metasomatism and undepleted mantle compositions: J. Petrol., v. 28, p. 37-74

Williams R.W., Gill J.B., and Bruland K.W., 1986, Ra-Th disequilibria systematics: Timescale of carbonatite magma formation at Oldoinyo Lengai volcano, Tanzania: Geochim. Cosmochim. Acta, v. 50, p. 1249-1259

Wilshire H.G., and Shervais J.W., 1975, Al-augite and Cr-diopside ultramafic xenoliths in basaltic rocks from western United States: Phys. Chem. Earth., v. 9, p. 257-272

Wilshire H.G., Calk L.C., and Schwarzman E.C., 1971, Kaersutite - a product of reaction between pargasite and basanite at Dish Hill, California: Earth Planet. Sci. Lett., v. 10, p. 281-284

Wilshire, H.G., Neilson-Pike, J.E., Meyer, C.E., and Schwarzman, E.C., 1980, Amphibole-rich veins in lherzolite xenoliths, Dish Hill and Deadman Lake, California: Amer. J. Sci., v. 280A, p. 576-593

Wilshire, H.G., and Trask, N.J., 1971, Structural and textural relationship of amphibole and phlogopite in peridotite inclusions, Dish Hill, California: Amer. Mineral., v. 56, p. 240-255

Wilshire H.G., Pike J.E.N., Meyer C.E., and Schwarzmann E.C., 1980, Amphibole rich veins in lherzolite xenoliths, Dish Hill and Deadman Lake, California: Amer. J. Sci., v. 280A, p. 576-593

Witt G., and Seck H.A., 1987, Temperature history of sheared mantle xenoliths from the West Eifel, West Germany: evidence for mantle diapirism beneath the Rhenish Massif: J. Petrol., v. 28, p. 475-493

Wood D.A., 1979, A variably veined sub-oceanic upper mantle -genetic significance for mid-ocean ridge basalts from geochemical evidence: Geology, v. 7, p. 499-504

Wyllie P.J., 1965, Melting relationships in the system $CaO-MgO-CO_2-H_2O$ with petrological applications: J. Petrol., v. 6, p. 101-123

Wyllie P.J., 1966, Experimental studies of carbonatite problems: The origin and differentiation of carbonatite magmas: Carbonatites, in O.F. Tuttle, and J. Gittins, Eds, New York, Interscience, p. 311-352

Wyllie P.J., 1978, Mantle fluid compositions buffered in peridotite-CO_2-H_2O by carbonates, amphibole, and phlogopite: J. Geol., v. 86, p. 687-713

Wyllie P.J., 1980, The origin of kimberlites: J. Geophys. Res., v. 85, p. 6902-6910

Wyllie P.J., 1987, Transfer of subcratonic carbon into kimberlites and rare earth carbonatites: Magmatic Processes: Physiochemical Principles, in Mysen B.O., Ed, The Geochemical Society Spec. Publ. 1, p. 107-120

Wyllie P.J., 1987, Discussion of recent papers on carbonated peridotite bearing on mantle metasomatism and magmatism: Earth Planet. Sci. Lett., v. 82, p. 391-397

Wyllie P.J., and Huang W.L., 1976, Carbonation and melting reactions in the system $CaO-MgO-SiO_2-CO_2$ at mantle pressures with geophysical and petrological applications: Contrib. Mineral. Petrol., v. 54, p. 79-107

Wyllie P.J., and Huang W.L., 1975, Peridotite, kimberlite, and carbonatite explained in the system $CaO-MgO-SiO_2-CO_2$: Geology, v. 3, p. 621-624

APPENDIX A

DATABASE OF AMPHIBOLES FROM NATURAL LHERZOLITES

List of samples, localitites, and references	120
Amphibole analyses	125
Coexisting orthopyroxene analyses	132
Coexisting clinopyroxene analyses	137
Coexisting spinel analyses	142
Coexisting garnet analyses	145
Coexisting mica analyses	146
Lherzolite bulk rock compositions	147

Appendix A. List of published analyses of pargasitic amphiboles from peridotite assemblages

Location	Sample	Reference	Co-existing phases	Published analyses
Lherzolites in Alkali Basalts				
Massif Central, France	Li-9	Brown et al 1980	Ol,opx,cpx,sp	Ol,opx,cpx,sp
	Li-35		Ol,opx,mica	Ol,opx,mica
	Li-52		Ol,opx,cpx,sp	Ol,opx,cpx
	Cp-15		Ol,opx,cpx,sp	Ol,opx,cpx,sp
	B182	Menzies et al 1987	Ol,opx,cpx,sp,mica	mica
	B101		Ol,opx,cpx,sp,mica	mica
Languedoc,S.France	H204B	Fabries et al 1987	Ol,opx,cpx,sp	Ol,opx,cpx,sp
	80-437		Ol,opx,cpx,sp	Ol,opx,cpx,sp
	80-442		Ol,opx,cpx,sp	Ol,opx,cpx,sp
	76-250		Ol,opx,cpx,sp	Ol,opx,cpx,sp
W. Eifel, Germany	DF78	Stosch & Seck 1980	-	-
	1	Witt & Seck 1987	-	-
	2		-	-
	3		-	-
	4		-	-
N.H.D, Germany	Pr.Nr.BDHX	Mengel 1981	Ol,opx,cpx,sp,mica	Ol,opx,cpx,mica
Deudesfeld, Germany	Deudes 1-82	Menzies et al 1987	Ol,opx,cpx,sp,mica	mica,BR
Nunivak Island, Alaska	10016	Francis 1976	Ol,opx,cpx,sp,mica	cpx,mica
	14001		Ol,opx,cpx,sp	-
	10067		Ol,opx,cpx,sp	-
	10050		Ol,opx,cpx,sp	-
	10006		Ol,opx,cpx,sp,mica	cpx,mica
	10013		Ol,opx,cpx,sp,mica	mica
	10052		Ol,opx,cpx,sp	-
	10051	Menzies et al 1987	Ol,opx,cpx,sp,mica	mica
Dish Hill,California	Ba-1-52	Wilshire & Trask 1971		
	Ba-2-1	Wilshire et al 1980	Ol,opx,cpx,sp	-
San Carlos,Arizona	PA-120G	Frey & Prinz 1978	Ol,opx,cpx,sp	Ol,opx,cpx,sp
Grand Canyon,Arizona	S6	Best 1974	Ol,opx,cpx,sp	-
	E25A		Ol,opx,cpx,sp	-
	E33		Ol,opx,cpx,sp	-
Hawaii	69ULUP	Sen 1987	Ol,opx,cpx,sp	Ol
	SL011	Goto & Yokoyama 1988	Ol,opx,cpx,sp	Ol,opx,cpx,sp
	SL138		Ol,opx,cpx,sp	Ol,opx,cpx,sp
Hoggar,Algeria	TAH4	Girod et al 1981	Ol,opx,cpx,sp	BR
	TAH88		Ol,opx,cpx,sp	BR
	ATK88		Ol,opx,cpx,sp	-
	V	Kornprobst et al 1987	Opx,cpx,sp,graphite	Opx,cpx,sp
	TAH276-35	Dautria et al 1987	Ol,opx,cpx,sp	BR

Location	Sample	Reference	Co-existing phases	Published analyses
Ataq	AT-15	Varne 1970	Ol,opx,cpx,sp	Ol,opx,cpx,BR
Tariat depression Mongolia	MO4230/16	Press et al 1986	Ol,opx,cpx,sp,mica	Ol,opx,cpx,sp,mica,BR
	MO104		Ol,opx,cpx,sp,mica	Ol,opx,cpx,sp,mica,BR
Ichinomegata, Japan	LHZ-13	Takahashi 1980	Ol,opx,cpx,sp	Ol,opx,cpx,sp
	Lhz-53		Ol,opx,cpx,sp	Ol,opx,cpx,sp
	Lhz-29		Ol,opx,cpx,sp	Ol,opx,cpx,sp
	#87	Kuno & Aoki 1970	Ol.opx,cpx,gt	Ol,opx,cpx
	I-014	Arai 1986	Ol,opx,cpx,sp	-
Lake Bullenmerri, Victoria	BM-9	Nickel & Green 1984	Ol,opx,cpx.sp	opx,cpx,sp
	BM-15		Ol,opx,cpx.sp	opx,cpx,sp
	BM-18		Ol,opx,cpx,sp,ap	opx,cpx,sp,BR
	BM-27		Ol,opx,cpx.sp	opx,cpx,sp
	BM-47		Ol,opx,cpx.sp	opx,cpx,BR
	BM-51		Ol,cpx,sp,ap	cpx,sp,BR
	BM-58		Ol,opx,cpx.sp	opx,cpx,sp
	BM-62		Ol,opx,cpx.sp	opx,cpx,sp
	BM-74		Ol,opx,cpx.sp	opx,cpx,sp
	BM-109		Ol,cpx,sp	opx,cpx,sp
	BM-116		Ol,opx,cpx.sp	opx,cpx,sp,BR
	BM-134		Ol,opx,cpx.sp	opx,cpx,sp,BR
	BM-135		Ol,opx,cpx.sp	cpx,BR
	BM-137		Ol,opx,cpx.sp	opx,cpx,sp,BR
	BM-139		Ol,opx,cpx.sp	opx,cpx,sp,BR
	BM-143		Ol,opx,cpx,sp,mica	opx,cpx,sp,mica,BR
	BM-147		Ol,opx,cpx.sp	opx,cpx,sp
	BM-154		Ol,opx,cpx.sp	opx,cpx,sp,BR
	BM-161		Ol,opx,cpx.sp	opx,cpx,sp
	BM-163		Ol,opx,sp	opx,sp,BR
	BM-166		Ol,opx,cpx.sp	opx,cpx,sp
	BM-167		Ol,opx,cpx,sp	opx,cpx,sp,BR
	BM-654	Griffin et al 1984	Ol,opx,cpx,sp,ap	opx,cpx,sp,BR
	BM-632		Ol,opx,cpx,sp,ap	opx,cpx
	BM-189		Ol,opx,cpx,sp	opx,cpx,sp
	Bm-18	Stoltz & Davies 1988	Ol,opx,cpx,sp	opx,cpx,sp
	BM635	O'Reilly & Griffin 1988	-	BR
	WGBM1		-	BR
	WGBM11		-	BR
	WGBM16		-	mica,BR
Mt Leura, Victoria	LE-2641	Nickel & Green 1984	Ol,opx,cpx,sp	opx,cpx,sp
	LE-2642	Frey & Green 1974	Ol,opx,cpx,sp	Ol,opx,cpx,sp,BR
Lake Gnotuk, Victoria	Gn-15	Stoltz & Davies 1988	Ol,opx,cpx,sp	opx,cpx,sp
	Gn-2		Ol,opx,cpx,sp	opx,cpx,sp
	Gn-3		Ol,opx,cpx,sp	opx,cpx,sp
	Gn-16		Ol,opx,cpx,sp	opx,cpx,sp
	Gn-20A		Ol,opx,cpx,sp	opx,cpx,sp
	Gn20B		Ol,opx,cpx,sp	opx,cpx,sp
	Gn-24		Ol,opx,cpx,sp	opx,cpx,sp
	Gn-26		Ol,opx,cpx,sp,mica	opx,cpx,sp,mica

Location	Sample	Reference	Co-existing phases	Published analyses
Lherzolite xenoliths in other magma types				
Fen, Norway	1	Griffin 1973	Ol,opx,cpx,sp	Ol,opx,cpx,sp
(~575my) Damkjernite	2		Ol,opx,cpx,sp	Ol,opx,cpx,sp,BR
	4		Ol,opx,cpx,sp	Ol,opx,cpx,sp
	9		Ol,opx,cpx,sp	Ol,opx,cpx,sp,BR
	10		Ol,opx,cpx,sp	Ol,opx,cpx,sp
Malaita	PHN4022	Neil 1988	Ol,opx,cpx,sp	Ol,opx,cpx,sp
(34my) Alnoite	PHN4028		Ol,opx,cpx,sp	Ol,opx,cpx,sp
	PHN4073		Ol,opx,cpx,sp	Ol,opx,cpx,sp
	PHN4074		Ol,opx,cpx,sp	Ol,opx,cpx,sp
	PHN4085		Ol,opx,cpx,sp	Ol,opx,cpx,sp
	CRN216		Ol,opx,cpx,sp	Ol,opx,cpx,sp
	PHN4002		Ol,opx,cpx,gt,sp	Ol,opx,cpx,gt,sp
	PHN4009		Ol,opx,cpx,gt,sp	Ol,opx,cpx,gt,sp
	PHN4013		Ol,opx,cpx,gt,sp	Ol,opx,cpx,gt,sp
	PHN4034		Ol,opx,cpx,gt	Ol,opx,cpx,gt
	PHN4069		Ol,opx,cpx,gt,sp	Ol,opx,cpx,gt,sp
	CRN209		Ol,opx,cpx,gt,sp	Ol,opx,cpx,gt,sp
	PHN3550B	Delaney et al 1979	Opx,mica	opx,gt
	PHN3567		Ol,opx,cpx,gt,sp	Ol,cpx
	PHN3534		Ol,opx,cpx,sp	opx
	CRN205	Neal & Nixon 1986	Ol,opx,cpx,sp	opx,cpx,sp
Rhode Is	LN-4	Leavy & Hermes 1979	Ol,opx,cpx,sp	BR
(Alnoite)				
Lherzolite xenoliths in Kimberlites				
Jagersfontein	311	Field et al 1988	Ol,opx,cpx,gt,mica	Ol,opx,cpx,gt,mica
	259		Ol,opx,cpx,gt	Cpx
	557		Ol,opx,cpx,sp,gt	Opx,cpx,sp,gt
	576		Ol,opx,cpx,sp,gt,mica	Opx,sp,gt,mica
	571		Ol,opx,cpx,mica	Ol,opx,cpx,mica
	585		Ol,opx,cpx,sp,gt,mica	Sp,mica
	595		Ol,opx,cpx	-
	558		Ol,opx,cpx	-
Monastery	7429	Boyd 1971	-	-
	BD1368	Dawson et al 1975	-	-
Bultfontein	BD3707	Dawson et al 1982	-	-
Bellsbank	PJL13	Nixon et al 1978	-	-
Lesotho	PHN2508	Griffin et al 1979	-	-
Tanzania	DU-18500	Dawson & Smith 1982	Ol,cpx,chromite	Ol,cpx,chromite
Green Knobs,	N53	Smith,1979	Ol,opx,cpx,sp	Ol,opx,cpx,sp
N.Mexico	N55		Ol,opx,cpx,sp	Ol,opx,cpx,sp

Location	Sample	Reference	Co-existing phases	Published analyses
Alpine Peridotites				
Finero, N.Italy	F2A	Ernst 1978	Ol,opx,cpx	Ol,opx,cpx,BR
	F69		Ol,opx,cpx,mica	Ol,opx,mica
	F2D		Ol,opx,cpx,sp,mica	Ol,opx,cpx,sp,mica,BR
	197	Cawthorn 1975	Ol,opx,cpx,sp,mica	Ol,opx,cpx,sp
	106		Ol,opx,cpx,sp,mica	Ol,opx,BR
Alpe Arami	F-16a	Ernst 1978	Ol,opx,cpx,gt	Ol,opx,cpx,gt,BR
	F-16c		Ol,opx,cpx,sp,plag	Ol,opx,sp,BR
	F-52c		Ol,opx,cpx,gt,sp	Ol,opx,cpx,BR
Balmuccia, W.Alps	B-3C	Ernst 1978	Ol,opx,cpx,sp	Ol,opx,cpx,sp,BR
	F-58		Ol,opx,cpx,sp	Ol,opx,cpx,sp,BR
Lien Perid., Norway	1K	Medaris 1980	Ol,opx,cpx,gt	Ol,opx,cpx,gt
	1J		Opx,cpx,gt	opx,cpx,gt
	5-4-21C	Medaris 1984	Ol,opx,cpx,gt	Ol,opx,gt
	USC-8A		Ol,opx,cpx,gt	Ol,opx,gt
Ronda, S.Spain	R501	Obata 1980	Ol,opx,cpx,sp,gt	Ol,opx,cpx,sp,gt
	R740		Ol,opx,cpx,sp,gt	Ol,opx,cpx,sp,gt
	R696		Ol,opx,cpx,sp,gt	Ol,opx,cpx,sp,gt
	R123		Ol,opx,cpx,sp,gt	Ol,opx,cpx,sp,gt
	R243		Ol,opx,cpx,sp	Ol,opx,cpx,sp
	7319		Ol,opx,cpx,sp	Ol,opx,cpx,sp
Zabargad	Z-37	Bonatti et al 1986	Ol,opx,cpx,sp,plag	Opx,cpx,sp,plag,BR
	Z-42a		Ol,opx,cpx,sp,mica	Opx,cpx,sp,mica
	Z-42b		Ol,opx,cpx,sp	Opx
	Z-35		Ol,opx,cpx,sp,mica	Sp,mica,BR
	Z-206a		Ol,opx,cpx,sp	Sp,BR
	Z-206b		Ol,opx,cpx,sp	Sp
East Timor	7	Berry 1981	Ol,opx,cpx,sp	Ol,opx,cpx,sp,BR
	11		Ol,opx,cpx,sp	Ol,opx,cpx,sp
	12		Ol,opx,cpx,sp	Ol,opx,cpx,sp,BR
S.W. Oregon	VH3	Henry & Medaris 1980	Ol,opx,cpx,sp	-
	VH6		Ol,opx,cpx,sp	-
	VH9		Ol,opx,cpx,sp	Ol,opx,cpx,sp
	CSZ12		Ol,opx,cpx,sp	Ol,opx,cpx,sp
	SB17		Ol,opx,cpx,sp	-
Lizard	90691	Green 1964	Ol,opx,cpx,sp	-
Kinugasa, Japan	K-3	Arai 1986	Ol,opx,cpx,sp,mica	-
Miyamori, Japan	77073113	Ozawa 1986	Ol,opx,cpx,sp	Ol,opx,cpx,sp
	77111919		Ol,opx,cpx,sp	Ol,opx,cpx,sp

Location	Sample	Reference	Co-existing phases	Published analyses
Tinaquillo, Venezuela	5	Deer et al 1963	-	-
	80-21	Seyler & Mattson 1989	Ol,opx,cpx,sp	Ol,opx,cpx,sp,BR
	80-20		Ol,opx,cpx,sp	Ol,opx,cpx,sp,BR
	80-64		Ol,opx,cpx,sp	Ol,opx,cpx,sp,BR
	80-11		Ol,opx,cpx,sp	Ol,opx,cpx,sp,BR
	80-12		Ol,opx,cpx,sp	Ol, cpx,BR
	80-17		Ol,opx,cpx,sp	Ol,opx,cpx,sp,BR
	79-59		Ol,opx,cpx,sp	Ol,opx,cpx,sp,BR
	80-58		Ol,opx,cpx,sp	Br
	80-55		Ol,opx,cpx,sp	Ol,cpx,BR
	80-49		Ol,opx,cpx,sp	-
Nonsberg peridotite Austridic crystaline complex,N.Italy	MK5D	Obata & Morten 1982	Ol,opx,cpx,gt,sp	Ol,opx,cpx,gt,sp,BR
	MO11		Ol,opx,cpx,gt,sp	Ol,opx,cpx,sp,gt,BR
	MK5C		Ol,opx,cpx,gt,sp	Ol,opx,cpx,gt,sp,BR
	MK1		Ol,opx,gt,sp	Ol,opx,gt,sp,Br
	ULT12		Ol,opx,gt,sp	Ol,opx,gt,sp,Br
	ULT4		Ol,opx,sp	Ol,opx,sp,Br
	300B		Ol,opx,sp	Ol,opx,sp,Br
	MO9		-	-

Amphibole (1)

Location	Massif Central					Languedoc					P.D'Aspet	NHD Deudesfeld	
Number	LI-9	LI-35	LI-52	Cp-15	B182	B101	H204B	80-437	80-442	76-250	322	BOHX	D1-82
SiO2	43 10	43 40	43.20	42 70	43 61	43 73	42 21	43 63	42 87	43 93	42 87	42 65	43 83
TiO2	2 06	0.57	0 75	2 83	0 72	2 33	1 82	2 32	1.34	2.73	0 77	1 33	2 22
Al2O3	14 20	12.60	13 90	13 80	13.32	12 89	15 30	14 78	15 04	14 86	16.01	14 02	12 04
Cr2O3	0 80	1 46	1.63	0 79	2 24	0 33	0 84	0 81	0 87	0 97	1 07	1 26	1 42
FeO	4 26	5 54	4 16	4 17	4 34	5 54	4.65	4 58	4 52	3 70	4 57	5 72	4 40
MgO	17.10	17 60	17.40	16 80	17 47	17 07	18 02	17 49	17 62	17 05	18 26	16 94	17 56
CaO	10.90	10 20	11 40	11 90	10 74	10 89	10.22	10 77	11.18	11 35	11 07	10 91	10 92
Na2O	3.36	3 81	3 17	3 41	3.38	3 05	4 02	3 97	3 36	3 67	3 52	3 20	3 19
K2O	0 40	0 69	0 51	0 04	1 11	1 39	0 06	0 11	0 06	0 51	0 05	1 44	1 34
Total	96 18	95 87	96 12	96 44	96 93	97 22	97 14	98 46	96 86	98 77	98 19	97 47	96 92
Si	6 213	6 332	6 242	6 143	6.282	6 297	6 035	6 148	6 136	6 089	6 030	6 154	6 321
Ti	0 223	0 063	0 082	0 307	0.078	0 252	0 196	0.245	0 144	0.292	0 081	0 144	0 241
Al	2 408	2 169	2 380	2 350	2 262	2 188	2 578	2 455	2 537	2 485	2.654	2 385	2 047
Cr	0 091	0 168	0 186	0 090	0 255	0 038	0 095	0 090	0 099	0 109	0 119	0 144	0 162
Fe	0 514	0 676	0.503	0 502	0 523	0 667	0 556	0 540	0 541	0 438	0 538	0 690	0 531
Mg	3 672	3 813	3 736	3.609	3 750	3 663	3 841	3.674	3.760	3 604	3 828	3 644	3 774
Ca	1 676	1 600	1 764	1 837	1 658	1 680	1 565	1.627	1.714	1 725	1 668	1 687	1 688
Na	0 940	1 078	0 889	0 953	0 944	0 852	1 115	1 085	0 932	1 010	0 960	0 895	0 892
K	0 074	0 128	0 094	0 007	0 204	0 255	0 010	0 020	0 011	0 092	0 001	0 265	0 247
Total	15 811	16 027	15 876	15 798	15.956	15 892	15 991	15 884	15 874	15 844	15.879	16 008	15 903
Mg#	87 7	84 9	88 1	87.8	87 8	84 6	87 4	87.2	87 4	89 2	87 7	84 1	87 7
Ca	28 6	26 3	29 4	30 9	27 9	28 0	26.2	27 9	28 5	29 9	27 6	28 0	28 2
Mg	62 6	62 6	62.2	60 7	63 2	60 9	64 4	62 9	62.5	62.5	63 4	60 5	63 0
Fe	8 8	11 1	8.4	8 4	8 8	11 1	9.3	9 2	9 0	7 6	8 9	11 5	8 9
Mg# Ol	89.9	87 5	90 2	89 7	-	-	89 9	89 8	90 1	91 0	-	-	-

Amphibole (2)

Location	W Eifel					Nunivak							
Number	DF78	1	2	3	4	10016	14001	10067	10050	10052	10006	10013	10051
SiO2	43 17	43 82	43.53	43 43	44 72	46 75	43 18	43 85	43 57	44.04	45 99	44 54	45 04
TiO2	0 18	1 25	1 08	1 28	0 24	0 11	1 67	0 37	0 97	0 43	0 08	0 38	1 68
Al2O3	14 81	12 79	12 77	13 70	12 61	11 51	14 87	14 54	14.18	14.64	12 91	13 42	12 74
Cr2O3	1 47	0 99	1 59	2 07	2 17	2.55	1 18	1.97	1 91	1.50	3.14	2 85	1 76
FeO	4.07	4 45	4 30	3 99	3 71	3 29	4 40	4 50	3.90	3 14	3 42	4 13	4 15
MgO	18.37	19 17	20 00	17 99	18 48	19 01	18.00	17 80	17.79	18 16	18 45	17 68	17 18
CaO	11 55	12 30	10 49	10 41	10 73	9.43	10 57	9 32	10 89	11 14	9 07	9 79	9.24
Na2O	3 17	2 98	3 88	3 11	3 38	4 39	3 09	3 84	2.96	3.18	4 79	3 83	4 21
K2O	0.90	0 12	0 19	1.35	1 04	0 72	1 63	1.24	1.63	1.09	0 92	1 31	1 18
Total	97 69	97 87	97.83	97.33	97 08	97 76	98 59	97 43	97.80	97.32	98 77	97 93	97 18
Si	6 421	6.231	6 192	6.218	6 398	6 595	6 111	6 258	6 211	6 206	6 449	6 336	6 433
Ti	0 020	0 134	0 116	0 138	0.026	0 012	0 178	0 046	0 104	0 042	0.008	0 041	0 180
Al	2 597	2.144	2 142	2 312	2.127	1 914	2 481	2.452	2 383	2.448	2 134	2 250	2 145
Cr	0.173	0 111	0 179	0 234	0 245	0 284	0 132	0 169	0 215	0 167	0 348	0 321	0 199
Fe	0.506	0 529	0 512	0 478	0 444	0 388	0 521	0 373	0 465	0 371	0 401	0 491	0 496
Mg	4.072	4 062	4 240	3 839	3 941	3 997	3 797	3 846	3 780	3 845	3 856	3 749	3 657
Ca	1 841	1.874	1.599	1.597	1 645	1 425	1 602	1 696	1 663	1 693	1 363	1 492	1 414
Na	0.915	0 822	1 070	0 863	0 938	1 201	0 848	0 876	0 818	0 872	1.302	1 056	1 166
K	0 171	0 022	0 034	0 247	0 190	0 130	0 294	0 198	0 296	0 196	0 165	0 238	0 215
Total	16.717	15 929	16.084	15 926	15.954	15 946	15 964	15 913	15 936	15 840	16 027	15 972	15 905
Mg#	88 9	88 5	89.2	88.9	89 9	91 1	87 9	91 2	89 0	91 2	90 6	88 4	88 1
Ca	28 7	29 0	25.2	27 0	27 3	24 5	27 1	28 7	28 2	28 7	24 2	26 0	25 4
Mg	63 4	62.8	66.8	64 9	65 4	68 8	64 1	65 0	64 0	65 1	68 6	65 4	65 7
Fe	7 9	8 2	8.1	8 1	7 4	6 7	8 8	6 3	7 9	6 3	7 1	8 6	8 9
Mg# Ol	-	-	-	-	-	-	-	-	-	-	-	-	-

Amphibole (3)

Location	Dish Hill	San Carlos			Grand Canyon		Hawaii			Hoggar			
Number	Ba-1-52	Ba-2-1	PA-120G	S6	E25A	E33	69ULUP	SL011	SL138	TAH4	TAH88	ATK88	V
SiO2	-	43 30	42.80	44 60	47 80	43.50	42 96	41 36	43 41	-	-	-	43 86
TiO2	-	1 80	1.20	1 20	0 10	0.30	3 20	0.82	1 60	-	-	-	2 49
Al2O3	-	15 40	13 80	13 40	9 80	15 00	12 58	14 21	13 57	-	-	-	12 99
Cr2O3	-	1 13	2 00	2 70	2 80	1.40	1 33	1 49	1 32	-	-	-	2 51
FeO	-	4 70	4.50	3 40	2 90	4.20	6 70	4 38	4 12	-	-	-	4.59
MgO	-	17 30	17 90	18 10	19.70	18 20	16 05	17 58	17 66	-	-	-	16 84
CaO	-	10 80	9 70	10 10	9 60	11.10	11.69	10 09	10 55	-	-	-	10 77
Na2O	-	3 50	3.70	3 40	4.50	3 50	2 83	3 38	3 33	-	-	-	3 13
K2O	-	0 02	1 13	1.30	0 30	0 40	1.03	1 17	1 03	-	-	-	0 86
Total	-	97 95	96 73	98.20	97 50	97 60	98 37	94 48	96 59	-	-	-	98 04
Si	6.144	6 126	6 177	6.306	6 744	6 180	6 175	6 145	6 276	6 006	6.106	6 131	6 247
Ti	0.145	0.192	0 130	0.128	0 011	0 032	0.346	0 092	0 174	0 111	0 151	0 257	0 267
Al	2 457	2 568	2 347	2.233	1 630	2.512	2.134	2 489	2 313	2 486	2 528	2 427	2 181
Cr	0 120	0.126	0 228	0.302	0 312	0.157	0 151	0 175	0 151	0 150	0 108	0 101	0.283
Fe	0 635	0 556	0 543	0 402	0.342	0 499	0.806	0.544	0 498	0 729	0 742	0 567	0 547
Mg	3 766	3 648	3 851	3 815	4 143	3 854	3 439	3.893	3 805	3 675	3 543	3 604	3 575
Ca	1.701	1 637	1 500	1.530	1 451	1 690	1 800	1 606	1.634	1 751	1 680	1.709	1 644
Na	0 830	0 960	1 035	0 932	1 231	0 964	0 789	0 974	0 934	0 898	0.840	0 861	0 864
K	0 053	0 004	0 208	0 235	0 054	0 073	0 189	0 222	0 190	0 153	0 274	0 191	0 156
Total	15 852	15 817	16 020	15 882	15 917	15 960	15 829	16 140	15 975	15 959	15.972	15 848	15 764
Mg#	85 6	86 8	87 6	90 5	92 4	88 5	81 0	87.7	88 4	83 4	82 7	86 4	86 7
Ca	27 9	28 0	25 5	26 6	24 4	28 0	29 8	26 6	27 5	28 4	28 2	29 1	28 5
Mg	61 7	62 5	65 3	66 4	69 8	63 8	56 9	64 4	64 1	59 7	59 4	61 3	62 0
Fe	10 4	9.5	9 2	7.0	5 8	8 3	13 3	9 0	8 4	11 8	12 4	9 6	9 5
Mg# Ol	-	-	89 1	-	-	-	84 6	-	-	87 9	85 2	89 8	-

Amphibole (4)

Location	Ataq	Tanat		Ichinomegata					Mt Leura		Lake Bullenmerri		
Number	AT-15	MO423016	MO104	LHZ-13	LHZ-53	LHZ-29	#87	I-014	LE-2641	LE-2642	BM-9	BM-15	BM-18
SiO2	44 73	43 73	42 78	44 36	44 54	41 76	44 21	45 11	43 02	45 19	42 12	42 51	45 98
TiO2	0 29	2 51	2 99	0 41	0 53	1.54	0.76	0 80	1 32	1 28	0 34	1 86	0 60
Al2O3	12 58	14 06	14 60	12 26	12 98	14 92	16 70	12 35	14 38	15 43	10 22	15 20	9 42
Cr2O3	2.43	0 68	0 96	1 08	1.12	1.06	-	1 11	1 13	0 97	3 19	0 78	2 26
FeO	3 37	3.89	3 60	4.74	4.00	4 51	4 52	4 22	2.99	3 51	2 95	4 09	3 02
MgO	19 17	17.46	16 66	18 18	18.37	17.86	18 78	18 95	18 16	17 98	17 04	17 07	19 12
CaO	10 95	11 02	10 57	12.69	12 53	11.64	11 88	11 95	10.99	10 11	9 42	10 70	10 03
Na2O	3 84	3.38	3 46	2.01	2 34	2 96	3 18	2 21	3 32	3 47	3 45	3 33	4 09
K2O	0 43	0.79	1 13	0 10	0 07	0 06	-	0 02	-	0.04	0.96	1 01	0 56
Total	97 79	97 52	96 75	95 83	96.48	96 31	100 03	96.72	95.31	97 98	89 69	96 55	95 08
Si	6 326	6 217	6 168	6.415	6 376	6 029	6 074	6 432	6 142	6 303	6 523	6 118	6 681
Ti	0 031	0.268	0 324	0 045	0 057	0 167	0 079	0 086	0 145	0 134	0.040	0.201	0 066
Al	2.097	2.357	2 482	2 090	2 190	2.539	2 704	2.076	2 477	2 537	1 865	2 578	1 613
Cr	0 272	0 076	0 109	0 124	0 127	0 121	0 000	0 125	0 131	0 107	0 391	0 089	0 260
Fe	0.397	0 463	0 434	0 573	0 479	0 545	0 519	0 503	0 366	0 371	0 382	0 492	0 367
Mg	4 041	3.700	3 580	3 919	3 920	3 843	3 846	4 027	3 957	3 738	3 933	3 662	4 141
Ca	1 659	1.679	1 633	1 966	1 922	1 800	1 749	1 826	1 721	1.511	1 563	1 650	1 562
Na	1 053	0 932	0 967	0 564	0 650	0 829	0 847	0 611	0 941	0 938	1 036	0 929	1 152
K	0 078	0 143	0 208	0 018	0 013	0.011	0 000	0 004	0 000	0 007	0 190	0 185	0 104
Total	15 953	15 835	15 904	15 713	15 733	15 883	15 818	15 689	15 879	15 647	15 922	15 905	15 945
Mg#	91 0	88 9	89 2	87 2	89 1	87 6	88 1	88 9	91 5	91 0	91 1	88 1	91 9
Ca	27.2	28 7	28 9	30 4	30 4	29 1	28.6	28 7	28 5	26.9	26 6	28 4	25 7
Mg	66 3	63 3	63 4	60 7	62 0	62 1	62.9	63 4	59 8	60 4	66.9	63 1	68 2
Fe	6 5	7.9	7 7	8.9	7 6	8 8	8.5	7.9	13 7	15 1	6.5	8 5	6 0
Mg# Ol	90 8	-	90 3	88 5	90 1	90	84 4	-	90 6	90 4	91.0	88.6	89 8

Amphibole (5)

Location Number	BM-27	BM-47	BM-51	BM-58	BM-62	BM-74	BM-109	BM-116	BM-134	BM-135	Lake Bullenmerri BM-137	BM-139	BM-143
SiO2	43 42	44 34	46 96	43 35	42 73	42 45	43 39	44.00	41 58	45 94	39 94	42 80	42 53
TiO2	1 63	-	0 25	1 20	0 54	1 14	0 48	0.52	0 36	0 89	1 54	0 90	3 59
Al2O3	15 08	13 47	9 86	15 15	14 05	14 28	13 80	15 26	12 45	10 13	13 99	14 70	14 76
Cr2O3	0.66	1 72	1.74	1 50	1 49	1 68	2.10	1 80	2 25	1 87	0 96	0 99	1 35
FeO	3.26	4.29	3 20	3.85	3 23	3 81	4 10	3 42	3 48	3.83	3 52	3 94	3 75
MgO	17.33	18 03	19 36	17.22	17.94	16 91	17.51	17 95	16 90	18 62	16 43	17 31	16 78
CaO	9 78	10 53	9 97	9 82	10 43	10 79	10 06	10 48	9 44	9 78	11.21	10 45	10 47
Na2O	3 26	3.29	4.48	3 28	3 57	2 97	3 38	3 30	3 89	4 10	2 66	3 50	3 01
K2O	0 92	-	0 66	1 57	-	0 92	0 79	0 98	0 32	0.83	0 80	1 22	1 78
Total	95 34	95 67	96 48	96 94	93 98	94 95	95 61	97 71	90 67	95.99	91 05	95 81	98 02
Si	6 261	6 395	6 718	6 206	6 262	6 208	6 297	6 225	6 352	6 634	6 100	6 208	6 054
Ti	0 177	-	0 027	0 129	0 060	0 125	0 052	0 055	0 041	0 097	0 177	0 098	0 384
Al	2.563	2.290	1 663	2 556	2 457	2 462	2 361	2 545	2 242	1.724	2 518	2 513	2 476
Cr	0 075	0 196	0 197	0 170	0 173	0 194	0 241	0 201	0 272	0 214	0.116	0 114	0 152
Fe	0 393	0 518	0 383	0 461	0 396	0 466	0 498	0 405	0 445	0 463	0 450	0 478	0 446
Mg	3 724	3 876	4 128	3 675	3 914	3 686	3 788	3 785	3.848	4 008	3 740	3 742	3 560
Ca	1 511	1 627	1 528	1.506	1 636	1.691	1.564	1 589	1 545	1 513	1 834	1 624	1 597
Na	0 911	0 920	1 243	0 910	1.014	0 842	0.951	0 905	1.152	1 148	0 788	0 984	0 831
K	0 169	-	0 120	0 287	-	0 172	0.146	0 177	0 062	0 153	0 156	0 226	0 323
Total	15.784	15 822	16 007	15.900	15.911	15 846	15 898	15 888	15 958	15 952	15 878	15 986	15 824
Mg#	90 5	88 2	91.5	88 9	90 8	88 8	88 4	90 3	89 6	89 7	89 3	88 7	88 9
Ca	26 8	27 0	25 3	26 7	27 5	28 9	26 7	27 5	26 5	25 3	30 4	27 8	28 5
Mg	66 2	64 4	68 4	65 1	65 8	63 1	64 8	65 5	65 9	67.0	62 1	64 0	63 5
Fe	7 0	8 6	6 3	8 2	6 7	8 0	8 5	7 0	7 6	7 7	7 5	8 2	8 0
Mg# Ol	90 2	86 9	89 8	90 6	89 8	89 2	88 9	90 1	89 7	87 9	89 7	88 6	90 4

Amphibole (6)

Location Number	BM-147	BM-154	BM-161	BM-163	BM-166	BM-167	BM-654	BM-632	BM-189	Bm-18	Lake Bullenmerri BM-635	WGBM1	WGBM11
SiO2	43 64	41 47	40 51	46 00	42 45	40 39	43.89	45 00	43 19	44 55	44 00	43 30	46 40
TiO2	0.31	1 25	1 27	0 20	1 33	1 62	0 69	0 57	0 7	1 33	1 14	1 70	0 25
Al2O3	13 63	12 22	13 83	10 53	14 65	14 59	13 97	12 54	14 72	11 71	13 30	15 50	10 70
Cr2O3	1 95	2 24	1 36	3 04	1 19	0 95	1 95	2 02	1 72	2.23	1 78	0 90	2 85
FeO	3.57	4 31	3 53	2 59	3 03	3 66	4 32	3 25	3 82	5 37	4 23	4 05	3 37
MgO	18 44	16.06	16 00	19 14	17 47	16 68	17 47	17 88	17 35	16 94	17 60	17 60	18 70
CaO	10 03	10 32	10 34	9 28	10 99	9 77	10.78	10 78	10 83	9 56	10 70	11 00	10 00
Na2O	4 02	2 85	2 86	4 61	3 49	3 35	3 38	3 58	3 91	3 75	3 34	3 75	4 31
K2O	0 57	1.23	0 86	0 62	0 20	-	1 04	0 70	0 19	1 08	1 16	0.39	0 72
Total	96.16	91 95	90 56	96 01	94 80	91 01	97 49	96.32	96 43	96 52	97.25	98 19	97 30
Si	6.288	6 307	6 204	6.612	6 177	6 121	6 270	6 458	6 203	6.454	6 303	6 113	6 607
Ti	0.034	0 143	0 146	0.022	0 146	0.185	0 074	0 062	0 076	0.145	0.123	0 180	0 027
Al	2 315	2.191	2 496	1.784	2 512	2 606	2.352	2 121	2 492	2 000	2.246	2 580	1 796
Cr	0.222	0.269	0 165	0 346	0 137	0 114	0 220	0 229	0 195	0 255	0 202	0 100	0 321
Fe	0 438	0 543	0 452	0.311	0 369	0 464	0 516	0 390	0 459	0 651	0.507	0 478	0 401
Mg	3 960	3 641	3 652	4 100	3 789	3 768	3 720	3 825	3 714	3 657	3 758	3 703	3 969
Ca	1 548	1 682	1 697	1 429	1.713	1 586	1 650	1 658	1 667	1.484	1 642	1 664	1 526
Na	1.123	0 840	0 849	1.285	0 985	0 984	0 936	0 996	1 089	1 054	0.928	1 026	1 190
K	0 105	0 239	0 168	0 114	0 037	-	0 190	0 128	0.035	0 200	0 212	0 070	0 131
Total	16 032	15 855	15 829	16 002	15 864	15 827	15.927	15 867	15 930	15 900	15 920	15 915	15 968
Mg#	90 0	87 0	89 0	92.9	91 1	89 0	87 8	90 7	89 0	84 9	88 1	88 6	90 8
Ca	26.0	28 7	29 2	24 5	29 2	27 3	28 0	28 2	28 5	25 6	27 8	28 5	25 9
Mg	66.6	62 1	63 0	70 2	64 5	64 8	63.2	65 1	63.6	63 1	59 4	57 9	59 4
Fe	7.4	9 3	7 8	5 3	6 3	8 0	8 8	6 6	7 9	11 2	18 2	17 3	14 1
Mg# Ol	-	87 1	89 7	91.4	90 5	89 5	87 6	89 9	89 1	84 7	-	-	-

Amphibole (7)

Location	L.Bullenm	Lake Gnotuk							Malaita				
Number	WGBM16	GN-15	GN-2	GN-3	GN-16	GN-20A	GN-20B	GN-24	GN-26	PHN3550B	PHN3567	PHN3534	CRN205
SIO2	42 60	46 59	45 09	43 73	42 75	44 72	43.32	40 91	41 20	43 70	44 00	44 80	44 06
TIO2	3.24	0 06	0 17	0 45	0 66	0 47	1.90	3 99	2 79	2 40	0 82	1 40	0 92
Al2O3	14 50	10 82	11 47	13.07	14 60	12 28	15 10	14.06	13 72	14 10	13 61	13 50	15 33
Cr2O3	1.38	2.90	1.95	1 75	1.54	1.52	0.82	0.70	1 32	1 50	1.00	1 40	0 84
FeO	4 22	2 99	4 69	4.19	4 18	3.71	3 85	5 09	5 75	4 40	4.50	4 00	3 93
MgO	16 90	19 30	18.21	17.63	17 34	18 82	17 67	16 30	15 95	18 00	18 40	18 60	17 82
CaO	10 80	10 00	10 07	10 49	10 46	10 31	11 06	11 40	10 40	9 80	11.30	10 80	10 79
Na2O	3 16	3.99	3 92	3.60	3 62	3 73	3 82	2 87	3 22	3.30	3 92	3 60	3 76
K2O	1 44	0 74	0 92	0 83	0.64	0.83	0 08	1 23	1.31	1.30	0 05	0 60	0 00
Total	98.24	97 39	96 49	95.74	95 79	96.39	97 62	96 55	95 66	98.50	97 60	98 70	97 45
SI	6 062	6 608	6.511	6 351	6 199	6.428	6 138	5 961	6 070	6 175	6 269	6 293	6 230
TI	0.347	0.006	0 019	0 049	0 072	0.051	0 203	0.437	0 309	0.255	0 088	0 148	0 098
AI	2.433	1.809	1 953	2.238	2 496	2 081	2.522	2 415	2.383	2 348	2.285	2 235	2 556
Cr	0.155	0 325	0 223	0.201	0 177	0 173	0.092	0 081	0.154	0 168	0 113	0 155	0 094
Fe	0.502	0 355	0 566	0.509	0 507	0 446	0 456	0 620	0.709	0 520	0.536	0 470	0 465
Mg	3 584	4 080	3 919	3 816	3 748	4 032	3.731	3 540	3.502	3 792	3 908	3 895	3 755
Ca	1 647	1.520	1.558	1 632	1 625	1.588	1 679	1 780	1.642	1 484	1 699	1 625	1 635
Na	0.872	1 098	1 099	1.015	1 019	1 041	1 051	0 812	0 921	0 904	1 083	0 980	1 031
K	0.261	0 134	0 170	0.154	0 118	0 152	0 015	0 229	0 246	0 234	0 009	0 108	0 000
Total	15 863	15 935	16 017	15.965	15 961	15.991	15 885	15 874	15 936	15 880	15 990	15.909	15 863
Mg#	87.7	92.0	87 4	88 2	88 1	90 0	89 1	85 1	83 2	87.9	87 9	89 2	89 0
Ca	28.7	25.5	25 8	27 4	27 6	26 2	28 6	30 0	28 1	25 6	27 7	27.1	27 9
Mg	58.7	60.9	59 6	59.0	58 6	60.5	57.8	57 7	57 7	65 4	63 6	65 0	64 1
Fe	18.1	12.9	20 0	18.2	18 3	16 0	16 6	22 0	25 2	9.0	8 7	7 8	7 9
Mg# Ol	-	91.0	85 1	87.7	89 4	89 0	89 0	85 4	82 6	-	-	-	-

Amphibole (8)

Location	Malaita												
Number	PHN4022	PHN4028	PHN4073	PHN4074	PHN4085	CRN205	CRN216	PHN4002	PHN4009	PHN4013	PHN4034	PHN4069	CRN209
SIO2	43 20	44 00	43 80	45 40	44 00	44 10	45 30	43 70	45.80	44 20	44 10	44 00	42 20
TIO2	1 08	1 34	0 91	1.33	0 87	0 92	0.73	0.30	0 95	0 79	2 02	0 94	3 09
Al2O3	15.90	14 70	14 00	10 70	14 30	15 30	13 00	15 30	12.10	14 50	13 40	13 90	14.20
Cr2O3	0.81	1.05	1 62	1.13	1.67	0 84	1 74	0 91	0 61	1 09	1 56	1 17	0 70
FeO	3 98	4 41	4 62	6 48	4 38	3 93	3 94	6 08	9 12	4.33	4 50	4 30	7 25
MgO	17.60	17 70	17 70	17.70	17 80	17 80	18 30	18 10	19.60	17 80	17 30	18 10	16 00
CaO	11 00	10 50	9 83	9.43	10 10	10 80	10.20	8 87	8 84	10 60	10 10	11 40	9 56
Na2O	4.07	3 36	4 49	4.81	4 09	3 76	3 35	4.06		3 75	3 40	3 47	3 53
K2O	0 02	0 56	0 64	0.76	0 51	-	0 70	0 15	0 17	0 32	1 41	0 06	1.19
Total	97 66	97.62	97 61	97.74	97.72	97 45	97 26	97.47	97.19	97.38	97 79	97 34	97 72
SI	6 135	6.237	6.243	6.514	6 243	6 224	6 246	6 213	6 472	6.274	6.273	6 259	6 091
TI	0 115	0.143	0 097	0.143	0 065	0 098	0 078	0 032	0.101	0.084	0.216	0 101	0 335
AI	2 609	2 462	2 352	1 810	2 391	2.552	2 179	2.570	2 016	2 424	2.256	2.334	2 406
Cr	0 090	0.118	0 183	0 128	0 188	0 094	0.195	0 102	0.084	0.122	0 175	0.131	0 080
Fe	0 472	0.524	0 551	0.778	0 520	0 464	0 467	0 724	0 525	0 514	0.536	0.511	0 875
Mg	3 753	3.732	3 771	3 782	3 768	3 753	3 873	3 823	3 978	3 772	3.680	3 833	3 441
Ca	1 667	1.591	1 500	1 449	1 468	1 634	1.546	1 351	1 536	1.615	1.544	1.734	1 478
Na	1 122	0 925	1 240	1 339	1 126	1 031	0 921	1.119	1 155	1 031	0.938	0 954	0 988
K	0 003	0 102	0 116	0 139	0 093	-	0.126	0 028	0 121	0 057	0.256	0 011	0 219
Total	15.966	15 834	16 053	16 082	15 862	15 850	15.631	15 962	15 988	15 893	15.874	15 868	15 913
Mg#	88.8	87.7	87 3	82 9	87.9	89 0	89 2	84 1	88.3	88.0	87 3	88 2	79 7
Ca	28.3	27 2	25 8	24 1	25 5	27 9	26 3	22 9	25 4	27.4	26 8	28 5	25 5
Mg	63 7	63 8	64.8	62.9	65 5	64 1	65 8	64.8	65 9	63 9	63 9	63 1	59 4
Fe	8 0	9 0	9.5	12.9	9 0	7.9	7.9	12 3	8 7	8.7	9 3	8 4	15 1
Mg# Ol	-	-	- -	-	-	-	-	-	-	-	-	-	

Amphibole (9)

Location	Fen					Monastery	Bultfontein		Bellsbank	Jagersfontein			
Number	1	2	4	9	10	7429	BD1368	BD3707	PJL13	311	259	557	576
SiO2	43 51	43 36	43 33	42.66	42 47	45.50	45 10	41 80	41.75	45 71	46.23	44 75	47 67
TiO2	0 49	0 57	-	-	-	0 01	0 00	0 20	0 25	0 48	0 34	0 06	0 06
Al2O3	14 74	13.87	14 96	14 88	15 17	11 10	11 10	15 80	16.64	12 13	11 11	11 83	10 56
Cr2O3	1 07	1 11	0.49	0 77	1.36	1.67	2 20	1 20	0 09	2 04	2 13	2 14	2 03
FeO	4 00	4.47	4 10	4 37	4 20	3 18	2 68	5 80	7 18	3 12	2.55	2 25	3.21
MgO	19 18	18.55	18 97	19 20	19 10	20 00	20 40	17.20	17.05	19 26	20 17	20 43	19 85
CaO	10.70	11.09	11.14	12 00	11 04	10 60	10 90	10 90	10 68	10 17	10.28	10 69	8 78
Na2O	3 93	3 65	4 06	3 79	3 49	3 79	3 23	2 70	3.07	3 39	3 93	4 23	4 72
K2O	0.19	-	-	-	-	0 60	1 34	1.60	0.62	1 34	1.03	0 64	0 79
Total	97 81	96 67	97 05	97 67	96.83	96 45	96 95	97 20	97 33	97 64	97.77	97 02	97 67
Si	6 159	6 222	6 180	6 077	6 080	6 520	6 453	6 044	6 015	6 475	6 530	6 379	6 716
Ti	0 052	0 062	-	-	-	0 001	0.000	0 022	0.027	0 051	0 036	0.006	0 006
Al	2 460	2.344	2 515	2 499	2 560	1 875	1 872	2 693	2 826	2 026	1.850	1 988	1 754
Cr	0 120	0 126	0 055	0 087	0 154	0 189	0 249	0 137	0 010	0 228	0 238	0 241	0 226
Fe	0 474	0 536	0 489	0 520	0 503	0 381	0 321	0 701	0 865	0 370	0 301	0 268	0 378
Mg	4 046	3 967	4 032	4 076	4 075	4 271	4 350	3 707	3.661	4 066	4.246	4 340	4 168
Ca	1 623	1 705	1 702	1 832	1 693	1 628	1 671	1 689	1.649	1.544	1 556	1 633	1 325
Na	1 079	1 106	1 123	1 046	0 969	1 053	0 896	0 757	0.858	0 931	1 076	1 169	1 289
K	0 034	-	-	-	-	0 110	0 245	0 295	0 114	0.242	0 186	0 116	0 142
Total	16 047	16 068	16 096	16 137	16 034	16 028	16 057	16 045	16 025	15 933	16 020	16 142	16 004
Mg#	89 5	88.1	89 2	88 7	89 0	91 8	93 1	84 1	80 9	91 7	93 4	94 2	91 7
Ca	26 4	27 5	27 4	28 5	27 0	25 9	26 4	27 7	26 7	25 8	25.5	26 2	22 6
Mg	65 9	63 9	64 8	63 4	65 0	68 0	68 6	60 8	59 3	68 0	69 6	69 5	71 0
Fe	7 7	8 6	7 9	8 1	8 0	6 1	5 1	11 5	14 0	6 2	4 9	4 3	6 4
Mg# Ol	90 2	89 6	89 6	89 1	89 3	-	-	-	-	-	-	-	-

Amphibole (10)

Location	Jagersfontein				Lesotho	Tanzania	Green Knobs		Rhode Is	Lien		W Gneiss	
Number	571	585	595	558	PHN2508	DU18500	N53	N55	LN-4	1K	1J	5421C	USC-8A
SiO2	50 57	47 42	46 62	47 82	44 00	49 00	42 60	43 60	42 07	45 80	46.00	44 90	45 10
TiO2	0 04	0 10	0 58	0 05	0 70	0 90	0 28	0 08	2 17	0.36	0 59	0 42	0 43
Al2O3	9 24	10.21	9 07	9 63	10 70	7 50	15 70	14 10	12 71	10 90	11 70	13 40	13 60
Cr2O3	2.19	2 09	1 26	1.83	-	2 10	0 80	0.75	2.22	1.72	0 41	1 49	1 68
FeO	3 38	2 76	4 98	3 04	10 10	2 80	3 91	4 10	3.56	3 94	4 73	3 39	2 26
MgO	19 29	20 44	19 53	19 96	16 10	20 80	18.30	18 60	18.07	19 40	18 70	18 70	19 00
CaO	6 80	9.94	9 19	8.13	10 80	9 60	12 00	12 20	11 20	12 30	11 10	12 10	12 20
Na2O	5 73	3.94	4 26	5 00	3 40	4 10	3 49	3 37	3.65	3 26	3 66	2 73	2 46
K2O	0 51	0 94	1 00	0 65	0.90	1 00	0 03	0 28	0.14	0 19	0 03	0 06	0 08
Total	97 75	97.84	96 49	96.11	96 70	97 80	97.11	97 08	95 79	97 87	96 92	97 19	96 81
Si	7.054	6 676	6 721	6 824	6 493	6 899	6 081	6.236	6 122	6 497	6 557	6.360	6 378
Ti	0 004	0 011	0 063	0 005	0 078	0 095	0 030	0 009	0.237	0 038	0 063	0 045	0 046
Al	1.520	1 695	1 542	1 620	1 862	1 245	2 642	2 377	2 181	1 822	1 966	2.237	2 267
Cr	0.242	0.233	0 144	0 206	-	0 234	0 090	0 085	0 255	0 193	0 046	0 167	0 188
Fe	0 394	0.325	0 600	0.363	1 247	0.330	0 467	0 490	0 433	0 467	0 564	0 402	0 267
Mg	4.010	4 289	4 196	4 245	3 541	4.365	3 893	3 965	3 919	4 102	3 973	3 948	4 005
Ca	1 016	1.499	1 420	1.243	1 708	1 448	1 835	1 870	1 746	1 869	1 695	1 836	1.848
Na	1.550	1 076	1 191	1 383	0 973	1 119	0 966	0 935	1 030	0 897	1 012	0 750	0 675
K	0 091	0 169	0 184	0 118	0 169	0 180	0 005	0 051	0 026	0 034	0 006	0 011	0 014
Total	15 881	15 972	16 060	16.008	16 070	15 915	16 009	16 017	15 950	15 919	15 880	15 756	15 687
Mg#	91 0	93 0	87 5	92 1	74 0	93 0	89 3	89 0	90 0	89 8	87 6	90 8	93 7
Ca	18 7	24 5	22 8	21.2	26 3	23 6	29 6	29.6	28.6	29 0	27 2	29 7	30 2
Mg	74 0	70 2	67 5	72 6	54 5	71 1	62 8	62 7	64 3	63 7	63 8	63 8	65 4
Fe	7 3	5 3	9 7	6.2	19 2	5 4	7 5	7.8	7 1	7 3	9 0	6 5	4 4
Mg# Ol	-	-	-	-	-	-	-	-	-	-	-	-	-

Amphibole (11)

Location	Finero					A Arami			Balmuccia		Timor		
Number	F2A	F69	F2D	197	106	F-16a	F-16c	F-52c	B-3C	F-58	7	11	12
SiO2	44 11	46 32	45 40	46 73	49 16	46 01	45 93	45 26	42 18	42 62	43.90	47 50	44 00
TiO2	0 61	1.24	0 44	0 61	0 08	0 45	0 39	0 39	2 72	3 17	1 42	0 63	1 23
Al2O3	12 55	9 76	11 67	10.80	10 08	11.53	13 37	14 01	14 39	14 73	13 90	9 88	14.90
Cr2O3	1 79	1 79	2 08	2 03	-	1 72	1 22	1 02	0 64	0 69	0 99	0 84	1 07
FeO	3 39	3.06	3 32	3.02	2 69	3 02	3 73	3 64	4 29	3 96	3 46	2 93	3 57
MgO	18 50	19.51	18 98	19 60	21 52	19 03	18 55	18 19	16 72	16 83	18 40	19 70	18 00
CaO	12.32	12 20	12 19	12 87	11 32	12 53	12 4	12 58	12 01	11 98	12.50	12 50	12 30
Na2O	2 45	2.23	2 19	2 21	1.66	2 21	1.87	2 03	4 00	3.72	2 72	2 06	2 82
K2O	0 70	0.71	1.08	0 56	0 44	0 51	0 18	0 05	0 19	0.23	-	-	-
Total	96 42	96 82	97 35	98 43	96 95	97 01	97 64	97 17	97 14	97.93	97.29	96 04	97.89
Si	6.344	6 607	6 464	6 557	6 869	6 535	6 458	6.395	6 060	6 052	6 240	6 760	6 200
Ti	0 066	0 133	0 047	0 064	0 008	0 048	0 041	0 041	0.294	0 339	0 150	0 070	0 130
Al	2 127	1.641	1 959	1 786	1 660	1 930	2 216	2 333	2 437	2 465	2 320	1 660	2 480
Cr	0 204	0 202	0 234	0 226	-	0 193	0 136	0 114	0 073	0 078	0 110	0 100	0 120
Fe	0 408	0 365	0 395	0 354	0 314	0 359	0 439	0 430	0 516	0 470	0 390	0 350	0 420
Mg	3 966	4 148	4 028	4 099	4 482	4 028	3 888	3 831	3 581	3 562	3 890	4 170	3 780
Ca	1 898	1 865	1 860	1.935	1 695	1 907	1.868	1 905	1 849	1 823	1 900	1 900	1 850
Na	0 683	0 617	0 605	0 601	0 450	0 609	0 510	0 556	1 114	1 024	0 750	0 570	0 770
K	0 128	0.129	0 196	0 100	0 078	0 092	0 032	0 009	0 035	0 042	-	-	-
Total	15 825	15 707	15 788	15 724	15 556	15.701	15 588	15 615	15 958	15 854	15 750	15 580	15 750
Mg#	90 7	91 9	91.1	92 0	93 4	91 8	89 9	89 9	87 4	88 3	90 9	92 3	90 0
Ca	30 3	29 2	29 6	30 3	26 1	30 3	30 2	30 9	31 1	31 1	30 7	29 6	30 6
Mg	63 2	65 0	64 1	64 2	69 0	64 0	62 8	62 1	60 2	60 8	62.9	65 0	62 5
Fe	6 5	5 7	6 3	5 5	4 8	5 7	7 1	7 0	8 7	8.0	6.3	5 5	6 9
Mg# Ol	91.3	91 6	91 3	-	-	91 0	89 6	89 7	89 7	90 0	89 5	90 2	89 8

Amphibole (12)

Location	Ronda						Zabargad						Lizard
Number	R501	R740	R696	R123	R243	7319	Z-37	Z-42A	Z-42B	Z-35	Z-206A	Z-206B	90691
SiO2	43 65	43 58	43 65	44.27	44 27	42 58	41.81	43 00	43 50	43 70	48 60	48 40	46 19
TiO2	1 96	2 35	2 72	2 87	2 87	1 87	4 49	1.73	1 79	3.53	0 06	0 05	0 96
Al2O3	15 15	14 62	13 81	14 03	14 03	14 11	12 46	14 40	14 50	12.70	8 34	8 21	12 83
Cr2O3	1.20	1 05	1.03	0 97	0 97	1.86	1 63	0 94	1 40	0 40	2 00	1 65	0.80
FeO	3 45	3 40	4 16	3 70	3 70	3 12	4 51	4 22	4 45	4 82	4.51	4.32	4 44
MgO	17 68	18 20	17 70	17.35	17 35	18 55	16 65	18 70	17.90	16 90	20.90	21.00	18 71
CaO	11.28	11 49	11 12	11 99	11 99	11 96	11 80	11.80	12.20	12 40	9 90	10 30	12 45
Na2O	3.68	3 47	3 25	3 20	3 20	3 64	3 16	3 35	3 25	2 86	2 19	2 21	1 87
K2O	0 00	0.00	0 00	0 00	0 00	0 00	0 90	0 90	1 09	0 91	0 45	0 37	0 27
Total	98 05	98 16	97 44	98 38	98 38	97 69	97 41	99 04	100 08	98 22	96 95	96 51	98 52
Si	6 145	6 131	6 197	6 092	6 216	6 053	6 033	6 063	6 103	6 219	6 879	6 880	6 458
Ti	0.207	0 249	0 290	0.312	0 303	0 200	0 487	0 183	0.189	0.378	0 006	0 005	0 101
Al	2 514	2 425	2 311	2 499	2 323	2 365	2 119	2 393	2 398	2 130	1 391	1 375	2 114
Cr	0 134	0.117	0 116	0 093	0 108	0 209	0 186	0 105	0 115	0 045	0 224	0 185	0 088
Fe	0 406	0 400	0 494	0 498	0 435	0 371	0 544	0 498	0.522	0.574	0 534	0.514	0 471
Mg	3 710	3 816	3 745	3 559	3 631	3 930	3.561	3 930	3 743	3 585	4.409	4.449	3 899
Ca	1.701	1.732	1 692	1 685	1 804	1 822	1 824	1 783	1 834	1 891	1.501	1 569	1 865
Na	1 004	0 947	0 895	1 107	0 871	1 003	0 884	0 916	0 884	0 789	0 601	0 609	0 507
K	0 000	0 000	0 000	0 000	0 000	0 000	0 166	0 162	0.195	0 165	0 081	0 067	0 048
Total	15.821	15.817	15 740	15 845	15 691	15 953	15 804	16 033	15 983	15 776	15 626	15 653	15 551
Mg#	90 1	90 5	88.3	87 7	89 3	91 4	86 7	88 8	87 8	86.2	89 2	89 6	89 2
Ca	29 2	29 1	28 5	29 3	30 7	29 8	30 8	28 7	30 1	31 3	23 3	24 0	29 9
Mg	63 8	64 2	63 1	62 0	61 9	64 2	60 1	63 3	61 4	59 3	68 4	68 1	62 5
Fe	7.0	6 7	8 3	8.7	7 4	6 1	9 2	8 0	8 6	9 5	8 3	7 9	7 6
Mg# Ol	-	-	-	-	-	-	89 1	89.2	-	88 4	89 6	-	-

Amphibole (13)

Location	Oregon					Myamori		Kinugasa	Nonsberg	Peridotite			
Number	VH3	VH6	VH9	CSZ12	SB17	77073113	77111919	K-3	MK5D	MO11	MK5C	MK1	ULT12
SiO2	41 60	42 70	42.70	43 40	45.80	45 92	46 12	45 79	44 72	45 58	46 02	44 89	45 34
TiO2	1 42	1 65	1.02	0.98	0 55	0 36	0 41	0 58	0.65	0 50	0 32	0 56	0 58
Al2O3	14 70	14 30	15 00	14 70	13 30	12 82	12 69	10 93	14.23	12 11	12 59	13 07	12 85
Cr2O3	1 17	1 15	1 10	1.24	1 15	1.25	1 12	1.73	1 12	1.36	1 22	1.28	1 37
FeO	3 43	3 14	3 63	3.14	3 41	3 62	3.68	3 98	2 92	3 12	2 69	2 75	3 30
MgO	18 00	18 10	18.20	18 50	18.40	18 22	18 52	19 26	19 54	19 53	19 27	19 31	19 30
CaO	11.90	11 60	11 90	12 30	12 60	12 80	12 45	12 95	11.69	12.57	12 64	12 43	12 43
Na2O	3 80	3.80	3 70	3 10	1.70	1.98	2 02	2 44	3 31	2 00	1 71	2 49	2 42
K2O	0 06	-	0 10	-	0 14	0 05	0 04	0 02	0 02	1 11	0 54	0 49	0 48
Total	96 08	96 44	97 35	97 36	97 05	97 02	97.05	97.68	98 20	97 88	97 00	97 27	98 07
Si	6 019	6 122	6 087	6 158	6 468	6 504	6 523	6 496	6.261	6 438	6 502	6 357	6 380
Ti	0 155	0.178	0.109	0.105	0.058	0 038	0 044	0.062	0 069	0.053	0 034	0 060	0 061
Al	2.511	2.423	2.524	2.452	2.221	2.141	2.116	1 828	2 348	2 016	2 097	2 182	2 132
Cr	0 134	0 130	0.124	0 139	0 128	0 140	0 125	0 194	0 124	0.152	0 137	0 144	0 152
Fe	0 415	0 377	0 433	0 373	0 403	0 429	0 435	0 472	0 342	0 369	0 318	0 326	0.388
Mg	3 876	3 880	3 862	3.913	3.871	3 846	3 904	4 072	4.078	4 113	4 059	4 076	4 049
Ca	1.845	1 786	1.815	1.876	1 902	1.943	1 887	1 969	1 754	1.903	1.913	1 885	1.874
Na	1 069	1 046	1.012	0.844	0 455	0.544	0.554	0 671	0 898	0.548	0 467	0 684	0 661
K	0.011	-	0 018	-	0 025	0 009	0 007	0 004	0 003	0.200	0 097	0 089	0 087
Total	16 035	15.942	15 984	15 860	15.531	15.594	15 594	15 768	15 877	15 792	15 624	15 803	15 784
Mg#	90 3	91 1	89.9	91.3	90 6	90 0	90 0	89.6	92 3	91 8	92 7	92 6	91 3
Ca	30 1	29 6	29.7	30 4	30 8	31 2	30.3	30 2	28 4	29.8	30 4	30 0	29 7
Mg	63.2	64 2	63 2	63 5	62 7	61.9	62 7	62 5	66 1	64 4	64 5	64 8	64 2
Fe	6 8	6.2	7 1	6.1	6.5	6 9	7 0	7.3	5 5	5 8	5 1	5 2	6 1
Mg# Ol	-	-	90.1	90 0	-	90 7	90 1	-	90 5	89 4	90.5	90 5	90 0

Amphibole (14)

Location				Tinaquillo									
Number	ULT4	300B	MO9	5	80-21	80-20	80-64	80-11	80-12	80-17	79-59	80-58	80-55
SiO2	46 58	46.97	45.77	43 61	42 21	42 96	42 48	44.32	43.71	43 80	43 87	44 31	44 46
TiO2	0 19	0 23	0 35	1.15	3.44	2 91	1.76	1.75	2 14	2 59	1.25	1 14	1 01
Al2O3	12 82	11.91	12 77	15 06	14.55	14 80	15 67	15 02	14 47	14 10	13 62	13 97	13 80
Cr2O3	1.18	0 80	1 50	-	1.08	0 95	0 96	0 59	1 02	1 11	1 34	0 87	0 74
FeO	3.15	2.87	3 05	6.57	4 00	3 67	3 56	3 66	3 59	3 55	3 48	3 62	3 87
MgO	19.17	19 55	19.22	16 53	16 76	16 84	17 41	17.76	17 69	16 97	18 04	17 98	17 91
CaO	12.98	12 86	12.59	11.80	11 72	12 05	11.95	11.98	12 24	11 96	12 54	12 90	12 46
Na2O	1.65	1.64	1.99	2 78	3 85	3.75	3 70	3 55	2 44	3 56	2.96	2 35	2 71
K2O	0 83	0.72	0 50	0.11	0 02	0.00	0 00	0.01	0.04	0 14	0 11	0 29	0 07
Total	98 55	97.55	97.74	97 61	97 63	97 93	97 49	98 64	97 34	97.78	97 21	97 43	97 03
Si	6 501	6.599	6 442	6.200	6 021	6 088	6.040	6 203	6.194	6 205	6.249	6 284	6 325
Ti	0 020	0 024	0 037	0.123	0 369	0 310	0 188	0 184	0 228	0 276	0.134	0 122	0 108
Al	2 108	1.972	2 118	2.524	2 447	2 472	2.626	2 478	2 417	2.355	2 287	2 336	2 315
Cr	0 130	0 088	0 167	0.000	0 122	0 106	0 108	0 065	0 114	0 124	0 151	0 098	0 083
Fe	0.368	0 337	0.359	0.781	0 477	0 435	0 423	0 428	0 425	0 421	0 415	0 429	0 460
Mg	3.988	4 095	4.033	3.503	3 563	3 556	3 689	3 704	3 736	3 583	3 830	3 800	3 797
Ca	1.941	1 936	1.898	1.797	1.791	1 830	1 820	1 796	1.858	1 815	1 914	1 960	1 899
Na	0 446	0 447	0 543	0.766	1.065	1 030	1 020	0 963	0 670	0 978	0.818	0 646	0 748
K	0.148	0 129	0 090	0 020	0 004	0 000	0 000	0 002	0 007	0 025	0 020	0 052	0 013
Total	15 650	15 627	15 687	15.714	15 859	15 828	15 915	15 824	15 651	15.781	15 817	15.727	15 748
Mg#	91 6	92 4	91.8	81.8	88 2	89 1	89 7	89 6	89 8	89 5	90 2	89 8	89 2
Ca	30.8	30 4	30 2	29.6	30 7	31 4	30 7	30.3	30 9	31.2	31 1	31 7	30 8
Mg	63.3	64 3	64 1	57.6	61 1	61 1	62 2	62 5	62 1	61 6	62.2	61 4	61 7
Fe	5.8	5.3	5 7	12 8	8 2	7 5	7 1	7 2	7 1	7.2	6 7	6.9	7 5
Mg# Ol	90.1	89 9	-	-	89 6	89 9	90 2	90 4	90 4	90 5	90 7	89 4	89 8

Orthopyroxene (1)

Location	Massif Central				Languedoc				SanCarlos	Hawaii	Hoggar	Ataq	
Number	Li-9	Li-35	Li-52	Cp-15	H204B	80-437	80-442	76-250	PA-120G	SL011	SL138	V	AT-15
SiO2	56 20	56 60	56 30	55 50	54.81	55 89	55 29	55 47	56 80	54 92	54 88	55 18	55 95
TiO2	0 10	0 04	0 04	0.08	0 02	0 10	0 09	0 09	0 03	0 03	0 06	0 08	-
Al2O3	3 64	1 53	2 66	3 90	4 29	3 65	4 03	4 76	2.75	4.59	5 13	2 28	1 36
Cr2O3	0 21	0 14	0.31	0.28	0 22	0 25	0 12	0.35	0.48	0.52	0 42	0 69	0 35
FeO	6 18	7 93	6.04	6 58	6 69	6 30	5.96	5 79	6 90	6 91	6 43	9 10	5 63
MgO	32 40	32 70	33 50	32 80	32.64	33 16	33 47	33 49	33 30	32 46	32 25	31 60	36 17
MnO	0 11	0 18	0.11	0 14	0 04	0 16	-	0 13	0 22	0 13	0 14	0 12	0 19
CaO	0.66	0 52	0 60	0.50	0.52	0 43	0 41	0 30	0 76	0 71	0 64	0 27	0 57
Total	99.50	99 64	99 56	99 78	99 23	99 94	99.37	100.38	101.24	100 27	99 95	99 32	100.22
Si	1 943	1.970	1.946	1.921	1.907	1 926	1.913	1 900	1 942	1 898	1 896	1 943	1 927
Ti	0 003	0 001	0.001	0.002	0 001	0 003	0 002	0.002	0.001	0 001	0 002	0 002	-
Al	0 148	0 063	0.108	0 159	0 176	0 148	0 164	0 192	0 111	0 187	0.209	0 095	0 055
Cr	0 006	0 004	0 008	0 008	0 006	0 007	0 003	0.010	0 013	0.014	0 011	0 019	0 010
Fe	0 179	0 231	0.175	0 190	0 195	0 182	0 173	0 166	0 197	0 200	0 186	0 268	0 162
Mg	1.668	1.698	1.728	1.690	1 692	1.703	1 727	1.710	1 697	1 672	1 661	1 658	1 857
Mn	0 003	0 005	0 003	0 004	0 001	0 005	-	0 004	0 006	0 004	0 004	0 004	0 005
Ca	0 024	0 019	0 022	0 019	0 019	0 016	0 015	0 011	0 028	0 026	0 024	0 010	0 021
Total	3.974	3 991	3 991	3 993	3 997	3 990	3 997	3 995	3.995	4 001	3 992	3 998	4 037
Mg#	90.3	88 0	90 8	89 9	89 7	90 3	90 9	91.2	89.6	89.3	89 9	86 1	92 0
Ca	1.3	1 0	1 1	1 0	1 0	0 8	0 8	0 6	1 4	1 4	1.3	0 5	1 0
Mg	89.2	87 2	89 8	89 0	88 8	89 6	90 2	90 6	88 3	88 1	88 8	85 6	91 0
Fe	9 6	11 9	9 1	10 0	10 2	9 6	9 0	8 8	10 3	10 5	9 9	13 8	7 9

Orthopyroxenes (2)

Location	Tariat	Ichinomegata				L Bullenmerri					Lake Bullenmerri		
Number	MO423016	MO104	LHZ-13	LHZ-53	LHZ-29	#87	BM-9	BM-15	BM-18	BM-27	BM-47	BM-58	BM-62
SiO2	54 65	55 18	54 26	55.73	53 52	54 73	57 59	55 09	58 28	54 97	56 17	54 72	56 45
TiO2	0.14	0 12	0 10	0 05	0 15	0 12	-	-	-	-	-	-	-
Al2O3	4.99	4 06	3 34	3 38	3 99	3 47	0.86	4 58	-	4 25	1 96	4 64	2 60
Cr2O3	0.27	0 35	0 42	0 39	0 56	0 45	0.25	-	-	0.25	0 26	0 48	0 28
FeO	6.98	5 83	7.53	6 32	6 56	6 32	5 55	6 93	6 22	6.13	7 97	5 96	6 27
MgO	32 03	33 44	32 82	33 59	32 59	34 20	35 57	32 76	35.14	33 69	33 13	32 76	34 02
MnO	0 15	0 16	0 20	0.15	0 15	0 12	-	-	-	-	-	-	-
CaO	0.51	0 41	0.55	0.46	0 79	0 72	0 26	0 64	0 36	0 54	0 51	0 69	0 38
Total	99.72	99 55	99.22	100 07	98 31	100.13	100 08	100.00	100 00	99 83	100 00	99 25	100 00
Si	1 897	1 908	1.903	1 921	1 888	1 887	1 976	1 904	2 004	1 897	1.952	1 900	1 945
Ti	0 004	0 003	0 003	0.001	0 004	0 003	-	-	-	-	-	-	-
Al	0 204	0 165	0 138	0 136	0 166	0 113	0.035	0 187	-	0 173	0.080	0 190	0 106
Cr	0 007	0 010	0 012	0 010	0 016	0 012	0 077	-	-	0 007	0 007	0 013	0 008
Fe	0.202	0 169	0.221	0.182	0 194	0 183	0 159	0.200	0.179	0 177	0 232	0 173	0 180
Mg	1.656	1.724	1 716	1.726	1 714	1 756	1.820	1.688	1 801	1 734	1.716	1 696	1 747
Mn	0.004	0 005	0 006	0 004	0 005	0 003	-	-	-	-	-	-	-
Ca	0 019	0 015	0 021	0 016	0 030	0 027	0 010	0 024	0 013	0 020	0 019	0 026	0 014
Total	3 993	3 999	4 020	3 996	4 017	3 984	4 077	4 003	3 997	4 008	4 006	3 998	4 000
Mg#	89 1	91 1	88.6	90 5	89 8	90 6	92 0	89 4	91 0	90.7	88 1	90 7	90 7
Ca	1 0	0 8	1 1	0.8	1 5	1 4	0 5	1 3	0.7	1 0	1 0	1 4	0 7
Mg	88 2	90 4	87 6	89 7	88 4	89 3	91 5	88 3	90 4	89.8	87 2	89 5	90 0
Fe	10 8	8 9	11.3	9.5	10 0	9 3	8 0	10 5	9.0	9 2	11 8	9 1	9 3

Orthopyroxene (3)

Location	Lake Bullenmerri									Lake Bullenmerri			
Number	BM-74	BM-109	BM-116	BM-134	BM-137	BM-139	BM-143	BM-147	BM-154	BM-161	BM-163	BM-166	BM-167
SiO2	55 62	55 95	55 96	56.61	56.00	55 66	54 17	55 93	56 06	55 62	56.57	55 70	54 87
TiO2	-	-	-	-	-	-	0 20	-	-	-	-	-	-
Al2O3	3 63	2 64	3 06	1.80	3 11	3 60	4 91	2 12	2 38	3.89	2 27	3 30	4 52
Cr2O3	0 29	0 46	0 35	0 28	-	0 22	0 54	0.31	0 30	0 24	-	0 27	0 25
FeO	6.39	6 79	5 70	6 30	6.59	6 97	5 99	6.61	7 58	6 18	5 30	5 94	6 53
MgO	33 08	33 59	34.11	34 47	33.99	33 01	33 10	34 43	32 67	33 16	35 17	34 31	33 04
MnO	-	-	-	-	-	-	-	-	-	-	-	-	-
CaO	0.39	0 57	0 47	0 24	0 31	0 62	0 84	0 38	0.39	0.39	0 32	0 28	0 41
Total	99 40	100 00	99 65	99 70	100 00	100 08	99 75	99 78	99 38	99 48	99 63	99 80	99 62
Si	1 922	1 935	1.928	1 953	1 931	1 924	1 874	1 935	1.947	1 919	1.943	1 919	1 897
Ti	-	-	-	-	-	-	-	-	-	-	-	-	-
Al	0 148	0 108	0 124	0.074	0 127	0 147	0 200	0 086	0 097	0 157	0.092	0 134	0 184
Cr	0.008	0.013	0 010	0.008	0 000	0 006	0 015	0 009	0 009	0 007	-	0 007	0 006
Fe	0.185	0 197	0 164	0 182	0 190	0 201	0 173	0 191	0.220	0 178	0 152	0 171	0 189
Mg	1 704	1.732	1 751	1.773	1 747	1 701	1 708	1.776	1 691	1.705	1 801	1.762	1.703
Mn	-	-	-	-	-	-	-	-	-	-	-	-	-
Ca	0 014	0 021	0.017	0 008	0 012	0 023	0 031	0 014	0 014	0.015	0 012	0 010	0 015
Total	3 981	4.006	3 994	3 998	4 007	4 002	4 001	4 011	3 978	3 981	4 000	4 003	3 994
Mg#	90.2	89 8	91.4	90 7	90 2	89 4	90 8	90 3	88 5	90 5	92 2	91.2	90 0
Ca	0 7	1 1	0.9	0 4	0 6	1.2	1 6	0 7	0 7	0.8	0 6	0.5	0 8
Mg	89.5	88 8	90.6	90 3	89 6	88 4	89 3	89.7	87 8	89.8	91 7	90 7	89 3
Fe	9 7	10 1	8 5	9 3	9 7	10 4	9 0	9 6	11 4	9 4	7 7	8.8	9 9

Orthopyroxene (4)

Location					Mt Leura		Lake Gnotuk		Lake Gnotuk				
Number	BM-654	BM-632	BM-189	Bm-18	LE-2541	LE-2642	Gn-15	Gn-2	Gn-3	Gn-16	Gn-20A	Gn-20B	Gn-24
SiO2	56.16	57 30	56.03	56 29	56 36	56 44	58 12	56 40	56 82	56.06	57 60	55 97	56 05
TiO2	-	-	-	0.05	-	0 14	0 02	0.02	0 02	0 03	0 01	0 06	0 02
Al2O3	2.18	1 92	3 21	1.51	3 17	3 77	0 67	0 81	1.36	2.40	1 06	3 31	2 64
Cr2O3	0 41	0 27	0 37	0 41	0 22	0 36	0 29	0 20	0.24	0.25	0 19	0 25	0 27
FeO	7 50	6 25	6 69	8 98	5 79	5 74	5 79	8 74	7 36	6 93	6 92	6 80	8 13
MgO	32 93	33.70	32 97	31.72	34 17	32 25	34 03	32.47	33 35	32 72	34 44	33 36	32 97
MnO	0 18	0 18	0 13	0 15	-	0 12	0 16	0.20	0 19	0.18	0 18	0 18	0 18
CaO	0 59	0 42	0 43	0 68	0 28	0 54	0 39	0 54	0 51	0 45	0 37	0 40	0 53
Total	99 95	100 04	99 83	99 79	99 99	99 36	99 47	99 38	99.85	99 02	100 77	100 33	100 79
Si	1 950	1 972	1 938	1.970	1 936	1.949	2 005	1.980	1 971	1.957	1 975	1 928	1 935
Ti	-	-	-	0 001	-	0 004	0 001	0 001	0 001	0 001	0 000	0 002	0 001
Al	0 089	0 078	0 131	0.062	0 128	0 154	0 027	0 034	0 056	0 099	0 043	0 134	0 107
Cr	0 011	0 007	0 010	0 011	0 006	0 010	0 008	0 006	0 007	0 007	0 005	0.007	0 007
Fe	0 218	0 180	0.194	0 263	0 166	0 166	0 167	0 257	0.214	0 202	0 198	0 196	0 235
Mg	1 704	1 728	1 699	1 654	1 749	1 660	1 750	1 698	1.725	1 702	1 760	1 713	1 697
Mn	0 005	0 005	0 004	0.004	-	0 004	0 005	0 006	0 006	0.005	0 005	0 005	0 005
Ca	0 022	0.015	0 016	0 025	0 010	0 020	0 014	0.020	0 019	0 017	0 014	0 015	0 020
Total	4 000	3 986	3 992	3 992	3 997	3 965	3 977	4 000	3 997	3 990	4 001	4 000	4.007
Mg#	88 7	90 6	89 8	86.3	91 3	90 9	91 3	86 9	89 0	89.4	89 9	89 7	87 8
Ca	1 1	0 8	0 8	1.3	0 5	1 1	0 7	1 0	1 0	0 9	0 7	0 8	1 0
Mg	87 7	89 8	89 0	85 2	90 8	89 9	90 6	86.0	88.1	88.6	89 2	89 0	87 0
Fe	11.2	9 4	10 1	13 5	8 6	9 0	8 7	13 0	10 9	10 5	10 1	10 2	12 0

Orthopyroxene (5)

Location	L Gnotuk	Fen					Malaita						
Number	Gn-26	1	2	4	9	10	PHN4022	PHN4028	PHN4073	PHN4074	PHN4085	CRN205	CRN216
SiO2	54 27	53 70	52 24	54 50	53 42	53 26	54.50	55 30	54 50	56 20	54 80	55 40	56 10
TiO2	0 22	0 05	0.05	-	-	-	0 10	0 04	0 11	0.14	0 08	0 11	0 07
Al2O3	2 81	4 20	4 56	4 55	4 40	4 47	4 10	4 50	4 29	1.15	5 17	4 69	3 07
Cr2O3	0 17	0 35	0 47	0 26	0 27	0 40	0 26	0 28	0 34	0.23	0 38	0 33	0 51
FeO	10.52	6 12	6 65	6 56	6 52	6 57	6 44	5 25	6 53	9.65	6 74	6 55	6 63
MgO	30 37	34 10	33 66	33 40	33 77	33 93	33 30	33 70	0 18	0 13	0 16	0 21	0 10
MnO	0.20	0 16	0 18	-	0 23	0 22	0 18	0 16	33 00	31.20	32 30	32 50	32 60
CaO	0 93	0 70	0.75	0 59	0 69	0.83	0 42	0.60	0 46	0 50	0 45	0 45	0 38
Total	99 49	99 38	98 56	99 86	99 30	99 68	99 32	99 83	99 41	99 20	100 08	100 24	99 46
Si	1 924	1.872	1 863	1.887	1 867	1 856	1 894	1 905	1.893	1.973	1 893	1 905	1 939
Ti	0.006	0 001	0 001	-	-	-	0 002	0 001	0 003	0 004	0 002	0 003	0 002
Al	0 117	0 173	0 172	0 186	0 181	0 184	0 167	0 180	0 176	0 047	0 210	0 190	0 125
Cr	0 005	0 010	0 010	0 007	0 007	0 011	0 008	0 008	0 008	0 006	0 010	0 009	0 014
Fe	0 312	0 178	0.177	0 190	0 191	0 192	0 186	0 151	0 190	0 284	0 194	0 189	0 192
Mg	1 604	1 771	1 792	1 723	1 759	1 762	1.718	1 727	0 005	0 004	0 005	0 006	0 005
Mn	0 006	0 005	0 005	-	0 007	0 006	0 005	0 005	1 709	1 633	1.662	1 668	1 683
Ca	0 035	0 026	0 026	0 002	0 026	0 031	0 016	0 022	0 017	0 019	0 013	0 017	0 014
Total	4 009	4 036	4 046	3 995	4 038	4.042	3 996	3 999	4 001	3 970	3 989	3 987	3 974
Mg#	83 7	90 9	91 0	90 1	90 2	90 2	90.2	92 0	90 0	85 2	89 5	89 8	89 8
Ca	1 8	1 3	1 3	0 1	1 3	1 6	0 8	1 2	0 9	1 0	0.7	0 9	0 7
Mg	82 2	89 7	89.8	90 0	89 0	88 8	89 5	90 9	89 2	84 3	88 9	89 0	89 1
Fe	16 0	9 0	8 9	9 9	9 7	9 7	9 7	7.9	9 9	14 7	10 4	10 1	10 2

Orthopyroxene (6)

Location	Malaita								Jagersfontein				Green Knobs
Number	PHN4002	PHN4009	PHN4013	PHN4034	PHN4069	CRN209	3550B	3534	311	557	576	571	N53
SiO2	56.30	55 20	55.10	55 90	55 50	55 00	56 60	56 11	57 94	58 71	58 39	58 68	54 30
TiO2	0 14	0 13	0 16	0 14	0 13	0 24	0 07	0 21	0 03	-	-	-	0 08
Al2O3	1 90	3 94	4 11	2 31	3 56	4 30	2.60	2 83	0 61	0 72	0 66	0 68	5 22
Cr2O3	0.32	0 28	0 38	0 47	0 39	1 10	0.41	0 44	0 22	0 24	0 29	0 27	0 47
FeO	6.76	6 63	6 69	6 02	6 61	5.55	6 00	6 13	5 28	4 58	5 59	5 21	6 07
MnO	0.14	0 16	0 14	0 11	0 10	0 10	34 26	34 15	34 88	34 68	35 33	35 13	32 80
MgO	34 10	33.00	32 90	33 50	33 10	31 60	0 13	0 15	0 34	0 11	0 21	0 15	0 16
CaO	0 50	0 41	0 41	0 56	0 40	1.74	0.51	0 55	0 18	0.60	0 16	0 18	0 77
Total	100 16	99 75	99 89	99 01	99 79	99 63	100 58	100 57	99 48	99.64	100 63	100.30	99 87
Si	1 944	1 909	1 905	1 942	1 918	1 905	1.939	1 926	1 996	2 010	1 991	2 001	1 879
Ti	0.004	0 003	0 004	0 004	0 003	0 006	0 002	0 005	0 001	-	-	-	0 002
Al	0 077	0 161	0 167	0 095	0 157	0 176	0 105	0 115	0 025	0.029	0 027	0 027	0 213
Cr	0 009	0.008	0 010	0 013	0 008	0 030	0 011	0.012	0 006	0 006	0 008	0 007	0 013
Fe	0 195	0 192	0 194	0.175	0 191	0.161	0 172	0 176	0.152	0 131	0 159	0 149	0 176
Mn	0.004	0.005	0 004	0 004	0 003	0 003	0 004	0 004	1 791	1 770	1 795	1 786	1 691
Mg	1.755	1 700	1.695	1 736	1.704	1 636	1.749	1 747	0 010	0.003	0 006	0 004	0 005
Ca	0 019	0 015	0 015	0 021	0 017	0 065	0 019	0 020	0 007	0 022	0 006	0 007	0 029
Total	4 007	3 993	3 994	3.990	4 001	3 982	4 001	4.005	3 987	3 972	3 992	3 981	4 007
Mg#	90 0	89 9	89.7	90.8	89 9	91 0	91 1	90 8	92.2	93 1	91 8	92 3	90 6
Ca	1 0	0 8	0 8	1.1	0 9	3 5	1 0	1 0	0 3	1 1	0 3	0 3	1 5
Mg	89 1	89 1	89 0	89 9	89 1	87 9	88 4	87 7	91.9	92 0	91 6	92 0	89 2
Fe	9 9	10 1	10 2	9 1	10 0	8 6	9 6	10 1	7 8	6 8	8 1	7 7	9 3

Orthopyroxene (7)

Location	Finero					Balmuccia		Zabargad			Timor		
Number	F2A	F69	F2D	197	106	B-3C	F-58	Z-37	Z-42A	Z-42B	7	11	12
SiO2	56 42	57 48	57 02	55 98	56 78	55 49	55 52	54 03	56 00	57 30	54 70	54 70	54 50
TiO2	0 01	0.10	0 08	0 04	0.02	0.06	0 08	0 15	0 10	0 07	-	-	-
Al2O3	1.20	0.65	1 40	1 16	1 44	3 18	4 05	3 97	3 50	2.89	5.11	5 69	5 44
Cr2O3	0.31	0.25	0 40	-	-	0 19	0 35	0 26	0 25	0 22	0 40	0 48	0 35
FeO	5 40	5.23	5 39	6 83	6 59	6 52	6 26	7 11	6 70	6 34	6 68	6 24	6 68
MgO	35 27	36 02	35 28	35 40	34.27	33 35	33 39	33 13	33 50	33 70	32 50	32 40	32 40
MnO	0 17	0 16	0 16	-	-	0 17	0 25	0 18	0 18	0 16	-	-	-
CaO	0.26	0 41	0 36	0 71	0 51	0 33	0 29	0 67	0 49	0.55	0 70	0 56	0 60
Total	99 04	100 30	100 09	100 12	99 61	99 29	100 19	99 50	100 72	101 23	100 09	100 07	99 97
Si	1 958	1.968	1.958	1 938	1 966	1 929	1 912	1 886	1 921	1.949	1 890	1 880	1 890
Ti	0 000	0 003	0 002	0 001	0 001	0 002	0 002	0 004	0 003	0 002	-	-	-
Al	0 049	0 026	0 057	0 047	0 059	0 130	0 164	0 163	0 142	0.116	0 210	0 230	0 220
Cr	0 009	0 007	0 011	0 000	0 000	0 006	0 009	0 007	0 007	0.006	0 010	0 010	0 010
Fe	0 157	0.150	0 155	0 198	0 191	0 190	0 180	0 208	0 192	0.180	0 190	0 180	0 190
Mg	1.825	1 839	1 806	1 827	1 769	1 728	1 714	1 724	1 713	1 708	1 670	1.660	1 670
Mn	0.005	0 005	0 005	0 000	0 000	0 005	0 007	0 005	0 005	0 005	-	-	-
Ca	0.010	0.015	0 013	0 026	0 019	0 012	0 011	0 025	0 018	0 020	0 030	0 020	0 020
Total	4 013	4 013	4 007	4 037	4 004	4 002	3 999	4 022	4 001	3 986	4 000	3 980	4 000
Mg#	92.1	92 5	92 1	90 2	90 3	90 1	90.5	89 2	89 9	90 5	89 8	90 2	89 8
Ca	0 5	0 7	0 7	1.3	1 0	0 6	0 6	1 3	0 9	1 0	1 6	1 1	1 1
Mg	91 6	91 8	91 5	89 1	89 4	89 5	90.0	88 1	89 1	89.5	88 4	89 2	88 8
Fe	7 9	7 5	7 9	9 6	9 6	9.8	9 4	10 6	10 0	9 4	10 1	9 7	10.1

Orthopyroxene (8)

Location	A Araml			Lien				Ronda					
Number	F-16A	F-16C	F52C	1K	1J	5421C	USC8A	R501	R740	R696	R123	R243	7319
SiO2	57.97	56 56	57 19	57.60	56 60	57 00	57 50	55 67	55 26	54 86	54 91	54 64	54 56
TiO2	0 07	0 00	0 05	0 03	0 04	0 01	0 04	0 07	0 12	0 14	0 17	0 10	0 07
Al2O3	0 82	1.65	0 68	0 59	0 48	0 34	0 29	3 13	3 28	3 43	4 06	4 04	3 69
Cr2O3	0 17	0 06	0 16	0 14	0 07	0 00	0 02	0 35	0 33	0 28	0.28	0 29	0 67
FeO	5.44	6 73	5 96	7 50	8 85	5 60	4 96	6 55	6.69	7 43	7 48	6 84	5 61
MgO	35 99	35 16	35 89	35 00	34 20	36.50	36 80	34.00	34 15	33 64	33 17	34 38	35 54
MnO	0 12	0 18	0 11	0 09	0 10	0 06	0 10	0 15	0 17	0.17	0 09	0 16	0 14
CaO	0.23	0 12	0 17	0 14	0 13	0 05	0 03	0.44	0 43	0 43	0 47	0 48	0 74
Total	100 81	100 46	100 21	101.09	100 47	99 56	99.74	100 36	100.43	100.38	100 63	100 93	101 02
Si	1 973	1.946	1 965	1 974	1 965	1 968	1 975	1 918	1.906	1.900	1 894	1.878	1 885
Ti	0 002	0 000	0 001	0 001	0.001	0 000	0 001	0 002	0.003	0 004	0 004	0 003	0 002
Al	0 033	0.067	0 028	0 024	0 020	0.014	0.012	0 127	0 133	0 140	0 165	0 164	0 150
Cr	0 005	0 002	0 004	0.004	0 002	0 000	0.001	0 010	0 009	0 008	0 008	0 008	0 018
Fe	0 155	0 194	0 171	0 215	0 257	0 162	0 142	0 189	0 193	0 215	0 216	0 197	0 162
Mg	1.826	1.803	1 838	1 787	1.770	1.878	1 884	1 745	1.755	1 736	1 705	1 761	1 779
Mn	0 003	0 005	0 003	0.003	0 003	0 002	0 003	0 004	0.005	0 005	0 003	0 005	0 004
Ca	0 008	0 004	0 006	0 005	0 005	0 002	0 001	0 016	0 016	0 016	0 017	0 018	0 027
Total	4.005	4.021	4 016	4 012	4 023	4 025	4 018	4 011	4 020	4.024	4 012	4 034	4 027
Mg#	92 2	90 3	91 5	89 3	87 3	92 1	93 0	90 2	90 1	89 0	88 8	89 9	91 7
Ca	0 4	0 2	0 3	0 3	0 2	0 1	0 1	0 8	0 8	0 8	0 9	0 9	1 4
Mg	91.8	90 1	91 2	89 0	87 1	92 0	92 9	89 5	89 4	88 3	88 0	89 1	90 4
Fe	7 8	9 7	8 5	10 7	12 6	7 9	7 0	9 7	9 8	10 9	11 1	10 0	8 2

Orthopyroxene (9)

Location	Miyamori		Oregon		Nonsberg peridotite			
Number	77073113	77111919	VH9	CSZ12	MK5D	MO11	MK5C	MK1
SiO2	55 23	55.28	55.80	54.40	55 48	56 65	56 18	56 33
TiO2	0 03	0 00	0.05	0 07	0 04	0 06	0 03	0 04
Al2O3	3 03	3 26	3.57	4 48	2 57	1.11	1 62	1.57
Cr2O3	0.38	0.45	0 29	0 49	0 34	0 16	0 20	0 19
FeO	5 99	6.75	6 40	6 20	5 82	6 43	6 09	6 20
MgO	33 55	33 60	33 70	33 20	34 76	35 31	35 00	35 57
MnO	0 13	0.14	0 15	0 14	0 11	0 14	0 12	0 13
CaO	0 52	0 35	0 44	0 86	0 20	0 19	.0 21	0 22
Total	98 86	99.83	100 40	99 84	99 32	100 05	99 45	100 25
Si	1.927	1.916	1 919	1 886	1 925	1 955	1.947	1.939
Ti	0 001	0.000	0 001	0 002	0.001	0 001	0 001	0 001
Al	0 125	0.133	0 141	0 183	0 105	0.045	0.066	0 064
Cr	0 010	0 012	0 008	0 013	0 009	0 004	0.005	0 005
Fe	0 175	0.196	0 184	0 179	0 169	0 186	0 176	0 178
Mg	1.744	1.736	1.724	1 716	1.798	1 816	1.808	1 826
Mn	0 004	0.004	0.004	0 004	0.003	0 004	0 003	0 004
Ca	0 019	0 013	0 016	0 032	0 008	0 007	0 008	0 008
Total	4 005	4.011	3 997	4 015	4 018	4 018	4.014	4 025
Mg#	90 9	89.9	90 4	90 6	91 4	90 7	91 1	91 1
Ca	1 0	0.7	0 8	1 7	0.4	0 3	0 4	0 4
Mg	90.0	89 3	89 6	89 1	91 0	90 4	90 8	90 8
Fe	9 0	10.1	9 6	9 3	8 6	9 3	8 8	8 8

Orthopyroxene (10)

Location	Nonsberg peridotite							
Number	ULT12	ULT4	80-21	80-20	80-64	80-11	80-17	79-59
SiO2	57 56	56.04	55 12	54 9	55 57	56 04	57 31	56 23
TiO2	0 08	0 00	0 8	0 1	0 06	0 03	0 02	0 03
Al2O3	1.50	1.85	3 94	4 53	3 56	3.57	2.24	1 97
Cr2O3	0 17	0 14	0 37	0 45	0 37	0 41	0.18	0 22
FeO	6 41	6 42	6 8	6 4	6 24	6 2	6 36	6 07
MgO	34 51	34 89	33 62	33 92	33 85	33 9	34.51	34 34
MnO	0 12	0.15	0 15	0 12	0 17	0.16	0 17	0 19
CaO	0 22	0.19	0 24	0.27	0 31	0 31	0 31	0 31
Total	100 57	99.68	101 04	100 69	100 13	100.62	101 1	99 36
Si	1.971	1.941	1.900	1 884	1.915	1.919	1 952	1.950
Ti	0 002	0.000	0 002	0 003	0 002	0.001	0 001	0 001
Al	0 061	0.076	0.160	0 183	0 145	0 144	0.090	0 080
Cr	0.005	0 004	0.010	0 012	0 010	0.011	0 005	0.006
Fe	0 184	0 186	0 196	0 184	0.180	0 178	0.181	0 176
Mg	1 761	1.801	1.728	1.734	1 738	1 730	1.752	1 774
Mn	0.004	0.005	0 004	0 003	0 005	0.005	0.005	0 006
Ca	0 008	0 007	0.009	0 010	0.011	0.011	0.011	0 012
Total	3 996	4.020	4 009	4 013	4 006	3 999	3.997	4 005
Mg#	90.5	90.6	89.8	90.4	90 6	90 7	90 6	91 0
Ca	0 4	0 4	0 5	0.5	0 6	0 6	0.6	0 6
Mg	90 2	90 3	89 4	89.9	90 1	90 2	90 1	90 4
Fe	9 4	9 3	10 1	9 5	9 3	9 3	9 3	9 0

Clinopyroxene (1)

Location	Massif Central			Languedoc				San Carlos	Hawaii		Hoggar	Nunivak	
Number	LI-9	LI-52	Cp-15	H204B	80-437	80-442	76-250	PA-120G	SL011	SL138	V	10016	10006
SiO2	52 30	52 30	52.50	51 77	52.50	51.19	52 21	52.20	53 14	52 36	51 79	54 83	55 64
TiO2	0 63	0 19	0.53	0 59	0.60	0.43	0 50	0.38	0 12	0 30	0 48	0 02	0 03
Al2O3	6.81	4 49	5.80	7.12	7.20	7 44	6.30	5.60	6 63	6 81	4 66	3 27	4 28
Cr2O3	0 65	0 82	0.73	0.71	0.85	0 84	0 88	1 12	1.11	0.87	1 58	0 78	0 87
FeO	2.91	2 89	2.29	2 68	3 06	2.88	2 65	3.30	2.82	2.89	3 86	2 42	2 80
MgO	14 60	16 20	14.20	14.91	14.51	14 22	0 07	15 60	14 69	14 56	15 38	16 22	15 94
MnO	0 09	0 05	0 05	-	0 13	0 16	14 97	0.12	0 03	0 06	0 12	0 13	0 13
CaO	20.50	21 60	21.50	20.19	19 43	20 56	21.30	18 20	18.59	19 13	20 84	19 89	17 61
NaO	1.43	1 10	1.73	1 68	1.72	1 08	1 39	2.14	2 52	2 13	0 92	2 12	2 71
Total	99 92	99.64	99.33	99 65	100.00	98 80	100 27	98 66	99 65	99 11	99 63	99 68	100 01
Si	1.888	1 906	1.912	1 876	1 888	1 867	1 886	1 911	1 919	1.904	1 896	1 981	1 991
Ti	0.017	0 005	0.015	0 016	0 016	0 012	0 014	0 010	0 003	0 008	0 013	0 001	0 001
Al	0.290	0 193	0.249	0 304	0 305	0.320	0 268	0 242	0 282	0.292	0.201	0 139	0 181
Cr	0.019	0 024	0 021	0 020	0 024	0 024	0 025	0 032	0 032	0 025	0 046	0 022	0 025
Fe	0 088	0 088	0 070	0.081	0 092	0 088	0 080	0 101	0 085	0 088	0 118	0 073	0 084
Mg	0 789	0 880	0 771	0 805	0 778	0 773	0 806	0 851	0.791	0 789	0 839	0 873	0 850
Mn	0 003	0 002	0 002	-	0 004	0 005	0 002	0 004	0 001	0 002	0 004	0 004	0 004
Ca	0 795	0.843	0 838	0 784	0 749	0 803	0 825	0 714	0.719	0 745	0 818	0 770	0 675
Na	0 100	0.078	0 122	0 118	0 143	0 113	0 097	0.152	0 179	0 150	0 065	0 148	0 188
Total	3 989	4.019	4 000	4.004	3 999	4 005	4 003	4 017	4 011	4 004	4 000	4 011	3 999
Mg#	90 0	90.9	91.7	90.9	89 4	89 8	91 0	89 4	90.3	90.0	87 7	92 3	91 0
Ca	47.5	46.5	49.9	46.9	46 3	48 3	48 2	42 9	45.1	45 9	46 1	44 9	42 0
Mg	47.2	48 6	45.9	48.2	48 1	46 5	47 1	51 1	49 6	48.6	47 3	50 9	52 8
Fe	5 3	4 9	4.2	4.9	5 7	5.3	4 7	6.1	5.3	5.4	6 7	4 3	5 2

Clinopyroxene (2)

Location	Ataq	Tariat	Ichinomegata				Lake Bullenmern						
Number	AT-15	MO423016	LHZ-13	LHZ-53	LHZ-29	#87	BM-9	BM-15	BM-18	BM-27	BM-47	BM-51	BM-58
SiO2	52 81	51.46	53 01	52 22	50 56	51 45	54.84	52.59	55 22	52 65	54 20	55 11	52 66
TiO2	0 07	0 80	0.09	0 20	0 42	0 50	-	0 41	-	0 24	-	-	-
Al2O3	3.00	7.34	1 92	3.61	4 70	4 11	3 34	6 68	1 80	5.94	3 47	2 88	7 19
Cr2O3	1.09	0 70	0 19	0 66	0 97	0 87	2 95	0 51	1.44	0.77	1 11	1 42	1.21
FeO	2 55	3 12	2 64	2 37	3 04	2 86	2 07	2.97	2.29	2 37	3 08	2 62	2 92
MgO	16 44	13 57	16 98	16 07	16 20	16 90	15 24	15 08	16 08	15 68	15 85	15 26	14 93
MnO	0.12	-	0 08	0.03	0.09	0 06	-	-	-	-	-	-	-
CaO	22.15	20 34	24 65	24.36	22 62	22 89	19 26	20.08	21 35	20 71	20.85	20 36	18 27
NaO	1.59	1 81	0.12	0.18	0.40	0.44	2.31	1 68	1.81	1.71	1 41	2 36	2 18
Total	99.82	99 14	99 68	99 70	99 00	100.08	100 01	100 00	99 99	100.07	99 97	100 01	99 36
Si	1.926	1 879	1.941	1.907	1 866	1.870	1.978	1.897	1.998	1 901	1.962	1 992	1.905
Ti	0 002	0.022	0.003	0 005	0 012	0.014	-	0 011	-	0.007	-	-	-
Al	0 129	0.316	0.083	0.155	0 205	0 176	0.142	0 285	0.077	0.253	0 148	0 123	0.307
Cr	0 030	0 020	0 006	0 018	0 028	0 003	0.084	0 014	0.041	0 022	0 032	0 041	0 034
Fe	0 072	0 095	0 081	0 072	0.094	0.087	0 063	0 090	0 069	0 072	0.093	0.079	0.088
Mg	0.894	0 738	0 927	0.875	0 891	0.915	0.819	0.811	0 867	0.844	0.855	0 822	0 805
Mn	0.004	-	0 003	0.000	0 003	0 002	-	-	-	-	-	-	-
Ca	0 866	0.796	0.967	0 953	0 894	0 891	0 744	0.776	0 828	0 801	0 809	0 789	0 708
Na	0 113	0.128	0 008	0.013	0 028	0 031	0 160	0 117	0 100	0 120	0 099	0 166	0 153
Total	4 036	3 994	4 019	3 998	4 021	3 989	3 990	4 001	3 980	4.020	3 998	4 012	4 000
Mg#	92 5	88 6	92.0	92.4	90 5	91 3	92 9	90 0	92.6	92.1	90 2	91 2	90 1
Ca	47.3	48 9	49.0	50.2	47 6	47 1	45 8	46.3	46 9	46 7	46 0	46 7	44 2
Mg	48 8	45 3	46.9	46.1	47 4	48 3	50 4	48 4	49 1	49 2	48 7	48 6	50 3
Fe	3 9	5 8	4 1	3 8	5 0	4 6	3 9	5 4	3 9	4 2	5 3	4 7	5 5

Clinopyroxene (3)

Location	Lake Bullenmerri												
Number	BM-62	BM-74	BM-109	BM-116	BM-134	BM-135	BM-137	BM-139	BM-143	BM-147	BM-154	BM-161	BM-166
SiO2	53.56	53.46	53.94	53.59	54.69	54 97	53 14	53.32	51 66	53 71	53 67	53 22	53 11
TiO2	-	-	-	-	-	-	-	-	0.78	-	-	-	0 24
Al2O3	4 73	5 14	4.50	5 14	4 28	2.22	4 64	6.25	6 99	4 70	4 34	5 77	4.86
Cr2O3	1 07	1.06	1 40	1.24	1.54	1 20	0 61	0.79	1.26	1 47	1 70	0 99	1 00
FeO	2 37	2 39	3 34	2.26	2 21	2.84	2.20	3.00	2 89	2 50	3 06	2 42	2 09
MgO	15.81	15.96	15 65	16 00	15.34	15 92	16.12	15 11	15 39	15.34	15 45	15 62	16 02
MnO	-	-	-	-	-	-	-	-	-	-	-	-	-
CaO	21.07	20 44	19.50	20.12	19.62	21 23	22 57	19.75	18 94	19 61	20 03	20.32	21 72
NaO	1.39	1.55	1.69	1.66	2 33	1 63	0 60	1 87	2.09	2.67	1 76	1 67	1 01
Total	100 00	100.00	100.02	100.01	100 01	100.01	99 88	100 09	100.00	100 00	100 01	100 01	100 05
Si	1.933	1.927	1 948	1.930	1 968	1 990	1.920	1.921	1 867	1 941	1 492	1 918	1 918
Ti	-	-	-	-	-	-	-	-	0 021	-	-	-	0.007
Al	0.202	0.219	0 192	0 218	0 182	0 094	0 198	0 266	0.298	0.200	0.186	0.245	0 207
Cr	0 031	0 030	0 040	0.036	0 044	0.034	0.017	0 022	0.036	0 042	0 049	0 028	0 029
Fe	0 071	0.072	0 101	0 068	0 066	0 086	0 067	0.090	0.087	0.075	0 093	0 073	0 063
Mg	0 851	0.858	0 842	0.859	0 822	0 859	0 868	0 811	0.829	0 827	0 833	0 839	0 862
Mn	-	-	-	-	-	-	-	-	-	-	-	-	-
Ca	0.815	0.790	0.755	0.777	0 757	0 824	0 874	0 763	0 733	0.759	0 777	0 784	0 841
Na	0 097	0.108	0.118	0.116	0 162	0 115	0 042	0 131	0.146	0 187	0 124	0 117	0 071
Total	4 000	4 004	3 996	4 004	4 001	4 002	3 986	4 004	4 017	4 031	3.554	4 004	3 998
Mg#	92 3	92 3	89 3	92 7	92 6	90.9	92 8	90.0	90.5	91 7	90 0	92 0	93 2
Ca	46 9	45.9	44 5	45 6	46 0	46 6	48.3	45 9	44 5	45 7	45 6	46 2	47 6
Mg	49 0	49 9	49 6	50 4	50 0	48 6	48 0	48.7	50 3	49 8	48 9	49 5	48 8
Fe	4.1	4 2	5 9	4.0	4 0	4.9	3 7	5 4	5 3	4 5	5 5	4 3	3 6

Clinopyroxene (4)

Location	Lake Bullenmerri					Mt Leura	Lake Gnotuk		Lake Gnotuk				
Number	BM-167	BM-654	BM-632	BM-189	Bm-18	LE-2641	LE-2642	Gn-15	Gn-2	Gn-3	Gn-16	Gn-20A	Gn-20B
SiO2	52 54	53 30	54 10	52 93	53 92	53 26	54.08	55 32	54 03	54 04	53 71	50 56	53 02
TiO2	0 36	-	-	0 25	0 14	0 22	0 46	0 02	0 02	0.06	0 06	0 45	0 45
Al2O3	6 60	4.52	3.90	5.02	3 27	4 99	4 42	3 16	3 08	3 88	4 34	6 82	5 97
Cr2O3	0 90	1.38	1.23	0 87	1.54	0 92	0 73	2 08	1 32	1.08	0 79	2 30	0 54
FeO	2 42	3.09	2 16	2.34	4 00	1 95	2.13	2 71	3.51	2.88	2 74	2 28	2 56
MgO	15 47	15.18	15 27	15 12	15 26	15 95	15 60	14 23	15 38	15.49	15 39	15 41	14 77
MnO	-	0 11	0 13	0 07	0.10		0 05	0 08	0 13	0.11	0 10	0 06	0 07
CaO	20 40	20.56	21 46	21.23	18 82	21.57	21.30	19 12	19 59	20.82	21 06	21 01	21 45
NaO	1.38	1.79	1 85	1.66	2 11	1 18	1 07	2.38	1 97	1.88	1.76	1 07	1 68
Total	100.07	99.93	100 10	99 49	99.16	100.04	99.84	99 10	99 03	100 24	99 95	99 96	100 51
Si	1.893	1.935	1 955	1 924	1.972	1 920	1 949	2.011	1.977	1.953	1.945	1 838	1 908
Ti	0 010	-	-	0 007	0 004	0.006	0 012	0 001	0.001	0 002	0 002	0.012	0 012
Al	0.280	0 193	0 166	0.215	0 141	0.212	0.188	0.135	0.133	0 165	0 185	0 292	0 253
Cr	0.026	0 040	0 035	0.025	0.045	0 026	0 021	0.060	0.038	0.031	0.023	0.066	0 015
Fe	0.073	0 094	0 065	0 071	0 122	0 059	0 064	0.082	0 107	0 087	0 083	0 069	0 077
Mg	0.831	0.821	0.822	0 819	0 832	0 857	0 838	0.771	0 839	0.834	0.830	0.835	0 792
Mn	-	0.003	0 004	0 002	0 003	0 000	0 002	0 002	0 004	0.003	0 003	0 002	0 002
Ca	0.787	0 800	0 831	0.827	0.738	0.833	0 823	0.745	0 768	0 806	0 817	0.818	0 827
Na	0.097	0 126	0.130	0.117	0 150	0 082	0 075	0.168	0.140	0 132	0 124	0 075	0 117
Total	3.997	4.012	4 009	4.007	4 006	3 996	3 971	3 975	4 007	4 013	4.011	4 008	4 004
Mg#	91 9	89.7	92.6	92.0	87.2	93 6	92.9	90 3	88.6	90.6	90 9	92 3	91 1
Ca	46 5	46.6	48.4	48 2	43 6	47 6	47.7	46 6	44 8	46 7	47.2	47 5	48.8
Mg	49.1	47.9	47.9	47 7	49 2	49 0	48 6	48.2	48 9	48.3	48.0	48 5	46 7
Fe	4 3	5 5	3.8	4 1	7.2	3 4	3 7	5.2	6 3	5.0	4 8	4 0	4 5

Clinopyroxene (5)

Location	Lake Gnotuk		Fen					Malaita					
Number	Gn-24	Gn-26	1	2	4	9	10	3567	PHN4022	PHN4028	PHN4073	PHN4074	PHN4085
SiO2	51 27	52 17	50.62	51 42	51.57	50 72	50.96	51 60	52.20	53.30	54 10	51.70	53 10
TiO2	0 60	0.90	0.21	0.18	-	-	-	0.69	0 42	0.10	0.16	0 53	0.24
Al2O3	5.64	5 40	5 90	6.25	6 80	5 87	5.99	4 91	5 28	5 06	2 35	6 00	4 59
Cr2O3	1.01	0.26	0 80	0 57	0.58	0 78	0 83	0 65	0 71	0.52	0.62	0 79	0 64
FeO	3.59	4 96	2 74	3 41	2.85	3 32	3 17	3 19	2 55	1 67	2 61	2 58	2 96
MgO	15.60	15 05	16 48	16 79	15.70	15 83	16.54	16 82	0 13	0 09	0 11	0 12	0 11
MnO	0.12	0 13	0 11	0.12	-	0 13	0 16	0.08	15 10	15 80	16 60	14 10	15.30
CaO	20 80	19 44	21 65	18 91	20 98	22 21	21 42	20 36	22 00	23 60	22 10	21 50	21 40
NaO	1.20	1.73	1.30	1.44	1.48	1.12	1.38	1 38	1.51	-	1 14	1.85	1 61
Total	99 83	100 04	99 81	99 09	99 96	99 98	100 45	98 68	99 90	100 14	99 79	99 17	99 95
Si	1.871	1 900	1.848	1 876	1 868	1.856	1.851	1 880	1 898	1.919	1.965	1 892	1 929
Ti	0.016	0 025	0 006	0.005	-	-	-	0 019	0.012	0.002	0 004	0 015	0 007
Al	0.243	0.232	0.254	0.269	0 291	0.253	0.256	0 211	0.226	0.215	0 101	0 259	0 196
Cr	0.029	0 007	0 023	0.016	0 017	0 023	0 024	0 019	0 020	0 015	0 018	0 023	0.018
Fe	0.110	0 151	0.084	0.104	0.087	0 102	0 096	0 097	0 077	0.051	0 080	0 079	0.090
Mg	0 848	0.817	0.897	0.913	0 849	0 863	0 895	0 913	0 044	0 003	0 003	0 004	0 004
Mn	0.004	0 004	0 003	0 004	-	0 005	0.004	0 002	0 819	0 848	0 897	0 769	0 831
Ca	0 813	0 759	0 847	0 739	0 816	0 871	0 834	0 795	0 856	0 910	0 861	0 845	0 824
Na	0 085	0.122	0 092	0 102	0 104	0 079	0.097	0 098	0 106	-	0 080	0 132	0.114
Total	4 019	4 017	4 054	4 028	4 034	4 053	4.058	4 035	4 058	3 963	4 009	4 018	4 013
Mg#	88 6	84 4	91 4	89.8	90 7	89 4	90.3	90 4	91 4	94 3	91 8	90 7	90 2
Ca	45 9	43 9	46 3	42 1	46.6	47 4	45.7	44.0	48 9	50 3	46 8	49 9	47 2
Mg	47 9	47.3	49 1	52 0	48.5	47 0	49 0	50 6	46 7	46 9	48 8	45 4	47 6
Fe	6 2	8 8	4 6	5 9	5 0	5 6	5 3	5 4	4 4	2.8	4 4	4 7	5 2

Clinopyroxenes (6)

Location	Malaita								Jagerstontain				Green Knob
Number	CRN205	CRN216	PHN4002	PHN4009	PHN4013	PHN4034	PHN4069	CRN209	311	259	557	571	N53
SiO2	52.90	51 10	52.70	52 50	53.00	53 50	53 00	52 80	54 89	54 07	55 71	56 19	52 60
TiO2	0 46	1.08	0.54	0 53	0.23	0 38	0 26	0 44	0 07	0 09	0 02	0 03	0 22
Al2O3	5 80	6 53	5 21	6 06	2 98	4.22	2 87	5 16	2 20	2.39	1.75	2 54	6 40
Cr2O3	0.64	0 78	0 76	0.76	0 63	1 38	0 64	2 30	1.59	1.78	1.52	1 78	0 87
FeO	2 62	2 51	2 73	2 61	2 72	2 66	2 68	3 82	1 75	1 54	1.27	1 60	2 20
MnO	0.09	0 06	0.05	0.11	0.07	0.06	0 05	0 11	16 00	16.58	17 02	14 82	15 90
MgO	15 00	13 80	14 80	14 70	16.50	15 40	16 40	18 40	0 12	0.04	0 12	0 11	0 10
CaO	21.30	21 50	21.00	20 90	23.00	20 40	22 60	14 80	21 48	21 30	21.59	20 64	20 20
NaO	1.39	2 07	0.76	1.84	0 87	1 91	0 77	1 86	1.45	2.10	1 53	2 30	1.67
Total	100.20	99 43	98 55	100 01	100.00	99 91	99 27	99 69	99 55	99 89	100 53	100 01	100 16
Si	1.907	1 867	1.915	1.901	1.930	1 938	1 943	1.902	1.990	1 960	1 996	2 020	1.893
Ti	0.013	0 030	0.015	0 015	0.006	0.010	0 007	0.012	0 002	0.002	0 001	0.001	0 006
Al	0.247	0 281	0.223	0.258	0 128	0.180	0 126	0 219	0 094	0.102	0.074	0 108	0 271
Cr	0.018	0.023	0 022	0 022	0 018	0 039	0 018	0 065	0 046	0.051	0.043	0 051	0.025
Fe	0 079	0 077	0 083	0 079	0 083	0.081	0 081	0 115	0 053	0 047	0 038	0 048	0 066
Mn	0 003	0 003	0 002	0 003	0 002	0 002	0 001	0 003	0.865	0 896	0 909	0 794	0 853
Mg	0.808	0 753	0 804	0 791	0 893	0 829	0 886	0.987	0 004	0 001	0 004	0 003	0 003
Ca	0 823	0 842	0 817	0.809	0.899	0 793	0.881	0.572	0 834	0 827	0 829	0 795	0 779
Na	0.097	0 147	0 133	0 129	0.061	0 134	0 063	0 130	0 102	0 148	0 106	0 160	0 117
Total	3 995	4 023	4 014	4 007	4.020	4 006	4 006	4 005	3 989	4 034	3.998	3 980	4.012
Mg#	91 1	90 7	90 6	90.9	91.5	91 1	91 6	89 6	94.2	95.0	96 0	94 3	92 8
Ca	48.1	50 4	47.9	48 2	47.9	46 6	47.7	34 2	47 6	46 7	46 7	48 6	45 9
Mg	47.3	45 0	47.2	47.1	47 6	48 7	47.9	59 0	49 3	50 6	51.2	48 5	50 2
Fe	4 6	4 6	4 9	4 7	4.4	4 8	4 4	6 9	3.0	2.6	2 1	2 9	3 9

Clinopyroxene (7)

Location	Tanzania	Finero			Alpe Arami		Balmuccia		Lien		Ronda		
Number	DU18500	F2A	F2D	197	F-16a	F-52c	B-3C	F-58	1K	1J	R501	R740	R696
SiO2	55.00	54 50	54 65	54 12	55 21	54 97	52 05	52 04	54 60	54 40	53 25	52 79	52 36
TiO2	0 14	0 06	0.08	0 06	0 16	0 10	0 36	0 46	0 07	0 09	0 50	0 46	0 85
Al2O3	1 40	0 79	1.20	1 39	1 32	1 40	5 35	6.03	1 89	3 00	5 40	5 38	6 52
Cr2O3	2 00	0 43	0 48	-	0 73	0 56	0 68	0 71	1 15	0.39	1.07	1 03	0 83
FeO	2.30	1 52	1 77	2 34	1 84	2 13	2 54	2 38	2 15	2 60	2 51	2 48	2 78
MgO	17 20	17 70	18 61	18 62	17 44	17.59	14 91	15 11	17 00	15 90	15 58	15 87	14 72
MnO	0 09	0 08	0 07	-	0 06	0 08	0 09	0 14	0 05	0 13	0 08	0 09	0 05
CaO	20 70	24 31	23 83	22 37	23 34	22 78	22 27	22 05	23.30	21 60	19 87	20 86	20 08
NaO	1 60	0 16	0 27	-	0 70	0 35	1 15	1 11	1.27	2.11	2 04	1 75	2 07
Total	100 43	99 55	100 96	98 90	100.80	99 96	99 40	100 03	101 48	100 22	100 30	100 71	100 26
Si	1.983	1 983	1.979	1.974	1 982	1.986	1.901	1 885	1 957	1 968	1.916	1 898	1 889
Ti	0.004	0 002	0.002	0 002	0 004	0.003	0 010	0 013	0 002	0 002	0 014	0 012	0 023
Al	0.060	0 034	0 051	0 060	0 056	0 060	0.230	0.257	0.080	0.128	0 229	0 228	0 277
Cr	0 057	0 012	0 014	-	0 021	0 016	0 020	0.020	0 033	0 011	0 030	0 029	0 024
Fe	0 069	0 046	0 054	0 071	0 055	0 064	0.078	0 072	0.064	0 079	0 076	0 075	0 084
Mg	0 924	0 960	0.950	1 012	0 933	0 947	0 812	0 816	0 908	0.857	0 836	0 850	0 791
Mn	0 003	0 002	0 002	-	0 002	0 002	0 003	0 004	0.002	0 004	0 002	0 003	0 002
Ca	0.800	0 948	0 925	0 874	0 898	0 882	0 871	0 856	0 895	0 837	0 766	0 804	0 776
Na	0 112	0 011	0 019	-	0 049	0 025	0 081	0 078	0.088	0 148	0 142	0 122	0 145
Total	4 011	3 998	3 996	3 994	4 000	3 985	4 006	4 001	4 029	4 034	4 011	4 021	4 011
Mg#	93.0	95 4	94 6	93 4	94 4	93 7	91 2	91 9	93 4	91.6	91 7	91 9	90 4
Ca	44 6	48 5	48 0	44 7	47 6	46 6	49 5	49 1	47 9	47 2	45 6	46 5	47 0
Mg	51.5	49 1	49.2	51 7	49 5	50 0	46 1	46 8	48 6	48 3	49 8	49.2	47 9
Fe	3 9	2 4	2 8	3 6	2 9	3 4	4 4	4 1	3 5	4 4	4 5	4 3	5 1

Clinopyroxene (8)

Location	Ronda			S W Oregon		Zabargad		East Timor			Miyamori	
Number	R123	R243	7319	VH9	CSZ12	Z-37	Z-42a	7	11	12	77073113	77111919
SiO2	51.84	51 60	52 18	51 40	51 80	50 87	46 30	50.80	51 50	51 10	51 80	53 04
TiO2	1 08	0 55	0.33	0 40	0 22	0 61	0 61	0 40	0 35	0 45	0 11	0 18
Al2O3	7.49	6 84	5.54	5 30	4 36	6 47	6 22	6 28	7 04	6 32	2 39	3 37
Cr2O3	0 64	0 75	1 61	0 64	0 71	0 68	0.80	1.08	1.10	0 73	0 43	0 71
FeO	3 07	2 87	2 41	2 45	2 44	2 62	2 71	2 47	2.47	2 39	2 21	2 43
MgO	14.27	15 20	15 66	15 90	16 70	15 13	15 60	15 30	15 00	16 00	16 95	16 59
MnO	0.10	0 13	0 10	0.08	0 09	0 08	0 07	-	-	-	0 04	0 06
CaO	19 77	20 40	21.01	22 60	22 90	21 79	21 20	23 60	21 70	22 50	24 19	24 04
NaO	2 32	1 55	1 41	0 99	0 50	1.23	1 41	-	0.91	0 46	0 12	0 28
Total	100 58	99 89	100 25	99 76	99 72	99 48	94 92	99 93	100 07	99 95	98 24	100 70
Si	1 886	1.870	1 887	1 874	1 890	1.858	1 866	1 850	1.860	1 850	1 922	1 917
Ti	0 029	0.015	0 009	0 011	0 006	0 017	0 017	0 010	0.010	0 010	0 003	0 005
Al	0 318	0.292	0 236	0.229	0 188	0 278	0.266	0 270	0 300	0 270	0 105	0 144
Cr	0.018	0 021	0 046	0 018	0 020	0 020	0 023	0 030	0 030	0 020	0 013	0 020
Fe	0 092	0 087	0 073	0 075	0 074	0 080	0 091	0.080	0.080	0 070	0 069	0 073
Mg	0 766	0 821	0 844	0 865	0.908	0 824	0 843	0 830	0 810	0 870	0 937	0 894
Mn	0 003	0 004	0 003	0 002	0 003	0 002	0 002	-	-	-	0 001	0 002
Ca	0 763	0.792	0.814	0.882	0.894	0 853	0 823	0 920	0 840	0.880	0 962	0 931
Na	0 162	0 109	0 099	0 070	0 035	0 087	0 099	-	0.060	0.030	0 009	0 020
Total	4.037	4 011	4 011	4 026	4.018	4 019	4 030	3 990	3.990	4.000	4 020	4 006
Mg#	89 3	90 4	92 0	92 0	92 5	91 2	90.3	91 2	91 0	92 6	93 2	92 4
Ca	47 1	46 6	47 0	48 4	47 7	48 5	46 8	50 3	48 6	48 4	48 9	49 0
Mg	47.3	48 3	48 8	47 5	48 4	46 9	48 0	45 4	46 8	47.8	47 6	47 1
Fe	5 7	5 1	4 2	4 1	3 9	4 6	5 2	4 4	4 6	3 8	3 5	3 9

Clinopyroxene (9)

Location	Austridic Complex			Tinaquillo							
Number	MK5D	MO11	MK5C	80-21	80-20	80-64	80-11	80-12	80-17	79-59	80-55
SiO2	53 49	54 67	54.23	53.43	52 59	51.90	53 41	53 82	54 78	53 57	53 14
TiO2	0.23	0.07	0.07	0 35	0 41	0.30	0 18	0 23	0.28	0 21	0 10
Al2O3	2.98	1 13	1.12	3 59	5 74	3 78	3 19	3.00	3 55	1 93	1 14
Cr2O3	0.79	0 19	0.29	0 46	0 75	0 64	0 43	0 38	0 48	0 38	0 14
FeO	1.52	1 78	1.62	2 43	2.25	2 21	2.20	2 00	2.12	1 98	1.97
MgO	16.34	18 04	18 14	16 27	14.84	16 23	16 32	16 41	16 26	17 12	17 70
MnO	0.06	0 05	0.07	0 08	0 07	0 07	0 07	0.07	0 08	0 09	0 11
CaO	22 89	24 16	24.05	22 50	21.53	23.22	22 73	23 28	23.32	23 76	24 79
NaO	1.18	0 18	0 19	1.07	1 46	0.90	0.83	0 83	0.96	0 27	0 15
Total	99 48	100 27	99.78	100.18	99 64	99 25	99.36	100 02	101 83	99 31	99.24
Si	1.947	1.974	1.969	1 933	1 907	1.904	1.946	1.949	1.947	1 956	1.951
Ti	0.006	0 002	0.002	0 010	0.011	0 008	0 005	0.006	0 007	0 006	0 003
Al	0 128	0.048	0.048	0 153	0.245	0 163	0.137	0 128	0 149	0 083	0 049
Cr	0 023	0.006	0.008	0.013	0 022	0.019	0.012	0 019	0 014	0 011	0 004
Fe	0.046	0.054	0.049	0.074	0 068	0.068	0 067	0.060	0 063	0 060	0 061
Mg	0.886	0.971	0 981	0 877	0.802	0.887	0.886	0.886	0 862	0 933	0.968
Mn	0.002	0.002	0.002	0.002	0 002	0 002	0 002	0 002	0 002	0 003	0 003
Ca	0.891	0.935	0.935	0.875	0 837	0 913	0.887	0.903	0 888	0 930	0 975
Na	0 083	0 013	0.013	0 075	0 103	0 640	0 059	0.059	0 066	0.019	0.010
Total	4 012	4.005	4 007	4.012	3 997	4.604	4 001	4.012	3.998	4 001	4 024
Mg#	95 1	94.7	95.2	92 2	92 2	92 9	93 0	93 7	93 2	94 0	94 1
Ca	48 9	47 7	47.6	47 9	49 0	48 9	48 2	48 8	49 0	48 4	48 7
Mg	48 6	49.5	49 9	48 0	47.0	47 5	48 2	47.9	47 5	48 5	48 3
Fe	2.5	2 8	2 5	4.1	4 0	3 6	3 6	3.2	3.5	3 1	3 0

Spinel (1)

Location	Massif Central		Languedoc				SanCarlos	Hawaii		Hoggar	Tariat	Ichinomegata	
Number	Li-9	Cp-15	H204B	80-437	80-442	76-250	PA-120G	SL011	SL138	V	MO423016	LHZ-13	LHZ-53
Al2O3	58 60	56 50	59 27	59 18	57 10	59 70	34 40	45 90	53.50	31 16	60 09	44 94	50 15
Cr2O3	8 60	9 83	7.63	8.07	9.60	8 09	32 30	20 35	13 19	33 45	7 67	18 59	15 92
Fe2O3	2 47	2 59	3 11	1.86	3 58	1 29	5 10	-	-	2 62	1 21	-	-
MgO	20.80	19 60	21.08	20.07	20.40	20 73	12.50	17.54	19 67	13 93	20 57	16 23	18 50
FeO	9 11	10 30	8 74	10 04	9 86	9 16	16 50	14 96	12 55	15 76	10 07	18 67	14 19
Total	99 58	98 82	99 83	99 22	100 54	98 97	100.80	98 75	98 91	96 92	99 61	98 43	98 76
Al	1 777	1 744	1.791	1 805	1 737	1 814	1 181	1 504	1.681	1 116	1 816	1 496	1 604
Cr	0 175	0 203	0.155	0 165	0 196	0 165	0 744	0 447	0.278	0 803	0 156	0 415	0 342
Fe3+	0.048	0 051	0 060	0 036	0 070	0 025	0 112	-	-	0 060	0 024	0 107	0 062
Mg	0.797	0 765	0 805	0 774	0 784	0 796	0 543	0 726	0.781	0.631	0 787	0 684	0 748
Fe2+	0 196	0 226	0 187	0 217	0 213	0 197	0 402	0.348	0 280	0 400	0 216	0 334	0.260
Total	2 993	2 989	2 997	2.997	2 999	2 998	2 982	3 025	3 020	3 010	2 999	3 036	3 016

Spinel (2)

Location	Ichinome	L.Bullenmerri											
Number	LHZ-29	BM-9	BM-15	BM-18	BM-27	BM-51	BM-58	BM-62	BM-74	BM-109	BM-116	BM-134	BM-137
Al2O3	50 85	16 75	58 04	11.83	58 57	13 89	51 94	47.95	47 68	36 44	43 71	33 04	59 55
Cr2O3	15 92	52.57	10 44	58 14	10 16	56 07	15 96	20 74	19 71	31.01	24 29	35 24	8 47
Fe2O3	-	-	-	-	-	-	-	-	-	-	-	-	-
MgO	19 40	13 14	20 24	11 26	20 14	11 24	19 77	18 12	18 82	15 56	18 93	15 55	20 67
FeO	13 70	16 88	11 28	18 66	10 11	18.80	11 47	12.26	12.61	16 23	12 16	15 42	10 64
Total	99 87	99 34	100.00	99 89	98 98	100 00	99 14	99 07	98 82	99.24	99 09	99 25	99 33
Al	1 603	0 625	1 770	0 456	1 769	0 530	1 611	1.531	1.525	1.235	1 417	1 137	1 803
Cr	0.337	1 316	0 214	1 502	0 206	1 435	0 333	0 444	0 423	0 706	0 528	0 814	0 172
Fe3+	0 069	-	-	-	-	-	-	-	-	-	-	-	-
Mg	0 774	0 620	0 780	0 547	0 770	0 543	0 776	0 732	0 761	0.667	0 777	0 675	0 792
Fe2+	0 235	0 447	0 244	0.510	0 217	0 509	0 252	0 278	0.286	0 391	0 280	0 377	0 229
Total	3 018	3 008	3 008	3 015	2 962	3 017	2 972	2 985	2 995	2 999	3 002	3 003	2 996

Spinel (3)

Location	Lake Bullenmerri									L Bullenmerri		Mt Leura	
Number	BM-139	BM-143	BM-147	BM-154	BM-161	BM-163	BM-166	BM-167	BM-654	BM-189	Bm-18	LE-2641	LE-2642
Al2O3	53 64	51 22	27.13	28 22	51 83	14 66	52 81	55 49	31.14	55.20	18 53	-	58 42
Cr2O3	15 02	16 48	41.74	37.55	15 80	56 07	15 42	11 54	36 71	14 55	44 27	-	11 44
Fe2O3	-	-	-	-	-	-	-	-	-	-	-	-	-
MgO	19.40	19 71	13 63	14.55	19 71	12 46	20 23	20 32	13 99	18 87	24 75	-	20 28
FeO	11.84	11.60	17.38	18.12	11 37	16 64	10 54	11 22	18 45	11 92	10 37	-	9 80
Total	99 90	99 01	99 88	98.44	98 71	99 83	99 00	98 57	100 29	100 54	97 92	-	99 94
Al	1 668	1 600	0.965	0.999	1 622	0 552	1 642	1 707	1 089	1.702	0 668	1 623	1 774
Cr	0.314	0.345	0 996	0 892	0 332	1 416	0 322	0 238	0 861	0.301	1 070	0 345	0 233
Fe3+	-	-	-	-	-	-	-	-	-	-	-	-	-
Mg	0 763	0 779	0.613	0 652	0 780	0 593	0 796	0 790	0.618	0 735	1 128	0 806	0 778
Fe2+	0 261	0 257	0 439	0 455	0.253	0 444	0 233	0.245	0 458	0.261	0 265	0 213	0 211
Total	3 006	2 981	3 013	2 998	2.987	3 005	2 993	2 980	3 025	2 999	3 131	2 987	2 997

Spinel (4)

Location	L.Gnotuk								Fen				
Number	GN-15	Gn-2	GN-3	Gn-16	Gn-20A	Gn-20B	Gn-24	Gn-26	1	2	4	9	10
Al2O3	27.42	17 31	29 57	46.81	23 82	60.32	42.92	44 05	54 22	55.62	57 29	56 85	51 93
Cr2O3	42.00	48.71	37.34	20 67	44 76	8 52	23 38	19 07	11 50	8 94	8 07	8 80	14 58
Fe2O3	-	-	-	-	-	-	-	-	-	-	-	-	-
MgO	11.96	22 03	17.79	14.33	18 38	10 68	18.04	18 88	11 40	12 83	11 81	12 96	12 99
FeO	18 44	9 83	13 82	17.23	12 90	20 81	15.88	16.75	20 50	19 69	21 10	19 54	19 08
Total	99 82	97.88	98.52	99.04	99 86	100.33	100.22	98 75	97 62	97.08	98 27	98 15	98 58
Al	0 983	0 631	1.036	1.543	0.842	1 895	1 408	1 456	1 780	1.815	1.849	1.828	1 695
Cr	1 010	1 190	0 877	0 457	1 061	0 180	0 514	0 423	0 253	0 196	0 175	0 190	0 319
Fe3+	-	-	-	-	-	-	-	-	-	-	-	-	-
Mg	0.542	1 015	0.788	0.597	0 821	0 424	0 748	0 789	0 473	0 529	0 482	0 527	0 536
Fe2+	0 469	0.254	0 343	0 403	0.324	0 464	0 369	0 393	0 477	0 456	0 483	0 446	0 442
Total	3.004	3.090	3 044	3 000	3 048	2.963	3.039	3 061	2.984	2.995	2 988	2 991	2 993

Spinel (5)

Location	Jagersfontein		Finero		A Aramı	Green Knob	Balmuccia		Ronda				
Number	557	576	F2D	197	F-16c	N53	B-3C	F-58	R501	R740	R696	R123	R243
Al2O3	17 85	51 82	20.66	19 71	58 86	56 90	58 46	60 94	45 30	50.20	54 50	58 40	58 70
Cr2O3	51 21	16 87	45.74	44 64	9.50	11 90	10 52	9 15	24.20	18 40	14 10	9 80	9 70
Fe2O3	3.22	5.72	-	-	-	-	-	-	-	-	-	-	-
MgO	13.57	22.34	9 65	11.48	18 51	19 10	18.35	18 52	13 10	11 80	12 00	12 10	11.00
FeO	13.81	5.72	23.61	22 91	12 01	12 20	13 58	12 76	17 70	19 30	19 40	19 60	20 30
Total	99.66	102 47	99 66	98 74	98 88	100 10	100.91	101.37	100 30	99 70	100 00	99 90	99 70
Al	0.659	1.565	0 777	0 749	1 796	1.749	1.782	1 824	1 454	1.578	1 684	1 779	1 783
Cr	1.268	0.342	1 154	1.138	0.194	0 245	0 215	0.184	0 521	0.388	0 291	0 200	0 196
Fe3+	0 076	0 110	-	-	-	-	-	-	0.024	0 035	0 024	0 019	0 019
Mg	0 633	0 853	0 459	0 552	0.714	0 742	0.708	0.701	0 720	0.768	0 756	0 754	0 779
Fe2+	0.362	0 123	0 630	0 618	0 260	0 266	0 294	0 271	0 275	0.229	0 240	0 243	0 219
Total	2.998	2.992	3.020	3 056	2 964	3 003	2 999	2 980	2 994	2 996	2.995	2 994	2 995

Spinel (6)

Location	Ronda	Zabargad				East Timor			Oregon	Miyamori			Nonsberg
Number	7319	Z-37	Z-42a	Z-35	Z-206a	7	11	12	VH9	CSZ12	77073113	77111919	MK5D
Al2O3	43.10	56.98	58 00	56 98	58 00	57 70	57 80	59 80	59.00	53 80	50 68	46 83	48 61
Cr2O3	25 30	9 17	10.30	9.17	10 30	10 90	11 50	8.54	8 70	13 30	16 49	19 01	20 10
Fe2O3	-	-	-	-	-	-	-	-	1.16	2 09	1 66	3 66	-
MgO	13.10	12.92	13.20	12 92	13 20	12 00	11 20	11 40	9 50	10 20	17 46	16 47	17.65
FeO	18.30	19.85	19.40	19 85	19 40	19 30	19 50	20 30	20 40	19 50	12 76	13 78	12 39
Total	99 80	98.92	100.90	98.92	100 90	99 90	100 00	100 04	98 76	98.89	99 05	99 75	98 75
Al	1 394	1.747	1 755	1 747	1 755	1 770	1 770	1 810	1.826	1 674	1 618	1 517	1 559
Cr	0.549	0 189	0 209	0 189	0.209	0.230	0 240	0 170	0 177	0 276	0 353	0 413	0 433
Fe3+	0 055	-	-	-	-	-	-	-	0.022	0.041	0 034	0 076	0 006
Mg	0 746	0 770	0 742	0 770	0.742	0 260	0 240	0 250	0 785	0.767	0 704	0 675	0 716
Fe2+	0.245	0.281	0 283	0 281	0.283	0 750	0.750	0 780	0 204	0 224	0 289	0.317	0 275
Total	2.989	2.987	2 989	2 987	2.989	3.010	3 000	3.010	3 014	2 982	2 998	2 997	2.989

Spinel (7)

Location	Nonsberg peridotite						Malaita						
Number	MO11	MK5C	MK1	ULT12	ULT4	300B	PHN4022	PHN4028	PHN4073	PHN4074	PHN4085	CRN205	CRN216
Al2O3	26 71	37 19	32 88	34 69	38 05	40 12	57 70	55 00	34.70	10 40	36 70	57 20	28 00
Cr2O3	39 64	31 15	35 46	33.51	29 73	29 26	9 87	11.30	29 30	35 00	29 60	9 30	35 70
Fe2O3	-	-	-	-	-	-	1 95	3.79	6.09	18 50	4 62	2 39	5 73
MgO	10.26	14 12	12.75	12 15	13 15	13 83	19.50	19 60	14 70	7.72	15 70	20 10	14.20
FeO	21 42	16 40	17.42	18 33	18 02	16 78	10 40	9 62	14 90	24 70	13 70	10 20	15 10
Total	98 03	98 86	98 51	98 68	98 95	99 99	99 42	99 31	99.69	96 32	100 32	99 19	98 73
Al	0 979	1.269	1.154	1.214	1 303	1.348	1 763	1 701	1 198	0.411	1 210	1 761	0 999
Cr	0 974	0 714	0 835	0.786	0 683	0 660	0 203	0.234	0.680	0.932	0 673	0 192	0 856
Fe3+	0 041	0.014	0.008	-	0 014	-	0.039	0.072	0 121	0 474	0 104	0 045	0 129
Mg	0 475	0 610	0.566	0 538	0 570	0 588	0 756	0 768	0 623	0.388	0 673	0.784	0 640
Fe2+	0.515	0 384	0 426	0 455	0 424	0 400	0 226	0.210	0 355	0.699	0 333	0 204	0 350
Total	2.984	2 990	2 989	2 993	2 993	2 995	2 986	2 985	2 976	2.903	2 993	2 986	2 974

Spinel (8)

Location	Malaita					Tinaquillo					
Number	PHN4002	PHN4009	PHN4013	PHN4069	CRN209	80-21	80-20	80-64	80-11	80-17	79-59
Al2O3	45 20	44 50	37.90	37.80	25 50	56 26	57 03	58 21	53 60	56 20	45 91
Cr2O3	21.30	21 10	24 80	24.80	38.40	12.33	11 65	13 07	15.10	13 55	21 89
Fe2O3	2 39	3 79	7 70	7.24	4 82	0 45	0 86	0 71	0 91	0 12	1.71
MgO	17.30	17.70	16 80	16 30	17 00	18 71	19.30	19.00	18 65	19 31	16 13
FeO	2 39	3 79	11.80	12 90	11 70	12 38	11.78	12 25	12.06	11.56	14 80
Total	88.58	90.88	99.00	99.04	97 42	100 13	100 62	103 24	100 32	100 74	100 44
Al	1.469	1.451	1.270	1.287	0 907	1 736	1 744	1.740	1.667	1 721	1 488
Cr	0.465	0 462	0.558	0 566	0 911	0.255	0 239	0.262	0.315	0.278	0 476
Fe3+	0 059	0 081	0 165	0.139	0 148	0 009	0 017	0.014	0 018	0 002	0.035
Mg	0 712	0 729	0 711	0 701	0 762	0 730	0 746	0 718	0 733	0 747	0 661
Fe2+	0.283	0 263	0.281	0 291	0 228	0.271	0 255	0 260	0.266	0.251	0.340
Total	2.987	2 985	2.984	2.982	2 955	3 000	3 000	2 992	3.000	2.999	3 000

Garnet (1)

Location	Jagersfontein			A Arami	Lein		Ronda				W Gneiss	
Number	311	557	567	F-16a	1K	1J	R501	R740	R696	R123	5421C	USC8A
SiO2	41.97	40 19	42 13	41 45	41 00	41 00	42 37	42 42	42 64	41 79	41 20	41 20
TiO2	0.03	0 03	0 01	0 11	0 09	0 09	0 17	0 17	0 15	0 30	0 25	0 13
Al2O3	22.16	23 87	21.85	22 86	21 90	22 60	22 46	22 58	22 83	22 90	21 90	21 30
Cr2O3	2 80	2 55	1 96	2 16	2.20	0 61	1.38	1 10	0 71	0 53	2 02	2 37
FeO	9 10	8 19	9 46	8 28	11 10	13 90	8 50	8 01	9 23	9 22	8 84	9 62
MgO	18 94	20 00	21 09	19 87	18 60	17 60	20 56	20 27	20.06	19 82	20 50	19 70
MnO	0 56	0 47	0 66	0 40	0 40	0 37	0 41	0 35	0.37	0 32	0 48	0 55
CaO	4 86	4 95	3 16	4 97	5 02	4 66	5 04	5 01	4 74	4 65	4 23	4 28
Total	100 42	100 25	100 32	100 10	100 31	100 83	100 89	99 91	100 73	99 53	99 42	99 15
Si	2 998	2 870	3 000	2 956	2 960	2 964	2 994	3.014	3 015	2 991	2 964	2 987
Ti	0 002	0 002	0 001	0 006	0 005	0 005	0 009	0 009	0 008	0 016	0 014	0 007
Al	1 866	2.010	1.834	1 922	1 864	1 926	1.870	1 891	1 902	1 932	1 858	1 820
Cr	0 158	0.144	0 110	0 122	0 126	0 035	0 077	0 062	0 040	0 030	0 115	0 136
Fe	0.544	0 489	0 563	0 494	0 670	0 840	0 502	0 476	0 546	0.552	0 532	0 583
Mg	2 016	2 129	2 238	2 112	2 002	1 896	2 165	2 147	2 114	2 115	2 198	2 128
Mn	0 034	0 028	0 040	0 024	0 024	0 023	0 025	0 021	0 022	0 019	0 029	0 034
Ca	0 372	0.379	0 241	0 380	0 388	0 361	0 382	0 381	0 359	0 357	0 326	0 332
Total	7 989	8 051	8 027	8 016	8 040	8 050	8 024	8 001	8.006	8 012	8 036	8 028
Mg#	78.8	81 3	79 9	81 0	74 9	69 3	81 2	81 9	79 5	79 3	80 5	78 5
Ca	12 7	12 6	7 9	12 7	12 7	11 7	12 5	12 7	11 9	11 8	10 7	10 9
Mg	68 8	71 0	73 6	70 7	65 4	61 2	71 0	71 5	70.0	69 9	71 9	69 9
Fe	18 5	16 3	18 5	16 5	21 9	27 1	16 5	15 8	18 1	18 3	17 4	19 2

Garnet (2)

Location	Nonsberg peridotite					Malaita					
Number	MK5D	MO11	MK5C	MK1	ULT12	3550B	PHN4002	PHN4009	PHN4013	PHN4069	CRN209
SiO2	42 19	42 44	41 91	42.31	42 24	42 77	41.80	41 90	41 70	41 70	41 70
TiO2	0 04	0 03	0 02	-	0 06	0 07	0 09	0 07	0 08	0 08	0 56
Al2O3	22 57	22 99	22 28	22 35	22 33	23 43	22 90	23 00	22 60	22 30	20 10
Cr2O3	1.02	0 64	1 36	1 44	1 42	1.39	1 01	0 61	1 32	1 32	4 90
FeO	9 90	10 34	10 20	9 79	10 05	8 00	9 36	9 12	8 97	8 99	6 23
MgO	19 16	18 89	18 23	18 81	18 65	20 67	19 20	19 60	18 60	18 80	20 90
MnO	0 47	0 63	0 62	0 57	0 49	0 41	0 41	0 53	0 47	0 49	0 24
CaO	4.97	5 35	5 84	5 64	5 48	5 36	5 02	4 84	6 00	5 89	5 54
Total	100 32	101 31	100 46	100 91	100 72	102 10	99 79	99 67	99 74	99 57	100 17
Si	3 012	3 007	3 005	3 011	3 015	2 979	2 985	2.991	2 989	3 004	2 976
Ti	0.002	0 001	0 001	-	0 003	0 004	0 005	0 004	0 005	0 005	0 030
Al	1 899	1 920	1 883	1 875	1 878	1 924	1 929	1 935	1 913	1.884	1 690
Cr	0 058	0 036	0 077	0 081	0 080	0 077	0 057	0.034	0 076	0 075	0 277
Fe	0.591	0 613	0.612	0 583	0 600	0 466	0 560	0.547	0 538	0 539	0 372
Mg	2 038	1 995	1.949	1 996	1.984	2 145	2 050	2 094	1.992	2 010	2 223
Mn	0 028	0 038	0 038	0 034	0 030	0 024	0 025	0 032	0 029	0.030	0 014
Ca	0 380	0 406	0 449	0 430	0 419	0 400	0.390	0.371	0 461	0.453	0 424
Total	8 008	8 016	8 014	8 010	8 009	8 018	8 001	8 008	8 003	8 000	8 006
Mg#	77 5	76 5	76 1	77 4	76 8	82 2	78 5	79 3	78 7	78 9	85 7
Ca	12.6	13 5	14 9	14 3	14 0	13 3	13 0	12 3	15 4	15 1	14 0
Mg	67.7	66 2	64 8	66 3	66 1	71 2	68 3	69 5	66 6	67 0	73 6
Fe	19.6	20 3	20 3	19 4	20 0	15 5	18 7	18 2	18 0	18 0	12 3

Mica (1)

Location	Massif Central			Nunivak				Tariat		Bullenmerri		Gnotuk
Number	LI-35	B128	B101	10016	10006	10013	10051	MO423016	MO104	BM-143	WGBM16	GN-26
SiO2	38 80	37 96	39.36	39 91	38 31	38 53	38 43	39 13	39.20	37 98	37.30	36 38
TiO2	0 86	0 39	3 13	0 20	0 14	0 43	2 73	4 71	4 49	6 04	4 96	3 83
Al2O3	16 20	16 72	16.24	17 75	16 72	17 62	16 25	15 74	17.00	17 13	17 04	16 40
Cr2O3	0 67	-	-	2 17	2 48	1 93	-	0 42	0 84	1 27	1 17	1 16
FeO	5 20	4.30	5 43	3 43	3 75	4 13	4 17	4 08	3.80	4 27	4 44	5 97
MgO	23 10	21 60	20.96	23.76	23.53	22 78	21 31	21.55	21.26	20 35	20 20	20 28
MnO	-	0 05	0.05	0 05	0 05	0 05	0 03	-	-	-	-	0 05
CaO	0.02	0 03	0 13	-	-	-	0 01	-	-	-	-	-
Na2O	1.60	1 02	0.98	1 47	0 82	0 92	1.21	0 71	0.67	0 79	0.87	1 01
K2O	7 87	9 04	8 15	7 30	9 19	8 60	9 02	8 37	8.74	9 17	8 38	8 44
Total	94 32	91 11	94 43	96 04	94 99	94 99	93 16	94 71	96.00	97 00	94 36	93 52
Si	5 551	5.612	5.607	5 540	5 464	5 470	5.558	6 004	5.942	5 551	5 787	5.765
Ti	0 093	0 044	-0.336	0 021	0.015	0 046	0 297	0 544	0 512	0 664	0.579	0 456
Al	2.733	2 914	2 727	2 904	2 811	2 948	2 771	2 847	3 038	2 951	3 117	3 064
Cr	0.076	-	-	0 238	0 280	0.217	-	0 051	0 101	0 146	0 144	0 145
Fe	0 622	0 532	0.647	0 398	0 447	0 490	0 504	0.524	0 482	0 522	0.576	0 791
Mg	4 934	4 759	4.450	4 916	5 003	4 820	4 594	4 928	4 803	4 435	4.671	4 790
Mn	-	0.006	0 006	0 006	0 006	0 006	0 004	-	-	-	-	0.007
Ca	0 003	0 005	0.020	-	-	-	0 002	-	-	-	-	-
Na	0 444	0.292	0 271	0.396	0 227	0.253	0 339	0.211	0 197	0 223	0 262	0 310
K	1 436	1.705	1 481	1 293	1.672	1 557	1 664	1 639	1.690	1 709	1 659	1 706
Total	15 892	15.869	15.545	15.712	15 925	15 807	15 733	16 747	16.765	16.201	16 794	17 035
Mg#	88 8	89 9	87.3	92 5	91 8	90 8	90 1	90 4	90 9	89 5	89 0	85 8

Mica (2)

Location	Jagersfontain				Nyanzian	Finero		Zabargad	
Number	311	576	571	585	Y1B1	F69	F2D	Z-42a	Z-35
SiO2	40.38	39 97	41.30	38 71	40 18	39 36	38 92	37 50	38 60
TiO2	3 37	0 19	0 15	0 37	0 81	1 79	0 71	3 51	3 89
Al2O3	14 78	15 14	13 87	14 45	14 93	14 53	16 02	17 40	15 80
Cr2O3	1.87	0 92	1 08	0 82	1 64	1.28	1.32	0 92	0.34
FeO	4,26	3 06	3 36	3 11	2.73	2 48	2 45	3 82	4.51
MgO	21.63	25 40	25 62	25 28	25 20	24 54	24 64	23 14	22 00
MnO	0.04	0.03	0 02	-	0 01	0 04	0 02	-	0.09
CaO	0 02	-	0.01	0 01	0 02	-	0 03	0 01	0.14
Na2O	0.31	1.02	1 82	0 96	1 55	0 90	0 81	1.34	0 91
K2O	9.07	7.61	6 80	7.21	8 03	9 11	8.91	7.85	8 78
Total	95 73	93 34	94.03	90 92	95 10	94 03	93.83	95 49	95.06
Si	5.949	5 955	6.099	5.923	6 108	6.109	6.032	5.707	5.956
Ti	0.373	0 021	0.017	0 043	0 093	0 209	0 083	0 402	0 451
Al	2.567	2.659	2.415	2 607	2 676	2 659	2 927	3.122	2.874
Cr	0.218	0 108	0.126	0.099	0 197	0 157	0 162	0 111	0 041
Fe	0 525	0 381	0 415	0 398	0.347	0.322	0 318	0 486	0.582
Mg	4 749	5 640	5 638	5.765	5.709	5 677	5 691	5.248	5 059
Mn	0.005	0 004	0.003	-	0 001	0.005	0 003	-	0 012
Ca	0.003	-	0 002	0 002	0 003	-	0 005	0 002	0.023
Na	0 089	0 295	0 521	0 285	0 457	0 271	0 243	0 395	0.272
K	1.705	1 447	1.281	1 407	1 557	1 804	1 762	1 524	1 728
Total	16.182	16 510	16.516	16 528	17 149	17 213	17.224	16 997	16.999
Mg#	90 0	93 7	93.1	93 5	94 3	94 6	94 7	91 5	89 7

Bulk Rock composition (1)

Location	San Carlos	Hoggar			Ataq	Tariat	L Bullenmerri					
Number	PA-120G	TAH4	TAH88	TAH276	AT-15	MO423016	MO104	BM-18	BM-47	BM-51	BM-134	BM-135
SiO2	43 65	44 20	46 45	44.18	42.84	44 08	44 08	42 30	44 40	42 36	43 15	42 13
TiO2	0 26	0.10	0 15	0 11	0 00	0 23	0 11	0 10	0 07	0 07	0 04	0 11
Al2O3	0 83	3 33	3.12	3 42	1.34	4 50	3 00	1 04	2 45	1 71	1 25	1 04
Cr2O3	0 41	-	-	-	0 11	0.39	0 31	0 39	0 44	0 51	0 35	0 34
Fe2O3	2.34	-	-	9 41	0 78	0 49	0.38	8 32	10.30	8 00	8 80	9 85
FeO	10 30	8.72	7 92	-	7.70	7.69	7.38	-	-	-	-	-
MnO	0.13	0 14	0 13	0 14	0 21	0 13	0 13	0 15	0 18	0.14	0 15	0 15
NiO	-	-	-	-	0 00	0 23	0 28	0 28	0 24	0 26	0 32	0 27
MgO	40 00	39 60	37.90	39 44	44 20	36 98	41 18	44 00	38 40	41 80	44 40	42 60
CaO	1 19	2 85	3 05	2 95	1.38	3 87	2 23	2 50	2 88	3.96	1 22	2 98
Na2O	0.14	0.23	0.30	0 18	0 40	0 23	0 15	0.51	0.55	0 82	0 32	0 46
K2O	0 06	0.04	0.01	0.01	0 02	0 05	0 01	0 07	0 14	0 11	0 03	0 06
Total	99 31	99.21	99 03	99 84	98 98	98 87	99 24	99.66	100 05	99 74	100 03	99 99

Bulk Rock composition (2)

Location	Finero			L.Bullenmerri								
Number	F2A	F2D	106	BM-139	BM-143	BM-154	BM-163	BM-167	BM-654	WGBM16	WGBM1	WGBM11
SiO2	41 31	43.00	48 06	44 51	45 67	43 34	43.39	44 30	44 02	44 97	44 11	42 54
TiO2	0 01	0.08	0.02	0 17	0 45	0 14	0 02	0 11	0 10	0 10	0.08	0 02
Al2O3	0 25	1.04	1 21	3 59	4 30	1 54	0 68	2.75	2.23	2 30	4 23	1 00
Cr2O3	0.09	0 39	-	0 41	0 67	0 40	0 38	0.37	0 34	0 29	0 43	0 32
Fe2O3	9 26	8 41	6 15	8 26	7.02	10 40	7 27	8.58	-	-	-	-
FeO	-	-	0.89	-	-	-	-	-	9 65	7 85	8 72	7 55
MnO	0.13	0.12	0.14	0 14	0 12	0.15	0.13	0 14	0.15	0 15	0 23	0 14
NiO	0.35	0 30	-	0 23	0 22	0 29	0 31	0 27	0 19	0 20	0 19	0 21
MgO	48 30	44.80	40.30	38 40	36.10	41 70	46 90	40 70	39 20	41 11	36 36	43 06
CaO	0 13	0 89	1.33	3 49	4 74	1 60	0 63	2 64	2 95	2 42	2 93	2 75
Na2O	-	0.38	0 09	0 72	0 64	0 30	0 24	0.19	0 50	0 13	0 10	0 25
K2O	0.01	0.47	0.06	0 17	0 08	0 04	0 02	0 00	0 11	0 00	0 02	0 03
Total	99 84	99 88	98.25	100 09	100 01	99 90	99 97	100 05	99 44	99 52	97 40	97 87

Bulk Rock composition (3)

Location	Leura	Fen		Rhode Is	A.Arami			Balmuccia		Zabargad		
Number	LE-2642	2	9	LN-4	F-16a	F-16c	F-52c	B-3C	F-58	Z-37	Z-35	Z-206a
SiO2	45.19	44 64	43.07	42 15	43.03	44 59	46.76	46 41	46.61	44 40	43 36	42 11
TiO2	0 06	0 10	0 13	0 07	0 15	0 21	0.21	0.13	0 13	0.20	0 15	0 02
Al2O3	2.98	3 47	2 96	1 87	1.41	1.94	1 70	1 40	1 44	4 01	3 57	1 98
Cr2O3	0 43	0 35	0 31		0 41	0 42	0.32	0.33	0 36	-	-	-
Fe2O3	1 50	2.62	2 74	1 40	8 30	8.37	8 15	8.50	8 15	1.92	2 14	1 65
FeO	6.30	5 56	5 88	6 60	-	-	-	-	-	6 75	7 30	7 50
MnO	0 13	0 12	0 12	0 11	0 12	0 12	0.12	0 13	0 12	0 14	0 16	0 14
NiO	0 27	-	-	-	0 26	0 24	0 23	0.24	0 23	-	-	-
MgO	40 60	36 60	37 70	40 30	41 10	38 50	38.60	40 30	39 50	38 20	39 10	41 00
CaO	2.50	2 38	3 09	2 75	1.61	2 69	2 81	2 70	2 48	3 29	2 76	3 45
Na2O	0 19	0 35	0.39	0.16	0 42	0 68	-	-	-	0 34	0 45	0 46
K2O	0 00	0 12	0 09	0 13	0 09	0 13	0 01	-	-	0 03	0 10	0 08
Total	100 15	97 31	96 48	95 54	96 90	97 89	98.91	100 14	99 02	99.28	99 09	98.39

Bulk Rock composition (4)

Location	Timor	Nonsberg peridotite								Nyanzian	Tinaquillo	
Number	7	12	MK5D	MO11	MK5C	MK1	ULT12	ULT4	300B	Y1B1	80-21	80-20
SiO2	44 49	45 63	41.34	42.67	42 02	43 57	45 06	42 52	45.44	41 48	45 77	44 59
TiO2	0.09	0 15	0.05	0 09	0.03	0 10	0 08	0.03	0 06	0 05	0 13	0 09
Al2O3	3.05	4 47	2.79	4 21	2 05	3 70	3 05	2 00	2 50	0 80	4 02	2 97
Cr2O3	0.47	0.51	0 44	0 33	0 41	0 31	0 36	0.39	0 30	-	0 41	0 4
Fe2O3	0.70	0 77	0.00	1.70	-	1 49	0 11	1.16	1.21	1 74	-	-
FeO	7.98	7 05	8.81	6 40	8 70	6 96	7.91	7 54	6 53	5 56	8 1	8 09
MnO	0 15	0 14	0 13	0 16	0 13	0 16	0 14	0.13	0 16	0 12	0 14	0 13
NiO	0.25	0 25	0 28	0 28	0 29	0 28	0 28	0 29	0 27	-	0 22	0 27
MgO	39 94	36.93	43 55	38 42	42 94	39 73	39 47	43 82	39 52	44 24	35 57	40 01
CaO	2.55	4 18	2.50	3 58	2 14	3 09	3 02	1 80	2.78	0 49	4 37	2 6
Na2O	0.18	0 35	0.18	0 27	0 15	0.27	0 26	0.17	0.20	0 26	0 29	0 2
K2O	0.01	0.00	0 02	0 10	0 04	0 05	0 05	0 09	0 08	0 14	-	-
Total	99.86	100.43	100 09	98.21	98 90	99 71	99 79	99.94	99 05	94 88	99 02	99 35

Bulk Rock composition (5)

Location	Tinaquillo						
Number	80-64	80-11	80-17	80-12	79-59	80-55	80-56
SiO2	42 03	43 04	42 81	43 44	42 4	44 44	44.53
TiO2	0.06	0.06	0 06	0 05	0 03	0.2	0 14
Al2O3	2 75	2 55	2 14	2 2	1 57	3.55	2.91
Cr2O3	0 44	0 5	0 4	0 42	0 45	0.38	0 42
Fe2O3	-	-	-	-	-	-	-
FeO	8.08	7 8	7.7	7.81	8 26	8 14	8 42
MnO	0.13	0 13	0 13	0 13	0 13	0 13	0.13
NiO	0 26	0 27	0 28	0.27	0 29	0 25	0 25
MgO	42 12	41 59	41 86	42 63	44 61	39 14	40 13
CaO	2.58	2 28	1 83	1 99	1 57	3 07	2 35
Na2O	0 15	0 12	0 15	0 09	0 05	0 45	0 29
K2O	-	0 01	0.01	0 01	-	0 05	0 03
Total	98 6	98 35	97.37	99 04	99 36	99 8	99 6

APPENDIX B

MINERAL ANALYSES FROM TINAQUILLO (WATER SATURATED AND WATER UNDERSATURATED) EXPERIMENTS

Olivine analyses	150
Orthopyroxene analyses	151
Clinopyroxene analyses	152
Amphibole analyses	153
Garnet analyses	153

Additional experimental analyses from Pyrolite + H_2O (Green, 1973, analysed as part of this project) and North Hessian Depression composition (Mengel and Green, 1989)

Additional amphibole analyses	154
Additional pyroxene analyses	155
Additional garnet analyses	156

Olivine (1), Tinaquillo -40% ol

	Water-undersaturated										
Pressure	10	15	15	20	20	20	25	25	25	28	28
Temperature	970	1000	1025	1000	1025	1100	1000	1025	1100	1050	1100
SiO2	39 79	40 98	40 42	40 65	40 81	40 84	40 73	41 00	40 85	40 90	40 67
FeO	11.03	10 41	10 64	10 73	10 11	9 94	10 39	9 87	10 29	10 07	10 29
NiO	0 55	0 61	0 59	0 75	0 60	0 44	0 61	0 62	0 60	0 67	0 66
MgO	46 98	47 99	48 34	47 87	48 49	48 79	48 27	48 51	48 27	48 36	48 37
Total	100 00	100 00	100 00	100 00	100 00	100 00	100 00	100 00	100 00	100 00	100 00
Si	0 9824	1 0076	0 9964	1 0023	1 0025	1 0017	1 0020	1 0058	1 0041	1 0048	1 0005
Fe	0 2276	0 2139	0 2194	0 2213	0 2077	0 2039	0 2139	0 2025	0 2115	0 2067	0 2116
NiO	0 0108	0 0122	0 0119	0 0149	0 0117	0 0086	0 0119	0 0122	0 0118	0 0127	0 0136
Mg	1 7286	1 7587	1 7760	1.7591	1 7755	1 7840	1.7702	1 7736	1 7685	1 7705	1 7739
Total	2 9948	2 9924	3 0036	2.9976	2 9975	2 9983	2 9980	2 9941	2 9959	2 9952	2 9995
Mg# Ol	88 4	89 2	89 0	88 8	89 5	89 7	89 2	89 8	89 3	89 5	89 3

Olivine (2), Tinaquillo -40% ol

	Water-saturated										
Pressure	10	15	15	15	20	25	25	28	28	28	28
Temperature	1000	900	950	1000	950	950	1000	1000	950	1000	1050
SiO2	40 83	41 19	40 63	40 54	41 21	40 98	40 73	40 79	40 67	40.44	41 62
FeO	10 09	10 61	10 63	10 56	10 44	9 85	10 04	10 42	9 88	10 17	10 17
NiO	0 71	0 53	0 49	0 49	0 68	0 62	0 69	0 74	0 71	0 71	0 89
MgO	48 37	47 55	47 89	48 41	47 34	48 25	48 19	47 77	48 74	48 50	47 14
CaO	-	0 12	0 36	-	0 33	0 30	0 35	0 28	-	0 18	0 18
Total	100 00	100 00	100 00	100 00	100 00	100 00	100 00	100 00	100 00	100 00	100 00
Si	1 0033	1 0128	1 0013	0 9982	1 0138	1 0062	1 0019	1 0047	0 9991	0 9958	1 0125
Fe	0 2072	0 2181	0 2191	0 2175	0 2148	0 2022	0 2066	0 2146	0 2029	0 2095	0 2071
Ni	0 0141	0.0105	0.0097	0 0097	0 0135	0 0123	0 0136	0 0147	0 0140	0 0140	0 0174
Mg	1 7721	1 7427	1 7591	1 7764	1 7353	1 7651	1 7668	1 7539	1 7849	1 7800	1 7457
Ca	-	0 0032	0 0095	-	0 0087	0 0079	0 0092	0 0074	-	0 0047	0 0048
Total	2 9967	2 9873	2 9987	3 0018	2 9861	2 9937	2 9981	2 9953	3 0009	3 0040	2 9875
Mg#	89 5	88 9	88 9	89 1	89 0	89 7	89 5	89 1	89 8	89 5	89 4

Orthopyroxene (1), Tinaquillo -40% ol

	Water-undersaturated											
Pressure	10	15	15	20	20	20	25	25	25	25	28	28
Temperature	970	1000	1025	1000	1025	1100	1000	1025	1050	1100	1050	1100
SiO2	54 74	55 11	54.27	55 44	55 05	54 93	56 54	54 99	55 71	54 27	56 58	55 58
Al2O3	4 73	4 64	3 63	3 81	4 58	4 74	2 51	4 83	3 98	5 80	2 70	3 13
Cr2O3	0.51	0 31	0 45	0 37	0 61	0 51	0 54	0 65	0 60	0 67	0 62	0 68
FeO	7 03	6 79	6 90	6 76	6 51	6 47	6 53	6 51	6 85	6 52	6 31	6 50
MgO	32 16	32 46	33 87	32 90	32 50	32 38	33 29	32 21	32 15	31 81	33 09	33 27
CaO	0 82	0 70	0.87	0 71	0 74	0 97	0 60	0 81	0 71	0 94	0 72	0 85
Total	100 00	100 00	100 00	100 00	100 00	100 00	100 00	100 00	100 00	100 00	100 00	100 00
Si	1 8969	1 9048	1.8856	1 9169	1 9026	1 8989	1 9510	1.9004	1 9257	1 8772	1 9508	1 9227
Al	0 1933	0 1887	0 1488	0 1555	0 1864	0 1933	0.1021	0 1969	0 1621	0 2364	0 1097	0 1278
Cr	0 0139	0 0084	0 0123	0 0103	0 0169	0 0139	0 0146	0 0176	0 0165	0 0183	0 0168	0 0185
Fe	0 2038	0 1962	0 2006	0 1956	0 1880	0 1872	0 1885	0 1881	0 1980	0 1885	0 1818	0 1878
Mg	1 6611	1 6724	1 7542	1 6957	1 6744	1 6684	1 7121	1 6592	1 6563	1 6404	1 7002	1 7158
Ca	0 0306	0 0260	0 0323	0 0263	0 0275	0 0358	0 0222	0.0300	0 0264	0 0347	0 0266	0 0315
Total	3 9995	3 9966	4 0339	4 0002	3 9958	3 9975	3 9906	3 9923	3 9850	3 9955	3 9859	4 0041
Mg#	89 1	89 5	89 7	89 7	89 9	89 9	90 1	89 8	89 3	89 7	90 3	90 1
Ca	1.6	1 4	1 6	1 4	1 5	1 9	1.2	1 6	1 4	1 9	1 4	1 6
Mg	87 6	88 3	88 3	88 4	88 6	88 2	89 0	88 4	88 1	88 0	89 1	88 7
Fe	10 8	10 4	10 1	10 2	9 9	9 9	9 8	10 0	10 5	10 1	9 5	9 7

Orthopyroxene (2), Tinaquillo -40% ol

	Water-saturated										
Pressure	10	15	15	15	20	25	25	28	30	30	30
Temperature	1000	900	950	1000	950	950	1000	1000	950	1000	1050
SiO2	54 72	53 01	53 84	55 23	54 80	56 71	55 78	54 98	56 82	56 17	55 53
Al2O3	4 65	7 51	5 36	4 49	4 00	2 11	2 74	1 99	1.78	1 73	2 28
Cr2O3	0 46	0 50	0 47	0 72	0 59	0 50	0 59	0 29	0 40	0 35	0 53
FeO	7 22	6 82	6 84	6 55	7 07	6 14	6 40	6 78	6 38	6 48	6 57
MgO	32 19	31 57	32 77	32 13	32 88	33 95	33 84	35 44	34 08	34 74	34 29
CaO	0 75	0 59	0 72	0 88	0 66	0 59	0 65	0 52	0 54	0 53	0 80
Total	100 00	100 00	100 00	100 00	100 00	100 00	100 00	100 00	100 00	100 00	100 00
Si	1 8974	1 8355	1 8666	1 9090	1 9007	1 9543	1 9280	1 9082	1 9597	1 9413	1 9237
Al	0 1903	0 3065	0 2190	0 1832	0 1635	0 0857	0 1114	0 0814	0 0724	0 0707	0 0932
Cr	0 0126	0 0137	0 0129	0 0198	0 0162	0 0136	0 0161	0 0080	0 0109	0 0096	0 0145
Fe	0.2094	0 1976	0 1983	0 1895	0 2050	0 1769	0 1850	0 1968	0 1841	0 1873	0 1904
Mg	1 6635	1 6292	1 6934	1 6556	1 6995	1 7438	1 7434	1 8334	1 7517	1 7900	1 7709
Ca	0 0279	0 0219	0 0271	0 0326	0 0246	0 0218	0 0241	0 0193	0 0200	0 0197	0 0297
Total	4 0011	4 0044	4 0173	3.9897	4 0095	3 9961	4 0080	4 0471	3 9988	4.0186	4 0224
Mg#	88 8	89 2	89 5	89 7	89 2	90 8	90 4	90 3	90 5	90 5	90 3
Ca	1 5	1 2	1 4	1 7	1 3	1.1	1 2	0 9	1 0	1 0	1 5
Mg	87 5	88 1	88 3	88 2	88 1	89 8	89 3	89 5	89 6	89 6	88 9
Fe	11 0	10 7	10 3	10 1	10 6	9 1	9 5	9 6	9 4	9 4	9 6

Clinopyroxene (1), Tinaquillo-40% ol

	Water-undersaturated											
Pressure	10	15	15	20	20	20	25	25	25	25	28	28
Temp	970	1000	1025	1000	1025	1100	1000	1025	1050	1100	1050	1100
SiO2	53 01	52 85	51 78	52 09	53 39	53.28	52 52	53 22	53 59	52 88	52 13	53 67
TiO2	0 00	0 23	0 31	0.21	-	0.21	0 32	0 24	0 18	-	0 25	-
Al2O3	3 69	3 60	4 51	4 89	3 52	3 51	4 26	3 22	3 04	4 53	4 60	2 64
Cr2O3	0 41	0 42	0 85	0 78	1.00	1 00	0 77	1 30	0 89	1 35	0 88	1 02
FeO	2 92	3 14	3 21	3 16	2 92	2 91	3 36	3 09	2 91	3 31	3 40	3 03
MgO	17 17	17 07	17 17	16 93	17 28	17 24	16 66	17 82	17 35	16 87	17 29	17 86
CaO	22 80	22 70	22 17	21 60	21 61	21 57	21 72	20 52	21 57	20 08	20 96	21 18
Na2O	-	-	-	0 34	0 28	0 28	0 37	0 58	0 47	0 98	0 49	0 40
Sum	100 00	100 00	100 00	100 00	100 00	100 00	100 00	100 00	100 00	100 00	100 00	100 00
Si	1 9218	1 9185	1 8825	1 8895	1 9320	1 8828	1 9069	1 9266	1 9401	1 9147	1 8916	1 9489
Ti	0 0000	0 0062	0 0085	0 0057	-	0 0054	0 0087	0 0066	0 0050	-	0 0069	-
Al	0 1579	0 1540	0 1931	0 2090	0 1502	0 2377	0 1826	0 1375	0 1296	0 1930	0 1965	0 1124
Cr	0 0119	0 0120	0 0244	0 0223	0 0286	0 0247	0 0221	0 0372	0 0256	0 0387	0 0252	0 0292
Fe	0 0884	0 0951	0 0977	0 0957	0 0883	0 1020	0 1021	0 0936	0 0881	0 1002	0 1033	0 0918
Mg	0 9276	0 9236	0 9304	0 9152	0 9318	0 9059	0 9017	0 9616	0 9359	0 9098	0 9353	0 9630
Ca	0 8858	0 8830	0 8636	0 8394	0.8379	0 8061	0 8451	0 7960	0 8365	0 7787	0 8147	0 8211
Na	-	-	-	0 0246	0 0197	0 0322	0 0259	0 0404	0 0329	0 0690	0 0346	0 0278
Sum	3 9933	3 9924	4 0003	4 0014	3 9885	3 9967	3 9951	3 9996	3 9937	4 0040	4 0080	3 9941
Mg#	91 3	90 7	90 5	90 5	91 3	89 9	89 8	91 1	91 4	90 1	90 1	91 3
Ca	46 6	46 4	45 7	45 4	45 1	44 4	45 7	43 0	45 0	43 5	44 0	43 8
Mg	48 8	48 6	49 2	49 5	50 2	49 9	48 8	51 9	50 3	50 9	50 5	51 3
Fe	4 6	5 0	5 2	5 2	4 8	5 6	5 5	5 1	4 7	5 6	5 6	4 9

Clinopyroxene (1), Tinaquillo-40% ol

	Water-saturated										
Pressure	10	15	15	15	20	25	25	28	30	30	30
Temp	1000	900	950	1000	950	950	1000	1000	950	1000	1050
SiO2	53 36	52 00	52 54	52 43	52 52	52 98	53 33	53 86	54 25	53 72	53 96
Al2O3	2 49	3 99	4 32	4 66	4 20	3 97	3 24	2 94	3 02	3 45	2 21
TiO2	0 20	-	-	-	0 29	0 22	0 21	-	-	-	-
Cr2O3	1 05	0 67	0 61	0 96	0 63	0 97	0 99	0 86	0 99	1 12	0 79
FeO	3 10	3 02	3 11	3 45	3 63	3 12	3 21	3 04	3 28	2 94	3 20
MgO	17 83	18 03	17 85	17.37	17 54	17 90	17 97	17 73	16 88	17 64	18 24
CaO	22 01	22 27	21 27	21 09	20 81	20 13	20 36	20 77	20 28	20 10	21 14
Na2O	-	-	0 30	-	0 38	0 71	0 69	0 80	1 30	1 03	0 46
Sum	100 00	100 00	100 00	100 00	100 00	100.00	100 00	100 00	100 00	100 00	100 00
Si	1 9353	1 8898	1 9022	1 8996	1 9041	1 9151	1 9296	1 9473	1 9619	1 9397	1.9534
Al	0 1066	0 1707	0 1843	0 1991	0 1794	0 1690	0 1383	0 1254	0 1288	0 1469	0 0946
Ti	0 0055	-	-	-	0.0079	0 0060	0 0057	-	-	-	-
Cr	0 0301	0 0193	0 0175	0 0275	0.0181	0 0277	0 0283	0 0246	0 0283	0 0320	0 0227
Fe	0 0941	0 0919	0 0942	0 1046	0 1100	0 0942	0 0972	0 0920	0 0993	0 0888	0 0969
Mg	0 9639	0 9765	0 9632	0 9378	0 9479	0 9641	0 9691	0 9558	0 9098	0 9494	0 9842
Ca	0 8553	0 8669	0 8251	0 8186	0 8083	0 7797	0 7891	0 8045	0 7858	0 7780	0 8200
Na	-	-	0 0211	-	0 0268	0 0497	0 0483	0 0561	0 0912	0 0721	0 0324
Sum	3 9908	4 0151	4 0076	3 9872	4 0025	4 0055	4 0056	4 0057	4 0051	4 0069	4 0042
Mg#	91.1	91 4	91.1	89 9	89 6	91 1	90 9	91 2	90 2	91 4	91 0
Ca	44 7	44 8	43 8	44 0	43 3	42 4	42 5	43 4	43 8	42 8	43 1
Mg	50 4	50 4	51 2	50 4	50 8	52 5	52 2	51.6	50 7	52 3	51 8
Fe	4 9	4 7	5 0	5 6	5 9	5 1	5 2	5 0	5 5	4 9	5 1

Amphiboles, Tinaquillo-40%ol,

	Water-saturated			Water-undersaturated					
Pressure	15	20	25	10	15	20		25	
Temp	925	950	950	970	1000	1000	1025	1000	1025
SiO2	49 42	46 54	47 90	45 44	51 35	44 05	43 74	44 77	48 75
TiO2	0 39	0 45	0 62	0 63	0 45	0 68	1 31	0 76	0 61
Al2O3	9 18	11.63	9 74	13 29	15 13	14 69	14 69	12 44	8.65
Cr2O3	0 62	1 09	1 48	1 31	0 45	1 22	0 25	1 27	0 41
FeO	5 39	4 39	4 88	4 02	6 26	3 70	7 06	3 87	4 95
MgO	24 90	21 21	22 05	19 64	17 19	19 03	19 04	20 85	17 10
CaO	7 46	10 38	9 01	11 42	6 58	11 17	9 54	10 58	16 51
K2O	-	0 25	0 70	0 32	0 24	0 56	0 59	0 51	0 17
Na2O	0 65	2 06	1 63	1 93	0 34	2 90	1 80	2 95	0 85
Total	98 00	98 00	98 00	98 00	98 00	98 00	98 00	98 00	98 00
Si	6 8213	6 5206	6 7053	6 3801	6 9854	6 2102	6 1969	6 3170	6 9022
Ti	0 0411	0 0475	0 0650	0 0657	0 0469	0 0715	0 1395	0 8000	0 0655
Al	1 4925	1 9201	1 6064	2 1995	2 4271	2 4408	2 4529	2 0688	1 4432
Cr	0 0676	0 1205	0 1637	0 1450	0 0492	0 1365	0 0278	0 1408	0 0454
Fe	0 6224	0 5142	0 5711	0 4720	0 7121	0 4363	0 8363	0 4574	0 5864
Mg	5 1231	4 4289	4 6007	4 1095	3 4850	4 0001	4 0210	4 3852	3 6081
Ca	1 1030	1 5587	1 3502	1 7187	0 9588	1 6867	1 4483	1 6000	2 5049
K	-	0 0053	0 0150	0 0565	0 0417	0 1011	0 1066	0 0913	0 0300
Na	0 1728	0 5588	0 4413	0 5261	0 0885	0 7939	0 4941	0 8064	0 2346
Total	15 4438	15 6746	15 5187	15 6731	14 7946	15 8770	15 7234	15 9468	15 4202
Mg#	89 2	89 6	89 0	89 7	83 0	90 2	82 8	90 6	86 0
Ca	16 1	24 0	20 7	27 3	18 6	27 5	23.0	24 8	37 4
Mg	74 8	68 1	70 5	65 2	67 6	65 3	63 8	68 1	53 9
Fe	9 1	7 9	8 8	7 5	13.8	7 1	13 3	7 1	8 8

Garnets Tinaquillo-40% ol

	Water-saturated							Water-undersaturated							
Pressure	20	25	25	28	30	30	30	20	20	25	25	25	25	28	28
Temp	950	950	1000	1000	950	1000	1050	1000	1100	1000	1025	1050	1100	1050	1100
SiO2	42 70	42 74	42 59	42 90	43 83	42 04	42 68	41 47	41 61	41 50	41 66	41 65	41 83	41 99	41 72
Al2O3	20 73	19 04	19 35	19 45	17 96	20 11	20 33	22 51	22 42	19 65	21.74	22 33	22 03	21 02	21 58
TiO2	0 17	0 34	0 21	0 28	0 26	0 34	0 25	0 24	0 16	0 20	0 38	0 40	0 24	0 17	0 19
Cr2O3	1 35	1 32	2 22	2 00	2 12	1 72	1 68	1 72	1 78	2 50	1 66	1 25	1 80	2 75	2 80
FeO	8 41	8 23	8 31	7 99	8 37	8 34	8 34	8 33	7 55	8 69	8.19	8 66	7 84	8 10	7 72
MgO	19 43	20 69	20 47	20 38	19 75	20 92	19 46	18 33	20 27	20 85	18 72	18 50	19 89	19 17	19 13
CaO	6 81	7 33	6 53	6 74	7 44	6 19	6 99	6 96	5 83	6 34	7 30	6 90	6 09	6 40	6 61
MnO	0 40	0 31	0 31	0 26	0 27	0 34	0 27	0 44	0 38	0 28	0 35	0 31	0 30	0 39	0 25
Total	100 00	100 00	100 00	100 00	100 00	100 00	100 00	100.00	100 00	100 00	100.00	100 00	100 00	100 00	100 00
Si	3 0578	3.0701	3 0334	3 0747	3 1501	3 0163	3 0593	2 9754	2 9667	2 9929	2 9903	2 9866	2 9869	3 0133	2 9901
Al	1 7504	1 6119	1 6921	1 6420	1 5214	1 7007	1 7182	1 9035	1 8839	1 6707	1 8391	1 8876	1 8537	1 7784	1 8225
Ti	0 0092	0 0184	0 0113	0 0151	0 0140	0 0183	0 0135	0 0131	0 0087	0 0107	0 0206	0 0216	0 0126	0 0096	0 0100
Cr	0 0766	0 0750	0 1247	0 1134	0 1207	0 0973	0 0953	0 0976	0 1005	0 1423	0 0942	0 0710	0 1017	0 1562	0 1583
Fe	0 5040	0 4944	0 4948	0 4785	0 5029	0 5004	0 5004	0 5001	0 4498	0 5242	0 4917	0 5195	0 4677	0 4861	0 4630
Mg	2 0746	2 2152	2 1730	2 1760	2 1164	2 2372	2 0800	1 9602	2 1539	2 2422	2 0034	1 9770	2 1167	2 0503	2 0426
Ca	0 5227	0 5641	0 4987	0 5170	0 5729	0 4755	0 5373	0 5344	0 4455	0 4894	0 5620	0 5304	0 4655	0 4920	0 5078
Mn	0 0243	0 0189	0 0188	0 0158	0 0164	0 0206	0 0164	0 0265	0 0232	0 0173	0 0211	0.0186	0 0180	0 0238	0 0151
Total	8 0196	8 0680	8 0468	8 0325	8 0148	8 0663	8 0204	8 0108	8 0322	8 0897	8 0223	8 0124	8 0227	8 0096	8 0094
Mg#	80 5	81 8	81 5	32 0	80 8	81 7	80 6	79 7	82.7	81 1	80 3	79 2	81 9	80 8	81 5
Ca	16 9	17 2	15 7	16 3	17 9	14 8	17 2	17 8	14 6	15 0	18 4	17 5	15 3	16 2	16 9
Fe	16 2	15.1	15 6	15 1	15 8	15 6	16 1	65 5	70 6	68 9	65 5	65 3	69 4	67 7	67 8
Mg	66 9	67 7	68 6	68 6	66 3	69 6	66 7	16 7	14 8	16 1	16 1	17 2	15 3	16 1	15 4

Additional Experimental Amphiboles (1)

	Pyrolite, water-saturated							Pyrolite + 0 2% H2O			
Pressure	10	15	15	15	15	15	20	27	15	19	19
Temperature	970	900	930	950	970	1000	950	970	1000	1000	1100
SiO2	44 00	46 67	46 37	45 73	46 05	44 40	44 30	45 86	44 96	44 11	44 07
TiO2	2 10	1 07	1 24	1 44	1 48	1 63	1 10	0 69	1 88	1 87	2 51
Al2O3	12 00	12 12	11 48	12 02	11 79	12 83	13 60	12 05	12 67	13 26	13 43
Cr2O3	2 60	0 96	1 25	1 26	1 02	1 84	1 10	0 98	1 29	1 30	1 42
FeO	5 60	5 40	5 25	5 18	5 39	5 86	5 50	4 21	5 34	4 94	4 85
MgO	18 10	19 15	19 19	18 31	18 45	19 07	19 10	20 68	18 07	18 97	18 58
CaO	11 30	10 45	10 78	11 40	11 26	9 81	10 40	9 31	11 08	10 21	9 74
Na2O	1 80	1 75	1 91	2 10	2 07	2 09	0 50	0 69	2 13	2 71	2 66
K2O	0 50	0 44	0 53	0 58	0 50	0 47	2 40	3 53	0 58	0 62	0 73
Sum	98 00	98 00	98 00	98 00	98 00	98 00	98 00	98 00	98 00	98 00	98 00
Si	6 275	6 556	6 538	6 469	6 507	6 293	6.272	6 455	6 369	6 247	6 235
Ti	0 225	0 112	0 131	0 154	0 158	0 174	0 117	0 073	0 200	0 199	0 267
Al	2 017	2 007	1.909	2 004	1 964	2 143	2 269	2 000	2 115	2 214	2 240
Cr	0 293	0 107	0 139	0 140	0 114	0.206	0 123	0 109	0 145	0 145	0 160
Fe	0 668	0 634	0 619	0 612	0 636	0 694	0 651	0 496	0 633	0 585	0 574
Mg	3 847	4 009	4 033	3 861	3 885	4 028	4 031	4 338	3 814	4 005	3 919
Ca	1 727	1 573	1 629	1 727	1 704	1 489	1 578	1 404	1 681	1 549	1 476
Na	0 498	0 476	0 523	0 574	0 565	0.575	0 659	0 963	0 586	0 745	0 729
K	0 091	0 078	0 095	0 104	0 089	0 086	0 090	0 123	0 104	0 111	0 131
Sum	15 641	15 551	15 616	15 644	15 623	15 688	15 790	15 961	15 646	15 802	15 729
Mg#	85 2	86 3	86 7	86 3	85 9	85 3	86 1	89 7	85 8	87 3	87 2
Ca	27 7	25 3	25 9	27 9	27 4	24 0	25 2	22 5	27 4	25 2	24 7
Mg	61 6	64 5	64 2	62 3	62 4	64 8	64 4	69 5	62 2	65 2	65 7
Fe	10 7	10 2	9 9	9 9	10 2	11 2	10 4	8 0	10 3	9 5	9 6

Additional Experimental Amphiboles (2)

	Pyrolite + 0 2 H2O							N H D (H2O sat)			
Pressure	20	21	22	22	23	25	28	25	25	25	28
Temperature	1100	1100	1000	1100	1000	1100	1100	975	1000	1150	1050
SiO2	43 99	44 73	44 22	43 23	44 56	43 82	45 68	44 38	45 14	43 81	45 01
TiO2	2 35	1 69	1 57	2 69	1 41	2 56	1 78	0 80	0 94	1 19	0 94
Al2O3	12 98	12 55	13 23	13 82	12 75	13 41	11 36	13 86	11 74	14 76	12 48
Cr2O3	1 50	1 60	1 68	1 57	1 32	1 57	1 07	1 03	1 74	1 69	1 22
FeO	4 69	4 76	4 61	5 15	4 39	4 84	4 64	3 65	3 64	3 80	3 87
MgO	18 39	18 37	18 38	17 50	19 34	18 47	19 27	19 41	20 25	18 57	19 58
CaO	10 15	10 83	10 55	10 33	9 96	9 04	9 95	11 59	11 02	11 26	10 85
Na2O	3 17	2 80	2 98	2 66	3 51	3 16	3 09	1 82	2 09	1 73	2 42
K2O	0 79	0 68	0 78	1 06	0 76	1 15	1 17	1 45	1 43	1 20	1 64
Sum	98 00	98 00	98 00	98 00	98 00	98 00	98 00	98 00	98 00	98 00	98 00
Si	6 245	6 343	6 273	6 157	6 310	6 217	6 470	6 306	6 425	6 216	6 417
Ti	0 251	0 180	0 167	0 287	0 150	0 273	0 189	0 086	0 100	0 127	0 101
Al	2 172	2 098	2 212	2 320	2 128	2 242	1 897	2 321	1 971	2 468	2 097
Cr	0 168	0 179	0 188	0 177	0 148	0 176	0 120	0 116	0 196	0 189	0 137
Fe	0 557	0 565	0 546	0 613	0 520	0 574	0 550	0 433	0 434	0 451	0 463
Mg	3 891	3 882	3 888	3 714	4 082	3 906	4 068	4 111	4 296	3 927	4 160
Ca	1 544	1 646	1 605	1 576	1 511	1 373	1 509	1 765	1 681	1 712	1 657
Na	0 871	0 771	0 820	0 735	0 966	0 869	0 851	0 502	0 577	0 477	0 669
K	0 143	0 122	0 142	0 193	0 137	0 208	0 211	0 263	0 259	0 216	0.298
Sum	15 841	15 785	15 841	15 771	15 953	15 839	15 864	15 904	15 939	15 783	15 998
Mg#	87 5	87 3	87 7	85 8	88 7	87 2	88 1	90 5	90 8	89 7	90 0
Ca	25 8	27 0	26 6	26 7	24 7	23 5	24 6	28 0	26 2	28 1	26 4
Mg	64 9	63 7	64 4	62 9	66 8	66 7	66 4	65 2	67 0	64 5	66 2
Fe	9 3	9 3	9 0	10 4	8 5	9 8	9 0	6 9	6 8	7 4	7 4

Additional Experimental Orthopyroxenes

	Pyrolite, watersaturated						Pyrolite, water-undersaturated									
P, kb	15	15	15	15	15	20	15	19	19	20	21	21	22	22	23	24
Temp	900	930	950	970	1000	950	1000	1000	1100	1100	1000	1100	1000	1100	1000	1000
SiO2	54 14	54 19	54 48	54 25	54 41	53 20	54 34	54 91	55 71	54 53	54 77	54 66	55 16	54 76	54 45	53 32
TiO2	0 26	0 22	0 26	0 37	0 60	0 40	0 36	0 45	-	0 54	0 43	0 23	-	0 46	0 25	-
Al2O3	3 83	3.51	3.73	3 90	3 68	5 40	3 48	3 37	4 24	4 37	3 81	3 88	2 91	4 07	2 12	2 41
Cr2O3	0 86	0 61	0 66	0 77	0 62	0 70	0 85	0 51	-	0 71	0 58	0 52	0 31	0 59	0 39	0 35
FeO	9 50	9 68	9.54	9 45	9 08	8 80	9 50	8 48	7 53	8 19	7 97	8 04	8 46	8 01	8 75	8 94
MgO	30 50	30 89	30 54	30 08	30 36	30 50	30 16	31 43	31 45	30 88	31 37	31 68	31 37	30 98	33 33	34 34
CaO	0 78	0 68	0 78	1.05	1 10	0 80	1 31	0 86	1.07	1 07	1 06	0 98	1 26	1 14	0 71	0 66
Sum	100 00	99 99	99 99	100 00	100 00	99 80	100 00	100 01	100 00	100 29	99 99	99 99	99 47	100 01	100 00	100 02
Si	1 902	1 905	1 911	1 905	1 908	1 866	1 910	1 916	1 930	1 897	1 909	1 905	1 934	1 908	1 908	1 875
Ti	0 007	0 006	0 007	0 010	0 016	0 011	0 010	0 012	-	0 014	0 011	0 006	-	0 012	0 007	-
Al	0 158	0 146	0 154	0 162	0 152	0 223	0 144	0 139	0 173	0 179	0 157	0 160	0 121	0 167	0 088	0 100
Cr	0 024	0 017	0 018	0 022	0 017	0 019	0 024	0 014	-	0 020	0 016	0 014	0 010	0 016	0.011	0 010
Fe	0 279	0 285	0 280	0 278	0 266	0 258	0 279	0 248	0.218	0 238	0 232	0 234	0 248	0 234	0 256	0 263
Mg	1 597	1 618	1 596	1 574	1 587	1 594	1 580	1 635	1 624	1 601	1 630	1 646	1 640	1 609	1 741	1 799
Ca	0 030	0 026	0 030	0 040	0 041	0 030	0 049	0 032	0 040	0 040	0 040	0 037	0 047	0 043	0 027	0 025
Sum	4 000	4 008	3 996	3 994	3 992	4 002	3 996	3 996	3 984	3 990	3 994	4 002	4 000	3 989	4 036	4 071
Mg#	85 1	85 0	85 1	85 0	85 6	86 1	85 0	86 8	88 2	87 1	87 5	87 5	86 9	87 3	87 2	87 3
Ca	1 5	1 3	1 5	2 1	2 2	1 6	2 6	1 7	2 1	2 1	2 1	1 9	2 4	2 3	1 3	1 2
Mg	83 8	83 9	83 8	83 2	83 8	84 7	82 8	85 4	86 3	85 2	85 7	85 9	84 7	85 4	86 0	86 2
Fe	14 6	14 8	14 7	14 7	14 1	13 7	14 6	12 9	11 6	12 7	12 2	12 2	12 8	12 4	12 7	12 6

Additional Experimental Clinopyroxenes

	Pyrolite, watersaturated						Pyrolite + 0 2% H2O							N H D (H2O-sat)			
P, kb	15	15	15	15	15	20	15	19	21	22	24	25	28	25	25	25	28
Temp	900	930	950	970	1000	950	1000	1000	1000	1100	1000	1100	1100	975	1000	1150	1050
SiO2	54 20	53 60	52 98	52 08	53 70	51 30	52 54	52 17	51 70	51 10	53 46	52 29	51 46	51 67	52 76	51 67	52 42
TiO2	0 37	0 69	0 48	0 71	0 67	0 30	0 75	0 90	1 25	1 29	0 46	1 16	1 10	0 44	0 36	0 33	0 37
Al2O3	2 28	3 31	3 24	4 02	3 48	4 60	3 77	4 24	5 54	6 98	2 88	5 35	5 72	4 51	3 98	4 75	3 96
Cr2O3	0 53	0 09	0 94	0 82	0 49	1 00	0 85	0 89	1 15	1 34	1 00	1 27	1 23	0 43	1 12	0 97	1 69
FeO	3 46	4 62	4 30	4 40	4 49	3 80	4 57	4 10	4 42	4 19	4 12	4 10	5 13	3 46	2 88	2 79	3 24
MgO	19 38	16 45	17 35	17 19	16 92	17 00	17 51	18 03	17 39	17 36	18 24	16 97	17 92	17 19	17 35	17 41	16 96
CaO	19 59	20 29	20 39	20 52	19 96	21 20	19 83	19 03	17 44	16 38	19 19	17 14	15 87	21 85	20 77	21 43	20 99
Na2O	0 18	0 26	0 33	0 26	0 20	0 70	0 18	0 63	1 11	1 35	0 65	1 71	1 43	0 45	0 78	0 46	0 96
Sum	100 01	99 91	99 91	100 00	99 91	99 90	100 00	99 99	100 00	100 00	100 00	99 99	99 86	100 00	100 00	99 81	100 61
Si	1 952	1 945	1 926	1 896	1 944	1 874	1 908	1 891	1 871	1 844	1 935	1 890	1 865	1 881	1 910	1 878	1 896
Ti	0 010	0 019	0 013	0 020	0 018	0 008	0 021	0 025	0 034	0 035	0 013	0 032	0 030	0 012	0 010	0 009	0 010
Al	0 097	0 142	0 139	0 172	0 149	0 198	0 161	0 181	0 236	0 297	0 123	0 228	0 245	0 194	0 170	0 204	0 170
Cr	0 015	0 020	0 024	0 024	0 014	0 029	0 024	0 026	0 033	0 038	0 029	0 036	0 035	0 012	0 032	0 028	0 048
Fe	0 105	0 140	0 131	0 134	0 136	0 116	0 139	0 124	0 134	0 127	0 125	0 124	0 156	0 105	0 087	0 085	0 098
Mg	1 041	0 890	0 940	0 932	0 913	0 925	0 948	0 974	0 938	0 934	0 985	0 914	0 968	0 932	0 936	0 943	0 914
Ca	0 756	0 789	0 794	0 800	0 774	0.830	0 772	0 739	0 676	0 633	0 744	0 664	0 616	0 852	0 806	0 835	0 814
Na	0 013	0 019	0 023	0 019	0 014	0 050	0 013	0 044	0 078	0 095	0 046	0 120	0 101	0 032	0 055	0 032	0 067
Sum	3 988	3 962	3 990	3 996	3 962	4 029	3 985	4 004	4 000	4 001	3 999	4 007	4 016	4 020	4 006	4 013	4 018
Mg#	90 9	86 4	87 8	87 4	87 0	88 9	87 2	88 7	87 5	88 1	88 8	88 1	86 2	89 9	91 5	91 7	90 3
Ca	39 8	43 4	42 6	42 9	42 5	44 3	41 5	40 2	38 7	37 4	40 2	39 0	35 4	45 1	44 0	44 8	44 6
Mg	54 7	48 9	50 4	49 9	50 1	49 5	51 0	53 0	53 7	55 1	53 1	53 7	55 6	49 3	51 2	50 6	53 1
Fe	5 5	7 7	7 0	7 2	7 5	6 2	7 5	6 8	7 6	7 5	6 7	7 3	8 9	5 6	4 8	4 6	5 4

Additional Experimental Garnets

	Pyrolite								NHD			
Pressure	21	21	22	22	23	24	25	28	25	25	25	28
Temperature	1000	1100	1000	1100	1000	1000	1100	1100	975	1000	1150	1050
SiO2	41 34	41 42	40 94	42 28	41 71	42 30	41 50	40 73	41 74	41.9	42 25	41 67
TiO2	1 34	0 98	0 70	1 09	0 71	1 38	1 57	1 26	0 46	0 96	0 54	0 64
Al2O3	19 73	20 60	19 98	17 66	20 64	18 91	19 13	19 48	21 15	21 34	20 87	20 31
Cr2O3	1 92	2.12	1.97	2 07	2 05	1 79	2 15	1 94	1 37	2 18	2 53	2 61
FeO	9 48	9 77	10 43	9 05	10 15	9 62	9 45	9 88	8 16	7 73	6 51	7 57
MnO	-	0 25	0 38	0 35	0 34	-	-	0 24	19 60	19 09	19 88	19 81
MgO	19 33	17 96	17 68	19 94	17 84	17 91	19 43	20 24	-	-	-	-
CaO	6 87	6 91	7 15	7.58	6 57	8 09	6 78	6 24	7 32	7 31	7 32	7 40
Sum	100 01	100 01	99 23	100 02	100 01	100 00	100 01	100 01	99 80	100 50	99 90	100 01
Si	2 989	2 998	3 002	3 064	3 019	3 064	3 003	2 955	2.998	2 988	3 015	2 992
Ti	0 073	0 053	0 038	0.059	0 039	0 075	0 085	0 069	0 025	0.051	0 029	0 035
Al	1 681	1 757	1 726	1 508	1 761	1 615	1 631	1 666	1 791	1 794	1 756	1 720
Cr	0 110	0 121	0 114	0 119	0 117	0 103	0.123	0 111	0 078	0 123	0 143	0 148
Fe	0 573	0 591	0 640	0 549	0 614	0 583	0 572	0 599	0 490	0 461	0 389	0 455
Mn	-	0 015	0 024	0 021	0 021	-	-	0 015	-	-	-	-
Mg	2 083	1 938	1 933	2 154	1 925	1 934	2 095	2 189	2 098	2 030	2 115	2 120
Ca	0 533	0 536	0 562	0 589	0 510	0 628	0 525	0 485	0 563	0 558	0 560	0 569
Sum	8.042	8 009	8 039	8 063	8 004	8 002	8.035	8 088	8 043	8 003	8 006	8 039
Mg#	78 4	76 6	75 1	79 7	75 8	76 8	78 6	78 5	81 1	81 5	84 5	82 3
Ca	16 7	17 5	17 9	17 9	16 7	20 0	16 5	14 8	17 9	18 3	18 3	18 1
Mg	65 3	63 2	61 7	65 4	63 1	61 5	65 6	66 9	66 6	66 6	69 0	67 4
Fe	18 0	19 3	20 4	16 7	20 2	18 5	17 9	18 3	15 6	15 1	12 7	14 5

APPENDIX C

MINERAL ANALYSES FROM PYROLITE + 1.4% $MgCO_3$ OR 5.0% $CaMg(CO_3)_2$ + 0.2% H_2O EXPERIMENTS

Olivine analyses	158
Orthopyroxene analyses	159
Clinopyroxene analyses	160
Garnet analyses	162
Amphibole analyses	163
Ilmenite analyses	165
Carbonate analyses	166
Mineral anayses from Brey and Green's (1983, unpublished) experiments on Pyrolite + 0.5% CO_2 + 0.2% H_2O (analysed as part of this project)	167

Olivine (1), Pyrolite + 1 4% $MgCO_3$ or 5 0%$CaMg(CO_3)_2$ +0 2%H_2O

	Subsolidus Carbonate Field								Subsolidus CO2 Field				
Pressure	17	20	22	25	28	31	31	32	15	20	20	20	20
Temperature	900	950	950	925	925	900	925	925	1050	975	1000	1050	1075
SiO_2	41 44	41 13	41 25	40 75	41 14	41 10	41.20	41 6	40 77	41 71	40 69	41 00	40 88
Al_2O_3	-	0 22	-	-	-	-	-	-	-	11 67	-	-	-
FeO	12 89	12 43	10 91	11.88	9 80	9 23	9.33	9 27	11 00	0 43	11 48	10 74	10 89
NiO	0 40	0 39	0 46	-	0 49	0 51	0 43	0.33	0 40	46 01	0 34	0 33	0 41
MgO	45 13	45 83	47 38	47.38	48 57	49 16	49 04	48 8	47 83	0 18	47 49	47 93	47 83
CaO	0 14	-	-	-	-	-	-	-	-	-	-	-	-
Sum	100 00	100 00	100 00	100 00	100.00	100 00	100 00	100	100 00	100 00	100 00	100 00	100 00
Si	1 0271	1 0176	1 0146	1 0059	1 0079	1 0049	1 0070	1 0148	1 0044	1 0281	1 0044	1 0080	1 0064
Al	-	0 0066	-	-	-	-	-	-	-	-	-	-	-
Fe	0 2671	0 2572	0 2244	0 2451	0 2008	0 1887	0 1908	0 1892	0 2267	0 2406	0 2369	0 2208	0 2242
Ni	0 0080	0 0078	0 0091	-	0 0096	0 0100	0 0084	0 0065	0 0079	0 0085	0.0068	0 0066	0 0080
Mg	1 6671	1 6900	1 7373	1 7431	1.7737	1 7915	1 7868	1 7746	1 7566	1.6902	1 7475	1 7565	1 7549
Ca	0 0036	-	-	-	-	-	-	-	-	0 0047	-	-	-
Sum	2 9729	2 9791	2 9854	2 9941	2 9921	2 9951	2 9929	2 9851	2 9956	2 9719	2 9956	2 9919	2 9936
Mg#	86 2	86 8	88 6	87 7	89 8	90 5	90 4	90 4	88 6		88 1	88 8	88 7

Olivine (2), Pyrolite + 1 4 $MgCO_3$ or 5 0%$CaMg(CO_3)_2$ +0 2%H_2O

	Carbonate Melt Field											
Pressure	21	22	22	22	25	25	27	27	27	28	29	29
Temperature	1025	975	1000	1050	950	975	950	1000	1050	1075	950	975
SiO_2	40 92	40 63	40 52	41 16	40 72	41 17	41 01	41 08	40 85	41 09	40 96	40 61
FeO	11 06	11 83	11 36	8 23	10 68	11 23	9 97	10 76	10 70	11 23	10 53	11 36
NiO	0 39	0 37	0 48	0 42	0 47	0 45	0 45	0 53	0 53	0.51	0.32	0 44
MgO	47 63	47 17	47 64	50 20	48 13	47 15	48 57	47 63	47 92	47 17	48 20	47 59
Sum	100 00	100 00	100 00	100.00	100 00	100 00	100 00	100 00	100 00	100 00	100 00	100 00
Si	1 0079	1 0047	1 0009	1 0017	1 0025	1 0143	1 0056	1 0107	1 0055	1.0128	1 0062	1 0027
Fe	0 2276	0 2447	0 2347	0 1676	0 2198	0 2314	0 2045	0 2214	0 2203	0 2315	0 2163	0 2345
Ni	0 0078	0 0074	0 0095	0 0081	0 0092	0 0089	0 0089	0 0106	0 0105	0 0100	0 0062	0 0088
Mg	1 7486	1 7383	1 7541	1 8209	1 7661	1 7311	1.7754	1 7467	1 7583	1 7328	1 7650	1 7512
Sum	2 9921	2 9953	2 9991	2 9983	2 9975	2 9857	2 9944	2 9893	2 9945	2 9872	2 9938	2 9973
Mg#	88 5	87 7	88 2	91 6	88 9	88 2	89 7	88 8	88 9	88 2	89 1	88 2

Olivine (3), Pyrolite + 1 4 $MgCO_3$ or 5 0%$CaMg(CO_3)_2$ +0 2%H_2O

	Silicate Melt Field										
Pressure	29	29	30	30	15	20	25	25	25	28	32
Temperature	1000	1025	950	1000	1075	1100	1100	1150	1200	1150	975
SiO_2	41 35	40 96	41 29	41 49	40 75	40 87	41 01	40 95	41.31	40 96	40 87
Al_2O_3	-	-	0 43	-	-	-	0 33	1 15	0 25	-	-
FeO	9 76	9 88	10 08	11 41	10.96	10 35	10 72	10 51	9 11	9 91	10 44
NiO	0 37	0 51	0 31	0 45	0 46	0 40	0 46	0 38	-	0 50	0 45
MgO	48 52	48 66	47 90	46 64	47 83	48 38	47 49	47 01	49 34	48 63	48 24
Sum	100 00	100 00	100 00	100 00	100 00	100 00	100 00	100 00	100 00	100 00	100
Si	1 0118	1 0045	1 0107	1 0219	1 0041	1.0040	1 0081	1.0044	1 0062	1 0045	1 0046
Al	-	-	0 0123	-	-	-	0 0094	0 0333	0 0071	-	-
Fe	0 1996	0 2026	0 2063	0 2350	0 2260	0 2127	0 2204	0 2155	0 1855	0 2033	0 2146
Ni	0 0072	0 0100	0 0062	0 0089	0 0092	0 0079	0 0090	0 0074	-	0 0098	0 0089
Mg	1 7696	1 7785	1 7477	1 7122	1.7567	1 7714	1 7402	1 7185	1 7914	1 7778	1 7673
Sum	2 9882	2 9955	2 9831	2 9781	2 9959	2 9960	2 9871	2 9790	2 9902	2 9955	2 9954
Mg#	89 9	89 8	89 4	87 9	88 6	89 3	88 8	88 9	90 6	89 7	89 2

Orthopyroxene (1), Pyrolite + 1 4% $MgCO_3$ or 5 0% $CaMg(CO_3)_2$ + 0 2% H_2O

	Subsolidus Field													
Pressure	15	16	17	18	20	20	20	20	20	22	25	28	30	31
Temp	1050	900	900	900	950	975	1000	1050	1075	950	925	925	900	900
SiO_2	54 73	54 83	54 86	56 01	57 28	54 96	54 38	54 25	54 86	54 99	55 61	56 85	55.65	56 50
TiO_2	0 29	0 27	0 29	0 18	-	0 20	0 29	0 34	0 28	0 18	0 17	-	0 34	-
Al_2O_3	2 70	3 57	4 02	2 66	2 21	4 05	4 48	4 48	3.84	4 19	3 12	1 75	2 78	2 35
Cr_2O_3	0.55	0 46	0 50	0 33	-	0 50	0 58	0 75	0 57	0 43	0 46	0 39	0 56	0 30
FeO	7 45	8 08	7 58	7 27	7 61	7 65	7 61	7.33	7 75	6 79	7.06	7 02	7 24	6 43
MgO	33 60	31 29	30 94	32 91	32 22	31 79	32 01	32 13	31 86	32 65	33 02	33 36	32 78	33 92
CaO	0 68	1 50	1 82	0 63	0 68	0 85	0 61	0 73	0 83	0 77	0 57	0 63	0 64	0 50
Sum	100 00	100 00	100 00	100 00	100 00	100 00	100 00	100 00	100 00	100.00	100 00	100 00	100 00	100 00
Si	1.9053	1 9136	1 9110	1 9402	1 9799	1 9098	1 8906	1 8858	1.9083	1 9034	1 9259	1 9658	1 9299	1 9485
Ti	0 0075	0.0070	0 0075	0.0047	-	0 0052	0 0076	0 0088	0 0072	0 0048	0 0043	-	0 0090	-
Al	0 1106	0 1468	0 1651	0 1088	0 0902	0 1659	0 1835	0 1834	0 1576	0 1710	0 1272	0 0711	0 1136	0 0957
Cr	0 0152	0 0127	0 0138	0 0092	-	0 0137	0 0150	0 0205	0 0158	0.0118	0 0125	0 0108	0 0154	0 0082
Fe	0 2168	0 2360	0 2207	0 2105	0 2199	0 2224	0 2213	0 2130	0 2256	0 1965	0 2045	0 2029	0 2101	0 1854
Mg	1.7435	1 6274	1 6062	1 6993	1 6600	1 6465	1 6587	1 6647	1 6522	1 6843	1 7044	1 7192	1 6946	1 7434
Ca	0 0255	0 0561	0 0679	0 0235	0 0250	0 0317	0 0258	0 0273	0 0310	0 0286	0 0211	0 0234	0 0239	0 0185
Sum	4 0243	3 9996	3 9921	3 9961	3 9750	3 9952	4 0025	4 0035	3 9978	4 0004	3 9999	3 9932	3 9966	3 9996
Mg#	88 9	87 3	87.9	89 0	88 3	88 1	88 5	88 7	88 0	89 6	89 3	89 4	89 0	90 4
Ca	1 3	2 9	3 6	1 2	1 3	1 7	1 4	1 4	1 6	1 5	1 1	1 2	1 2	1
Mg	87 8	84 8	84 8	87 9	87 1	86 6	87 0	87 4	86 6	88 2	88 3	88 4	87 9	89 5
Fe	10 9	12 3	11.6	10 9	11 5	11 7	11 6	11 2	11 8	10 3	10 6	10 4	10 9	9 5

Orthopyroxene (2), Pyrolite + 1 4% $MgCO_3$ or 5 0% $CaMg(CO_3)_2$ + 0 2% H_2O

	Subsolidus Field		Carbonate Melt Field										
Pressure	31	32	21	22	22	22	25	25	25	27	27	27	28
Temp	925	925	1025	975	1000	1050	950	975	1000	950	1000	1050	1075
SiO_2	54 90	56 81	54 81	54 95	54 87	54 84	54 50	55 67	54 55	56 10	55 80	55 11	55 57
TiO_2	0 28	-	0 29	0 31	0 27	0 19	0 34	0 24	0 18	0 19	0 19	0 29	0 41
Al_2O_3	2 81	2 20	4 22	3 94	4 12	4 34	4 28	2 86	4 05	2 80	2 81	4 01	3 10
Cr_2O_3	0 49	0 34	0 43	0 45	0 55	0 45	0 88	0 55	0 59	0 37	0 43	0 65	0 47
FeO	7 55	6 76	7.37	7 46	7 23	6 42	7 31	7 34	7 28	6 67	6 97	6 65	7 35
MgO	33 23	33 45	32 08	32 00	32 22	32 89	32 11	32 62	32 72	33 11	33 13	32 55	32 25
CaO	0 75	0 44	0 80	0 89	0 75	0 88	0 58	0.71	0 63	0 72	0 67	0 74	0 85
Sum	100 00	100 00	100 00	100 00	100 00	100 00	100 00	100 00	100 00	100 00	100.00	100 00	100 00
Si	1.9107	1 9602	1 9024	1 9087	1 9035	1 8965	1 8931	1 9314	1 8945	1 9382	1 9321	1 9070	1 9281
Ti	0 0073	-	0 0075	0 0080	0 0069	0 0048	0 0088	0 0063	0 0047	0 0048	0 0051	0 0076	0 0107
Al	0 1151	0 0893	0 1727	0 1612	0 1685	0 1769	0 1754	0 1168	0 1658	0 1164	0 1145	0 1634	0 1269
Cr	0 0135	0 0093	0 0117	0 0124	0 0150	0 0122	0 0242	0 0152	0 0162	0.0100	0 0118	0 0177	0 0130
Fe	0 2196	0 1950	0 2140	0 2168	0 2098	0 1857	0.2123	0 2131	0.2113	0 1926	0 2017	0 1924	0 2133
Mg	1 7236	1 7205	1 6598	1 6564	1 6663	1 6955	1 6629	1 6869	1 6938	1 7053	1 7095	1 6791	1 6678
Ca	0 0278	0 0162	0 0299	0 0331	0 0278	0 0326	0 0216	0 0265	0 0234	0 0265	0 0249	0 0276	0 0315
Sum	4 0177	3 9905	3 9979	3 9965	3 9978	4 0041	3 9983	3 9963	4 0098	3 9938	3 9996	3 9949	3 9913
Mg#	88 7	89 8	88 6	88 4	88 8	90 1	88 7	88 8	88 9	89 9	89 4	89 7	88 7
Ca	1 4	0 8	1 6	1 7	1 5	1 7	1 1	1 4	1 2	1 4	1 3	1 5	1 6
Mg	87 4	89 1	87 2	86 9	87 5	88 6	87 7	87 6	87 8	88 6	88 3	88 4	87 2
Fe	11 1	10 1	11 2	11 4	11 0	9 7	11.2	11 1	11 0	10 0	10 4	10 1	11 2

Orthopyroxene (3), Pyrolite + 1 4% $MgCO_3$ or 5 0% $CaMg(CO_3)_2$ + 0 2% H_2O

	Carbonate Melt Field					Silicate Melt Field							
Pressure	29	29	29	29	30	30	15	20	25	25	25	28	32
Temp	950	975	1000	1025	950	1000	1075	1100	1100	1150	1200	1150	975
SiO_2	56 60	56 23	56 23	56 76	56 58	55 81	56 51	56 01	55 30	55 42	55 10	53 60	57 00
TiO_2	0 16	0 18	0 19	-	0 20	0 20	-	0 18	0 24	0 21	0 25	0 30	-
Al_2O_3	2 24	1 95	2 49	2 28	1.67	2 94	2 37	2 79	2 94	2 92	3 30	4 96	2 11
Cr_2O_3	0 40	0 03	0 39	0 33	0 32	0.50	0 52	0 37	0 58	0 59	0 57	0 97	0 20
FeO	6 84	7 12	6 74	6 76	7 13	7 08	7 12	7 11	7 93	7 89	7 31	7 27	5 81
MgO	33 01	33 40	33 32	33 24	33 49	32 57	32 61	32 82	32 34	32 36	32 66	32 10	34 31
CaO	0 75	0 76	0 65	0 63	0 60	0 90	0 87	0 72	0 66	0 62	0 81	0 79	0 57
Sum	100 00	100 00	100 00	100 00	100.00	100 00	100 00	100 00	100 00	100 00	100 00	100 00	100 00
Si	1 9562	1 9483	1 9435	1 9594	1 9586	1 9341	1 9563	1 9393	1 9247	1 9276	1 9139	1 8658	1 9592
Ti	0 0043	0.0047	0 0050	-	0 0053	0 0053	-	0 0047	0 0064	0 0054	0 0065	0 0079	-
Al	0 0911	0 0797	0 1012	0 0929	0 0683	0 1199	0 0968	0 1138	0 1205	0 1197	0 1349	0 2037	0 0854
Cr	0 0109	0 0098	0 0106	0 0090	0 0089	0 0137	0.0142	0 0101	0 0161	0 0164	0 0156	0 0266	0 0055
Fe	0 1978	0 2062	0 1947	0 1950	0 2063	0 2052	0 2061	0 2059	0 2307	0 2294	0 2124	0 2117	0 1671
Mg	1 7003	1 7250	1 7163	1 7102	1 7277	1 6820	1 6825	1 6936	1.6774	1 6774	1 6909	1 6658	1 7574
Ca	0 0279	0 0284	0 0241	0 0232	0 0224	0 0334	0 0323	0 0267	0 0248	0 0230	0 0302	0 0296	0 0208
Sum	3 9885	4 0022	3 9955	3 9897	3 9975	3 9938	3 9882	3 9941	4.0006	3 9990	4 0044	4 0111	3 9954
Mg#	89 6	89 3	89 8	89 8	89 3	89 1	89 1	89 2	87 9	88 0	88 8	88 7	91 3
Ca	1 4	1 4	1 2	1 2	1 1	1 7	1.7	1 4	1 3	1 2	1 6	1 5	1 1
Mg	88 3	88 0	88 7	88 7	88 3	87 6	87 6	87 9	86 8	86.9	87 5	87 3	90 3
Fe	10 3	10 5	10 1	10 1	10 5	10 7	10 7	10 7	11 9	11.9	11 0	11 1	8 6

Clinopyroxene (1), Pyrolite + 1 4% $MgCO_3$ or 5 0% $CaMg(CO_3)_2$ + 0 2% H_2O

	Subsolidus Field											
Pressure	15	18	20	20	20	20	20	22	25	28	30	31
Temperature	1050	900	950	975	1000	1050	1075	950	925	925	900	900
SiO_2	51 65	52 97	51 31	52.36	51 39	51 52	51 11	52 49	53 13	53 49	52 97	53 51
TiO_2	1 12	0 40	0 63	0 63	0 84	0 79	1 13	0 51	0 53	0 51	0 51	0 35
Al_2O_3	4 28	3 29	3 03	4 20	4 79	4 78	5 66	3 24	3 36	3 34	3 15	3 27
Cr_2O_3	1 33	0 70	0 57	0 95	0 98	0 94	1 25	0 67	0 65	0 74	0 85	0 65
FeO	3 51	3 30	4 76	3 71	3 85	4 53	4 09	3 80	3 42	3 54	3 52	2 91
MgO	16 90	17 33	17 23	16 10	16 64	16 53	15 92	17 81	17 23	16 81	17 21	16 78
CaO	20 74	21 66	21 87	21 40	20 86	20 03	19 91	21 18	21 30	20 59	21 34	21 62
Na_2O	0 47	0 34	0 59	0 64	0 65	0 88	0 93	0 30	0 38	0 98	0 45	0 91
Sum	100 00	100 00	100 00	100 00	100.00	100 00	100 00	100 00	100 00	100 00	100 00	100
Si	1 8790	1 9224	1 8856	1 9053	1 8726	1 8787	1 8610	1 9090	1 9263	1 9387	1 9242	1 9388
Ti	0 0306	0 0110	0 0173	0 0172	0 0229	0 0216	0 0310	0 0139	0 0143	0 0139	0 0140	0 0094
Al	0 1837	0 1409	0 1313	0 1803	0 2057	0 2055	0 2427	0 1388	0 1436	0 1427	0 1347	0 1397
Cr	0 0382	0 0201	0 0166	0 0274	0 0282	0 0271	0 0359	0 0193	0 0187	0 0213	0 0244	0 0187
Fe	0 1067	0 1001	0 1463	0 1129	0 1174	0 1383	0 1244	0.1157	0 1036	0 1072	0 1069	0 0882
Mg	0 9164	0 9376	0 9439	0 8735	0 9036	0 8986	0 8639	0 9654	0 9310	0 9080	0 9319	0 9063
Ca	0 8082	0 8422	0 8611	0 8344	0 8142	0 7826	0 7767	0 8253	0 8273	0 7994	0 8305	0 8392
Na	0 0333	0 0236	0 0420	0 0452	0 0460	0 0620	0 0660	0 0214	0 0269	0 0689	0 0314	0 0641
Sum	3 9961	3 9979	4 0441	3 9962	4 0105	4 0144	4 0016	4 0088	3 9917	3 9999	3 9980	4 0046
Mg#	89 6	90 3	86 6	88 6	88 5	86 7	87 4	89 3	90 0	89 4	89 7	91 1
Ca	44 1	44 8	44 1	45 8	44 4	43 0	44 0	43 3	44 4	44 1	44 4	45 8
Mg	50 0	49 9	48 4	48 0	49 2	49 4	48 9	50 6	50 0	49 9	49 9	49 4
Fe	5 8	5 3	7.5	6 2	6 4	7 6	7 0	6 1	5 6	6 1	5 7	4 8

Clinopyroxene (2), Pyrolite + 1 4% $MgCO_3$ or 5 0% $CaMg(CO_3)_2$ + 0 2% H_2O

	Carbonate Melt Field											
Pressure	32	21	22	22	22	25	25	25	27	27	27	28
Temperature	925	1025	975	1000	1050	950	975	1000	950	1000	1050	1075
SiO_2	54 12	52 07	52 90	51 68	50 99	52 21	52 45	52 71	53 63	52 38	52 16	52 18
TiO_2	0 28	0 79	0 61	0 84	0 89	0 71	0 75	0 52	0 37	0 65	0 71	0 74
Al_2O_3	2 72	4 71	3 39	4 78	5 53	5 57	4 63	3 79	3 30	4 77	5 09	4 19
Cr_2O_3	0 66	0 83	0 96	1 01	0 90	0 79	1 14	0.68	0 70	0 89	0 86	0 80
FeO	3 67	3 94	3 63	3 65	4 43	3 50	3 24	3 59	3 55	3 77	4 50	3 86
MgO	16 19	16 31	16 94	16 52	15 83	15 89	15 98	16 96	17 05	16 13	16 07	16 39
CaO	21 16	20 74	20 83	20 52	20 49	20 43	20 98	21 20	20 86	20 49	19 13	21 15
Na_2O	1 19	0 61	0 72	1 00	0 94	0 91	0 83	0 55	0 54	0 91	1 49	0 66
Sum	100	100 00	100 00	100 00	100 00	100 00	100 00	100 00	100 00	100 00	100 00	100 00
Si	1 9647	1 8927	1 9217	1 8804	1 8618	1 8911	1 9030	1 9141	1 9415	1 9017	1 8961	1 8996
Ti	0 0076	0 0216	0 0168	0 0229	0 0244	0 0192	0 0205	0 0142	0 0101	0 0177	0 0193	0 0203
Al	0 1163	0 2019	0 1453	0 2050	0 2381	0 2380	0 1978	0 1621	0 1408	0 2042	0.2182	0 1798
Cr	0 019	0 0239	0 0276	0 0292	0 0260	0 0226	0 0326	0 0194	0 0200	0 0255	0 0247	0 0231
Fe	0 1115	0 1198	0 1103	0 1110	0 1354	0 1061	0 0982	0 1091	0 1076	0 1146	0 1369	0 1182
Mg	0 8761	0 8836	0 9172	0 8960	0 8613	0 8578	0 8642	0 9179	0 9200	0 8728	0 8705	0 8893
Ca	0 8231	0 8078	0 8107	0 8000	0 8015	0 7927	0 8157	0 8247	0 8090	0 7969	0 7451	0 8248
Na	0 0835	0 0431	0 0508	0 0703	0 0668	0 0636	0 0585	0 0389	0 0381	0 0643	0 1048	0 0467
Sum	4 0018	3 9943	4 0005	4 0148	4 0152	3 9912	3 9905	4 0004	3 9871	3 9978	4 0456	4 0019
Mg#	88 7	88 1	89 3	89 0	86 4	89 0	89 8	89 4	89 5	88 4	86 4	88 3
Ca	45 5	44 6	44 1	44 3	44 6	45 1	45 9	44 5	44 0	44 7	42 5	45 0
Mg	48 4	48 8	49 9	49 6	47 9	48 8	48 6	49 6	50 1	48 9	49 7	48 5
Fe	6.2	6 6	6 0	6 1	7 5	6 0	5 5	5 9	5 9	6 4	7 8	6 5

Clinopyroxene (3), Pyrolite + 1 4% $MgCO_3$ or 5 0% $CaMg(CO_3)_2$ + 0 2% H_2O

	Carbonate Melt Field						Silicate Melt Field						
Pressure	29	29	29	29	30	30	15	20	25	25	25	28	32
Temperature	950	975	1000	1025	950	1000	1075	1100	1100	1150	1200	1150	975
SiO_2	54 48	53 15	53 04	53 54	53 32	52 83	53 02	51 34	52 44	52 25	50 51	51 81	53 13
TiO_2	0 58	0 82	0 63	0 61	0 48	0 73	0 80	1 08	0 48	0 56	1 30	0 88	0 46
Al_2O_3	3 60	3 47	3 55	4 00	3 29	4 22	4 09	6 09	3 44	3 84	7 29	4 92	4 16
Cr_2O_3	0 53	1 10	1 07	0 95	0 67	1 02	0 86	1 25	0 59	0 93	1 12	1.01	0 64
FeO	3 82	3 92	4 65	3 47	3 90	3 46	3 60	3 39	3 91	3 70	4 09	3 61	4 06
MgO	16 63	16 33	15 34	16 64	16 37	16 24	17 03	16 58	16 80	17 07	16 10	16 88	16 08
CaO	18 89	19 76	20 34	19 25	21 46	20 62	20 24	19 39	21 98	21 08	18 44	20 03	20 03
Na_2O	1 48	1 46	1 37	1 54	0 52	0 88	0 37	0 87	0 35	0 57	1 13	0 86	1 45
Sum	100 00	100 00	100 00	100 00	100 00	100 00	100.00	100 00	100 00	100 00	100 00	100 00	100
Si	1 9637	1 9309	1 9351	1.9350	1 9375	1.9155	1 9172	1 8587	1 9115	1 9010	1 8314	1 8804	1 9287
Ti	0 0156	0 0223	0 0173	0 0165	0 0131	0 0200	0 0219	0 0295	0 0133	0 0153	0 0356	0 0239	0 0126
Al	0 1529	0 1486	0 1527	0 1705	0 1407	0 1803	0 1742	0 2600	0 1480	0 1645	0 3116	0 2105	0 178
Cr	0 0150	0 0315	0 0307	0 0272	0 0193	0 0292	0 0245	0 0359	0 0170	0 0266	0 0322	0 0291	0 0183
Fe	0 1150	0 1192	0 1420	0 1050	0 1185	0 1048	0 1090	0 1025	0 1193	0 1127	0 1241	0 1097	0 1231
Mg	0 8934	0 8840	0 8343	0 8964	0 8866	0 8776	0 9178	0 8944	0 9130	0 9259	0 8703	0 9130	0 8698
Ca	0 7295	0 7690	0 7952	0 7452	0 8354	0 8011	0 7840	0 7520	0 8585	0 8219	0 7162	0 7790	0 7789
Na	0 1032	0 1025	0 0971	0 1079	0 0367	0 0622	0 0258	0 0614	0 0245	0 0405	0 0796	0 0606	0 1024
Sum	3 9883	4 0080	4 0044	4 0037	3 9877	3 9908	3 9745	3 9945	4 0050	4 0084	4 0009	4 0062	4 0118
Mg#	88 6	88 1	85 5	89 5	88 2	89 3	89 4	89 7	88 4	89 1	87 5	89 3	87 6
Ca	42 0	43 4	44 9	42 7	45 4	44 9	43 3	43 0	45 4	44 2	41 9	43 2	44
Mg	51 4	49 9	47 1	51 3	48 2	49 2	50 7	51 1	48 3	49 8	50 9	50 7	49 1
Fe	6 6	6 7	8 0	6 0	6 4	5 9	6 0	5.9	6 3	6 1	7 3	6 1	7

Garnet (1), Pyrolite + 1 4% $MgCO_3$ or 5 0% $CaMg(CO_3)_2$ + 0 2% H_2O

	Subsolidus						Carbonate Melt Field					
Pressure	22	25	28	30	31	32	22	22	25	25	25	27
Temperature	950	925	925	900	900	925	975	1000	950	975	1000	950
P_2O_5					0 18							
SiO_2	41 62	41 44	42 29	42 67	42 46	40 12	41 28	41.29	41 24	41 43	41 72	41 94
TiO_2	0 37	0 35	0 50	0 80	0 62	3 51	0 73	0 96	0 95	0 64	1 38	0 55
Al_2O_3	22 03	20 14	20 52	19 88	19 57	18 94	20 71	20 13	20 65	21 22	19 76	20 34
Cr_2O_3	1 14	1 98	1 71	1 11	1 25	1 85	1 66	1 97	1.81	2 15	2 26	1 63
FeO	9.25	9 75	9 73	9 90	8 94	10 5	9 73	9 16	9 76	9 19	8 79	9 16
MnO	0 46	0 32	0 31	0 32	0 33	0 24	0 34	0 31	0 26	0 44	-	0 37
MgO	18 38	19 26	18 21	18 88	19 34	18 1	17 84	18.79	17 25	17 97	18 16	19 00
CaO	6 76	6 76	6 73	6 44	7.30	6 75	7 72	7 38	8 09	6 95	7 93	7 02
Sum	100 00	100 00	100 00	100 00	100 00	100	100 00	100 00	100 00	100 00	100 00	100 00
P					0 0111							
Si	2 9933	3 0008	3 0500	3 0735	3 0560	2 9286	2 9926	2 9886	2 9935	2 9919	3 0153	3 0246
Ti	0 0202	0 0192	0 0273	0 0433	0 0333	0 1929	0 0396	0 0522	0.0520	0 0348	0 0750	0 0299
Al	1.8671	1 7182	1 7441	1 6879	1 6604	1 6292	1 7698	1 7168	1 7663	1 8058	1 6830	1 7284
Cr	0 0645	0 1135	0 0975	0 0632	0 0712	0 1067	0 0950	0 1128	0 1038	0 1229	0 1294	0 0927
Fe	0 5563	0 5905	0 5868	0 5965	0 5383	0 6409	0 5899	0 5547	0 5922	0 5549	0 5310	0 5526
Mn	0 0277	0 0197	0 0190	0.0198	0 0200	0 0148	0 0209	0 0190	0 0163	0 0269	-	0 0224
Mg	1 9707	2 0780	1 9569	2 0266	2 0747	1 9695	1 9280	2 0275	1 8660	1 9338	1 9559	2 0422
Ca	0 5206	0 5241	0 5201	0 4967	0 5632	0 5278	0 5997	0.5726	0 6290	0 5378	0 6136	0 5423
Sum	8 0206	8 0640	8 0019	8 0075	8 0282	8 0104	8 0354	8 0442	8 0193	8 0089	8 0033	8 0349
Mg#	78.0	77 9	76.9	77 3	79 4	75 4	76 6	78 5	75 9	77 7	78 6	76 7
Ca	17 1	16 4	17 0	15 9	17 7	16 8	19 2	18 2	20 4	17 8	19 8	17 3
Mg	64 7	65 1	63 9	65 0	65 3	62 8	61 8	64 3	60 4	63 9	63 1	65 1
Fe	18 3	18 5	19 2	19 1	16 9	20 4	18 9	17 6	19 2	16 3	17 1	17 6

Garnet (2), Pyrolite + 1 4% $MgCO_3$ or 5 0% $CaMg(CO_3)_2$ + 0 2% H_2O

										Silicate Melt Field		
Pressure	27	27	28	29	29	29	29	30	30	25	25	28
Temperature	1000	1050	1075	950	975	1000	1025	950	1000	1100	1150	1150
SiO_2	41 60	41 59	40 98	41 35	41 42	41 76	41 81	41 64	41 31	41 75	41 47	41 51
TiO_2	0 74	0 64	0 79	0 73	1.07	0 65	0 52	0 91	2 19	1 21	0 98	0 79
Al_2O_3	21 41	20 82	20 16	21 00	20 26	20 90	21 81	21 39	19 58	21 05	20 64	20 38
Cr_2O_3	1 64	2 29	1 94	2 19	2 01	1 87	1 59	1 50	1 49	2 06	2 37	3 16
FeO	8 49	8 96	9 27	9 66	9 43	8 71	8 68	9 28	10.71	8 11	8 47	7 98
MnO	0 38	0 27	0 39	0 29	0 25	-	0 37	0 23	-	-	0 30	0 29
MgO	18 57	18 91	19 18	17 49	18 30	19 15	19 42	17 90	18 51	19 00	19 27	19 14
CaO	7 17	6 51	7 29	7 28	7 26	6 96	5 80	7 14	6 20	6 82	6 50	6 75
Sum	100 00	100 00	100 00	100 00	100 00	100.00	100 00	100 00	100 00	100 00	100 00	100 00
Si	2 9913	2 9962	2 9701	2 9942	2 9975	3 0016	2 9939	3 0002	2 9952	2 9932	2 9846	2 9888
Ti	0.0398	0 0349	0.0429	0 0398	0 0585	0 0353	0.0281	0 0493	0 1195	0 0655	0 0531	0 0428
Al	1 8142	1 7678	1.7220	1 7919	1 7282	1 7703	1 8407	1 8165	1 6734	1 7781	1 7508	1.7292
Cr	0.0933	0 1306	0 1113	0 1254	0 1151	0 1063	0 0902	0 0857	0 0857	0 1169	0 1349	0 1797
Fe	0 5107	0 5401	0 5619	0 5852	0 5707	0 5234	0.5201	0 5594	0 6496	0 4860	0 5095	0 4803
Mn	0 0232	0 0167	0 0242	0 0178	0 0151	-	0 0222	0 0138	-	-	0 0181	0 0180
Mg	1 9900	2 0305	2 0718	1 8881	1 9744	2 0516	2 0725	1 9228	2 0007	2 0303	2 0670	2 0543
Ca	0 5524	0 5028	0 5658	0 5649	0 5629	0 5363	0 4447	0 5515	0 4815	0 5237	0 5014	0 5207
Sum	8 0150	8 0196	8 0701	8 0073	8 0223	8 0247	8 0124	7 9993	8 0056	7 9937	8 0193	8 0138
Mg#	79.6	79 0	78 7	76 3	77 6	79 7	79 9	77 5	75 5	80 7	80 2	81 1
Ca	18 1	16 4	17 7	18 6	18 1	17 2	14 6	18 2	15 4	17 2	16 3	17 0
Mg	65 2	66 1	64 8	62 1	63 5	65 9	68 2	63 4	63 9	66 8	67 2	67 2
Fe	16 7	17 6	17 6	19 3	18 4	16 8	17 1	18 4	20 7	16 0	16 6	15 7

Amphibole (1), Pyrolite + 1 4% $MgCO_3$ or 5 0% $CaMg(CO_3)_2$ + 0 2% H_2O

	Subsolidus										
Pressure	15	16	17	18	20	20	20	20	20	22	25
Temperature	1050	900	900	900	950	975	1000	1050	1075	950	925
SiO_2	45 29	46 19	45 94	44 74	44 28	44 63	44 27	43 62	43 63	45 04	44 97
TiO_2	2 67	1 27	1 21	1 38	1 79	1 58	1 73	1 97	1 97	1 24	0 96
Al_2O_3	12 10	11 61	13 07	12 51	13 22	11 81	13 19	13 43	13 44	12 67	13 51
Cr_2O_3	1 09	1.27	1 04	1 22	1 05	1 12	1.28	1 21	1.21	1 17	1 22
FeO	5 02	5 56	5 24	5.00	4 73	4 77	4 84	5 40	5 40	5.20	4 19
MgO	19 80	20 99	20 52	18 88	18 35	18 24	18 41	18 05	18 05	19 36	18 96
CaO	9 37	10 62	10 25	11 08	11.08	10 97	10 78	10 76	10 76	10 53	10 61
K_2O	0 46	0 41	0 44	0 46	1 00	0 61	0 65	0 67	0 67	0 49	0 55
Na_2O	2 23	2 08	2 29	2 73	2 43	2 56	2 89	2 89	2 89	2 30	3 00
Sum	98 00	100 00	100 00	98 00	98 00	96 32	98 00	98 00	98 00	98 00	98 00
Si	6 3728	6 4036	6 3460	6 3415	6 2851	6 4282	6 2779	6.2101	6 1751	6.3655	6 3407
Ti	0 2818	0 1321	0 1261	0 1468	0 1912	0 1707	0 1845	0 2115	0 2519	0 1317	0 1021
Al	2 0066	1 8961	2 1280	2 0908	2 2119	2 0098	2 2044	2 2542	2 2041	2 1101	2 2450
Cr	0 1207	0 1397	0 1133	0 1362	0 1173	0 1279	0 1427	0 1365	0 1347	0 1307	0 1356
Fe	0 5899	0 6448	0 6050	0 5921	0 5620	0 5750	0 5699	0 6419	0 6810	0 6149	0 4945
Mg	4 1514	4 3369	4 2253	3 9894	3 8815	3 9155	3 8899	3 8294	3 9183	4 0766	3 9854
Ca	1 4126	1 5770	1 5178	1 6838	1 6851	1 6924	1 6376	1 6413	1 5955	1 5944	1 6038
K	0 0822	0 0730	0 0783	0 0834	0 1816	0 1112	0 1187	0 1207	0 1253	0 0879	0 0992
Na	0 6098	0 5591	0 6126	0 7511	0 6678	0 7138	0 7952	0 7952	0 7603	0 6286	0 8201
Sum	15 6277	15 7623	15 7525	15 8152	15 7836	15 7445	15 8210	15 8408	15 8463	15 7405	15 8264
Mg#	87 6	87 1	87 5	87.1	87 4	87 2	87 2	85 6	85 2	86 9	89 0
Ca	23 0	24 0	23 9	26 9	27 5	27 4	26 9	26 9	25 8	25 4	26 4
Mg	67 5	66 1	66 6	63 7	63 3	63 3	63 8	62 6	63 3	64 9	65 5
Fe	9 6	9 8	9 5	9 4	9 2	9 2	9 3	10 5	11 0	9 8	8 1

Amphibole (2), Pyrolite + 1 4% $MgCO_3$ or 5 0% $CaMg(CO_3)_2$ + 0 2% H_2O

			Carbonate Melt Field									
Pressure	30	31	21	22	22	22	25	25	25	27	27	27
Temperature	900	900	1025	975	1000	1050	950	975	1000	950	1000	1050
SiO_2	45 57	45 98	44 49	45 12	44 70	44 63	44 79	44 79	44 68	44 12	45 21	45 62
TiO_2	1 10	1 36	1 58	1 41	1 75	1 37	1 28	1 50	1 27	1 14	1 42	1 22
Al_2O_3	11 48	11 48	12 54	12 16	12 46	12 43	13 14	12 44	12 69	13 70	12 20	11 70
Cr_2O_3	0 83	0 79	1 09	1.32	1 16	1 06	1 55	1 33	1 04	1 86	0 95	1 15
FeO	5 55	4 43	5 26	4 72	4 66	5 41	3 84	4 87	4 81	4 91	4 75	4 64
MgO	19 27	19 56	18 74	18 90	18 51	18 66	18 70	18 40	18 82	19 57	19 15	18 92
CaO	11 09	11 01	10 90	11 07	11 12	10 78	10 86	11 36	11 06	10 92	10 51	10 80
K_2O	0 54	0 52	0.54	0 59	0 58	0 62	0 90	0 41	0 68	0 70	0 63	0 72
Na_2O	2 57	2 86	2 84	2 69	3 05	3 05	2 93	2.90	2 97	3 07	3 19	3 24
Sum	98 00	98 00	98 00	98 00	98 00	98 00	98 00	98 00	98 00	100 00	98 00	98 00
Si	6 4636	6 4872	6 3188	6 3909	6 3403	6 3440	6 3312	6 3538	6 3365	6 1580	6 3985	6 4617
Ti	0 1165	0 1446	0 1697	0 1505	0 1868	0 1467	0 1359	0 1601	0 1357	0 1195	0 1513	0 1295
Al	1 9183	1 9101	2.0983	2 0294	2 0825	2 0836	2 1891	2 0797	2 1205	2 2543	2 0342	1 9546
Cr	0 0932	0 0872	0 1216	0 1478	0 1304	0 1193	0 1734	0 1490	0 1163	0 2057	0 1065	0 1285
Fe	0 6586	0 5225	0 6256	0 5590	0 5526	0 6434	0 4550	0 5779	0 5701	0 5728	0 5614	0 5489
Mg	4 0752	4 1147	3 9687	3 9898	3 9122	3 9539	3 9396	3 8904	3 9784	4 0710	4 0393	3 9944
Ca	1 6863	1 6641	1 6592	1 6797	1 6900	1 6411	1 6448	1 7256	1 6817	1 6333	1 5935	1 6386
K	0 0972	0 0937	0.0968	0 1061	0 1041	0 1113	0 1622	0 0743	0 1226	0 1255	0 1141	0 1303
Na	0 7072	0 7842	0 7821	0 7392	0 8392	0 8403	0 8029	0 7961	0 8177	0 8301	0 8757	0 8912
Sum	15 8161	15 8084	15 8409	15 7925	15 8380	15.8403	15 8340	15 8068	15 8794	15 9702	15 8745	15 8778
Mg#	86 1	88.7	86 4	87 7	87 6	86 0	89 6	87 1	87.5	87 7	87 8	87 9
Ca	26 3	26 4	26 5	27 0	27 5	26 3	27 2	27 9	27 0	26 0	25 7	26 5
Mg	63 5	65 3	63 5	64 1	63 6	63 4	65 2	62 8	63 9	64 9	65 2	64 6
Fe	10 3	8 3	10 0	9 0	9 0	10 3	7 5	9 3	9 2	9 1	9 1	8 9

Amphibole (3), Pyrolite + 1 4% $MgCO_3$ or 5 0% $CaMg(CO_3)_2$ + 0 2% H_2O

							Silicate Melt Field			
Pressure	28	29	29	29	29	30	30	32	20	25
Temperature	1075	950	975	1000	1025	950	1000	975	1100	1200
SiO_2	45.12	46 38	45 62	45 65	46 15	48 91	46 66	46 55	39 98	41 23
TiO_2	2 23	0 99	1 17	1 34	1 40	0 89	1 15	1 09	5 42	4 42
Al_2O_3	12 15	12 04	10 79	11 53	12 64	9 82	10 78	11 24	15 74	15 48
Cr_2O_3	1.02	0 79	1 26	1 16	1 18	0 86	1 10	0 68	0 00	0 00
FeO	4 73	4 40	4 66	5 23	4 66	4 98	4 33	4 76	7 90	9 48
MgO	18 37	19 05	20 43	18 53	19 12	21 07	19 39	19 40	15 39	14 60
CaO	10 01	10 56	10 16	10 32	10 42	10 32	9 76	10 67	9 43	8 99
K_2O	1.20	0 67	0 98	1 23	1 12	0 45	1 38	0 68	0 51	0 79
Na_2O	3 16	3 13	2 91	3 01	3 29	2 70	3 44	2 95	3 52	3 03
Sum	98 00	98 00	98 00	98 00	100 00	100 00	98 00	98 00	98 00	98 00
Si	6 3995	6 5313	6 4658	6 4879	6 4083	6 7331	6 5997	6 5688	5 7713	5 9556
Ti	0 2376	0 1052	0 1256	0 1439	0 1467	0 0920	0 1223	0 1156	0 5889	0 4799
Al	2 0304	1.9988	1 8028	1 9313	2 0684	1 5938	1 7966	1 8677	2 6769	2 6357
Cr	0 1149	0 0879	0 1415	0 1303	0 1297	0 0933	0 1230	0 0753		
Fe	0 5611	0 5180	0 5520	0 6220	0 5413	0 5739	0 5129	0 5617	0 9537	1 1456
Mg	3.8820	3 9980	4 3157	3 9248	3 9576	4 3226	4 0886	4 0781	3 3118	3 1422
Ca	1.5212	1 5934	1 5431	1 5714	1 5510	1 5224	1 4790	1 6128	1 4581	1 3908
K	0 2181	0 1204	0 1785	0 2217	0 1986	0 0793	0 2498	0 1215	0 0947	0 1446
Na	0 8688	0 8538	0 8012	0 8293	0 8870	0 7207	0 9423	0 8064	0 9865	0 8491
Sum	15 8335	15 8070	15.9262	15 8627	15 8886	15 7312	15 9142	15 8079	15 8680	15 7434
Mg#	87 4	88 5	88 7	86 3	88 0	88 3	88 9	87 9	77 6	73 3
Ca	25 5	26 1	24 1	25 7	25 6	23 7	24 3	25 8	25 5	24 5
Mg	65 1	65 4	67 3	64 1	64 4	67 3	67 2	65.2	57 9	55 3
Fe	9 4	8 5	8 6	10 2	8 9	8 9	8 4	9 0	16 7	20 2

Spinels, Pyrolite + 1 4% $MgCO_3$ or 5 0% $CaMg(CO_3)_2$ + 0 2% H_2O

	Subsolidus				+Carbonate Melt		+ Silicate Melt	
Pressure	15	20	20	20	21	22	20	25
Temperature	1050	1000	1050	1075	1025	1050	1100	1200
SiO_2	7 21	6 16	3 17		5 73		1.48	1 26
TiO_2	2 14	1 26	2 69	2 15	2 46	2 3	1 3	1 28
Al_2O_3	26 78	36.42	30 44	31 44	21 77	26 97	38 34	35 48
Cr_2O_3	25 91	18 68	20 22	24 96	21 83	14 97	25.73	29 27
FeO	17.2	17 03	25 66	27	27 42	38 28	13 97	13 97
NiO	0 39	0 39	0 43		0 48	0 73		
MgO	19.72	19 87	17 21	14 45	18 29	16 75	18 82	19 66
CaO	0 32	0 19	0 18		2 04		0 36	0 35
Sum	99 67	100	100	100	100	100	100	101 27
Si	0.2053	0 1697	0 0932		0 1733		0 0413	0 0352
Ti	0 0458	0 0261	0 0596	0 0487	0 0559	0 0547	0 0272	0 0268
Al	0.8989	1 1831	1 0564	1 1184	0 7757	1 0055	1 2611	1 1677
Cr	0 5833	0 407	0 4707	0 5956	0 5219	0 3743	0 5677	0 6463
Fe	0 4096	0 3924	0 6319	0 6813	0 6933	1 0126	0 3261	0 3263
Ni	0 0088	0 0088	0 0103		0 0117	0 0185		
Mg	0 8369	0 8162	0 7556	0 6499	0 8242	0 7895	0 7827	0 8181
Ca	0.0097	0 0057	0 0058		0 0659		0 0109	0 0106
Sum	3 0167	3 009	3 0835	3 0941	3 1219	3 2552	3 017	3 0308
Mg#	67 1	67 5	54 5	48 8	54 3	43 8	70 6	71 5

Ilmenite (1), Pyrolite + 1 4% $MgCO_3$ or 5 0% $CaMg(CO_3)_2$ + 0 2% H_2O

	Subsolidus Carbonate Field								Subsolidus CO2 Field				
Pressure	17	18	20	22	25	28	30	31	32	16	20	20	20
Temperature	900	900	950	950	925	925	900	900	925	900	975	1000	1050
SiO_2	2 09	-	-	-	-	-	0 20	-	-	-	2 74	-	-
TiO_2	48 98	51 26	52 32	44 27	55 02	42 23	50 44	43 58	45 82	55 81	48 11	53 66	46 44
Al_2O_3	2 77	0 60	1 38	1.21	0 41	1 00	0 66	0 92	0 65	0 55	0 95	0 74	0 87
Cr_2O_3	3 56	1 98	2 55	4 65	1 89	2 64	2 05	2.55	2 24	1 06	2 79	2 57	3 41
FeO	28 69	33 18	30 63	38 90	29 26	43 11	35 05	40 94	39 44	29 31	30 84	29 10	33 30
NiO	-	-	0 46	0 45	-	0 41	0 64	0 61	-	-	0 45	-	-
MgO	13 23	12 43	12 08	10 36	13 27	10 36	10 75	11 19	11 61	12 64	13 90	13 75	13 98
CaO	0 30	0 16	0 23	0 16	0 16	0 25	0 20	0 22	0 24	0 19	0 23	0 17	-
MnO	0 38	0 38	0 36	-	-	-	-	-	-	0 44	-	-	-
Sum	100 00	100 00	100 00	100 00	100 00	100 00	100 00	100 00	100 00	100 00	100 00	100 00	100 00
Si	0.0955	-	-	-	-	-	0 0095	-	-	-	0 1264	-	-
Ti	1.6831	1.8172	1 8346	1 6274	1 9077	1 5812	1 8073	1 6142	1 6773	1 9357	1 6706	1 8613	1 7193
Al	0 1490	0 0332	0 0757	0 0698	0 0222	0 0589	0 0372	0 0533	0 0373	0 0300	0 0519	0 0404	0 0483
Cr	0 1287	0 0739	0 0938	0 1796	0 0690	0 1039	0 0771	0 0993	0 0864	0 0387	0 1017	0 0936	0 1273
Fe	1 0961	1 3081	1 1944	1 5904	1 1281	1 7949	1 3965	1 6860	1 6054	1 1304	1 1911	1 1226	1 3145
Ni	-	-	0 0172	0 0178	-	0 0162	0 0246	0 0240	-	-	0 0166	-	-
Mg	0 9007	0 8733	0 8392	0 7547	0 9118	0 7688	0 7636	0 8211	0 8420	0 8687	0 9566	0 9455	0 9835
Ca	0 0147	0 0083	0 0113	0 0082	0 0079	0 0135	0 0104	0 0117	0 0126	0 0095	0 0113	0 0084	-
Mn	0 0149	0 0153	0 0144	-	-	-	-	-	-	0 0170	-	-	-
Sum	4 0826	4 1293	4 0807	4 2479	4 0468	4 3374	4 1261	4 3097	4 2609	4 0301	4 1262	4 0718	4 1929
Mg#	45 1	40 0	41 3	32 2	44 7	30 0	35 4	32 8	34 4	43 5	44 5	45 7	42 8

Ilmenite (2), Pyrolite + 1 4% $MgCO_3$ or 5 0% $CaMg(CO_3)_2$ + 0 2% H_2O

	Carbonate Melt Field												
Pressure	21	22	22	22	25	25	25	27	27	27	28	29	29
Temperature	1025	975	1000	1050	950	975	1000	950	1000	1050	1075	950	975
SiO_2	-	-	-	2 54	-	-	-	-	0 96	-	0 24	0 29	-
TiO_2	47 08	54 14	53 54	27 65	54 71	54 04	52 74	50 21	50 33	52 71	53 33	53 58	54 33
Al_2O_3	1 20	0 51	0 69	3 13	0 59	0 54	1.71	0 95	0 92	0 80	0 84	0 58	0 47
Cr_2O_3	3 51	2 27	3 16	5 90	2 20	3 35	3 36	3 43	3 44	3 41	2 43	2 31	2 06
FeO	36 25	28 93	28 05	51 73	27 35	27.20	26 74	31 37	29 56	28 03	28 44	29 56	28 60
NiO	-	0 36	-	-	0 38	0 44	0 53	-	0 41	-	-	0 49	0 41
MgO	11 82	13 61	14 56	9 05	14 52	14.21	14 75	13.83	14 08	14 46	14 51	13 01	13 93
CaO	0 14	0 18	-	-	0 25	0 22	0 17	0 20	0 31	0 17	0 22	0 18	0 21
Sum	100 00	100 00	100 00	100 00	100 00	100 00	100 00	100 00	100 00	100 00	100 00	100 00	100 00
Si	-	-	-	0 1312	-	-	-	-	0 0445	-	0 0109	0 0132	-
Ti	1 6970	1 8794	1 8490	1 0761	1 8840	1 8653	1 8126	1 7653	1 7511	1 8184	1 8413	1 8651	1 8827
Al	0 0680	0 0278	0 0373	0 1911	0 0319	0 0294	0 0923	0 0524	0 0499	0 0434	0 0453	0 0319	0 0255
Cr	0 1329	0 0827	0 1149	0 2413	0 0798	0 1214	0 1214	0 1269	0 1258	0 1236	0 0880	0 0845	0 0749
Fe	1 4532	1 1168	1.0771	2 2387	1 0474	1 0440	1 0219	1 2266	1 1437	1 0751	1 0921	1 1443	1 1021
Ni	-	0 0135	-	-	0 0140	0 0164	0 0194	-	0 0154	-	-	0 0181	0 0152
Mg	0 8445	0 9361	0 9966	0 6979	0 9908	0 9723	1 0045	0 9640	0 9711	0 9884	0 9927	0 8972	0 9565
Ca	-	0 0091	-	-	0 0124	0 0106	0 0084	0 0099	0 0152	0 0085	0 0109	0 0092	0 0104
Sum	4 2026	4 0654	4 0750	4 5764	4 0603	4 0594	4 0806	4 1451	4 1166	4 0737	4.0813	4 0635	4 0672
Mg#	36 8	45 6	48 1	23 8	48 6	48 2	49 6	44 0	45 9	47 9	47 6	43 9	46 5

Carbonates, Pyrolite + 1 4% $MgCO_3$ or 5 0% $CaMg(CO_3)_2$ + 0 2% H_2O

	Dolomite					Magnesite				Magnesite	Dolomite
Pressure	17	18	20	25	27	28	30	31	32	32	32
Temperature	900	900	950	925	950	925	900	900	925	975	975
P_2O_5	-	-	-	-	-	-	-	0 18	-	0 16	-
SiO_2	1 47	0 50	6 04	-	-	0 22	0 19	-	-	0 24	0 25
Al_2O_3	-	0 20	-	-	-	0 25	0 20	0 31	0 27	0 37	-
FeO	2 87	2 75	4 62	0 58	0 27	5 09	3 89	3 46	4 38	4 69	2 57
MgO	19 92	18 46	21 07	20 63	20 93	38 54	38 83	38 00	37 85	36 40	18 97
CaO	29 13	31 19	27 84	30 03	29 49	2 88	1 62	1 98	1 75	3 86	28 73
Sum	53 39	53 09	59 57	51 24	50 69	46 99	44 74	43 93	44.25	45 72	50 53
P	-	-	-	-	-	-	-	0 0149	-	0 0128	-
Si	0 1327	0 0461	0 4698	-	-	0 0204	0 0183	-	-	0 0226	0 0245
Al	-	0 0217	-	-	-	0 0273	0 0226	0 0347	0 0303	0 0407	-
Fe	0 2173	0 2136	0 3005	0 0462	0 0214	0 3889	0 3070	0 2775	0 3521	0 3691	0 2092
Mg	2 6894	2 5566	2 4411	2 9093	2 9700	5 2472	5 4587	5 4299	5 4217	5 1036	2 7486
Ca	2 8277	3 1049	2.3186	3 0444	3 0084	0 2820	0 1636	0 2032	0 1805	0 3888	2 993
Sum	5 8671	5 9429	5 5301	5 9998	5 9998	5 9658	5 9703	5 9602	5 9847	5 9376	5 9753
Mg#	92 5	92 3	89 0	98 4	99 3	93 1	94 7	95 1	93 9	93 3	92 9
Ca#	49.3	52 8	45 8	50 7	50 1	4 8	2 8	3 4	3 0	6 6	50 3
Mg#	46 9	43 5	48 2	48 5	49 5	86 7	92 1	91 9	91 9	87 1	46 2
Fe#	3 8	3 6	5 9	0 8	0 4	6 6	5 2	4 7	5 9	6 3	3 5

Apatites, Pyrolite + 1 4% $MgCO_3$ or 5 0% $CaMg(CO_3)_2$ + 0 2% H_2O

Pressure	16	18	30
Temperature	900	900	900
P_2O_5	42 72	41 52	41 10
SiO_2	0 26	-	0 93
Al_2O_3	-	-	0 15
FeO	0 62	0 70	0 68
MgO	1 1	0 90	1.61
CaO	55 02	53 08	52 24
Cl	0 25	0 50	0 21
Sum	99 98	96 70	96 91
P	5 994	6 000	6 001
Si	0 044	-	0 160
Al	-	-	0 031
Fe	0 086	0 100	0 098
Mg	0 272	0 229	0 413
Ca	9.770	9 706	9 651
Cl	0 070	0 146	0 060
Sum	16 235	16 181	16 415
Mg#	76 1	69 5	80 9
Ca	96 5	96 7	95 0
Mg	2 7	2 3	4 1
Fe	0 8	1 0	1 0

Melt, Pyrolite + 1 4% $MgCO_3$ or 5 0% $CaMg(CO_3)_2$ + 0 2% H_2O

	25	25
	1100	1150
SiO_2	30 84	29 42
TiO_2	1 80	1 91
Al_2O_3	7 07	9 88
Cr_2O_3	0 29	-
FeO	6 31	7 06
MnO	-	-
MgO	19 09	15 95
CaO	7 97	9 99
Na_2O	3 11	3 01
K_2O	0 70	1 32
Sum	77.20	80 10
Mg#	84 3	80 1
Ca	20.2	26 5
Mg	67 3	58 9
Fe	12 5	14 6

* Melt compositions are from area scans and are quench modified

Mineral analyses from Brey (1983 unpublished) experiments

Olivines, Pyrolite -40% ol, + 5 0%CO2 + 0 2% H2O						Opx				Cpx				
Pressure	25	27	27	27	29	25	27	27	29	25	27	27	27	29
Temperature	1100	1050	1100	1140	1100	1100	1100	1140	1100	1100	1050	1100	1140	1100
SiO2	41 47	39 99	40 74	40 47	41 19	55 53	55 18	55 08	55 83	51 62	52 03	52 87	52 81	53 10
TiO2	-	-	-	-	-	0 32	0 47	0 41	0 32	1 11	0 64	0 89	0 91	1 10
Al2O3	0 40	-	-	-	-	3 39	3 44	3 90	2 77	5 01	3 52	4 38	4 25	4 35
Cr2O3	-	-	-	-	-	0 58	0 65	0 65	0 54	1 17	1 06	1 30	1 20	1 28
FeO	10 45	13 10	11.10	11.06	10 05	7 13	7 37	7 57	6 10	4 00	4 45	3 58	3 64	3 70
NiO	-	-	0 38	-	-	-	-	-	-	-	-	-	-	-
MgO	47 39	46 91	47 79	48 21	48 49	32 34	32 20	32 11	33 45	17 63	19 69	17 07	17 79	17 14
CaO	0 30	-	-	-	0 26	1 03	1 04	1 03	0 99	18 47	17 90	18 77	18 33	18 24
Na2O	-	-	-	-	-	-	-	-	-	0 87	0 80	1 14	1 09	1 34
Sum	100 00	100 00	100 00	99 74	100 00	100 33	100 32	100 75	100 00	99 86	100 00	100 00	100 02	100 25
Si	1 016	0 994	1 004	0 999	1.009	1 920	1 912	1 902	1.928	1 873	1 887	1 911	1 907	1 913
Ti	-	-	-	-	-	0 008	0 012	0 011	0 008	0 030	0 017	0 024	0 025	0 030
Al	0 012	-	-	-	-	0 138	0 141	0 159	0 113	0 214	0.151	0 187	0 181	0 185
Cr	-	-	-	-	-	0 016	0 018	0 018	0 015	0 034	0 031	0 037	0 034	0 036
Fe	0 214	0.272	0 229	0 228	0 206	0 206	0 213	0 219	0 176	0 121	0 132	0 108	0 110	0 112
Ni	-	-	0 008	-	-	-	-	-	-	-	-	-	-	-
Mg	1 730	1 739	1 756	1 774	1 770	1 667	1 663	1 653	1 722	0 953	1 064	0 920	0 957	0 920
Ca	0 008	-	-	-	0 007	0 038	0 039	0 038	0 037	0 718	0 696	0 727	0 709	0 704
Na	-	-	-	-	-	-	-	-	-	0 061	0 056	0 080	0 077	0 094
Sum	2 979	3 006	2 996	3 001	2 991	3 994	3 997	3 999	4 000	4 004	4 033	3 993	3 999	3 993
Mg#	89 0	86 5	88 5	88 6	89 6	89 0	88 6	88 3	90 7	88 7	89 0	89 5	89 7	89 2
Ca	0 4	0 0	0 0	0 0	0 3	2 0	2 0	2 0	1 9	40 1	36 8	41 4	39 9	40 6
Mg	88 6	86 5	88 5	88 6	89 3	87 2	86 8	86 6	89 0	53 2	56 3	52 4	53 9	53 0
Fe	11 0	13 5	11 5	11 4	10 4	10 8	11 1	11 4	9 1	6 8	7 0	6 2	6 2	6 4

Amphiboles,Pyrolite - 40% ol, +CO2						Garnets				Ilmenite
Pressure	25	27	27	27	29	25	27	27	29	27
Temperature	1100	1050	1100	1140	1100	1100	1050	1100	1100	1050
SiO2	45 05	44 64	47 01	46.57	48 14	42 49	41 68	41 70	42 12	-
TiO2	1 95	1 45	2 06	1 95	1 62	1 08	0 85	0 99	1 77	55 66
Al2O3	11 63	11 83	9 73	11 18	10 82	18 87	21 22	21 39	19 28	0 48
Cr2O3	1 56	1 26	0 50	0 57	0 83	1 95	2 20	2 71	2 58	2.29
FeO	4 18	5 21	7 37	5 80	4 74	8 34	10 20	8 58	8 51	26 81
MnO	-	-	-	-	-	0 33	0 39	0 38	0 27	0 29
MgO	20 72	20 71	19 12	19 40	20 79	20 82	18 26	19 12	18 72	14 14
CaO	9 79	9 53	8 48	10 34	9 49	6 61	6 94	6 68	7.68	0 32
K2O	0 80	0 84	1 44	0 46	0 11	-	-	-	-	-
Na2O	2 31	2 51	2 30	1 73	1 45	-	-	-	-	-
Sum	98 00	98 00	98 00	98 00	98 00	100 48	101 74	101 62	100 93	99 99
Si	6 354	6 326	6 683	6 558	6 696	3 042	2 972	2 963	3 017	-
Ti	0 207	0 155	0 220	0 207	0 169	0 058	0 046	0 053	0 095	1 862
Al	1 935	1 976	1 630	1 855	1 775	1 592	1 783	1 787	1 628	0 026
Cr	0 173	0.141	0 057	0 064	0 092	0 111	0 124	0 152	0 146	0 083
Fe	0 473	0.618	0 875	0 682	0 552	0 499	0 608	0 509	0 510	1 024
Mn	-	-	-	-	-	0 020	0 024	0 023	0 016	0 011
Mg	4 357	4 376	4 051	4 071	4 309	2 221	1 941	2 021	1 998	0 962
Ca	1 479	1 447	1 291	1 560	1 414	0 507	0.530	0 508	0 589	0 015
K	0 145	0 152	0 261	0 083	0 391	-	-	-	-	
Na	0 632	0 692	0 634	0 473	0 020	-	-	-	-	
Sum	15 754	15 883	15 702	15 554	15 417	8 049	8 028	8 015	8 000	4 034
Mg#	90 2	87 6	82 2	85 6	88 6	81 7	76 1	79 9	79 7	48 4
Ca	23 4	22 5	20 8	24 7	22 5	15 7	17 2	16 7	19 0	0 8
Mg	69 1	67 9	65 2	64 5	68 7	68 8	63 0	66 5	64 5	48 1
Fe	7 5	9 6	14 1	10 8	8 8	15 5	19 7	16 8	16 5	51 2

APPENDIX D

LIST OF PROBE MOUNTS AND TUMUT - EUCUMBENE SAMPLE NUMBERS

Appendix D. List of probe mounts

Probe Mount#		Sample#	P	T
Chapter 1, Tinaquillo - 40% Ol				
H-526	1	T-1833	Starting Mix	
	2	T-1838	28	1100
	3	T-1840	25	1100
	4	T-1842	28	1050
	5	T-1848	20	1100
	6	T-1853	30	1050
H-535	1	T-1859	25	1000
H-558	1	T-1890	25	1050
	2	T-1895	25	1025
	3	T-1902	20	1025
	4	T-1912	Starting Mix	
	5	T-1920	15	1000
H-586	1	T-1944	20	1000
	2	T-1952	15	1025
	3	T-1979	10	1000
	4	T-1998	10	970
H-619	1	T-2007	10	1000
	2	T-2024	27	950
	3	T-2055	20	980
Chapter 2, Pyrolite -40% Ol				
H-713	1	T-2195	25	1050
	2	T-2198	27	1050
	3	T-2228	25	1000
	4	T-2235	25	1000
H-716	1	T-2246	25	1100
	2	T-2262	25	1150
	3	T-2267	25	1200
H-721	1	T-2272	28	1150
	2	T-2278	20	1000
	3	T-2279	22	1000
H-732	1	T-2290	22	1050
	2	T-2296	22	950
	3	T-2300	27	1050
	4	T-2314	20	1100
	5	T-2319	27	1000
	6	T-2321	20	1050
H-740	1	T-2344	21	1025
	2	T-2354	20	1075
	3	T-2361	28	1000
	4	T-2367	20	950
H-746	1	T-2379	15	1075
	2	T-2384	29	1000
	3	T-2388	22	975
	4	T-2390	29	975
	5	T-2392	29	950
H-750	1	T-2399	30	950
	2	T-2400	18	900
	3	T-2403	17	900
	4	T-2405	29	1025
	5	T-2406	16	900
	6	T-2407	20	975
H-751	1	T-2296	22	950
	2	T-2279	22	1000
	3	T-2290	22	1050
	4	T-2235	25	1000
	5	T-2410	28	1075
	6	T-2419	30	1000
H-756	1	T-2414	15	1050
	2	T-2429	30	900
	3	T-2434	31	925
	4	T-2440	25	975

Appendix D. List of probe mounts

Probe Mount#		Sample#	P	T
H-758	1	T-2428	30	900
	2	T-2441	31	950
	3	T-2444	31	925
H-765	1	T-2450	25	925
	2	T-2454	25	950
	3	T-2457	27	950
	4	T-2296	22	950
	5	T-2300	27	1050
	6	T-2319	27	1000
H-770	1	T-2467	22	975
	2	T-2467	22	975
	3	T-2464	28	925
H-772	1	T-2476	25	920

Chapter3, Sandwich experiments and reversals

Probe Mount#		Sample#	P	T
H-776	1	2489	22	975
	2	2479	31	900
	3	2483	32	925
	4	2488	32	975
	5	Carbonatite mix #1		
H-778	1	T-2490	25	900
	2	T-2493	19	950
H-792	1	T-2508	22	1000
H-798	1	T-2517	22	1000
H-809	1	T-2534	25	1000
H-810	1	T-2536	18	1000
H-811	1	T-2535	22	900
	2	T-2439	18	1000
H-812	1	T-2545	19	1040

Tumut-Eucumbene xenolith sample numbers

46375 = DHG 2823

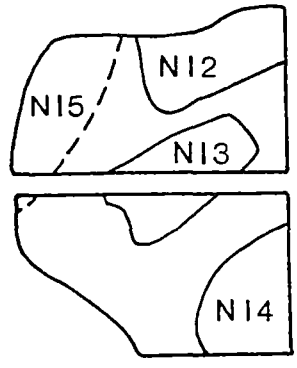

46376 = DHG 2824

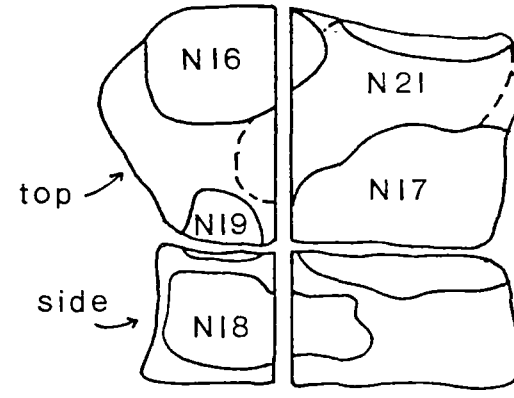

46377 = DHG 2825

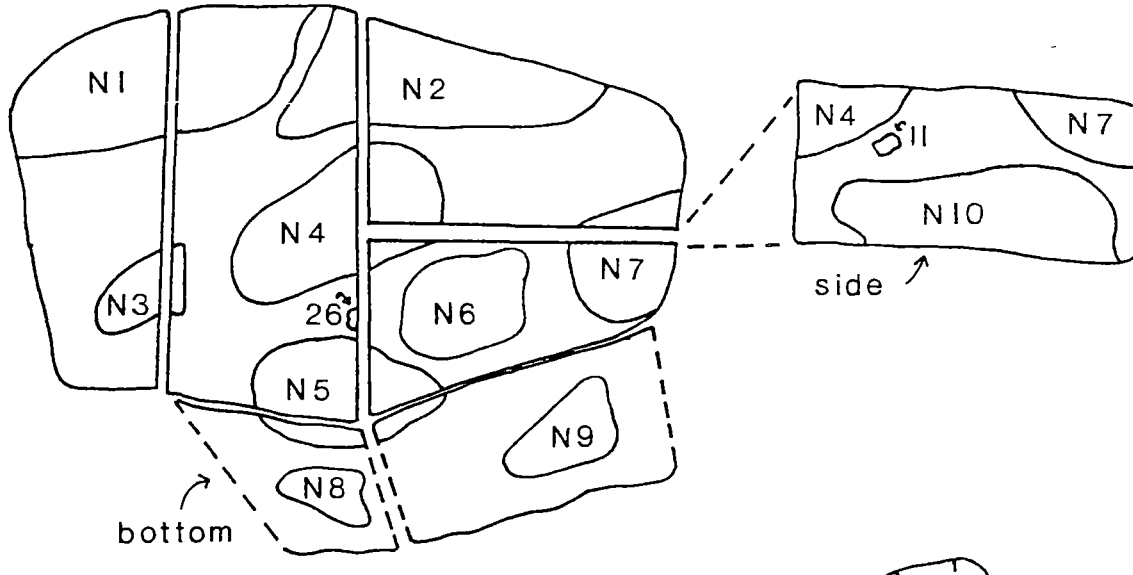
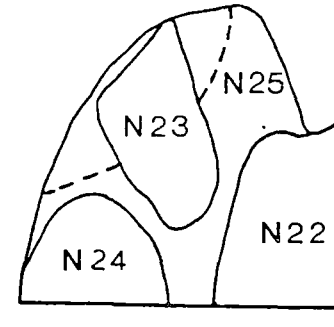
46378
= DHG 2826